Justus-Liebig-Universität Gießen

Fachbereich Medizin

Medizinisches Zentrum / Medizinische Klinik II und Poliklinik

Klinische Forschungsgruppe: ‚Lungenfibrose'

„Verständnis der entscheidenden Auswirkungen von deregulierter Autophagie und lysosomalem Stress bei diffusen parenchymalen Lungenerkrankungen"

„Understanding the crucial impact of deregulated autophagy & lysosomal stress in diffuse parenchymal lung diseases"

Habilitationsschrift

zur Erlangung der Lehrbefähigung für das Fach Experimentelle Pulmonologie

im Fachbereich Medizin der Justus-Liebig-Universität Gießen

vorgelegt von

Dr. rer. nat. Poornima Mahavadi

Gießen, 2021

To

my husband, my children and my parents

Table of contents

List of Abbreviations ..... **I**
1. Introduction **1**
1.1 Autophagy 1
1.2 Autophagy and the lysosome 4
1.3 The complex role of autophagy in cell survival and cell death 5
1.4 Diffuse parenchymal lung diseases (DPLDs) 6
1.5 Idiopathic Pulmonary Fibrosis (IPF) and animal models of lung fibrosis 7
1.6 Role of lysosomal stress and autophagy in lung fibrosis 9
2. Aims and objectives of this study **10**
3. Results and publications **11**
3.1 Animal models of lung fibrosis 11
3.2 Dysregulated autophagy in lung fibrosis 12
3.3 Role of LC3B in the development of lung fibrosis 13
3.4 Expanding the current understanding on the role of autophagy in lung fibrosis 14
4. Discussion **17**
4.1 HPS1/2 & amiodarone treated mice as animal models of lung fibrosis 17
4.2 Altered surfactant homeostasis is a common feature of DPLDs 19
4.3 Deregulation of autophagy taking the center stage in lung fibrosis 20
4.3.1 Lung fibrosis from the perspective of autophagy proteins 21
4.4 Contribution of HPS gene products to defective autophagy 22
4.5 A closer look into amiodarone induced excessive autophagy 24
4.6 Defective autophagy in IPF 25
4.8 Concomitant cellular stress pathways in IPF and other DPLDs 26
5. Summary and outlook **29**
6. Zusammenfassung **31**
7. References **33**
8. Publications **43**
8.1. Mahavadi et al., 2010
*8.2. Mahavadi et al., 2014*3
8.3. Birkelbach, …., Mahavadi, Knudsen* et al., 2015*
8.4. Mahavadi et al., 2015
8.5. Ahuja, …., Guenther, Mahavadi* et. al., 2016*
8.6. Kesireddy, …, Mahavadi et. al., 2019

9. Acknowledgements.....44
10. Declaration.....46

List of Abbreviations

ABCA3	ATP-binding cassette subfamily A member 3
AD	Amiodarone
AECII	Alveolar epithelial cell type II
AP3	Adaptor protein 3
Atg	Autophagy-related genes / gene products
ATP	Adenosine triphosphate
BAG3	Bcl2 athanogene 3
BCL2L13	B-cell lymphoma 2-like protein 13
Bcl-xL	B-cell lymphoma-extra large
BNIP3	BCL2/adenovirus E1B 19 kd-interacting protein-3
CFTR	Cystic fibrosis transmembrane conductance regulator
CHS	Chediak-Higashi syndrome
CLEAR	Coordinated Lysosomal Expression and Regulation
CMA	Chaperone-mediated autophagy
COPD	Chronic obstructive pulmonary disease
CoxIV	Cytochrome c oxidase subunit IV
CTL	Cytotoxic T lymphocytes
DPLD	Diffuse parenchymal lung disease
DPPC	Dipalmitoylphosphatidylcholine
Drp1	Dynamin-related protein 1
E64d	(2S,3S)-trans-Epoxysuccinyl-L-leucylamido-3-methylbutane ethyl ester
EDTA	Ethylenediaminetetraacetic acid
EM	Electron microscopy
ER	Endoplasmic reticulum
GABARAP	Gamma-aminobutyric acid receptor-associated protein
GAPDH	Glyceraldehyde-3-phosphate dehydrogenase
GFP	Green fluorescent protein
HE	Hematoxylin and eosin
HEPES	4-(2-hydroxyethyl)-1-piperazineethanesulfonic acid
HMGB1	High mobility group box 1 protein
HO1	Heme oxygenase 1
HPS	Hermansky-Pudlak syndrome
HPSIP	Hermansky-Pudlak syndrome-associated interstitial pneumonia
HRCT	High resolution computer tomography

IF	Immunofluorescence
IHC	Immunohistochemistry
IIP	Idiopatthic interstitial pneumonia
IPF	Idiopathic pulmonary fibrosis
ITS	Insulin-transferrin-sodium selenite supplement
K	Lysine
kDa	Kilo Daltons
Keap1	Kelch-like ECH-associated protein 1
KO	Knockout
LAMP	Lysosome-associated membrane protein
LB	Lamellar bodies
LC3B	Microtubule-associated protein 1A/1B light chain 3B
(LC-MS/MS)	Liquid chromatography coupled mass spectrometry
LIR	LC3-interacting region
LROs	Lysosome related organelles
LSDs	Lysosomal storage diseases
MLE12	Mouse lung epithelial 12
mTORC1	Mammalian target of rapamycin complex 1
MW	Molecular weight
NBR1	Neighbor of breast cancer 1
NPC	Niemann-Pick C
NK cells	Natural killer cells
Nrf2	Nuclear factor erythroid 2-related factor 2
PAGE	Polyacrylamide gel electrophoresis
PARP	Poly ADP-ribose polymerase
PCLS	Precision cut lung slices
PHB2	Prohibitin2
PI3K	Phosphatidyl-inositol-3-kinase
PINK1	Phosphatase and Tensin homolog-induced kinase 1
Pro-SPC	pro-surfactant protein C
ROS	Reactive oxygen species
SSc.ILD	Systemic sclerosis associated interstitial lung disease
TERT	Telomerase reverse transcriptase
TFEB	Transcription factor EB
TGFβ1	Transforming growth factor β1
Tom20	Translocase of outer mitochondrial membrane 20
UBD	Ubiquitin binding domain

UIP	Usual interstitial pneumonia
ULK1	Unc-51 like autophagy activating kinase 1
UPS	Ubiquitin-Proteasome system
Veh	Vehicle
WB	Western blot
α-SMA	Alpha smooth muscle actin
-/-	Knockout

1. Introduction

1.1 Autophagy

Autophagy is a lysosome dependent quality control mechanism that rejuvenates a cell by degrading long-lived proteins and non-functional organelles to maintain cellular homeostasis (1, 2). The term 'autophagy' literally means self-eating and it has been known for several decades as an adaptation to starvation and as a major pathway responsible for the turnover of long-lived proteins (3-5). Discovery of many autophagy related genes (*ATG)* in the yeast *Sacharomyces cerevesiae*, whose gene products are specifically involved in this catabolic pathway, led to a better understanding of the process (6). The discovery of homologues of these autophagy-related genes in eukaryotic organisms unveiled the relevance of autophagy in many physiological processes (7, 8). It is now known that autophagy plays an effective role in development and differentiation, type II programmed cell death, elimination of protein aggregates and protection against tumors and pathogen invasion (1, 9-12).

In the current literature, autophagy is classified into three types: 1. Microautophagy, 2. Macroautophagy and 3. Chaperone mediated autophagy (Figure 1).

Microautophagy involves pinching of cytoplasmic components for degradation directly by the lysosomal membrane (13). It has been described very well in yeast, but it is yet not well characterized in eukaryotic organisms with the exception of one study which reported that microautophagy may be involved in cellular mechanisms like the biogenesis of multivesicular bodies (14). **Macroautophagy** involves sequestration of cargo into a double membranous structure called autophagosome that ultimately fuses with the lysosome for degradation of its contents. This process is divided into four morphological steps: **1.** induction, when the formation of autophagosome formation is initiated, **2.** formation and completion of the autophagosome, during which the cargo gets enclosed into the vesicle, **3.** docking & fusion, during which the outer membrane of an autophagosome tethers and fuses to a lysosome, and **4.** degradation, involving lysis of the inner vesicle and breakdown of the cargo (15). Of

late, transcription factor EB (TFEB) has been associated to lysosomal biogenesis and was shown to play the role of a 'master chef' of macroautophagy under starvation conditions (16, 17). **Chaperone mediated autophagy** (CMA), unlike micro- and macroautophagy, is a selective form of autophagy and is mainly induced during stress conditions (18, 19). It involves recognition of a pentapeptide motif (KFERQ) on the amino terminus of the substrates by chaperones such as cytosolic and luminal heat shock cognate protein (hsc) 70 and hsc90. In addition, the CMA substrate proteins bind to monomers of the lysosome associated membrane protein (LAMP)-2A splice variant of the LAMP2 gene. This binding drives the LAMP-2A organization into multimeric complexes, which is essential for substrate translocation into lysosomes finally leading to their degradation (19).

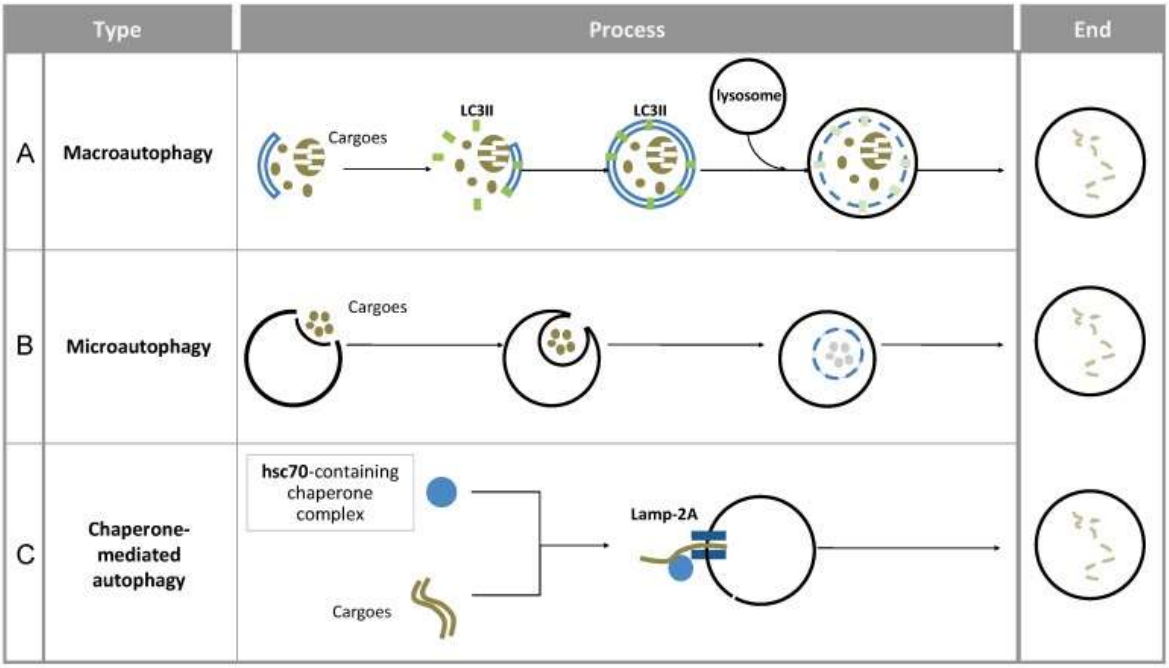

features are presented (1).

Apart from the classification mentioned above, another category of autophagy entitled '**selective autophagy**' has been described, that represents the selective elimination of unwanted components, protein aggregates, damaged/ dysfunctional organelles and invading pathogens (20). The selectivity of this pathway is achieved either via ubiquitin binding proteins or via specific autophagy adaptors/ autophagy receptors. Under certain settings,

when the ubiquitin-proteosomal system (UPS) is overloaded, protein aggregates are targeted to autophagic clearance through K-63 linkages, which are recognized by the ubiquitin binding domains (UBD) of p62 and neighbor of breast cancer 1 (NBR1) forming inclusion bodies. These are then directed to the autophagosome by binding to LC3B through the LC3 interacting region (LIR motif) of p62 and NBR1. Alternatively, K-63 linked protein aggregates are recognized by the UBD domain of HDAC6 (and p62 & NBR1), which form aggresomes that are directed to proteasomal or autophagic degradation. Binding of p62 & NBR1 to LC3B through their LIR motif targets the protein aggregates to autophagosome and subsequent degradation (20, 21).

In mammalian cells, a certain form of autophagy, aiming at selective removal of mitochondria has been identified and termed as 'mitophagy'. Here, the ubiquitin-binding protein p62 accumulates on damaged mitochondria and interacts with LC3B to target the damaged organelles to autophagic degradation (22). But other pathways of mitophagy exist too. The PTEN induced putative kinase 1 / parkinson protein 2, E3 ubiquitin protein ligase (PINK1/ Parkin) pathway of mitophagy has emerged as an important pathway that regulates mitophagy in mammalian cells. PINK1 is imported constitutively into the mitochondrial inner membrane where it is proteolytically cleaved. Upon loss of mitochondrial membrane potential ($\Delta\psi m$), PINK1 is stabilized on the outer mitochondrial membrane, thereby serving as a sensor for mitochondrial damage (23, 24). Parkin is a cytosolic protein under basal conditions. Upon loss of $\Delta\psi m$ and/ or upon accumulation of PINK1 on the mitochondrial membrane, it translocates rapidly to the mitochondrial membrane, where it ubiquitinates several mitochondrial proteins and serves as a signal for mitophagy. Although PINK1 has been shown to promote Parkin mediated mitophagy, some reports reveal that it is not required for the function of Parkin (25), indicating that the relationship between PINK1 and Parkin in mitophagy is still not very clear.

Mitochondrial Nix/BNIP3L and BCL2/adenovirus E1B 19 kd-interacting protein-3 (BNIP3) are autophagy receptors that have been shown to promote mitophagy in mammalian cells by directly binding to the LC3B via their LIR motifs (26). Nix is a Bcl2-related mitochondrial outer

membrane protein, that has been shown to selectively eliminate mitochondria, but not other organelles in reticulocytes (27). Because of its LIR motif, it is speculated to act as a receptor for targeting mitochondria to autophagosomes. Both Nix and BNIP3 have been shown to be involved in hypoxia-induced mitophagy in mammalian fibroblasts via the activation of hypoxia-inducible factor (28). Active mitophagy occurs under steady-state conditions in cells. It is further stimulated on exposure to oxidative stress (and subsequent ROS production) or due to altered mitochondrial dynamics or both. The precise regulation of autophagy and / or mitophagy by ROS is yet unclear. Because of its ability to facilitate the turnover of bulk amount of proteins/ organelles, autophagy is generally accepted to represent a cellular response to oxidative stress, either as a mechanism for sensitization or as a mechanism for resistance to oxidative stress. For example, it has been shown that the autophagy protein Atg4B is subjected to redox regulation (29) and the ubiquitin binding protein p62 is transcriptionally regulated by oxidative stress response proteins (30). In addition, it is reported that increased oxidative stress prevents mitophagy by inactivating Parkin (26).

1.2 Autophagy and the lysosome

Independent of the type, the last leg of autophagy requires the efficient fusion of autophagosomes with lysosomes to enable the degradation of autophagic cargo. Generally, during macroautophagy, autophagosomes fuse with lysosomes by a two-step process. The first step is the migration of autophagsomes towards lysosomes and this is enabled by microtubules. The second step is the fusion event resulting in the formation of autolysosomes that is dependent on SNARE proteins. Proteins of the Rab family which are small GTPases actively participate in these membrane trafficking events. The pH of these acidic compartments may also bear a pivotal role in the fusion event. Both autophagosomal as well as lysosomal pathways have complex functions in classical secretory cells that contain specialized secretory organelles which are either secretory lysosomes or lysosome related organelles (LROs). These organelles share their features with conventional lysosomes as well as secretory granules but use unique components of the secretory

machinery to perform their secretory functions. Classical examples of such organelles include melanosomes of melanocytes, lytic granules of activated cytotoxic T lymphocytes (CTL) and natural killer (NK) cells, azurophil granules of neurophilic leukocytes, *Drosophila* pigment granules, MHC class II compartments, platelet-dense granules of platelets and lamellar bodies of alveolar epithelial cells. Defects in such LROs give rise to a varied number of lysosome storage diseases which are discussed in the upcoming chapters.

1.3 The complex role of autophagy in cell survival and cell death

Basal autophagy is extremely important to breakdown unnecessary cargo and non-functional cellular organelles, thereby generating nutrients for the cell to sustain. This pathway was thus implied in cell survival (3, 31, 32). However, recent discoveries provide evidence that this pathway may also be involved in cell death mechanisms, especially in apoptosis (3, 33, 34). Some studies reveal that several common cellular stressors regulate both autophagy and apoptosis. Reactive oxygen species (ROS) for example trigger both apoptosis and autophagy (35, 36). The autophagy related protein 5 (Atg5), apart from regulating autophagy, has also been shown to regulate apoptosis. Atg5 is cleaved by the calcium-dependent protease calpain upon apoptotic stimulus and the cleavage product translocates onto the mitochondria, triggers cytochrome c release and caspase activation (37, 38). In addition, members of Bcl2-family and Beclin-1 serve as a point of crosstalk between autophagy and apoptosis pathways. It has been demonstrated that under normal conditions, Beclin1 complexes with Bcl2 and Bcl-xL to maintain autophagy at basal levels. Dissociation of Beclin1 from this complex activates the autophagy pathway (35). Proteins like high mobility group box 1 (HMGB1) and BNIP3 compete with Bcl2 and direct Beclin1 towards autophagosome formation and activation of apoptosis (35, 38).

Altered autophagic flux is mainly implicated in cancer, several neurodegenerative diseases and in lysosome related disorders. Many anti-cancer drugs are known to both stimulate and inhibit this pathway. Deregulation of both macroautophagy and chaperone mediated autophagy in the brain of Parkinson's disease patients (39) and insufficient autophagy due to

prolonged unfolded protein response (UPR) in Alzheimer's disease patients have been implicated (40). In addition, mouse models of lysosome storage diseases (LSDs), with severe neurodegenerative outcome like multiple sulfatase deficiency (MSD) and mucopolysaccharidosis type IIIA (MPS-IIIA), were shown to exhibit impaired autophagy (41, 42). A mouse model of Gaucher's disease, another LSD and neurodegenerative disease, displays abnormal autophagosomes and lysosomes implicating impaired autophagy (43). Altered autophagy was also reported in Niemann-Pick C (NPC) -/- mice as well as in fibroblasts from patients with NPC disease, a lipid storage disorder with disruption of cholesterol trafficking (44, 45). Researchers thus speculate on the role of autophagy in the pathogenesis especially of lysosome related disorders. Hence, targeting the autophagic pathway is one of the important issues being currently considered, albeit on a preclinical level. In spite of the wealth of information about autophagy and appreciable studies from many researchers in the field, the precise role of autophagy still remains to be elucidated in many other diseases and tissues of the body.

1.4 Diffuse parenchymal lung diseases (DPLDs)

DPLDs or interstitial lung diseases (ILDs) are a group of more than 300 heterogenous lung disorders that mainly affect the pulmonary interstitium, the alveolar epithelium and the capillary endothelium. Impaired gas exchange, reduced lung compliance and increase in the connective tissue are key characteristic features of DPLDs (46). The etiology of some DPLDs may be associated with a well-defined cause for example, silicosis, or drug-induced forms like amiodarone or bleomycin. Some DPLDs lack an obvious origin, for example, idiopathic interstitial pneumonia (IIP). IIPs are majorly grouped into chronic fibrosing and non-fibrosing interstitial pneumonia. Idiopathic pulmonary fibrosis (IPF) falls under the chronic fibrosing IIPs (Figure 2).

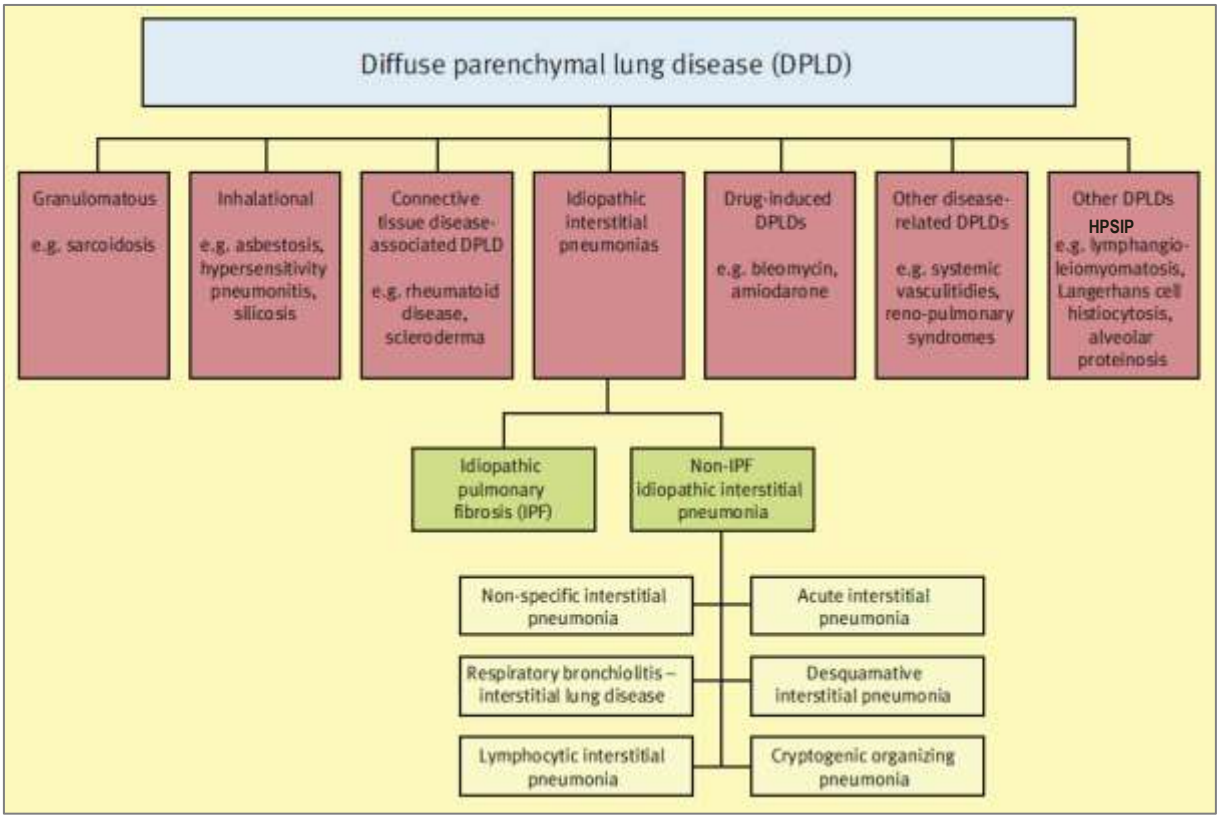

Figure 2. Schematic diagram showing a general classification for diffuse parenchymal lung diseases. Hermansky-Pudlak syndrome associated interstitial pneumonia (HPSIP) is now included for a better understading. Adapted from Maher et al., 2012.

1.5 Idiopathic Pulmonary Fibrosis (IPF) and animal models of lung fibrosis

IPF, as the name suggests, has an unknown etiology and is the most important form of idiopathic interstitial pneumonias (IIPs). It represents one of the most aggressive forms of organ fibrosis, killing patients within few years of diagnosis (47). IPF is characterized by a progressive decline in lung function and is associated with the histological appearance of usual interstitial pneumonia (UIP). The pathogenesis of IPF still remains to be fully elucidated, but may be based on chronic epithelial injury, disturbed epithelial-mesenchymal cross-talk, activation of fibroblasts, excessive collagen deposition and disruption of the delicate alveolar architecture, altogether resulting in progressive dyspnea, decline of lung function and, ultimately, death (48, 49). Several papers published in the past underscore the importance of the alveolar epithelium in the evolution of IPF. The very first report by Myers & Katzenstein on IPF disclosed the observation of extensive alveolar epithelial cell death and

suggested a pathomechanistic role for the epithelium (50). This concept has been further supported by appealing observations like severe and pro-apoptotic endoplasmic reticulum (ER) stress signaling in alveolar epithelial cells type II (AECII) from usual interstitial pneumonia (UIP) lungs due to familial and sporadic IPF (51, 52) and shortened telomere length in sporadic IPF epithelium (53). AECII are classical secretory cells of the alveolus that secrete the surface tension reducing lung surfactant. Lamellar bodies of the AECII are lysosome related organelles that store and secrete surfactant proteins and phospholipids (54). As an attempt to define the pathogenesis of lung fibrosis and to identify therapeutic options, several mouse models of lung fibrosis have been developed. Bleomycin is the most frequently used agent to drive lung fibrosis through intratracheal administration in mice (55). The concept of AECII injury as a triggering factor in lung fibrosis (56, 57) was supported by experimental data from some of these animal models, for example, prevention of bleomycin-induced lung fibrosis by use of anti-apoptotic agents (58), and the induction of lung fibrosis by initiation of AECII cell death via AECII specific diphtheria toxin receptor expression (59).

Hermansky-Pudlak syndrome (HPS) is an autosomal recessive disorder, and mutations in HPS genes are known to effect lysosome related organelles including lamellar bodies of the lungs in mice and men (60). Patients with mutations in some HPS genes (HPS1, HPS2 and HPS4) are reported to develop lung fibrosis (61-63), the clinical course and the histological presentation (UIP pattern) of which shows great similarities with IPF (64). Single HPS mutant mice (HPS1, HPS2) display alveolar macrophage activation (65) and increased susceptibility to bleomycin challenge (66).

Amiodarone (AD) is a highly efficient antiarrhythmic drug with potentially serious side effects. Severe pulmonary toxicity is reported in patients receiving AD even at low doses, and may cause interstitial pneumonia as well as lung fibrosis and can also result in an IPF-like disease (67-69). Again, apoptosis of AECII has been suggested to play an important role in this disease (70). Although molecular events underlying AD induced pulmonary toxicity are not clearly settled, certain mechanisms like cytotoxicity (71), intracellular phospholipidosis (72), alterations in the angiotensin signaling pathway (73), generation of oxidants (74) and

inflammatory reactions (75) have been indicated to be pivotal events. Taken together, severe injury to the AECII resulting in apoptosis is a common feature in IPF lungs and several animal models of lung fibrosis.

1.6 Role of lysosomal stress and autophagy in lung fibrosis

The regulation of autophagy in lung diseases represents a growing field of research. So far, increased autophagy resulting in apoptotic cell death has been shown under conditions of chronic obstructive pulmonary disease (COPD) (76). In cystic fibrosis, defective autophagy seems to occur and rescuing the autophagy pathway improved the trafficking of the cystic fibrosis transmembrane conductance regulator (CFTR) (77). More recent studies on the regulation of autophagy in lung fibrosis report that autophagy is either not activated or is insufficient in patients with idiopathic pulmonary fibrosis (IPF) and that TGFβ-1 inhibits autophagy in lung fibroblasts *in vitro* (78, 79). Another study revealed an alteration in the Bcl-2-binding protein Beclin1 (80), providing a hint towards a dysfunction in the autophagy/apoptosis system in IPF fibroblasts. In addition, defective PINK1 dependent autophagy was indicated in IPF AECII (81). Nevertheless, the precise role of autophagy within the alveolar epithelial cells largely remains unexplored in IPF as well as in other forms of DPLDs.

2. Aims and objectives of this study

In view of the studies so far, it is clear that lung fibrosis may result following several insults to the alveolar epithelial cells type II (AECII). AECII contain a great percentage of lysosome related organelles, the so called lamellar bodies. We hence hypothesized that injury to the lysosomal compartment may contribute to progressive AECII apoptosis and consecutive lung fibrosis. Hence, the overarching aim of this study was to understand if and how lysosome related alterations in the lysosomal compartment contribute to cellular stress in and apoptosis of AECII under conditions of lung fibrosis. In order to achieve this broad objective, we identified the following aims:

1. Establish new animal models of lung fibrosis that may enrich the portfolio of animal models and may be exploited in subsequent studies
2. Identify the contribution of lysosome related stress events, including the autophagy pathway towards AECII apoptosis in established animal models as well as in clinical samples of IPF and HPSIP patient lungs
3. Understanding the pathomechanistic significance of autophagy and autophagy related proteins in lung fibrosis

3. Results and publications

3.1 Animal models of lung fibrosis

We first established two mouse models of lung fibrosis, the HPSIP [Mahavadi et al., 2010; (82)] and the amiodarone (AD) induced lung fibrosis model [Mahavadi et al., 2014; (83)]. HPS is a rare autosomal recessive disorder and several HPS genes are identified in both human and mice. HPS genes encode protein complexes that affect the synthesis of various lysosome related organelles (LROs) including lamellar bodies of the lungs. The function of these protein complexes is not fully known. The radiologic appearance and the histopathology (UIP) of HPSIP is comparable to that of IPF and the clinical course is similar to IPF. Pulmonary fibrosis is the major complication and cause of mortality in patients with some forms of HPS (HPS1, HPS2 and HPS4). One unique feature of HPSIP is the development of foamy AECII with increased lamellar body size and number termed as "giant lamellar body degeneration". The mono mutant mouse models, HPS1 and HPS2, unlike HPS patients do not develop lung fibrosis (82). We then analyzed the lungs of HPS1/2 double mutant mice. Firstly, HPS1/2 mice at 3 months start to develop patchy and sub-pleural lung fibrosis that progresses as they reach 9 months age. HPS1/2 mice as well as lung samples from HPSIP patients display apoptosis of AECII via caspase 3 activation. HPS1/2 mice also display severe accumulation of surfactant lipids as well as surfactant proteins within the lung tissue and the mature / functional surfactant is either not detected or is greatly reduced in the broncho alveolar lavage fluids (BALF), indicating impaired surfactant secretion by AECII. These observations are also associated with enhanced and early lysosomal stress and late endoplasmic reticulum (ER) stress in the AECII. We also identified that cathepsin D, a lysosomal stress marker, is increased in the AECII of HPS1/2 mice as well as in HPSIP patients. *In vitro*, overexpression of cathepsin D in mouse lung epithelial (MLE12) cells led to activation of caspase 3 and proliferation of lung fibroblasts.

We next attempted to establish another murine model of lung fibrosis that is induced by amiodarone (AD) (83). We treated C57BL/6 mice every fifth day intratracheally with 0.8 mg/

kg body weight AD. Significant septal thickening, patchy interstitial lung fibrosis, extracellular matrix deposition, increased collagen fibrils, areas of dense fibrosis and areas with roughly preserved lung structure with increased AECII size was observed at day 7 after AD treatment. In addition, a significant increase in hydroxyproline levels was observed. AD treated mice also displayed altered surfactant homeostasis and apoptosis of AECII. Of interest and similar to HPS1/2 mice, AD treated mouse lungs also displayed increased levels of the lysosomal stress marker cathepsin D and an increase in ER stress markers. However, knockdown of cathepsin D *in vitro* did not decrease AD induced caspase 3 activation thus indicating that other alternate pathways might contribute towards the AECII apoptosis in AD model of lung fibrosis.

Such observations in the AD model were paralleled by readouts of design-based stereology approach [Birkelbach,…, Mahavadi*, Knudsen*, 2015; (84)] where progressive AECII hypertrophy and a high correlation between AECII related ultrastructural changes and collagen fibril deposition through septal walls was established. In the lungs of IPF patients, we reported similar qualitative alterations within the AECII, indicating that the observed ultrastructural alterations are tightly correlated with the progression of fibrotic remodeling.

3.2 Dysregulated autophagy in lung fibrosis

In an attempt to analyze alternate lysosomal pathways that may drive AECII apoptosis, we sought to study the autophagy pathway in AD and in HPS models of lung fibrosis. In the amiodarone model [Mahavadi et al., 2015; (85)], analysis of autophagy parameters revealed that both the autophagy marker protein LC3B and substrate protein p62 were increased. According to the guidelines for monitoring autophagy, an increase in LC3B protein with a concomitant increase in p62 may indicate defective autophagy. However, we observed an up-regulation of p62 transcript which might have compensated for its protein level. Analysis of autophagic flux using autophagy inhibitors chloroquine and a combination of pepstatin and E64D revealed that AD in fact increases autophagy flux. MLE12 cells knocked down for

LC3B showed decreased caspase 3 activation and SP-C accumulation indicating that AD induced autophagy is at least in part mediated via the autophagy marker protein, LC3B.

Next, in HPSIP patients and in the HPS model, autophagy marker proteins, LC3B and the standard autophagy substrate protein p62 were analyzed. In patients with HPSIP, we observed that the levels of p62 protein increased in AECII. Similar observations were made in HPS1/2 mouse model. The levels of p62 inversely correlated with the autophagic activity. The increase in p62 protein in HPS associated lung fibrosis revealed a decreased clearance of this protein, indicating defective autophagy. *In vitro*, knockdown of HPS1 drove A549 cells to apoptosis but when such cells were overexpressed with GFP-LC3B the activation of cleaved caspase was decreased. Altogether, our analysis indicated that loss of HPS1 results in impaired autophagy that is restored by overexpression of LC3B and that defective autophagy may play a vital role in AECII apoptosis and thereby in the development and progression of lung fibrosis in HPSIP [Ahuja,…, Guenther*, Mahavadi*, 2016; (86)].

One interesting and novel observation from our studies was revealed is that, immunogold labelling for LC3B with subsequent electron microscopic analysis revealed a preferential staining for LC3B in lamellar bodies of AECII in HPS model, AD model as well as in control mice (85). In HPS1/2 mice, LC3B was localized to the lumen of the lamellar bodies, in AD and in healthy control mice, LC3B-bound gold particles were identified in close proximity to the limiting membrane of lamellar bodies (86). More so, in AD treated mice, membrane sharing between autophagosomes and lamellar bodies was observed. Observations from these studies clearly indicate that autophagy markers in general and LC3B in particular may be involved in lamellar body functions and hence, surfactant homeostasis.

3.3 Role of LC3B in the development of lung fibrosis

In view of our observations so far, we further sought to particularly understand the role of LC3B in the development of lung fibrosis. We first investigated the lung structure of LC3B-/- mice. At 3 months of age, the LC3B-/- mice showed regular lung architecture with no signs of lung abnormalities. However, upon aging until 9 months, LC3B-/- mice developed thickened

septae, smaller lamellar body profiles, altered surfactant homeostasis, severe lysosomal and ER stress as well as AECII apoptosis [Kesireddy,…, Mahavadi, 2019; (87)]. We identified that autophagosomal soluble N-ethylmaleimide–sensitive factor attachment protein receptor, syntaxin 17, is increased in the AECII of the aged LC3B-/- mice, but not in the younger mice and speculated that syntaxin 17 might have compensated for the LC3B function in the younger LC3B-/- mice. Such increase in syntaxin 17 was also observed in the AECII of IPF patient lungs as compared to the AECII of donor lungs. *In vitro,* knockdown of LC3B in MLE12 cells sensitized them to bleomycin induced apoptosis, while overexpression of LC3B rendered protection. Supporting these *in vitro* observations, upon low doses of bleomycin treatment for 7 days, LC3B-/- mice developed extensive fibrosis when compared to control mice treated with the same dose of bleomycin. In order to further gain an insight into the mechanisms underlying LC3B mediated autophagy and apoptosis, we performed immunoprecipitation of LC3B in MLE 12 cells followed by liquid chromatography coupled mass spectrometry (LC-MS/MS) and identified novel interacting partners. Of particular interest, we identified the lysosomal protective protein, Cathepsin A as a novel interacting protein of LC3B. This LC3B-cathepsin A interaction was confirmed by co-immunoprecipitation analysis as well as reverse immunoprecipitation. We then analyzed cathepsin A in the AECII of LC3B-/- as well as in IPF patients. Interestingly, we could show Cathepsin A is increased in the AECII of both aged LC3B-/- mice and IPF patients. Analysis of cathepsin A protein sequence revealed 5 putative LC3B-interacting regions (LIRs). Our data so far suggest that LC3B mediated autophagy protects AECII from apoptosis and subsequent lung injury and fibrosis by modulating the functions of pivotal lysosomal proteins like Cathepsin A (87).

3.4 Expanding the current understanding on the role of autophagy in lung fibrosis

In IPF lungs, the highly proliferative and apoptosis-resistant behaviour of IPF fibroblasts contributes to excessive extracellular matrix deposition, matrix stiffening and perpetuation of

the fibrotic response via biochemical stress. It is hence imperative to identify precise molecular mechanisms and subsequent targets not only in the alveolar epithelium but also in the interstitial fibroblasts of IPF lungs. In addition, the autophagy-lysosomal system has been reported to be deregulated in fibroblasts (79) alongside with the AECII in IPF lungs (81). In this context, we identified that Bcl2 athanogene 3 (BAG3), a co-chaperone that regulates selective autophagy, is significantly increased in interstitial fibroblasts of IPF patients as compared to those of healthy donor lungs (Figure 3A, 3C, unpublished). BAG3 belongs to the BAG family of proteins which regulates protein folding and activity by interacting with heat shock protein 70 (Hsp70) (88, 89). BAG3, in particular, is known to control protein degradation in a highly specific manner via autophagy (90, 91). Its interaction with the two molecular chaperones, HSP70 and HSPB8 results in the formation of the multi-chaperone complex BAG3-HSPB8-HSP70. Formation of this complex together with HSP70-interacting ubiquitin ligase CHIP facilitates ubiquitination of substrate proteins (92). This enables BAG3 to recruit HSP70 substrates to the autophagy adaptor protein SQSTM1/ p62. Since p62 can simultaneously bind to ubiquitinated clients and the autophagy marker protein, LC3B (93), the substrates are degraded by autophagy in the lysosome. Along with an increase in BAG3, we also observed an increase in its substrate protein filamin C, confirming a dysregulation of BAG3 mediated autophagy in IPF fibroblasts (Figure 3D, 3E, unpublished), further hinting towards the involvement of the BAG3-HSPB8-HSP70 mutichaperone complex in defective autophagy as observed in IPF fibroblasts.

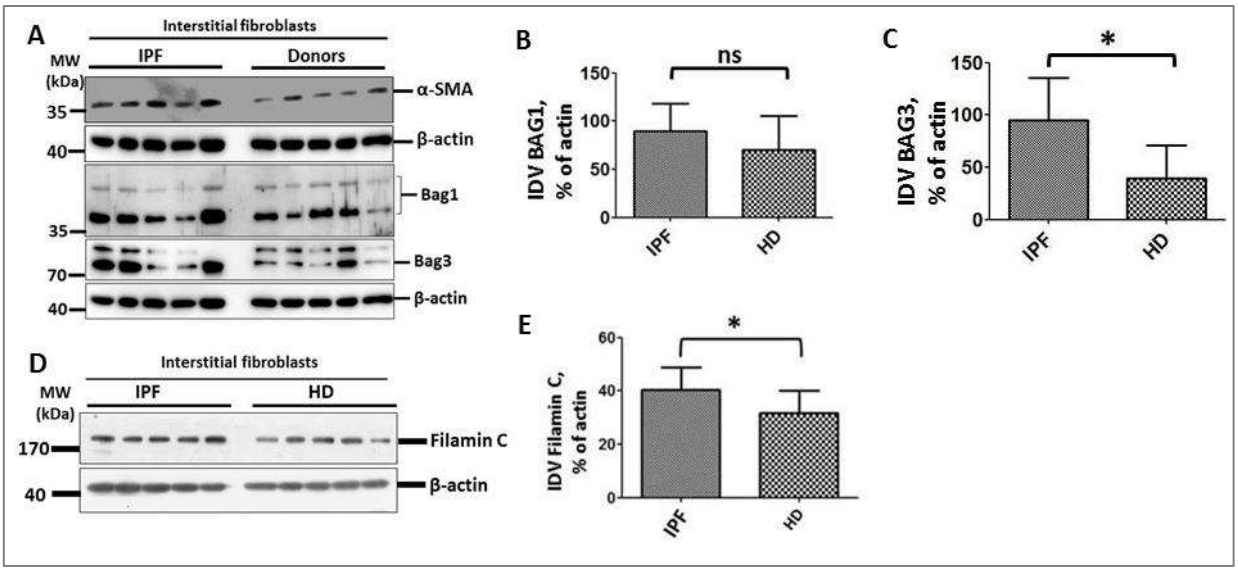

Figure 3. A glimpse of preliminary data, procured from experiments performed in primary interstitial fibroblasts of IPF and donor lungs. **A.** Representative western blot images for the indicated proteins followed by **B & C.** respective densitometric quantifications showing an increase in BAG3 in IPF fibroblasts as compared to donors. **D.** western blots for filamin C and **E.** its quantification showing its significant increase in IPF fibroblasts as compared to donor fibroblasts. Representative bots from 5 patient fibroblasts are shown here and analysis was performed from 8-10 IPF and donor lung fibroblasts. Significance: *P<0.05. (Manuscript under review).

4. Discussion

Important advances in the past decade increased our understanding of DPLDs and enabled development of effective drugs for these diseases. Pirfenidone and nintedanib are such drugs that have been reported to show a reduction in the decline in lung capacity and improved survival in IPF patients (94, 95). More recently, nintedanib has also been shown to reduce the rate of lung function decline also in patients with systemic sclerosis associated interstitial lung disease (SSc.ILD) (96). Combination treatment with both pirfenidone and nintedanib also showed encouraging results in IPF patients, but also an increased frequency of side effects (97). However, these drugs at best slow progression of the disease but cannot reverse fibrosis or improve breathlessness. Therefore, prognosis of IPF patients still remains poor and warrants a continuous search not only for drugs that target the progression of lung fibrosis, but which target trigger mechanisms of pathomechanistic significance. In this regard, both basic research and preclinical studies on model systems play important roles in identifying novel molecular mechanisms of the disease process.

4.1 HPS1/2 & amiodarone treated mice as animal models of lung fibrosis

So far, several animal models that mimic the development of lung fibrosis have been developed. Amongst them are the models based on bleomycin with single and repetitive dosing, asbestosis, radiation, silica, fluorescein isothiocyanate, ageing, diphtheria toxin and models based on overexpression of pro fibrotic factors like TGF-α & TGF-β and mutations in TERT, SFTPC or SFTPA2 genes. While these animal models provided us with invaluable insights into the pathogenesis of lung fibrosis, several limitations exist (98, 99), making not all of them suitable to fully represent the human disease. Bleomycin induced lung fibrosis is the most frequently used mouse model for lung fibrosis. Mice instilled with bleomycin intratracheally develop fibrosis in about 2-4 weeks, which is a relatively short period of time. This model has been constantly criticized due to several reasons: 1. Inflammation based model with extensive inflammation being observed in the first week, prior to the development of fibrosis; 2. The histopathological alterations in these mice do not fully represent the

characteristic UIP pattern that is observed in IPF patients; 3. Mice treated with single-dose of bleomycin resolve over time; 4. Mice respond to bleomycin in a strain dependent manner, with C57Bl/6 demonstrating the highest susceptibility; 5. Not a truly alveolar epithelial cell injury driven model rather many other cell types are involved, for example, endothelial cells, fibroblasts/ myofibroblasts, fibrocytes, several inflammatory cells, pericytes, airway epithelial cells and stem/ progenitor cells. 6. Broad range of its dosing regimen and high mortality rates add to the other drawbacks of this model (98). Recent studies following a repetitive application resulted in septal thickening and enlarged alveoli, develop hyperplastic club cells and infiltration of perialveolar ducts by inflammatory cells, again not fully representing the human situation (99, 100). In this regard, the here in reported HPS model developing on the basis of natural mutations in both HPS1 (pale ear) and HPS2 (pearl) genes is characterized by spontaneous lung fibrosis with limited inflammation, AECII hyperplasia, giant lamellar bodies, early AECII injury and apoptosis and age-related onset of the disease. These HPS1/2 mice therefore offer as a better model for IPF/ UIP (64, 82). This is also supported by the fact that clinical course of HPSIP largely coincides with that of the IPF patients and that the histopathological and radiopathologic pattern is that of UIP. One major limitation of the HPS1/2 mouse model however is their poor breeding capacity, resulting in limited numbers of littermates. In order to overcome this, our current strategy focusses on generating AECII targeted conditional knockout of HPS1 and HPS2.

Next, we reported that intratracheal administration of AD in mice leads to sub-pleural fibrosis with limited inflammation and massive AECII apoptosis. Ultrastructural analysis of AD treated mice lungs showed interstitial remodeling with considerable increase in collagen fibrils, septal wall thickness, injury to the blood-gas barrier, denuded basement membrane and larger lamellar body profiles in the AECII. Such alterations in different ultrastructural components with denudation of basal lamina and increased AECII profiles were also observed in IPF lungs, strengthening the concept that extent and significance of alveolar epithelial injury in AD model is similar to that in IPF patients (83, 84). In view of the ultrastructural alterations of the lungs along with AECII apoptosis, we believe that the HPS1/2 and AD models offer a lot

of similarities to the ultrastructural alterations and epithelial pro-apoptotic signaling in IPF and other DPLDs and may be exploited to study novel pathomechanistic mechanisms of lung fibrosis.

4.2 Altered surfactant homeostasis is a common feature of DPLDs

Having in mind the extensive alterations in the lamellar bodies in our models, it is imperative that pulmonary surfactant is altered under conditions of IPF, HPS1/2 or in AD induced lung fibrosis. In fact, impaired surface activity due to pronounced disturbances in biochemical and physical properties of surfactant had been reported in patients with interstitial lung diseases including IPF already two decades ago (101). In addition, it is well documented that mutations in the SFTPC gene, showing barely detectable active SP-C but high amounts of misfolded protein, are the reason for some familial forms of interstitial lung diseases (102-104) . Dense fibrosis with distorted AECII due to aberrant subcellular localization of the misfolded protein is a prominent observation in such patients (105). In the same line, *in vitro* studies showed that mutations in both the BRICHOS and the non-BRICHOS domains of SP-C lead to defects in cellular quality control mechanisms (106, 107). The lungs of induced mutant SP-C (SftpcC121G) mice developed spontaneous pulmonary fibrosis and restrictive lung impairment (108). Next, pediatric patients with mutations in the ATP binding cassette subfamily A/3 (ABCA3) gene display severe surfactant deficiency and interstitial lung disease (109, 110). ABCA3 plays a major role in the exocytosis of surfactant lipids. Abnormally small lamellar bodies within the AECII accompanied by pulmonary fibrosis have also been reported in adolescent patients with ABCA3 mutations (111). Similarly, surfactant alterations appear to be responsible for the observed phenotypes in several animal models of lungs fibrosis as well as lysosome storage diseases (LSDs). Such LSDs include Chediak-Higashi syndrome (CHS) (beige mouse as murine counterpart) showing accumulation of lamellar body lipids (112, 113), chocolate mice with mutations in Rab38 gene a small GTPase that participates in regulating vesicular trafficking (114) and Niemann-Pick type C2 (NPC2) which is caused by acid sphingomyelinase deficiency (115, 116). We observed significant alterations of

surfactant homeostasis in HPS1/2 as well as in AD treated mice. Severe accumulation of mature surfactant proteins and pro SP-C as well as altered surfactant phospholipid content and profile within the lungs was a persistent observation in both models. Lipidomic profiling of lung tissues revealed an increased percentage of phosphatidylcholine (PC) in HPS1/2 and AD treated mice (82, 83). More so, in HPS1/6 and in HPS1/2 mice lung homogenates, a significant increase in saturated PC was observed, which could be ascribed to the marked accumulation of the surface tension reducing dipalmitoylphosphatidylcholine (DPPC, PC-32:0). Supporting this, defects in pulmonary surfactant secretion in HPS1/2 mice were reported by us (82) and others (117), an observation not made in the AD mouse model. Since surfactant storage, processing and secretion in AECII occurs in the lysosomal compartment, altered intracellular surfactant homeostasis in both HPS1/2 as well as AD mouse models indicates altered lysosomal homeostasis. In this regard, we observed that the lysosomal aspartyl protease, cathepsin D, is increased in the lungs of both HPS1/2 as well as in the AD model. Cathepsin D activates both intrinsic and extrinsic apoptotic signaling cascades (118). In the HPS1/2 model, we observed that AECII apoptosis is mediated by cathepsin D. In the AD model, however, although an increase in cathepsin D was observed in the lungs, our *in vitro* observations revealed that the increase in cathepsin D upon AD treatment alone is not sufficient to trigger apoptosis. This prompted us to identify other lysosome related events driving AECII apoptosis under conditions of AD treatment. Taken together, disturbed surfactant trafficking in the AECII seems to provoke chronic injury of AECII and elicits cellular stress mechanisms.

4.3 Deregulation of autophagy taking the center stage in lung fibrosis

Autophagy-lysosomal pathway and the ubiquitin-proteasomal pathway are the two protein quality control mechanisms of a cell. They govern the turnover of all intra and many extracellular proteins and organelles at broadly differing rates, from minutes to days to months. While the autophagy-lysosomal system governs the turnover of long-lived proteins and unwanted organelles, the ubiquitin-proteasomal system is mostly responsible for the

rapid degradation of substrates (119, 120). The ubiquitin-proteasomal pathway has not been studied so far in the alveolar epithelium under conditions of lung fibrosis, but has been suggested to be activated in the mesenchymal compartment of IPF subjects and in the bleomycin model of lung fibrosis (121, 122). On the contrary, the autophagy pathway has been shown to be defective in the IPF fibroblasts. It has been reported that the autophagy pathway is either not activated or is insufficient in the fibroblasts of IPF lungs and has been suggested to play a role in their proliferation (78, 79).

4.3.1 Lung fibrosis from the perspective of autophagy proteins

In our studies, dysregulation of autophagy was observed in the alveolar epithelium in both HPS associated lung fibrosis as well as in AD model of lung fibrosis which emphasize the pivotal roles of autophagy proteins in several key functions of the AECII. In our attempts to add a fresh perspective to our understanding about the critical roles of autophagy proteins in AECII, we sought to study lung fibrosis from the perspective of autophagy proteins. In this regard, we identified that LC3B mediated autophagy plays protective role in the development of lung fibrosis as LC3B-/- mice upon aging develop septal thickening, AECII injury and apoptosis and are prone to secondary hits like bleomycin (87). Our study complements a previous study where mice deficient in ATG4B, a cysteine protease that cleaves the C—terminal of LC3B resulted in increased sensitivity to bleomycin induced lung injury and fibrosis (123). Protective roles of LC3B under several settings have been reported previously (124, 125), but our study showed that loss of LC3B can result in overt lung injury. This concept is supported by previous studies which show that loss of the most proximal protein of the autophagy cascade, autophagy activating kinase ULK1/2 (yeast Atg1 homolog), (126, 127), or loss of Atg5 display lung defects at a very early age (128). Loss of ULK1/2 or ATG5 results in a cumulative loss of function of all downstream autophagy proteins that may result in early lung phenotypes in such mice. LC3B on the other hand, is the most distal protein in the autophagy cascade and most likely the reason for the delayed appearance of the phenotype in LC3B-/- mice. Our study also identified Cathepsin A as a novel interacting protein of LC3B that is increased in the AECII of IPF patients as well. Cathepsin A has been

reported to modulate chaperone induced autophagy (CMA) and it remains to be studied how LC3B-cathepsin A interaction could influence the CMA pathway in healthy as well as under fibrotic conditions.

4.4 Contribution of HPS gene products to defective autophagy

Defective autophagy, resulting in impaired clearance of toxic proteins in several tissues of the body, is well established in several LSDs (129). Likewise, in HPS1/2 mice as well as in HPSIP patients, we reported that autophagy is defective within the AECII. *In vitro*, overexpression of LC3B rescued *HPS1* knockdown-mediated defective autophagy. HPS1 and HPS4 proteins are subunits of a large protein complex, the biogenesis of lysosome related organelle complex-3 (BLOC3), the precise function of which remains obscure (130, 131). The complex was however speculated to regulate the movement and distribution of lysosome related organelles (131). One straight forward explanation could be that one or more subunits of this complex directly interacts with motility factors in the cytoskeleton and absence of HPS1 or HPS4 might result in mistargeting the motility factor thereby leading to impaired movement of lamellar bodies to move towards plasma membrane to secrete surfactant or towards lysosome to degrade the accumulated proteins. It may also be speculated that, since the autophagy marker protein LC3B is an inherent microtubule associated protein, HPS1 or HPS4 might interact with LC3B and facilitate autophagy-lysosome mediated degradation of autophagic cargo. In our studies, we also reported that LC3B is localized in lamellar bodies in both HPS1/2 mice and wild type mice. Immunogold labeling for LC3B was found to be pronounced in the lamellar body lumen of HPS mice, while, in wild type mice, gold particles for LC3B were localized to the limiting membrane of lamellar bodies. Although not shown in our studies, this observation points out a putative role of LC3B in particular and autophagy in general in regulating lamellar bodies, and hence, surfactant secretion. However, LC3B-/- mice do not show any lung abnormalities at birth or reveal abnormal surfactant secretion. One explanation for this observation is that Gamma-aminobutyric acid receptor-associated proteins (GABARAPs) which are also LC3B family of

proteins may compensate for the loss of LC3B at earlier ages (132, 133). Studies in the past showed that autophagy plays a regulatory role in phospholipid and cholesterol-rich multi vesicular body / multi lamellar body formation and in lamellae formation in secondary lysosomes (134, 135). In addition, autophagic delivery of phospholipids from the Golgi apparatus to late lysosomal organelles has been shown to promote multi lamellar body expression in mink lung type II alveolar epithelial cell line (135). Another observation in support of this concept comes from studies in Pompe disease, a lysosomal glycogen storage disease, in which a pivotal role of autophagy in cellular clearance and exocytosis of lysosomal glycogen was observed in muscle cells (136). This wealth of literature and our findings revealing LC3B localization to the lamellar bodies and autophagic rescue upon LC3B overexpression in *HPS1* knockdown-induced defective autophagic cells argue that lamellar bodies are autolysosomes. However, experimental evidence for lytic and surfactant secretory functions of these organelles is lacking and is currently underway. In addition, our *in silico* analysis revealed three putative LC3B interacting regions (LIRs) in the human HPS1 protein sequence (unpublished), which again strengthens our hypothesis that HPS1 interacts with LC3B and this interaction may be important to stimulate surfactant secretion and/ or cargo degradation via the autophagy pathway in the lung AECII.

We also reported defective autophagy in the AECII of patients with HPS2 mutations and associated pulmonary fibrosis (137). HPS2 gene product is adaptor protein 3 (AP-3) which is known to bind to tyrosine sorting signals and for efficient delivery of tyrosinase to the melanosomes (138). More than one AP-3 dependent lysosome related pathways exist. For example, AP-3 delivers endolyn, a lysosomal mucosialin from trans-golgi network to lysosomes through an intracellular route bypassing early endosomes or it recruits LAMP3/CD63 directly to the lysosomes via early and late endosomes (139, 140). Additionally, AP-3 null cells were shown to mistarget both LAMP1 and LAMP2 proteins (141). LAMP2 represents the receptor for autophagosome-lysosome fusion, its mistargeting in the absence of AP-3 indicates defective autophagy. Further, lung lamellar bodies are in fact LAMP3 positive organelles (134) and it is currently under investigation if autophagy proteins

like LC3B may directly bind to AP-3 to facilitate the recruitment of LAMP3 to lamellar bodies or lysosomes in the AECII.

4.5 A closer look into amiodarone induced excessive autophagy

AD is an extremely effective anti-arrhythmic drug but exerts severe side effects particularly pulmonary toxicity with confluent lung fibrosis that remains as the main cause of mortality in patients receiving AD even at low doses. Foamy macrophages, characteristic AECII hyperplasia and apoptosis are typical features of AD induced lung fibrosis (142-144). Due to its unusually long half-life, AD gets enriched in lysosomes and results in lamellar body accumulation in several cell types. We and others reported induction of autophagy upon AD or its derivative dronedarone treatment in several tissues including the lungs (85, 145, 146). In fact, we reported that AD treatment increases autophagy flux and induces the fusion of phagophores (early autophagosomal structures) with lamellar bodies in the AECII. By use of electron microscopic tomography analysis, we showed a fusion and membrane sharing between these organelles. This interesting finding again supports the role of autophagy in lamellar body biogenesis and emphasizes the inevitable role of autophagy in degrading lamellar body contents and/ or in surfactant secretion.

Our *in vitro* studies showed that inhibiting the terminal autophagy pathway by knocking down *LC3B* transiently reduced AD induced apoptosis of MLE12 cells. This is in full support of a previous study showing that blockade of angiotensin formation *via* angiotensin converting enzyme captopril or angiotensin 1 receptor antagonist losartan inhibited AECII apoptosis and lung fibrosis in a rat model of AD induced lung fibrosis (147). It may be intriguing to note that both captopril and losartan are in fact autophagy inhibitors (148, 149) and might have exerted their protective effects by inhibiting the autophagy pathway as well.

Of note, AD is a cationic amphiphilic drug (CAD) and CADs are known to exert their first impact on lysosomes and induce phospholipidosis in several cell types (150). We also observed AD induced phospholipidosis in both lung tissue and BAL fluid. It has been suggested that phospholipidosis may be a defense mechanism of a cell in response to CAD

treatment, as lamellar bodies with increased phospholipids undergo exocytosis immediately in order to get rid of the intracellular build-up of toxins (150). This may be the reason behind increased surfactant phospholipid concentration in AD treated mice BAL fluids. However, once saturation levels are reached, lysosomal leaking is a possible event and elicits other events like mitochondrial dysfunction (150). Supporting this view, it has been shown that AD is metabolized via the P450 enzyme system and AD and its chief metabolite desethylamiodarone lead to the disruption of mitochondrial function, reactive oxygen species (ROS) production, decrease in mitochondrial membrane potential and cytochrome-c release. Our unpublished studies reveal that AD actually induces mitochondrial autophagy (mitophagy) in AECII. We also identified that mitophagy is elicited not only via autophagy receptor protein p62, but also via novel mitophagy protein, Bcl2L13. Our data show that mitochondrial integrity in the AECII is lost upon AD treatment and such disintegrated mitochondria are targeted to the autophagy-lysosomal system for degradation by aberrantly activated mitophagy receptors like p62 and Bcl2L13. It is being investigated if healthy mitochondria are also prone to autophagic degradation due to excessive autophagic turnover upon AD treatment and if rescuing such aberrant mitochondrial autophagy may prove beneficial for cells and mice treated with AD.

4.6 Defective autophagy in IPF

Inability of aging cells to maintain a highly efficient protein quality control is well established and IPF, being a remarkably aging associated disease, represents no exception from this rule. Insufficient autophagy has been reported in both the mesenchymal as well as the alveolar compartment of IPF patient lungs. Defective mitophagy within the AECII of IPF patients was specifically identified by Bueno and colleagues. Unpublished data from our group also show similar results in addition to the aberrantly increased mitophagy marker, namely Bcl2L13, within the IPF AECII. In addition, we also identified that autophagy related chaperones and co-chaperones, namely Hsp70 & BAG3 play significant roles in the fibroblasts of IPF patients (unpublished) where defective autophagy is a key player as well

(78, 79). Studies revealing the role of autophagy in AECII apoptosis and fibrosis are scarce. But it may be speculated that like in our animal models of lung fibrosis, defective autophagy in IPF AECII may contribute towards AECII apoptosis, increased profiles of lamellar bodies, altered surfactant protein processing or impaired activity of lung surfactant. Since both AECII and fibroblasts are reported to exhibit defective autophagy in IPF, it may be reasonable to consider pharmacological 'fine-tuning' of these cells which on the one hand would rescue AECII from apoptosis and on the other hand inhibit fibroblast proliferation.

4.8 Concomitant cellular stress pathways in IPF and other DPLDs

An accepted pathological concept of IPF is that repetitive AECII injury including genetic or aging related risk factors trigger impaired wound healing response and subsequent fibroblast activation and development of scar tissue. But what precisely leads to AECII death is a matter of extensive investigation. Studies from our group and by others underscored the importance of 'maladaptive' pro-apoptotic ER stress in the AECII of sporadic and familial IPF patients (51, 52, 151, 152). We were also able to show that provoking ER stress by CHOP alone in AECII is sufficient to trigger AECII apoptosis and a pro-fibrotic environment *in vitro* (153) and *in vivo* (unpublished). However, such *Chop* transgenic mice did not develop full-blown fibrosis, indicating that further pro-fibrotic cellular stress pathways or a second-hit that activates such pathways is required to push the lung to develop the disease. It is noteworthy that two antagonistic functions for CHOP have been suggested: it regulates the transcription of several autophagy genes and of apoptotic proteins to facilitate pro-survival autophagy or cell death, respectively. However, it is not yet studied if the prolonged induction of autophagy genes that is triggered by CHOP is also involved in apoptosis. In this regard, we observed in our *in vitro* model of *Chop* overexpression, an altered autophagy flux (unpublished) as well as increased apoptosis, warranting further studies on the regulatory role of CHOP in autophagy and apoptosis.

A prominent role for such ER stress was also established in asbestos-induced AECII apoptosis and lung fibrosis (154). Further, in HPSIP, in AD induced lung fibrosis, as well as

in aged LC3B-/- mice, we observed an increase in ER stress markers. It is intriguing to note that in HPSIP and in LC3B-/- mice, early lysosomal and late ER stress is a prominent finding. Although this was not clearly observed in the AD model, our *in vitro* observations from MLE 12 cells revealed a similar phenomenon after treating MLE12 cells with AD for short time periods (30 minutes – 4 hrs; unpublished). Taken together, our studies hint towards retrograde activation of ER stress by early lysosomal stress events under conditions of lung fibrosis. Whether this holds true for AECII of IPF patients as well remains a matter of future investigations.

Additionally, in the alveolar epithelium, an imbalance in the oxidative-antioxidative response leading to mitochondrial dysfunction was reported (155). It has been suggested that environmental factors may induce ROS generation via induction of ER stress, thereby promoting AECII apoptosis with subsequent secretion of pro-fibrotic cytokines and growth factors that activate fibroblasts. Depletion of antioxidant mechanisms in the IPF AECII may also render these cells sensitive to several kinds of insults and trigger pro-fibrotic environment. Mitochondrial dysfunction was one of the first reported observations in AD treated rat livers (156, 157) . AD has been reported to inhibit –oxidation of fatty acids, disable complex I and complex II of the respiratory chain and to decrease ATP formation resulting in enhanced ROS production and lipid peroxidation (157, 158). In the same line, we also observed an increased ROS production and altered mitochondrial dynamics in AD model of lung fibrosis.

About 8-15% of familial IPF and about 11% of sporadic IPF patients in a lung transplant cohort were identified to carry mutations in genes related to telomerase elongating enzyme, telomerase reverse transcriptase regulator of telomere elongation helicase 1 or poly(A)-specific ribonuclease (159, 160). In addition, IPF subjects with no known mutations in telomerase related genes are reported to display shortened telomere length as compared to their healthy counterparts in peripheral blood as well as in AECII (53, 161-163). This indicates destabilized chromosomes and increased percentage of DNA strand breaks. Such

DNA damage stress was also reported in some mouse models of lung fibrosis, namely the bleomycin and silica inhalation model (164, 165).

In conclusion, deregulated autophagy and subsequent lysosomal stress are important pathological events in lung fibrosis. This, in addition to dysfunctional mitochondria, severe ER stress and other accompanying stress factors like DNA damage may result in a fully deregulated organelle crosstalk, thereby leading to a defective protein and organelle quality control and, ultimately, AECII death and fibrosis (Figure 4). It appears extremely complex to therapeutically target all these pathways in a fibrotic lung, especially as the hierarchy of these cellular surveillance systems is currently unknown. However, pharmacological intervention on the level of some of these key pathways may prove beneficial in fibrotic lung diseases based on chronic AECII injury.

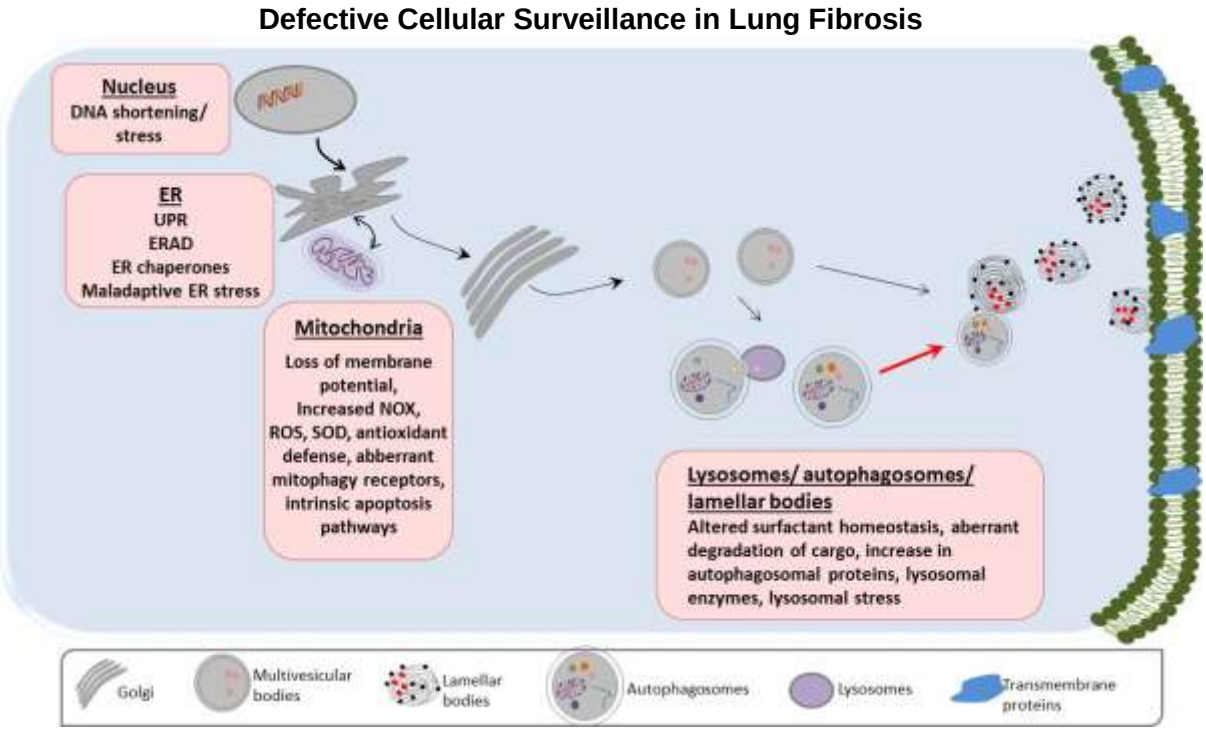

Figure 4. Defective cellular surveillance in alveolar epithelial cells in lung fibrosis. Illustration of the general protein transport path through different organelles in eukaryotic cells. Depicted here is a simplified version of organelle stress observed in the AECII of different forms of lung fibrosis. DNA damage, ER stress, mitochondrial dysfunction and lysosomal stress are common parameters that are observed in lung fibrosis which lead to deregulated organelle crosstalk resulting in defective protein and organelle quality control. These events trigger AECII apoptosis and ultimately, lung fibrosis. Red arrow indicates still unknown molecular mechanisms behind fusion of autophagosomes and lamellar bodies in some forms of lung fibrosis.

5. Summary and outlook

In summary, the data provided in this work strongly support the concept that alterations in the autophagy-lysosomal system contribute to alveolar epithelial cell injury and apoptosis, representing a key trigger in the development of lung fibrosis. Altered surfactant homeostasis in HPSIP and AD induced lung fibrosis, in addition to the previous reports in IPF lungs, were first indicators of an effect on the lysosomal compartment of AECII. Further evidence for lysosomal stress stems from the observation of increased markers of autophagy in IPF patient lungs and HPSIP as well as in the AD models of lung fibrosis. One discrepancy that we reported is, however, that autophagic activity is increased under conditions of amiodarone treatment, while it is impaired in HPS associated lung fibrosis. Such defective autophagy has also been reported in AECII of IPF patient lungs. This indicates that, depending on the type, level and mode of insult, autophagy is differentially regulated in different models of lung fibrosis. The same holds true for the unfolded protein response: both, too little and too intensive (pro-apoptotic) ER stress might be detrimental for the cell. In addition, enhanced ER stress signatures as well as oxidative stress, indicative of mitochondrial dysfunction add another level of complexity to our understanding of the epithelial injury in the evolution of fibrotic diseases. It is known that, despite being discrete signalling components, these cellular organelles play a concerted role to maintain cellular homeostasis in response to any insult. In aging lungs like IPF, or in lungs with a genetic predisposition like HPSIP or in lungs affected by drugs like AD, such organelle crosstalk is disrupted creating an imbalance, which might fuel common cell death mechanisms. The immediate next steps will be aimed at understanding if pharmacological correction of autophagy-lysosomal system, eg., by autophagy inducing drugs, would be beneficial in rescuing the fibrotic AECII from toxic proteins and to re-direct them to pro-survival programs. That said, the indubitable role of other cellular compartments like the ER or mitochondria in the process of epithelial injury and lung fibrosis underscores the need for further research,

aiming to identify molecular machineries coordinating organelle crosstalk in injured AECII and to develop novel molecular switches affecting all of these surveillance programs.

6. Zusammenfassung

Zusammenfassend lässt sich sagen, dass die Ergebnisse, die in dieser Arbeit präsentiert werden zeigen, dass Veränderungen im autophagie-lysosomalen System zu alveolar-epithelialen Zellschädigungen und Apoptose beitragen, welche einen zentralen Auslöser bei der Entstehung der Lungenfibrose darstellen. Eine veränderte Surfactant Homöostase beim HPSIP und bei AD induzierter Lungenfibrose, wie sie bereits in IPF Lungen gezeigt wurde, waren die ersten Hinweise, die einen Einfluss auf das lysosomale Kompartiment von AECII vermuten ließen. Weitere Anzeichen für lysosomalen Stress lieferte die Beobachtung erhöhter Autophagiemarker-Level in Lungen von IPF Patienten und bei HPSIP, ebenso wie bei AD Modellen der Lungenfibrose. Wir haben jedoch auch eine Abweichende Beobachtung gemacht und in unserer Publikation gezeigt, dass die Autophagie-Aktivität unter Aminodarone erhöht ist, jedoch während sie in HPS assoziierter Lungenfibrose reduziert ist. Eine derart gestörte Autophagie wurde zudem bereits bei AECII in Lungen von IPF Patienten gezeigt. Diese Beobachtung deutet darauf hin, dass die Autophagie in Abhängigkeit von Typ, Grad und Art der Schädigung in den unterschiedlichen Modellen der Lungenfibrose differentiell reguliert ist, ähnlich wie bei der Unfolded Protein Response, ist zu geringer ER Stress ebenso schädlich für die Zelle, wie zu intensiver (pro-apoptotischer) ER Stress. Erhöhte ER Stress Marker und oxidativer Stress, bezeichnend für mitochondriale Dysfunktion, fügen eine weitere Ebene der Komplexität zu unserem Verständnis der epithelialen Verletzung bei der Entstehung von fibrosierenden Erkrankungen hinzu. Es ist bekannt, dass diese zellulären Organellen zusätzlich zu ihrer Aufgabe als eigenständige Signalkomponenten eine fein aufeinander abgestimmte Rolle spielen, bei der Aufrechterhaltung der zellulären Homöostase nach jeglicher Schädigung. Bei alternden Lungen, wie bei der IPF, in Lungen mit einer genetischen Prädisposition wie beim HPSIP oder bei Lungen, die durch Medikamente wie AD beeinträchtigt sind, ist dieser Cross-Talk der Organellen beeinträchtigt, wodurch ein Ungleichgewicht entsteht, welches möglicherweise die für den Zelltod verantwortlichen Mechanismen ankurbelt. In den unmittelbar nächsten Schritten wird es darum gehen zu verstehen, ob pharmakologische

Korrekturen des autophagy-lysosomalen Systems, beispielsweise mittels Autophagie-induzierender Medikamente, dabei behilflich sein können, die fibrotischen AECII vor toxischen Proteinen zu schützen und sie hin zu einem pro-survival Programm umzulenken. Die zentrale Rolle, die andere Zellkompartimente wie das ER oder die Mitochondrien beim Prozess der epithelialen Verletzung und der Lungenfibrose spielen, unterstreicht den Bedarf an weiterer Forschung, durch welche weitere zelluläre Maschinerien identifiziert werden können, die den Cross-Talk der Organellen in verletzten AECII koordinieren und neuartige molekulare Schalter gefunden werden können, die alle diese Surveillance Programme beeinflussen können.

7. References

1. Yang, J., Carra, S., Zhu, W. G., and Kampinga, H. H. (2013) The regulation of the autophagic network and its implications for human disease. *International journal of biological sciences* 9, 1121-1133
2. Maiuri, M. C., and Kroemer, G. (2019) Therapeutic modulation of autophagy: which disease comes first? *Cell death and differentiation* 26, 680-689
3. Codogno, P., and Meijer, A. J. (2005) Autophagy and signaling: their role in cell survival and cell death. *Cell death and differentiation* 12 Suppl 2, 1509-1518
4. Mizushima, N., and Klionsky, D. J. (2007) Protein turnover via autophagy: implications for metabolism. *Annual review of nutrition* 27, 19-40
5. Wirawan, E., Vanden Berghe, T., Lippens, S., Agostinis, P., and Vandenabeele, P. (2012) Autophagy: for better or for worse. *Cell research* 22, 43-61
6. Klionsky, D. J., Cregg, J. M., Dunn, W. A., Jr., Emr, S. D., Sakai, Y., Sandoval, I. V., Sibirny, A., Subramani, S., Thumm, M., Veenhuis, M., and Ohsumi, Y. (2003) A unified nomenclature for yeast autophagy-related genes. *Developmental cell* 5, 539-545
7. Levine, B., and Klionsky, D. J. (2004) Development by self-digestion: molecular mechanisms and biological functions of autophagy. *Developmental cell* 6, 463-477
8. Reggiori, F., and Klionsky, D. J. (2002) Autophagy in the eukaryotic cell. *Eukaryotic cell* 1, 11-21
9. Mehrpour, M., Esclatine, A., Beau, I., and Codogno, P. (2010) Autophagy in health and disease. 1. Regulation and significance of autophagy: an overview. *American journal of physiology. Cell physiology* 298, C776-785
10. Czaja, M. J. (2010) Autophagy in health and disease. 2. Regulation of lipid metabolism and storage by autophagy: pathophysiological implications. *American journal of physiology. Cell physiology* 298, C973-978
11. Sandri, M. (2010) Autophagy in health and disease. 3. Involvement of autophagy in muscle atrophy. *American journal of physiology. Cell physiology* 298, C1291-1297
12. Reggiori, F., and Klionsky, D. J. (2005) Autophagosomes: biogenesis from scratch? *Current opinion in cell biology* 17, 415-422
13. Mijaljica, D., Prescott, M., and Devenish, R. J. (2011) Microautophagy in mammalian cells: revisiting a 40-year-old conundrum. *Autophagy* 7, 673-682
14. Sahu, R., Kaushik, S., Clement, C. C., Cannizzo, E. S., Scharf, B., Follenzi, A., Potolicchio, I., Nieves, E., Cuervo, A. M., and Santambrogio, L. (2011) Microautophagy of cytosolic proteins by late endosomes. *Developmental cell* 20, 131-139
15. Yang, Z., and Klionsky, D. J. (2010) Mammalian autophagy: core molecular machinery and signaling regulation. *Current opinion in cell biology* 22, 124-131
16. Cuervo, A. M. (2011) Cell biology. Autophagy's top chef. *Science* 332, 1392-1393
17. Settembre, C., Di Malta, C., Polito, V. A., Garcia Arencibia, M., Vetrini, F., Erdin, S., Erdin, S. U., Huynh, T., Medina, D., Colella, P., Sardiello, M., Rubinsztein, D. C., and Ballabio, A. (2011) TFEB links autophagy to lysosomal biogenesis. *Science* 332, 1429-1433
18. Kaushik, S., Bandyopadhyay, U., Sridhar, S., Kiffin, R., Martinez-Vicente, M., Kon, M., Orenstein, S. J., Wong, E., and Cuervo, A. M. (2011) Chaperone-mediated autophagy at a glance. *Journal of cell science* 124, 495-499
19. Orenstein, S. J., and Cuervo, A. M. (2010) Chaperone-mediated autophagy: molecular mechanisms and physiological relevance. *Seminars in cell & developmental biology* 21, 719-726
20. Johansen, T., and Lamark, T. (2011) Selective autophagy mediated by autophagic adapter proteins. *Autophagy* 7, 279-296
21. Shaid, S., Brandts, C. H., Serve, H., and Dikic, I. (2013) Ubiquitination and selective autophagy. *Cell death and differentiation* 20, 21-30

22. **Ashrafi, G., and Schwarz, T. L. (2013) The pathways of mitophagy for quality control and clearance of mitochondria.** ***Cell death and differentiation*** **20, 31-42**
23. **Matsuda, S., Kitagishi, Y., and Kobayashi, M. (2013) Function and characteristics of PINK1 in mitochondria.** ***Oxidative medicine and cellular longevity*** **2013, 601587**
24. **Ding, W. X., and Yin, X. M. (2012) Mitophagy: mechanisms, pathophysiological roles, and analysis.** ***Biological chemistry*** **393, 547-564**
25. **Park, J., Lee, S. B., Lee, S., Kim, Y., Song, S., Kim, S., Bae, E., Kim, J., Shong, M., Kim, J. M., and Chung, J. (2006) Mitochondrial dysfunction in Drosophila PINK1 mutants is complemented by parkin.** ***Nature*** **441, 1157-1161**
26. **Kubli, D. A., and Gustafsson, A. B. (2012) Mitochondria and mitophagy: the yin and yang of cell death control.** ***Circulation research*** **111, 1208-1221**
27. **Zhang, J., and Ney, P. A. (2008) NIX induces mitochondrial autophagy in reticulocytes.** ***Autophagy*** **4, 354-356**
28. **Zhang, J., and Ney, P. A. (2009) Role of BNIP3 and NIX in cell death, autophagy, and mitophagy.** ***Cell death and differentiation*** **16, 939-946**
29. **Scherz-Shouval, R., Shvets, E., Fass, E., Shorer, H., Gil, L., and Elazar, Z. (2007) Reactive oxygen species are essential for autophagy and specifically regulate the activity of Atg4.** ***The EMBO journal*** **26, 1749-1760**
30. **Jain, A., Lamark, T., Sjottem, E., Larsen, K. B., Awuh, J. A., Overvatn, A., McMahon, M., Hayes, J. D., and Johansen, T. (2010) p62/SQSTM1 is a target gene for transcription factor NRF2 and creates a positive feedback loop by inducing antioxidant response element-driven gene transcription.** ***The Journal of biological chemistry*** **285, 22576-22591**
31. **Klionsky, D. J. (2004) Cell biology: regulated self-cannibalism.** ***Nature*** **431, 31-32**
32. **Cuervo, A. M. (2010) Chaperone-mediated autophagy: selectivity pays off.** ***Trends in endocrinology and metabolism: TEM*** **21, 142-150**
33. **Wirawan, E., Vande Walle, L., Kersse, K., Cornelis, S., Claerhout, S., Vanoverberghe, I., Roelandt, R., De Rycke, R., Verspurten, J., Declercq, W., Agostinis, P., Vanden Berghe, T., Lippens, S., and Vandenabeele, P. (2010) Caspase-mediated cleavage of Beclin-1 inactivates Beclin-1-induced autophagy and enhances apoptosis by promoting the release of proapoptotic factors from mitochondria.** ***Cell death & disease*** **1, e18**
34. **Corcelle, E. A., Puustinen, P., and Jaattela, M. (2009) Apoptosis and autophagy: Targeting autophagy signalling in cancer cells -'trick or treats'?** ***The FEBS journal*** **276, 6084-6096**
35. **Nishida, K., Yamaguchi, O., and Otsu, K. (2008) Crosstalk between autophagy and apoptosis in heart disease.** ***Circulation research*** **103, 343-351**
36. **Chen, Y., and Gibson, S. B. (2008) Is mitochondrial generation of reactive oxygen species a trigger for autophagy?** ***Autophagy*** **4, 246-248**
37. **Yousefi, S., Perozzo, R., Schmid, I., Ziemiecki, A., Schaffner, T., Scapozza, L., Brunner, T., and Simon, H. U. (2006) Calpain-mediated cleavage of Atg5 switches autophagy to apoptosis.** ***Nature cell biology*** **8, 1124-1132**
38. **Marquez, R. T., and Xu, L. (2012) Bcl-2:Beclin 1 complex: multiple, mechanisms regulating autophagy/apoptosis toggle switch.** ***American journal of cancer research*** **2, 214-221**
39. **Levy, O. A., Malagelada, C., and Greene, L. A. (2009) Cell death pathways in Parkinson's disease: proximal triggers, distal effectors, and final steps.** ***Apoptosis : an international journal on programmed cell death*** **14, 478-500**
40. **Scheper, W., Nijholt, D. A., and Hoozemans, J. J. (2011) The unfolded protein response and proteostasis in Alzheimer disease: preferential activation of autophagy by endoplasmic reticulum stress.** ***Autophagy*** **7, 910-911**
41. **Ballabio, A. (2009) Disease pathogenesis explained by basic science: lysosomal storage diseases as autophagocytic disorders.** ***International journal of clinical pharmacology and therapeutics*** **47 Suppl 1, S34-38**

42. **Settembre, C., Fraldi, A., Jahreiss, L., Spampanato, C., Venturi, C., Medina, D., de Pablo, R., Tacchetti, C., Rubinsztein, D. C., and Ballabio, A. (2008) A block of autophagy in lysosomal storage disorders. *Human molecular genetics* 17, 119-129**

43. **Sun, Y., and Grabowski, G. A. (2010) Impaired autophagosomes and lysosomes in neuronopathic Gaucher disease. *Autophagy* 6, 648-649**

44. **Pacheco, C. D., and Lieberman, A. P. (2008) The pathogenesis of Niemann-Pick type C disease: a role for autophagy? *Expert reviews in molecular medicine* 10, e26**

45. **Pacheco, C. D., and Lieberman, A. P. (2007) Lipid trafficking defects increase Beclin-1 and activate autophagy in Niemann-Pick type C disease. *Autophagy* 3, 487-489**

46. **Maher, T. M. (2012) Diffuse parenchymal lung disease. *Medicine* 40, 314-321**

47. **King, T. E., Jr., Pardo, A., and Selman, M. (2011) Idiopathic pulmonary fibrosis. *Lancet* 378, 1949-1961**

48. **Selman, M., and Pardo, A. (2006) Role of epithelial cells in idiopathic pulmonary fibrosis: from innocent targets to serial killers. *Proceedings of the American Thoracic Society* 3, 364-372**

49. **(2002) American Thoracic Society/European Respiratory Society International Multidisciplinary Consensus Classification of the Idiopathic Interstitial Pneumonias. This joint statement of the American Thoracic Society (ATS), and the European Respiratory Society (ERS) was adopted by the ATS board of directors, June 2001 and by the ERS Executive Committee, June 2001. *American journal of respiratory and critical care medicine* 165, 277-304**

50. **Myers, J. L., and Katzenstein, A. L. (1988) Epithelial necrosis and alveolar collapse in the pathogenesis of usual interstitial pneumonia. *Chest* 94, 1309-1311**

51. **Lawson, W. E., Crossno, P. F., Polosukhin, V. V., Roldan, J., Cheng, D. S., Lane, K. B., Blackwell, T. R., Xu, C., Markin, C., Ware, L. B., Miller, G. G., Loyd, J. E., and Blackwell, T. S. (2008) Endoplasmic reticulum stress in alveolar epithelial cells is prominent in IPF: association with altered surfactant protein processing and herpesvirus infection. *American journal of physiology. Lung cellular and molecular physiology* 294, L1119-1126**

52. **Korfei, M., Ruppert, C., Mahavadi, P., Henneke, I., Markart, P., Koch, M., Lang, G., Fink, L., Bohle, R. M., Seeger, W., Weaver, T. E., and Guenther, A. (2008) Epithelial endoplasmic reticulum stress and apoptosis in sporadic idiopathic pulmonary fibrosis. *American journal of respiratory and critical care medicine* 178, 838-846**

53. **Alder, J. K., Chen, J. J., Lancaster, L., Danoff, S., Su, S. C., Cogan, J. D., Vulto, I., Xie, M., Qi, X., Tuder, R. M., Phillips, J. A., 3rd, Lansdorp, P. M., Loyd, J. E., and Armanios, M. Y. (2008) Short telomeres are a risk factor for idiopathic pulmonary fibrosis. *Proceedings of the National Academy of Sciences of the United States of America* 105, 13051-13056**

54. **Gunther, A., Korfei, M., Mahavadi, P., von der Beck, D., Ruppert, C., and Markart, P. (2012) Unravelling the progressive pathophysiology of idiopathic pulmonary fibrosis. *European respiratory review : an official journal of the European Respiratory Society* 21, 152-160**

55. **Moeller, A., Ask, K., Warburton, D., Gauldie, J., and Kolb, M. (2008) The bleomycin animal model: a useful tool to investigate treatment options for idiopathic pulmonary fibrosis? *The international journal of biochemistry & cell biology* 40, 362-382**

56. **Noble, P. W., and Homer, R. J. (2005) Back to the future: historical perspective on the pathogenesis of idiopathic pulmonary fibrosis. *American journal of respiratory cell and molecular biology* 33, 113-120**

57. **Selman, M., and Pardo, A. (2002) Idiopathic pulmonary fibrosis: an epithelial/fibroblastic cross-talk disorder. *Respiratory research* 3, 3**

58. **Wang, R., Ibarra-Sunga, O., Verlinski, L., Pick, R., and Uhal, B. D. (2000) Abrogation of bleomycin-induced epithelial apoptosis and lung fibrosis by captopril or by a caspase inhibitor. *American journal of physiology. Lung cellular and molecular physiology* 279, L143-151**

59. **Sisson, T. H., Mendez, M., Choi, K., Subbotina, N., Courey, A., Cunningham, A., Dave, A., Engelhardt, J. F., Liu, X., White, E. S., Thannickal, V. J., Moore, B. B., Christensen, P. J., and Simon, R. H. (2010) Targeted injury of type II alveolar epithelial cells induces pulmonary fibrosis.** ***American journal of respiratory and critical care medicine*** **181, 254-263**
60. **Nakatani, Y., Nakamura, N., Sano, J., Inayama, Y., Kawano, N., Yamanaka, S., Miyagi, Y., Nagashima, Y., Ohbayashi, C., Mizushima, M., Manabe, T., Kuroda, M., Yokoi, T., and Matsubara, O. (2000) Interstitial pneumonia in Hermansky-Pudlak syndrome: significance of florid foamy swelling/degeneration (giant lamellar body degeneration) of type-2 pneumocytes.** ***Virchows Archiv : an international journal of pathology*** **437, 304-313**
61. **Gahl, W. A., Brantly, M., Troendle, J., Avila, N. A., Padua, A., Montalvo, C., Cardona, H., Calis, K. A., and Gochuico, B. (2002) Effect of pirfenidone on the pulmonary fibrosis of Hermansky-Pudlak syndrome.** ***Molecular genetics and metabolism*** **76, 234-242**
62. **Anderson, P. D., Huizing, M., Claassen, D. A., White, J., and Gahl, W. A. (2003) Hermansky-Pudlak syndrome type 4 (HPS-4): clinical and molecular characteristics.** ***Human genetics*** **113, 10-17**
63. **Gochuico, B. R., Huizing, M., Golas, G. A., Scher, C. D., Tsokos, M., Denver, S. D., Frei-Jones, M. J., and Gahl, W. A. (2012) Interstitial lung disease and pulmonary fibrosis in Hermansky-Pudlak syndrome type 2, an adaptor protein-3 complex disease.** ***Mol Med*** **18, 56-64**
64. **Mahavadi, P., Guenther, A., and Gochuico, B. R. (2012) Hermansky-Pudlak syndrome interstitial pneumonia: it's the epithelium, stupid!** ***American journal of respiratory and critical care medicine*** **186, 939-940**
65. **Young, L. R., Borchers, M. T., Allen, H. L., Gibbons, R. S., and McCormack, F. X. (2006) Lung-restricted macrophage activation in the pearl mouse model of Hermansky-Pudlak syndrome.** ***J Immunol*** **176, 4361-4368**
66. **Young, L. R., Pasula, R., Gulleman, P. M., Deutsch, G. H., and McCormack, F. X. (2007) Susceptibility of Hermansky-Pudlak mice to bleomycin-induced type II cell apoptosis and fibrosis.** ***American journal of respiratory cell and molecular biology*** **37, 67-74**
67. **Chang, S. N., Hwang, J. J., Hsu, K. L., Tsai, C. T., Lai, L. P., Lin, J. L., Tseng, C. D., and Chiang, F. T. (2007) Amiodarone-related pneumonitis.** ***Journal of the Formosan Medical Association = Taiwan yi zhi*** **106, 411-417**
68. **Charles, P. E., Doise, J. M., Quenot, J. P., Muller, G., Aube, H., Baudouin, N., Piard, F., Besancenot, J. F., and Blettery, B. (2006) Amiodarone-related acute respiratory distress syndrome following sudden withdrawal of steroids.** ***Respiration; international review of thoracic diseases*** **73, 248-249**
69. **Ott, M. C., Khoor, A., Leventhal, J. P., Paterick, T. E., and Burger, C. D. (2003) Pulmonary toxicity in patients receiving low-dose amiodarone.** ***Chest*** **123, 646-651**
70. **Bargout, R., Jankov, A., Dincer, E., Wang, R., Komodromos, T., Ibarra-Sunga, O., Filippatos, G., and Uhal, B. D. (2000) Amiodarone induces apoptosis of human and rat alveolar epithelial cells in vitro.** ***American journal of physiology. Lung cellular and molecular physiology*** **278, L1039-1044**
71. **Ashrafian, H., and Davey, P. (2001) Is amiodarone an underrecognized cause of acute respiratory failure in the ICU?** ***Chest*** **120, 275-282**
72. **Martin, W. J., 2nd, Kachel, D. L., Vilen, T., and Natarajan, V. (1989) Mechanism of phospholipidosis in amiodarone pulmonary toxicity.** ***The Journal of pharmacology and experimental therapeutics*** **251, 272-278**
73. **Uhal, B. D., Zhang, H., Abdul-Hafez, A., Shu, R., and Li, X. (2007) Amiodarone induces angiotensinogen gene expression in lung alveolar epithelial cells through activation protein-1.** ***Basic & clinical pharmacology & toxicology*** **100, 59-66**
74. **Sarma, J. S., Pei, H., and Venkataraman, K. (1997) Role of Oxidative Stress in Amiodarone-induced Toxicity.** ***Journal of cardiovascular pharmacology and therapeutics*** **2, 53-60**

75. **Wilson, B. D., Clarkson, C. E., and Lippmann, M. L. (1991) Amiodarone-induced pulmonary inflammation. Correlation with drug dose and lung levels of drug, metabolite, and phospholipid.** ***The American review of respiratory disease*** **143, 1110-1114**

76. **Chen, Z. H., Kim, H. P., Sciurba, F. C., Lee, S. J., Feghali-Bostwick, C., Stolz, D. B., Dhir, R., Landreneau, R. J., Schuchert, M. J., Yousem, S. A., Nakahira, K., Pilewski, J. M., Lee, J. S., Zhang, Y., Ryter, S. W., and Choi, A. M. (2008) Egr-1 regulates autophagy in cigarette smoke-induced chronic obstructive pulmonary disease.** ***PloS one*** **3, e3316**

77. **Luciani, A., Villella, V. R., Esposito, S., Brunetti-Pierri, N., Medina, D., Settembre, C., Gavina, M., Pulze, L., Giardino, I., Pettoello-Mantovani, M., D'Apolito, M., Guido, S., Masliah, E., Spencer, B., Quaratino, S., Raia, V., Ballabio, A., and Maiuri, L. (2010) Defective CFTR induces aggresome formation and lung inflammation in cystic fibrosis through ROS-mediated autophagy inhibition.** ***Nature cell biology*** **12, 863-875**

78. **Patel, A. S., Lin, L., Geyer, A., Haspel, J. A., An, C. H., Cao, J., Rosas, I. O., and Morse, D. (2012) Autophagy in idiopathic pulmonary fibrosis.** ***PloS one*** **7, e41394**

79. **Araya, J., Kojima, J., Takasaka, N., Ito, S., Fujii, S., Hara, H., Yanagisawa, H., Kobayashi, K., Tsurushige, C., Kawaishi, M., Kamiya, N., Hirano, J., Odaka, M., Morikawa, T., Nishimura, S. L., Kawabata, Y., Hano, H., Nakayama, K., and Kuwano, K. (2013) Insufficient autophagy in idiopathic pulmonary fibrosis.** ***American journal of physiology. Lung cellular and molecular physiology*** **304, L56-69**

80. **Ricci, A., Cherubini, E., Scozzi, D., Pietrangeli, V., Tabbi, L., Raffa, S., Leone, L., Visco, V., Torrisi, M. R., Bruno, P., Mancini, R., Ciliberto, G., Terzano, C., and Mariotta, S. (2013) Decreased expression of autophagic Beclin 1 protein in idiopathic pulmonary fibrosis fibroblasts.** ***Journal of cellular physiology*** **228, 1516-1524**

81. **Bueno, M., Lai, Y. C., Romero, Y., Brands, J., St Croix, C. M., Kamga, C., Corey, C., Herazo-Maya, J. D., Sembrat, J., Lee, J. S., Duncan, S. R., Rojas, M., Shiva, S., Chu, C. T., and Mora, A. L. (2015) PINK1 deficiency impairs mitochondrial homeostasis and promotes lung fibrosis.** ***The Journal of clinical investigation*** **125, 521-538**

82. **Mahavadi, P., Korfei, M., Henneke, I., Liebisch, G., Schmitz, G., Gochuico, B. R., Markart, P., Bellusci, S., Seeger, W., Ruppert, C., and Guenther, A. (2010) Epithelial stress and apoptosis underlie Hermansky-Pudlak syndrome-associated interstitial pneumonia.** ***American journal of respiratory and critical care medicine*** **182, 207-219**

83. **Mahavadi, P., Henneke, I., Ruppert, C., Knudsen, L., Venkatesan, S., Liebisch, G., Chambers, R. C., Ochs, M., Schmitz, G., Vancheri, C., Seeger, W., Korfei, M., and Guenther, A. (2014) Altered surfactant homeostasis and alveolar epithelial cell stress in amiodarone-induced lung fibrosis.** ***Toxicological sciences : an official journal of the Society of Toxicology*** **142, 285-297**

84. **Birkelbach, B., Lutz, D., Ruppert, C., Henneke, I., Lopez-Rodriguez, E., Gunther, A., Ochs, M., Mahavadi, P., and Knudsen, L. (2015) Linking progression of fibrotic lung remodeling and ultrastructural alterations of alveolar epithelial type II cells in the amiodarone mouse model.** ***American journal of physiology. Lung cellular and molecular physiology*** **309, L63-75**

85. **Mahavadi, P., Knudsen, L., Venkatesan, S., Henneke, I., Hegermann, J., Wrede, C., Ochs, M., Ahuja, S., Chillappagari, S., Ruppert, C., Seeger, W., Korfei, M., and Guenther, A. (2015) Regulation of macroautophagy in amiodarone-induced pulmonary fibrosis.** ***The journal of pathology. Clinical research*** **1, 252-263**

86. **Ahuja, S., Knudsen, L., Chillappagari, S., Henneke, I., Ruppert, C., Korfei, M., Gochuico, B. R., Bellusci, S., Seeger, W., Ochs, M., Guenther, A., and Mahavadi, P. (2016) MAP1LC3B overexpression protects against Hermansky-Pudlak syndrome type-1-induced defective autophagy in vitro.** ***American journal of physiology. Lung cellular and molecular physiology*** **310, L519-531**

87. **Kesireddy, V. S., Chillappagari, S., Ahuja, S., Knudsen, L., Henneke, I., Graumann, J., Meiners, S., Ochs, M., Ruppert, C., Korfei, M., Seeger, W., and Mahavadi, P. (2019) Susceptibility of microtubule-associated protein 1 light chain 3beta (MAP1LC3B/LC3B)**

knockout mice to lung injury and fibrosis. *FASEB journal : official publication of the Federation of American Societies for Experimental Biology* 33, 12392-12408

88. Gamerdinger, M., Carra, S., and Behl, C. (2011) Emerging roles of molecular chaperones and co-chaperones in selective autophagy: focus on BAG proteins. *J Mol Med (Berl)* 89, 1175-1182

89. Takayama, S., and Reed, J. C. (2001) Molecular chaperone targeting and regulation by BAG family proteins. *Nature cell biology* 3, E237-241

90. Arndt, V., Dick, N., Tawo, R., Dreiseidler, M., Wenzel, D., Hesse, M., Furst, D. O., Saftig, P., Saint, R., Fleischmann, B. K., Hoch, M., and Hohfeld, J. (2010) Chaperone-assisted selective autophagy is essential for muscle maintenance. *Current biology : CB* 20, 143-148

91. Ulbricht, A., Gehlert, S., Leciejewski, B., Schiffer, T., Bloch, W., and Hohfeld, J. (2015) Induction and adaptation of chaperone-assisted selective autophagy CASA in response to resistance exercise in human skeletal muscle. *Autophagy* 11, 538-546

92. Rosati, A., Graziano, V., De Laurenzi, V., Pascale, M., and Turco, M. C. (2011) BAG3: a multifaceted protein that regulates major cell pathways. *Cell death & disease* 2, e141

93. Katsuragi, Y., Ichimura, Y., and Komatsu, M. (2015) p62/SQSTM1 functions as a signaling hub and an autophagy adaptor. *The FEBS journal* 282, 4672-4678

94. <205832s004lbl.pdf>.

95. <esbriet_prescribing.pdf>.

96. Wollin, L., Distler, J. H. W., Redente, E. F., Riches, D. W. H., Stowasser, S., Schlenker-Herceg, R., Maher, T. M., and Kolb, M. (2019) Potential of nintedanib in treatment of progressive fibrosing interstitial lung diseases. *The European respiratory journal* 54

97. Flaherty, K. R., Fell, C. D., Huggins, J. T., Nunes, H., Sussman, R., Valenzuela, C., Petzinger, U., Stauffer, J. L., Gilberg, F., Bengus, M., and Wijsenbeek, M. (2018) Safety of nintedanib added to pirfenidone treatment for idiopathic pulmonary fibrosis. *The European respiratory journal* 52

98. B, B. M., Lawson, W. E., Oury, T. D., Sisson, T. H., Raghavendran, K., and Hogaboam, C. M. (2013) Animal models of fibrotic lung disease. *American journal of respiratory cell and molecular biology* 49, 167-179

99. Tashiro, J., Rubio, G. A., Limper, A. H., Williams, K., Elliot, S. J., Ninou, I., Aidinis, V., Tzouvelekis, A., and Glassberg, M. K. (2017) Exploring Animal Models That Resemble Idiopathic Pulmonary Fibrosis. *Frontiers in medicine* 4, 118

100. Lee, S. H., Lee, E. J., Lee, S. Y., Kim, J. H., Shim, J. J., Shin, C., In, K. H., Kang, K. H., Uhm, C. S., Kim, H. K., Yang, K. S., Park, S., Kim, H. S., Kim, Y. M., and Yoo, T. J. (2014) The effect of adipose stem cell therapy on pulmonary fibrosis induced by repetitive intratracheal bleomycin in mice. *Experimental lung research* 40, 117-125

101. Gunther, A., Schmidt, R., Nix, F., Yabut-Perez, M., Guth, C., Rosseau, S., Siebert, C., Grimminger, F., Morr, H., Velcovsky, H. G., and Seeger, W. (1999) Surfactant abnormalities in idiopathic pulmonary fibrosis, hypersensitivity pneumonitis and sarcoidosis. *The European respiratory journal* 14, 565-573

102. Nogee, L. M. (2002) Abnormal expression of surfactant protein C and lung disease. *American journal of respiratory cell and molecular biology* 26, 641-644

103. Nogee, L. M., Dunbar, A. E., 3rd, Wert, S., Askin, F., Hamvas, A., and Whitsett, J. A. (2002) Mutations in the surfactant protein C gene associated with interstitial lung disease. *Chest* 121, 20S-21S

104. Cameron, H. S., Somaschini, M., Carrera, P., Hamvas, A., Whitsett, J. A., Wert, S. E., Deutsch, G., and Nogee, L. M. (2005) A common mutation in the surfactant protein C gene associated with lung disease. *The Journal of pediatrics* 146, 370-375

105. Thomas, A. Q., Lane, K., Phillips, J., 3rd, Prince, M., Markin, C., Speer, M., Schwartz, D. A., Gaddipati, R., Marney, A., Johnson, J., Roberts, R., Haines, J., Stahlman, M., and Loyd, J. E. (2002) Heterozygosity for a surfactant protein C gene mutation associated with usual

interstitial pneumonitis and cellular nonspecific interstitial pneumonitis in one kindred. ***American journal of respiratory and critical care medicine*** **165, 1322-1328**

106. Kabore, A. F., Wang, W. J., Russo, S. J., and Beers, M. F. (2001) Biosynthesis of surfactant protein C: characterization of aggresome formation by EGFP chimeras containing propeptide mutants lacking conserved cysteine residues. ***Journal of cell science*** **114, 293-302**

107. Hawkins, A., Guttentag, S. H., Deterding, R., Funkhouser, W. K., Goralski, J. L., Chatterjee, S., Mulugeta, S., and Beers, M. F. (2015) A non-BRICHOS SFTPC mutant (SP-CI73T) linked to interstitial lung disease promotes a late block in macroautophagy disrupting cellular proteostasis and mitophagy. ***American journal of physiology. Lung cellular and molecular physiology*** **308, L33-47**

108. Katzen, J., Wagner, B. D., Venosa, A., Kopp, M., Tomer, Y., Russo, S. J., Headen, A. C., Basil, M. C., Stark, J. M., Mulugeta, S., Deterding, R. R., and Beers, M. F. (2019) An SFTPC BRICHOS mutant links epithelial ER stress and spontaneous lung fibrosis. ***JCI insight*** **4**

109. Moore, G. P., Lines, M. A., Geraghty, M. T., de Nanassy, J., and Kovesi, T. (2014) Novel mutation in ABCA3 resulting in fatal congenital surfactant deficiency in two siblings. ***American journal of respiratory and critical care medicine*** **189, 750-752**

110. Matsumura, Y., Ban, N., and Inagaki, N. (2008) Aberrant catalytic cycle and impaired lipid transport into intracellular vesicles in ABCA3 mutants associated with nonfatal pediatric interstitial lung disease. ***American journal of physiology. Lung cellular and molecular physiology*** **295, L698-707**

111. Young, L. R., Nogee, L. M., Barnett, B., Panos, R. J., Colby, T. V., and Deutsch, G. H. (2008) Usual interstitial pneumonia in an adolescent with ABCA3 mutations. ***Chest*** **134, 192-195**

112. McGarry, M. P., Reddington, M., Novak, E. K., and Swank, R. T. (1999) Survival and lung pathology of mouse models of Hermansky-Pudlak syndrome and Chediak-Higashi syndrome. ***Proc Soc Exp Biol Med*** **220, 162-168**

113. Prueitt, J. L., Chi, E. Y., and Lagunoff, D. (1978) Pulmonary surface-active materials in the Chediak-Higashi syndrome. ***Journal of lipid research*** **19, 410-415**

114. Osanai, K., Oikawa, R., Higuchi, J., Kobayashi, M., Tsuchihara, K., Iguchi, M., Jongsu, H., Toga, H., and Voelker, D. R. (2008) A mutation in Rab38 small GTPase causes abnormal lung surfactant homeostasis and aberrant alveolar structure in mice. ***The American journal of pathology*** **173, 1265-1274**

115. Palmeri, S., Tarugi, P., Sicurelli, F., Buccoliero, R., Malandrini, A., De Santi, M. M., Marciano, G., Battisti, C., Dotti, M. T., Calandra, S., and Federico, A. (2005) Lung involvement in Niemann-Pick disease type C1: improvement with bronchoalveolar lavage. ***Neurological sciences : official journal of the Italian Neurological Society and of the Italian Society of Clinical Neurophysiology*** **26, 171-173**

116. Bjurulf, B., Spetalen, S., Erichsen, A., Vanier, M. T., Strom, E. H., and Stromme, P. (2008) Niemann-Pick disease type C2 presenting as fatal pulmonary alveolar lipoproteinosis: morphological findings in lung and nervous tissue. ***Medical science monitor : international medical journal of experimental and clinical research*** **14, CS71-75**

117. Guttentag, S. H., Akhtar, A., Tao, J. Q., Atochina, E., Rusiniak, M. E., Swank, R. T., and Bates, S. R. (2005) Defective surfactant secretion in a mouse model of Hermansky-Pudlak syndrome. ***American journal of respiratory cell and molecular biology*** **33, 14-21**

118. Minarowska, A., Minarowski, L., Karwowska, A., and Gacko, M. (2007) Regulatory role of cathepsin D in apoptosis. ***Folia histochemica et cytobiologica*** **45, 159-163**

119. Chen, B., Retzlaff, M., Roos, T., and Frydman, J. (2011) Cellular strategies of protein quality control. ***Cold Spring Harbor perspectives in biology*** **3, a004374**

120. Dubnikov, T., Ben-Gedalya, T., and Cohen, E. (2017) Protein Quality Control in Health and Disease. ***Cold Spring Harbor perspectives in biology*** **9**

121. **Semren, N., Welk, V., Korfei, M., Keller, I. E., Fernandez, I. E., Adler, H., Gunther, A., Eickelberg, O., and Meiners, S. (2015) Regulation of 26S Proteasome Activity in Pulmonary Fibrosis.** ***American journal of respiratory and critical care medicine*** **192, 1089-1101**

122. **Mutlu, G. M., Budinger, G. R., Wu, M., Lam, A. P., Zirk, A., Rivera, S., Urich, D., Chiarella, S. E., Go, L. H., Ghosh, A. K., Selman, M., Pardo, A., Varga, J., Kamp, D. W., Chandel, N. S., Sznajder, J. I., and Jain, M. (2012) Proteasomal inhibition after injury prevents fibrosis by modulating TGF-beta(1) signalling.** ***Thorax*** **67, 139-146**

123. **Cabrera, S., Maciel, M., Herrera, I., Nava, T., Vergara, F., Gaxiola, M., Lopez-Otin, C., Selman, M., and Pardo, A. (2015) Essential role for the ATG4B protease and autophagy in bleomycin-induced pulmonary fibrosis.** ***Autophagy*** **11, 670-684**

124. **Mai, S., Muster, B., Bereiter-Hahn, J., and Jendrach, M. (2012) Autophagy proteins LC3B, ATG5 and ATG12 participate in quality control after mitochondrial damage and influence lifespan.** ***Autophagy*** **8, 47-62**

125. **Pyo, J. O., Yoo, S. M., Ahn, H. H., Nah, J., Hong, S. H., Kam, T. I., Jung, S., and Jung, Y. K. (2013) Overexpression of Atg5 in mice activates autophagy and extends lifespan.** ***Nature communications*** **4, 2300**

126. **Alers, S., Loffler, A. S., Wesselborg, S., and Stork, B. (2012) Role of AMPK-mTOR-Ulk1/2 in the regulation of autophagy: cross talk, shortcuts, and feedbacks.** ***Molecular and cellular biology*** **32, 2-11**

127. **Alers, S., Loffler, A. S., Wesselborg, S., and Stork, B. (2012) The incredible ULKs.** ***Cell communication and signaling : CCS*** **10, 7**

128. **Cheong, H., Wu, J., Gonzales, L. K., Guttentag, S. H., Thompson, C. B., and Lindsten, T. (2014) Analysis of a lung defect in autophagy-deficient mouse strains.** ***Autophagy*** **10, 45-56**

129. **Seranova, E., Connolly, K. J., Zatyka, M., Rosenstock, T. R., Barrett, T., Tuxworth, R. I., and Sarkar, S. (2017) Dysregulation of autophagy as a common mechanism in lysosomal storage diseases.** ***Essays in biochemistry*** **61, 733-749**

130. **Carmona-Rivera, C., Simeonov, D. R., Cardillo, N. D., Gahl, W. A., and Cadilla, C. L. (2013) A divalent interaction between HPS1 and HPS4 is required for the formation of the biogenesis of lysosome-related organelle complex-3 (BLOC-3).** ***Biochimica et biophysica acta*** **1833, 468-478**

131. **Nazarian, R., Falcon-Perez, J. M., and Dell'Angelica, E. C. (2003) Biogenesis of lysosome-related organelles complex 3 (BLOC-3): a complex containing the Hermansky-Pudlak syndrome (HPS) proteins HPS1 and HPS4.** ***Proceedings of the National Academy of Sciences of the United States of America*** **100, 8770-8775**

132. **Nguyen, T. N., Padman, B. S., Usher, J., Oorschot, V., Ramm, G., and Lazarou, M. (2016) Atg8 family LC3/GABARAP proteins are crucial for autophagosome-lysosome fusion but not autophagosome formation during PINK1/Parkin mitophagy and starvation.** ***The Journal of cell biology*** **215, 857-874**

133. **Martens, S. (2016) No ATG8s, no problem? How LC3/GABARAP proteins contribute to autophagy.** ***The Journal of cell biology*** **215, 761-763**

134. **Hariri, M., Millane, G., Guimond, M. P., Guay, G., Dennis, J. W., and Nabi, I. R. (2000) Biogenesis of multilamellar bodies via autophagy.** ***Molecular biology of the cell*** **11, 255-268**

135. **Lajoie, P., Guay, G., Dennis, J. W., and Nabi, I. R. (2005) The lipid composition of autophagic vacuoles regulates expression of multilamellar bodies.** ***Journal of cell science*** **118, 1991-2003**

136. **Feeney, E. J., Spampanato, C., Puertollano, R., Ballabio, A., Parenti, G., and Raben, N. (2013) What else is in store for autophagy? Exocytosis of autolysosomes as a mechanism of TFEB-mediated cellular clearance in Pompe disease.** ***Autophagy*** **9, 1117-1118**

137. **Hengst, M., Naehrlich, L., Mahavadi, P., Grosse-Onnebrink, J., Terheggen-Lagro, S., Skanke, L. H., Schuch, L. A., Brasch, F., Guenther, A., Reu, S., Ley-Zaporozhan, J., and Griese, M. (2018) Hermansky-Pudlak syndrome type 2 manifests with fibrosing lung disease early in childhood.** ***Orphanet journal of rare diseases*** **13, 42**

138. Chapuy, B., Tikkanen, R., Muhlhausen, C., Wenzel, D., von Figura, K., and Honing, S. (2008) AP-1 and AP-3 mediate sorting of melanosomal and lysosomal membrane proteins into distinct post-Golgi trafficking pathways. *Traffic* 9, 1157-1172

139. Ihrke, G., Kyttala, A., Russell, M. R., Rous, B. A., and Luzio, J. P. (2004) Differential use of two AP-3-mediated pathways by lysosomal membrane proteins. *Traffic* 5, 946-962

140. Rous, B. A., Reaves, B. J., Ihrke, G., Briggs, J. A., Gray, S. R., Stephens, D. J., Banting, G., and Luzio, J. P. (2002) Role of adaptor complex AP-3 in targeting wild-type and mutated CD63 to lysosomes. *Molecular biology of the cell* 13, 1071-1082

141. Styers, M. L., Salazar, G., Love, R., Peden, A. A., Kowalczyk, A. P., and Faundez, V. (2004) The endo-lysosomal sorting machinery interacts with the intermediate filament cytoskeleton. *Molecular biology of the cell* 15, 5369-5382

142. Bedrossian, C. W., Warren, C. J., Ohar, J., and Bhan, R. (1997) Amiodarone pulmonary toxicity: cytopathology, ultrastructure, and immunocytochemistry. *Annals of diagnostic pathology* 1, 47-56

143. Nagata, N., Suematsu, R., Yoshii, C., Miyazaki, H., Sueishi, K., and Kido, M. (1997) Characterization of amiodarone pneumonitis as related to inflammatory cells and surfactant apoprotein. *Chest* 112, 1068-1074

144. Somani, P., Bandyopadhyay, S., Gross, S. A., Morady, F., and Dicarlo, L. A. (1987) Amiodarone and multilamellar inclusion bodies. *British journal of clinical pharmacology* 24, 237-239

145. Belur Nagaraj, A., Joseph, P., Kovalenko, O., Wang, Q., Xu, R., and DiFeo, A. (2018) Evaluating class III antiarrhythmic agents as novel MYC targeting drugs in ovarian cancer. *Gynecologic oncology* 151, 525-532

146. Lin, C. W., Chen, Y. S., Lin, C. C., Chen, Y. J., Lo, G. H., Lee, P. H., Kuo, P. L., Dai, C. Y., Huang, J. F., Chung, W. L., and Yu, M. L. (2015) Amiodarone as an autophagy promoter reduces liver injury and enhances liver regeneration and survival in mice after partial hepatectomy. *Scientific reports* 5, 15807

147. Uhal, B. D., Wang, R., Laukka, J., Zhuang, J., Soledad-Conrad, V., and Filippatos, G. (2003) Inhibition of amiodarone-induced lung fibrosis but not alveolitis by angiotensin system antagonists. *Pharmacology & toxicology* 92, 81-87

148. Xiao, R., Teng, M., Zhang, Q., Shi, X. H., and Huang, Y. S. (2012) Myocardial autophagy after severe burn in rats. *PloS one* 7, e39488

149. Moon, J. H., Jeong, J. K., Hong, J. M., Seol, J. W., and Park, S. Y. (2019) Inhibition of Autophagy by Captopril Attenuates Prion Peptide-Mediated Neuronal Apoptosis via AMPK Activation. *Molecular neurobiology* 56, 4192-4202

150. Anderson, N., and Borlak, J. (2006) Drug-induced phospholipidosis. *FEBS letters* 580, 5533-5540

151. Maguire, J. A., Mulugeta, S., and Beers, M. F. (2011) Endoplasmic reticulum stress induced by surfactant protein C BRICHOS mutants promotes proinflammatory signaling by epithelial cells. *American journal of respiratory cell and molecular biology* 44, 404-414

152. Mulugeta, S., Nguyen, V., Russo, S. J., Muniswamy, M., and Beers, M. F. (2005) A surfactant protein C precursor protein BRICHOS domain mutation causes endoplasmic reticulum stress, proteasome dysfunction, and caspase 3 activation. *American journal of respiratory cell and molecular biology* 32, 521-530

153. Klymenko, O., Huehn, M., Wilhelm, J., Wasnick, R., Shalashova, I., Ruppert, C., Henneke, I., Hezel, S., Guenther, K., Mahavadi, P., Samakovlis, C., Seeger, W., Guenther, A., and Korfei, M. (2019) Regulation and role of the ER stress transcription factor CHOP in alveolar epithelial type-II cells. *J Mol Med (Berl)* 97, 973-990

154. Kamp, D. W., Liu, G., Cheresh, P., Kim, S. J., Mueller, A., Lam, A. P., Trejo, H., Williams, D., Tulasiram, S., Baker, M., Ridge, K., Chandel, N. S., and Beri, R. (2013) Asbestos-induced alveolar epithelial cell apoptosis. The role of endoplasmic reticulum stress response. *American journal of respiratory cell and molecular biology* 49, 892-901

155. Cheresh, P., Kim, S. J., Tulasiram, S., and Kamp, D. W. (2013) Oxidative stress and pulmonary fibrosis. *Biochimica et biophysica acta* 1832, 1028-1040

156. Fromenty, B., Fisch, C., Berson, A., Letteron, P., Larrey, D., and Pessayre, D. (1990) Dual effect of amiodarone on mitochondrial respiration. Initial protonophoric uncoupling effect followed by inhibition of the respiratory chain at the levels of complex I and complex II. *The Journal of pharmacology and experimental therapeutics* 255, 1377-1384

157. Fromenty, B., Fisch, C., Labbe, G., Degott, C., Deschamps, D., Berson, A., Letteron, P., and Pessayre, D. (1990) Amiodarone inhibits the mitochondrial beta-oxidation of fatty acids and produces microvesicular steatosis of the liver in mice. *The Journal of pharmacology and experimental therapeutics* 255, 1371-1376

158. Fromenty, B., and Pessayre, D. (1995) Inhibition of mitochondrial beta-oxidation as a mechanism of hepatotoxicity. *Pharmacology & therapeutics* 67, 101-154

159. Talbert, J. L., Schwartz, D. A., and Steele, M. P. (2014) Familial Interstitial Pneumonia (FIP). *Clinical pulmonary medicine* 21, 120-127

160. Petrovski, S., Todd, J. L., Durheim, M. T., Wang, Q., Chien, J. W., Kelly, F. L., Frankel, C., Mebane, C. M., Ren, Z., Bridgers, J., Urban, T. J., Malone, C. D., Finlen Copeland, A., Brinkley, C., Allen, A. S., O'Riordan, T., McHutchison, J. G., Palmer, S. M., and Goldstein, D. B. (2017) An Exome Sequencing Study to Assess the Role of Rare Genetic Variation in Pulmonary Fibrosis. *American journal of respiratory and critical care medicine* 196, 82-93

161. Armanios, M. (2012) Telomerase and idiopathic pulmonary fibrosis. *Mutation research* 730, 52-58

162. Snetselaar, R., van Moorsel, C. H. M., Kazemier, K. M., van der Vis, J. J., Zanen, P., van Oosterhout, M. F. M., and Grutters, J. C. (2015) Telomere length in interstitial lung diseases. *Chest* 148, 1011-1018

163. Snetselaar, R., van Batenburg, A. A., van Oosterhout, M. F. M., Kazemier, K. M., Roothaan, S. M., Peeters, T., van der Vis, J. J., Goldschmeding, R., Grutters, J. C., and van Moorsel, C. H. M. (2017) Short telomere length in IPF lung associates with fibrotic lesions and predicts survival. *PloS one* 12, e0189467

164. Shoeb, M., Mustafa, G. M., Joseph, P., Umbright, C., Kodali, V., Roach, K. A., Meighan, T., Roberts, J. R., Erdely, A., and Antonini, J. M. (2019) Initiation of Pulmonary Fibrosis after Silica Inhalation in Rats is linked with Dysfunctional Shelterin Complex and DNA Damage Response. *Scientific reports* 9, 471

165. Lopez-Larraza, D., De Luca, J. C., and Bianchi, N. O. (1990) The kinetics of DNA damage by bleomycin in mammalian cells. *Mutation research* 232, 57-61

8. Publications

8.1. Mahavadi et al., 2010

8.2. Mahavadi et al., 2014

8.3. Birkelbach, …., Mahavadi, Knudsen* et al., 2015*

8.4. Mahavadi et al., 2015

8.5. Ahuja, …., Guenther, Mahavadi* et. al., 2016*

8.6. Kesireddy, …, Mahavadi et. al., 2019

Epithelial Stress and Apoptosis Underlie Hermansky-Pudlak Syndrome–associated Interstitial Pneumonia

Poornima Mahavadi[1], Martina Korfei[1], Ingrid Henneke[1], Gerhard Liebisch[2], Gerd Schmitz[2], Bernadette R. Gochuico[3], Philipp Markart[1,4], Saverio Bellusci[4], Werner Seeger[1,4], Clemens Ruppert[1,4]*, and Andreas Guenther[1,4,5]*

[1]Department of Internal Medicine II, University of Giessen Lung Center, Giessen; [2]Institute of Clinical Chemistry and Laboratory Medicine, University of Regensburg, Regensburg, Germany; [3]Medical Genetics Branch, National Human Genome Research Institute, National Institutes of Health, Bethesda, Maryland; [4]Excellence Cluster "Cardiopulmonary System," University of Giessen Lung Center, Giessen; and [5]Lung Clinic Waldhof-Elgershausen, Greifenstein, Germany

Rationale: **The molecular mechanisms underlying Hermansky-Pudlak syndrome–associated interstitial pneumonia (HPSIP) are poorly understood but, as in idiopathic pulmonary fibrosis, may be linked to chronic alveolar epithelial type II cell (AECII) injury.**

Objectives: **We studied the development of fibrosis and the role of AECII injury in various murine models of HPS.**

Methods: **HPS1, HPS2, and HPS6 monomutant mice, and HPS1/2 and HPS1/6 double-mutant and genetic background mice, were killed at 3 and 9 months of age. Quantitative morphometry was undertaken in lung sections stained with hemalaun–eosin. The extent of lung fibrosis was assessed by trichrome staining and hydroxyproline measurement. Surfactant lipids were analyzed by electrospray ionization mass spectrometry. Surfactant proteins, apoptosis, and lysosomal and endoplasmic reticulum stress markers were studied by Western blotting and immunohistochemistry. Cell proliferation was measured by water-soluble tetrazolium salt-1 and bromodeoxyuridine assays.**

Measurements and Main Results: **Spontaneous and slowly progressive HPSIP was observed in HPS1/2 double mutants, but not in other HPS mutants, with subpleural onset at 3 months and full-blown fibrosis at 9 months. In these mice, extensive surfactant abnormalities were encountered in AECII and were paralleled by early lysosomal stress (cathepsin D induction), late endoplasmic reticulum stress (activating transcription factor-4 [ATF4], C/EBP homologous protein [CHOP] induction), and marked apoptosis. These findings were fully corroborated in human HPSIP. In addition, cathepsin D overexpression resulted in apoptosis of MLE-12 cells and increased proliferation of NIH 3T3 fibroblasts incubated with conditioned medium of the transfected cells.**

Conclusions: **Extensively impaired surfactant trafficking and secretion underlie lysosomal and endoplasmic reticulum stress with apoptosis of AECII in HPSIP, thereby causing the development of HPSIP.**

Keywords: pulmonary surfactant; biogenesis of lysosome-related organelle complex; adaptor protein-3; apoptosis; cathepsin D

(*Received in original form September 21, 2009; accepted in final form March 31, 2010*)

* These authors contributed equally to this article.

Supported by research grants from the European Commission through FP7 (European IPF Network [www.pulmonary-fibrosis.net] and European Lipidomics Initiative [www.lipidomics.net]), the German Research Council (Clinical Research Group 118 "Lung Fibrosis" and Excellence Cluster "Cardiopulmonary System" [www.eccps.de]), and in part by the Intramural Research Program of the National Human Genome Research Institute, National Institutes of Health, Bethesda, MD.

Correspondence and requests for reprints should be addressed to Andreas Guenther, M.D., Ph.D., Department of Internal Medicine II, University of Giessen Lung Center (UGLC), Klinikstrasse 36, 35392 Giessen, Germany. E-mail: Andreas.Guenther@uglc.de

This article has an online supplement, which is accessible from this issue's table of contents at www.atsjournals.org

Am J Respir Crit Care Med Vol 182. pp 207–219, 2010
Originally Published in Press as DOI: 10.1164/rccm.200909-1414OC on April 8, 2010
Internet address: www.atsjournals.org

AT A GLANCE COMMENTARY

Scientific Knowledge on the Subject

No reports are available to date regarding the development of pulmonary fibrosis in murine models of Hermansky-Pudlak syndrome and the underlying mechanisms of Hermansky-Pudlak syndrome–associated interstitial pneumonia in mice and humans.

What This Study Adds to the Field

Apoptosis of alveolar epithelial type II cells in Hermansky-Pudlak syndrome–associated interstitial pneumonia in both mice and humans, due to severe lysosomal and endoplasmic reticulum stress, may represent a prominent reason for development of lung fibrosis.

Hermansky-Pudlak syndrome (HPS) is a rare autosomal recessive disorder associated with oculocutaneous albinism and hemorrhagic diathesis (1). Several HPS genes have been identified in both humans and mice that encode several protein complexes, the precise function of which is only partially known and that affect various lysosome-related organelles (LROs), including the lamellar bodies of the lungs. Hence, on the basis of their role in LRO trafficking, these genes have an enormous impact on a wide range of basic physiological processes such as immune recognition, coagulation, and neuronal function (2).

Pulmonary fibrosis due to HPS, entitled Hermansky-Pudlak syndrome–associated interstitial pneumonia (HPSIP), is known to develop in patients with HPS1 and HPS4 mutations, the genes of which encode the "biogenesis of lysosome-related organelle complexes" (BLOC)-3 (2–5). HPSIP is the most serious complication and the main reason for death of patients with HPS (6–8) and usually evolves during the third or fourth decade of life. The clinical course of HPSIP shows great similarities to the disastrous fate of patients with idiopathic pulmonary fibrosis (IPF). Accordingly, the radiographic appearance of HPSIP is comparable to that of IPF and the predominant histopathological pattern is that of usual interstitial pneumonia (UIP) (9, 10).

In contrast to IPF/UIP, however, a characteristic foamy swelling of alveolar epithelial type II cells (AECII) with lamellar bodies of increased size and number ("giant lamellar body degeneration") is regularly observed in patients with HPSIP (10).

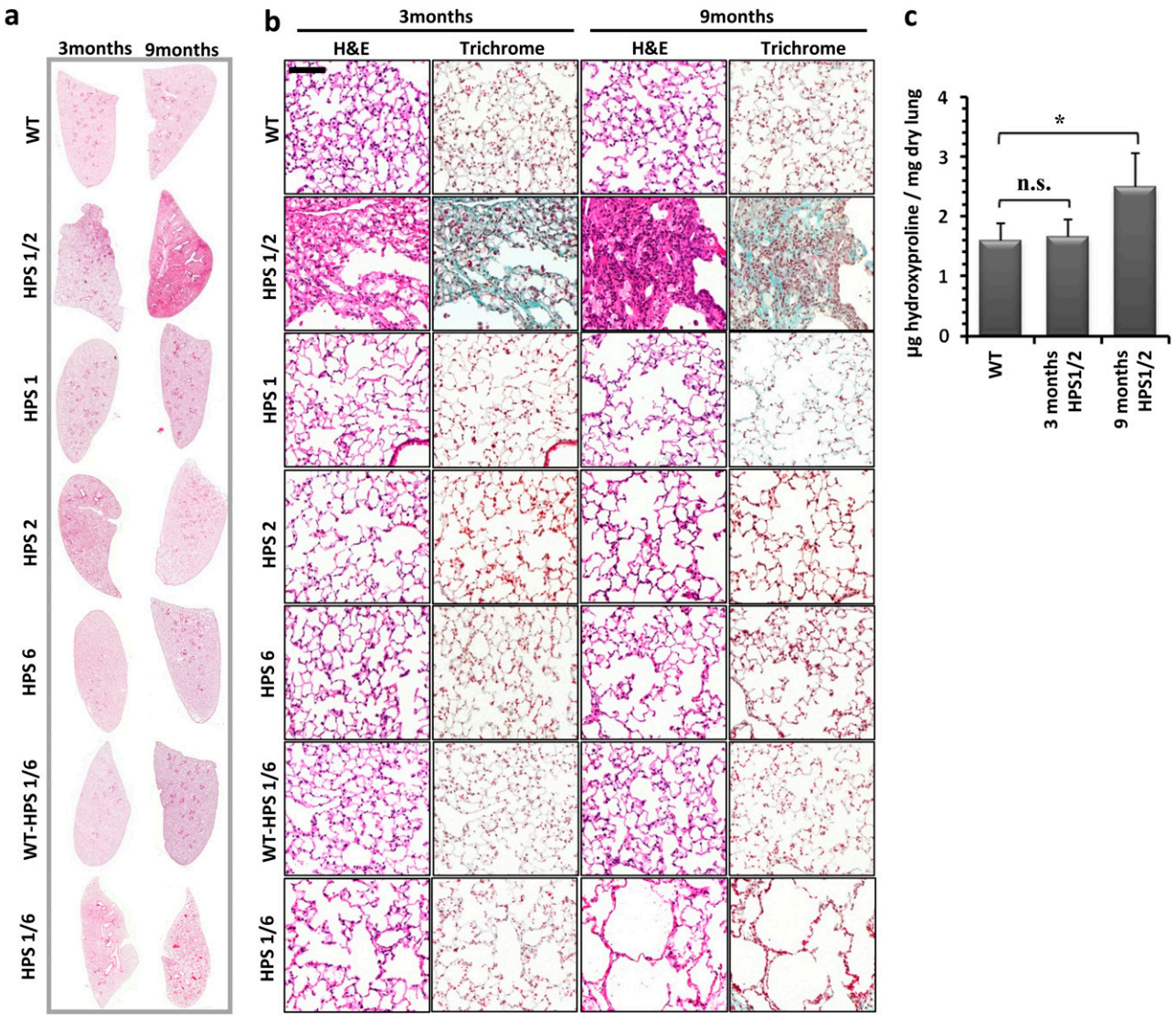

Figure 1. Development of pulmonary fibrosis only in HPS1/2 double-mutant mice: (*a*) Representative hematoxylin–eosin (H&E) stainings of complete right lungs of HPS monomutant mice, double-mutant mice, and background wild-type (WT) control mice at the ages of 3 and 9 months. (*b*) Higher magnification pictures of H&E- and trichrome-stained lungs of all the HPS mutants and WT controls analyzed in this study at the ages of 3 and 9 months. Original magnification, ×200 (scale bar, 100 μm). (*c*) Quantitative determination of lung hydroxyproline concentration in HPS1/2 double-mutant mice in comparison with WT control mice. *$P < 0.05$, n = 5 mice per group. n.s. = not significant.

As the proteins encoded by the HPS genes and their precise functions are only partly known, the pathogenesis of HPSIP is still poorly understood. However, in light of the previously mentioned histopathological findings, it has already been speculated that—like in IPF—chronic AECII injury may underlie the development of lung fibrosis (10, 11).

Interestingly, the HPS mutations occur not only in humans but also in mice, and several mono-, double-, and triple-mutant HPS mice have been characterized largely on the basis of coat color and platelet function. In some of these mice, including the herein studied HPS1/2 (*ep/pe*) mice, abnormal lung structure and abnormalities of surfactant transport and secretion in AECII had been described (12, 13). However, the development of HPSIP has not yet been described in murine HPS.

These reports prompted us to carefully assess a potential development of HPSIP in several of these murine models and to disclose potential underlying pathways. Some of the results of this study have been previously reported in the form of two abstracts (14, 15).

METHODS

Mice

Breeding pairs of HPS monomutant mice and HPS1/6 double-mutant mice were purchased from Jackson Laboratory (Bar Harbor, ME). Breeding pairs of HPS1/2 double-mutant mice were a kind gift from R. Swank (Roswell Park, Buffalo, NY). C57BL/6J was the background strain for the HPS1, HPS2, HPS6, and HPS1/2 mice. HPS1/6 mice were on the B6C3Fe background. All mice were mated and maintained under specific pathogen–free conditions, and five mice per group were killed at the ages of 3 and 9 months and genotyped as described in the online supplement.

Quantification of Lung Collagen

Hydroxyproline levels in murine lungs were determined as described elsewhere (16) and in the online supplement.

Computerized Lung Morphometry

Morphometric analysis was performed on hematoxylin and eosin–stained lung tissue sections by determining the mean interalveolar distance and mean septal thickness (linear intercept measurement). AxioVision

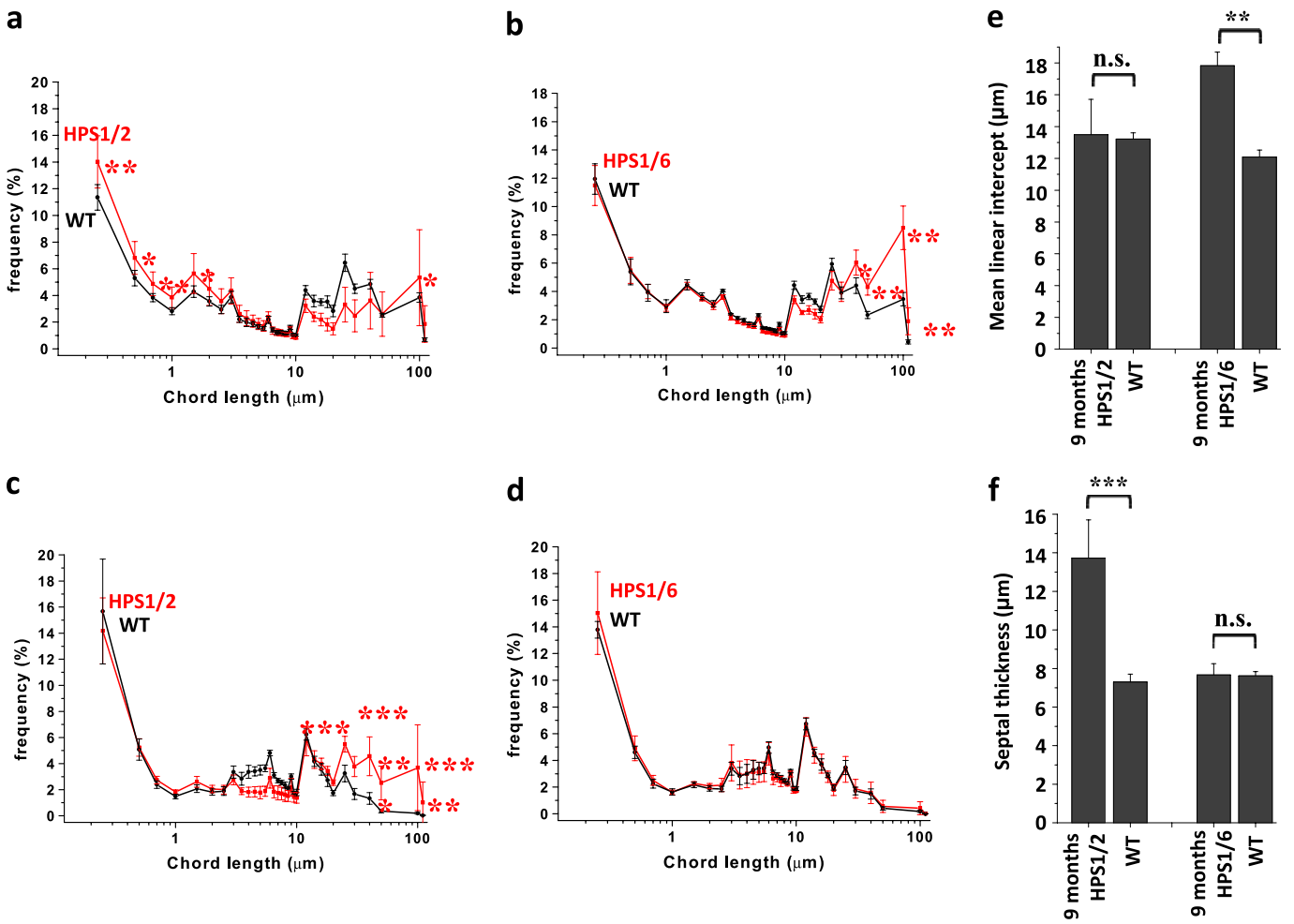

Figure 2. Increase in mean linear intercept in Hermansky-Pudlak syndrome (HPS) mice: Graphic representation of the length distribution of airspaces in (*a*) HPS1/2 mice and (*b*) HPS1/6 mice as well as the length distribution of septal thickness of (*c*) HPS1/2 mice and (*d*) HPS1/6 mice in comparison with respective wild-type (WT) controls. Twenty to 30 regions, covering the entire periphery of one digitally scanned lung slide stained with hematoxylin–eosin, were introduced with grids, comprising a total of 40,000 chords in the horizontal and vertical directions, with a distance of 40 μm. Each caption was analyzed by automated line-to-line intercept analysis, according to the criteria mentioned in METHODS. Five 9-month-old mice per group were analyzed and the data are represented as the frequency distribution of either (*a* and *b*) alveolar diameter or (*c* and *d*) septal thickness. In addition, the conventional parameters "mean linear intercept" and septal thickness are indicated in (*e*) and (*f*), respectively. ***$P < 0.001$,**$P < 0.01$, *$P < 0.05$; n.s. = not significant.

software (Carl Zeiss MicroImaging GmbH, Jena Germany) was used for the analysis as outlined in the online supplement.

Isolation of Murine Alveolar Epithelial Type II Cells

Murine AECII from the lungs of 3-month-old HPS1/2 and wild-type (WT) control mice were isolated according to the protocol given in the online supplement.

Cloning and Cell Culture

Full-length murine cathepsin D was cloned into the pcDNA3.1 expression vector and transfected into mouse lung epithelial (MLE)-12 cells, using primers and protocols described in the online supplement. NIH 3T3 mouse fibroblasts were then incubated with conditioned medium from either cathepsin D– or empty vector–transfected MLE-12 cells (24 h posttransfection). WST-1:4-[3-(4-iodophenyl)-2-(4-nitrophenyl)-2H-5-tetrazolio]-1,3-benzene disulphonate or BrdU: 5-bromo-2′-deoxyuridine (Roche Applied Science, Mannheim, Germany) was added as described in the online supplement and absorbance was measured at 450 nm.

Western Blot

Samples were subjected to denaturing sodium dodecyl sulfate–polyacrylamide gel electrophoresis followed by electroblotting on polyvinylidene difluoride membrane and immunostaining for the desired proteins. Protocol and the source of antibodies are given in the online supplement.

Phospholipid Analysis, Isolation of Large Surfactant Aggregates, and Assessment of Surface Activity

Phospholipids (PLs) were extracted from bronchoalveolar lavage fluid (BALF) or tissue extracts according to the Bligh and Dyer method as referred to in the online supplement. Characterization and surface activity of large surfactant aggregates (LAs) was undertaken as outlined in the online supplement.

Lipidomics

Lipids were quantified by electrospray ionization–tandem mass spectrometry in positive ion mode, as described in the online supplement.

Immunohistochemistry and *in Situ* Apoptosis Assay

ZytoChem Plus (AP) Broad Spectrum (Fast Red) kit (ZytoMed systems, Berlin, Germany) was used with paraffin-embedded lung sections for immunohistochemical localization of proteins according to the manufacturer's instructions. The protocol and source of antibodies are given in the online supplement. The degree of cellular

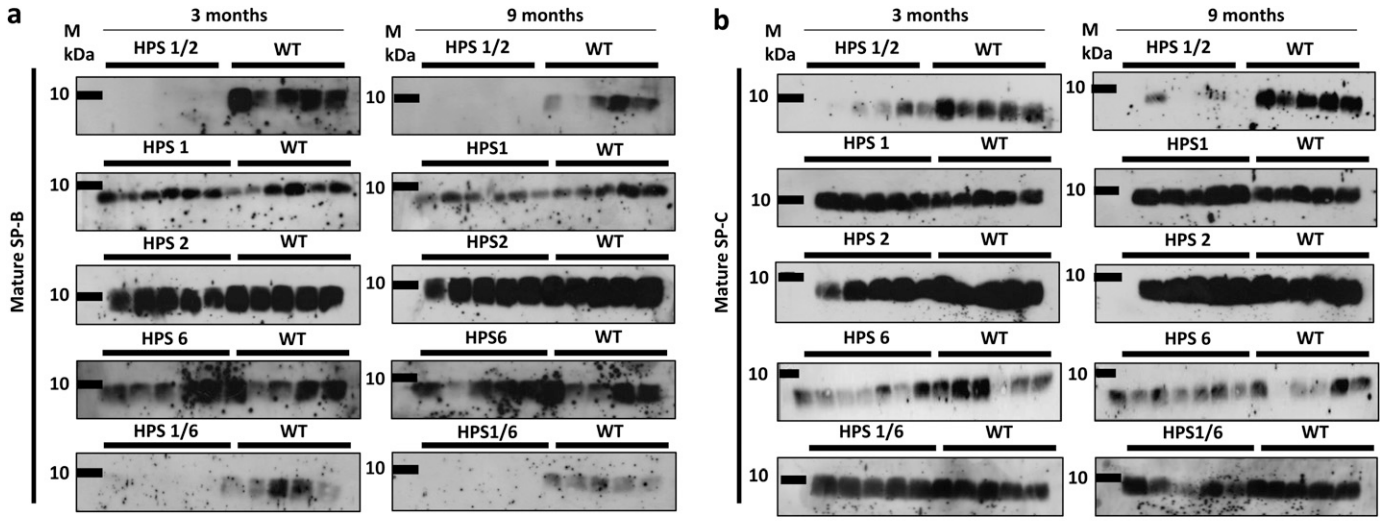

c

	Total PL content (μg/ml)	LA content (%)
WT	195.7 ± 5.86	91.3 ± 2.97
3months HPS1/2	121.5 ± 2.98 *	84.8 ± 8.13
9months HPS1/2	108.1 ± 11.18**	92.3 ± 4.81

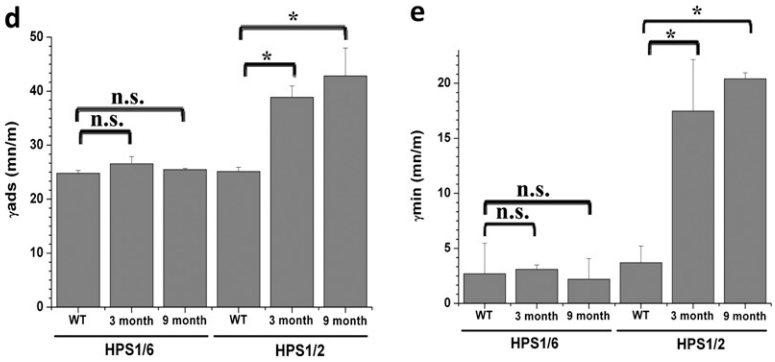

Figure 3. Loss of surfactant in bronchoalveolar lavage fluid (BALF) of HPS1/2 mice: Western blot analysis of (*a*) mature surfactant protein (SP)-B and (*b*) mature SP-C in BALF from Hermansky-Pudlak syndrome (HPS) mice along with their respective wild-type (WT) control mice at the ages of 3 and 9 months. An equal volume (20 μl per sample) of BALF was used for each analysis. (*c*) Data set showing phospholipid (PL) concentration and the relative amount of large surfactant aggregates (LA content, given as a percentage of total PL) in BALF of HPS1/2 and WT control mice. (*d* and *e*) Surface activity of LA from HPS1/2, HPS1/6, and WT control mice was characterized at a PL concentration of 2 mg/ml, employing a pulsating bubble surfactometer. (*d*) γ_{ads} (surface tension after 12 s of film adsorption) and (*e*) γ_{min} (minimal surface tension after 5 min of film oscillation) are given as millinewtons per meter (mN/m). *$P < 0.05$, **$P < 0.01$; n = 5 mice per group.

apoptosis was determined by the terminal deoxynucleotidyltransferase dUTP nick end labeling (TUNEL) method, using the *in situ* cell death detection kit, AP (Roche Applied Science) according to the manufacturer's instructions. All stained sections were analyzed on digital slide scanning, employing a Mirax scanner (Carl Zeiss GmbH, Jena, Germany). Mirax Viewer software (Carl Zeiss GmbH) was used to analyze and make snapshots of the stained tissue sections.

Statistics

Unless indicated otherwise, all data are expressed as means ± SEM of at least five mice. Statistical evaluation was performed by Mann-Whitney *U* test (comparison of two groups) and by Kruskal-Wallis *H* test (if more than two groups were analyzed). The level of significance is indicated in the figure legends and footnotes as follows: $^{*/\#}P < 0.5$, $^{**/\#\#}P < 0.01$, $^{***/\#\#\#}P < 0.001$.

RESULTS

Development of Pulmonary Fibrosis in HPS1/2

In HPS1/2 double-mutant mice, but not in HPS1/6 or HPS1, HPS2, or HPS6 mice, spontaneous development of lung fibrosis was evident at the age of 3 months (Figure 1a, *left*). Being patchy and subpleural at the beginning, the extent of lung fibrosis progressed over the age of 9 months (Figure 1a, *right*). Although fibrosis was encountered in all the 9-month-old HPS1/2 mice analyzed in this study, the extent of fibrosis differed somewhat from mouse to mouse. At higher magnification, lymphoplasmacellular infiltration and extracellular matrix deposition, with a dramatic increase in AECII size but roughly preserved lung structure, were evident at 3 months (Figure 1b). In contrast, dense fibrosis with extensive remodeling of the alveolar lung structure was prominent in 9-month-old HPS1/2 mice (Figure 1b, second row), because of which quantitative lung morphometric analysis did not reveal any significant increase in enlarged airspaces in HPS1/2 mice (Figure 2a) but revealed a more than twofold increase in septal thickness, when

TABLE 1. DIFFERENTIAL BRONCHOALVEOLAR LAVAGE COUNTS IN VARIOUS HERMANSKY-PUDLAK SYNDROME GROUPS

	AMs	PMNs	Lymphocytes
C57BL/6 controls	99.5 ± 0.7	0	0.5 ± 0.7
HPS1/2	74.6 ± 5.4	10.7 ± 6.4	14.6 ± 3.5
HPS1	67 ± 40.0	0	33 ± 40.0
HPS2	93.6 ± 10.4	0.6 ± 0.8	5.8 ± 10.4
HPS6	43.8 ± 17.9	0.4 ± 0.2	55.8 ± 23
HPS1/6 controls	99 ± 1.0	0	0.5 ± 0.7
HPS1/6	11.5 ± 4.8	0	88.5 ± 4.8

Definition of abbreviations: AMs = alveolar macrophages; HPS = Hermansky-Pudlak syndrome; PMNs = polymorphonuclear lymphocytes.
Data represent means ± SD.

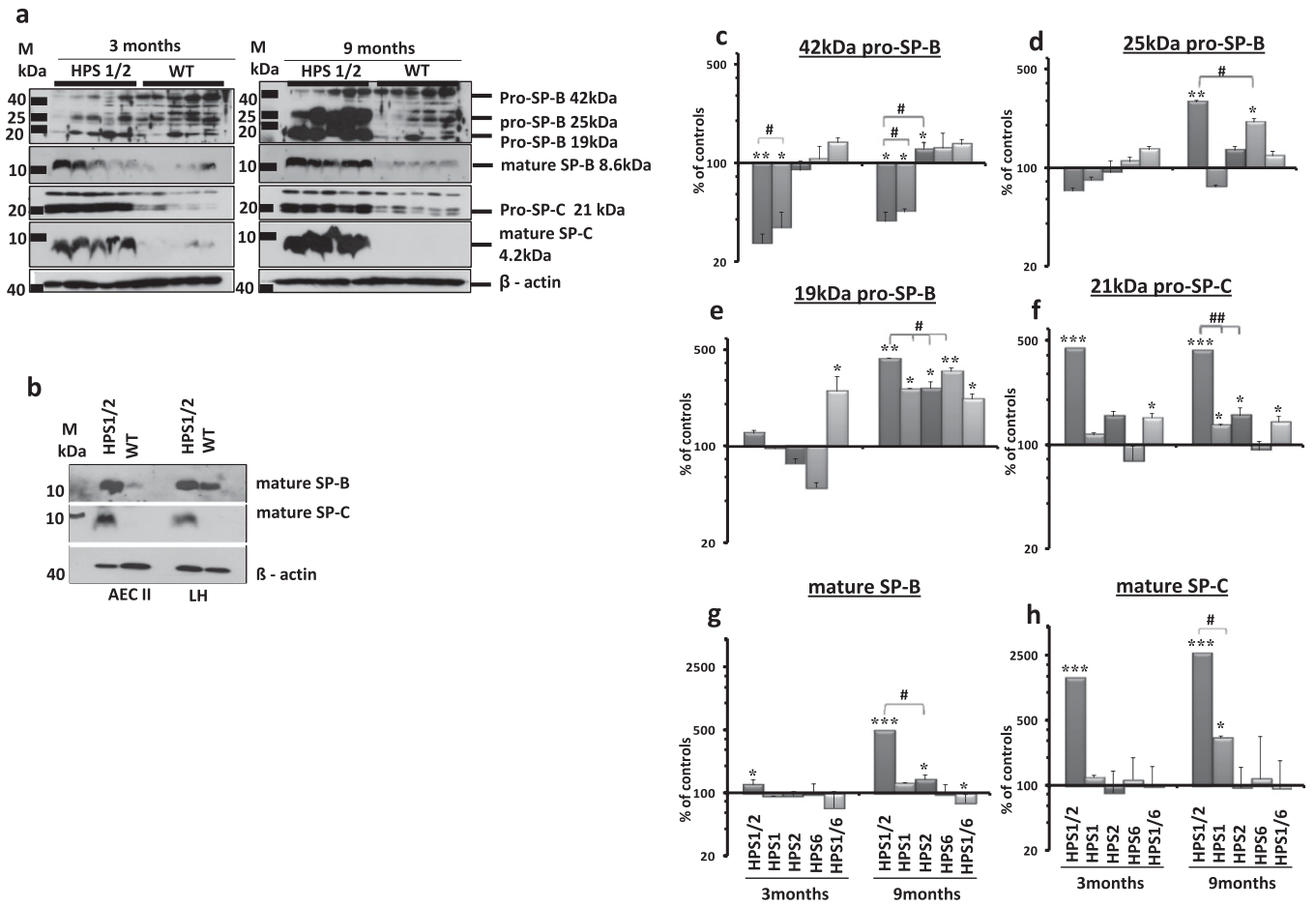

Figure 4. Accumulation of hydrophobic surfactant proteins in HPS1/2 lung tissues: (*a*) Western blot analysis of lung homogenates (LH; equal protein load) of (*left*) 3-month-old and (*right*) 9-month-old HPS1/2 double-mutant and wild-type (WT) controls for pro–surfactant protein (SP)-B, mature SP-B, pro–SP-C, and mature SP-C. (*b*) Western blot analysis of isolated alveolar epithelial type II cells (AECII; equal protein load) and LH for mature SP-B and mature SP-C from 3-month-old HPS1/2 mice and WT controls. [Please note that the blots in (*a*) and (*b*) have been developed to show adequate staining for HPS1/2 mouse samples; longer development forwarded staining for mature SP-C also in AECII and LH of WT mice.] Representative blots are from n = 5 mice per group, and three independent experiments are shown. (*c–h*) Densitometry was performed from all Western blot analyses of all HPS mouse lung homogenates. The target protein/β-actin ratio was calculated and is given as a percentage of the respective WT controls. ***$P < 0.001$,**/##$P < 0.01$, */#$P < 0.05$; n = 5 mice per group.

compared with WT controls (Figures 2c and 2e; and *see* Figure E1 in the online supplement). As a result of such fibrotic changes, lung hydroxyproline content was significantly elevated (Figure 1c). In HPS1/2 mice at 3 months, HPS1 and HPS2 monomutant mice at 9 months, and even more in HPS1/6 double-mutant mice at 9 months, airspace enlargement was a prominent finding (Figure 1b; and Figures 2b, 2d, and 2f).

Disturbed Composition and Function of the Alveolar Surfactant Pool in HPS1/2 Mice

As compared with WT mice, mature surfactant protein (SP)-B was undetectable in BALF from 3- and 9-month-old HPS1/2 mice and appeared greatly reduced in HPS1/6 mice of the same age. In contrast, BALF levels of mature SP-B remained unchanged in any of the other monomutant HPS mice (Figure 3a). Similarly, significantly reduced levels of mature SP-C were observed in the BALF of HPS1/2 mice at 3 and 9 months, but appeared unchanged in all other HPS mutants (Figure 3b). In addition, the total phospholipid content, but not the relative content of large surfactant aggregates (LAs), was significantly decreased in BALF from HPS1/2 mice (Figure 3c). As compared with WT controls, LA preparations from HPS1/2 BALF, but not from HPS1/6 BALF, showed a significant reduction in surface activity (Figures 3d and 3e). From these data, we concluded that HPS1/2 mice do have a significant defect in surfactant secretion, resulting in inappropriately low alveolar phospholipid and surfactant protein concentrations, thus leading to increased alveolar surface tension.

In addition, BALF cellular profiles from various HPS mice were analyzed. Of interest, many enlarged alveolar macrophages were encountered (data not shown), especially in HPS1/2 mice. In addition, a modest lymphocytic alveolitis was observed in all of the HPS mice analyzed (Table 1), and there was no significant difference between HPS1/2 and the other mice.

Accumulation of Hydrophobic Surfactant Proteins in HPS1/2 Lungs

A dramatic increase in intracellular content of almost all forms of the pro- and mature forms of the hydrophobic surfactant proteins SP-B and SP-C was encountered in lungs of HPS1/2 mice in comparison with their respective WT controls (Figure 4a). At the age of 3 months, especially 21-kD pro–SP-C, mature SP-B, and mature SP-C were elevated. In 9-month-old HPS1/2 mice, a more extensive accumulation of all pro- and mature

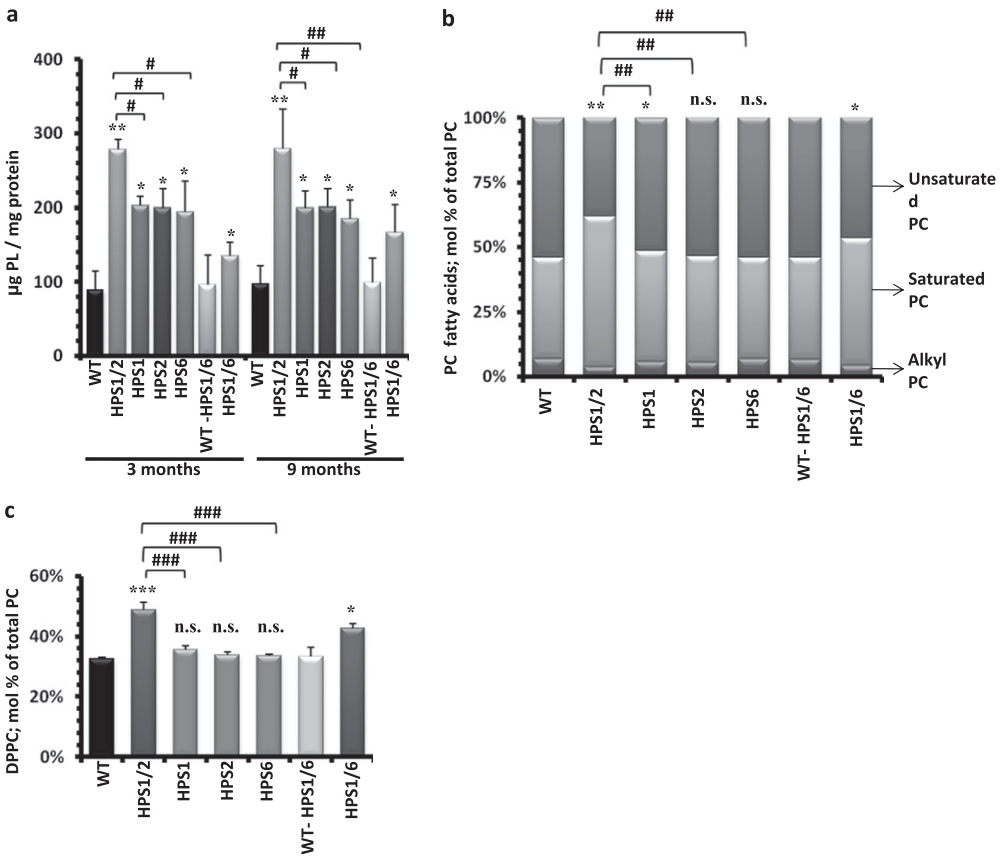

Figure 5. Accumulation of surfactant phospholipids in HPS1/2 mouse lungs: (*a*) Total phospholipids were extracted from lung tissue of all 3- and 9-month-old Hermansky-Pudlak syndrome (HPS) and wild-type (WT) control mice. The resulting phospholipid (PL) concentrations were normalized against their respective protein concentrations and values are expressed as micrograms of phospholipids per milligram of protein. (*b* and *c*) Lipidomic study was performed for 9-month-old HPS mice as compared with the respective WT control mice. *Columns* depicted here represent fatty acid distribution of (*b*) the phosphatidylcholine (PC) fraction and (*c*) the relative content of dipalmitoylated phosphatidylcholine (DPPC) within the PC fraction. Values are expressed as the molar percentage (mol %) of the respective lipid class, related to total PC. $^{*/\#}P < 0.05$, $^{**/\#\#}P < 0.01$, $^{***/\#\#\#}P < 0.001$; n.s. = not significant; n = 5 mice per group.

forms of SP-B/C, with the exception of 42-kD pro–SP-B, was encountered (Figure 4a). Densitometric analysis revealed a 25-fold increase in mature SP-C and a 5-fold increase in mature SP-B in HPS1/2 lung homogenates (Figures 4g and 4h). To confirm that such accumulation would reflect the situation within the AECII, the intracellular SP-B/C content was analyzed in AECII isolated from 3-month-old HPS1/2 mice and WT mice. Accumulation of mature SP-B and SP-C was seen exclusively in the AECII of HPS1/2 mice (Figure 4b), but not in any other HPS mutants (Figure E2). Regarding the proforms, only 19-kD pro–SP-B appeared highly up-regulated in all HPS mice (although significantly higher in HPS1/2), and some minor increases were encountered for 21-kD pro–SP-C and 25-kD pro–SP-B in these mice (Figures 4c−4f; and *see* Figure E2). Gene expression analysis did not show any differences in the expression of SP-B and SP-C between HPS1/2 and control mice (Figure E3a). Consistent with previous reports on the subcellular distribution of pro- and mature forms of the hydrophobic surfactant proteins in healthy AECII (17, 18) and with the ultrastructural appearance of AECII in humans with HPSIP (10), mature surfactant compounds seem to accumulate in the distal part of the lysosomal transport axis of AECII from HPS1/2, and hence largely in lamellar bodies.

Accumulation of Surfactant Phospholipids in HPS1/2 Lungs

We next analyzed the total phospholipid content of lung homogenates in all HPS mono- and double-mutant mice along with their WT controls. Phospholipid content was increased in all HPS mice, but to various extents. The strongest increase was found in HPS1/2 mice (approximately threefold), which was also significantly higher as compared with all other HPS mice (Figure 5a). It seems noteworthy to mention that, in contrast to the changes in mature SP-B/C, the phospholipid content of HPS1/2 lung homogenates did not further increase beyond the age of 3 months. In AECII, the combinatory loss of HPS1 and HPS2 genes thus does not seem to affect early lysosomal transport processes, as suggested for HPS1 or HPS2 gene products in other cell types (19, 20).

Lipidomic Profiling in HPS Mice

Because we observed differences in total phospholipids in HPS mice, we further performed mass spectrometry–based lipidomics analysis of lung tissues from all 9-month-old HPS and WT control mice. As evident from Table E1 in the online supplement and Figure 5a, extensive alterations of the phospholipid profile were encountered. In particular, HPS1/2 mice showed a significant increase in phosphatidylcholine (PC). To some extent this also held true for HPS1/6 mice. Of note, phosphatidylethanolamine plasmalogens were markedly depressed in HPS1/2 versus the other mice (Table E1). Moreover, a significant increase in saturated PC species was encountered in HPS1/2 mice and, to some extent, also in HPS1/6 mice (Figure 5b), which could be ascribed almost entirely to a marked increase in dipalmitoylated phosphatidylcholine (DPPC, PC-32:0; Figure 5c). Another interesting observation was a significant increase in glucosylceramides (GlcCer) in 9-month-old HPS1/2 mice, with a ceramide/GlcCer ratio of 3.9 in HPS1/2 mice compared with 7.6 in controls (*see also* Table E2). Because the expression level of the synthesizing enzyme (glucosylceramide synthase) remained unchanged (data not shown), the observed accumulation of GlcCer in HPS1/2 mice might be due to their decreased clearance.

AECII Apoptosis in HPS1/2 Mice

Accumulation and impaired secretion of pulmonary surfactant may have resulted in chronic cell stress and apoptosis of AECII

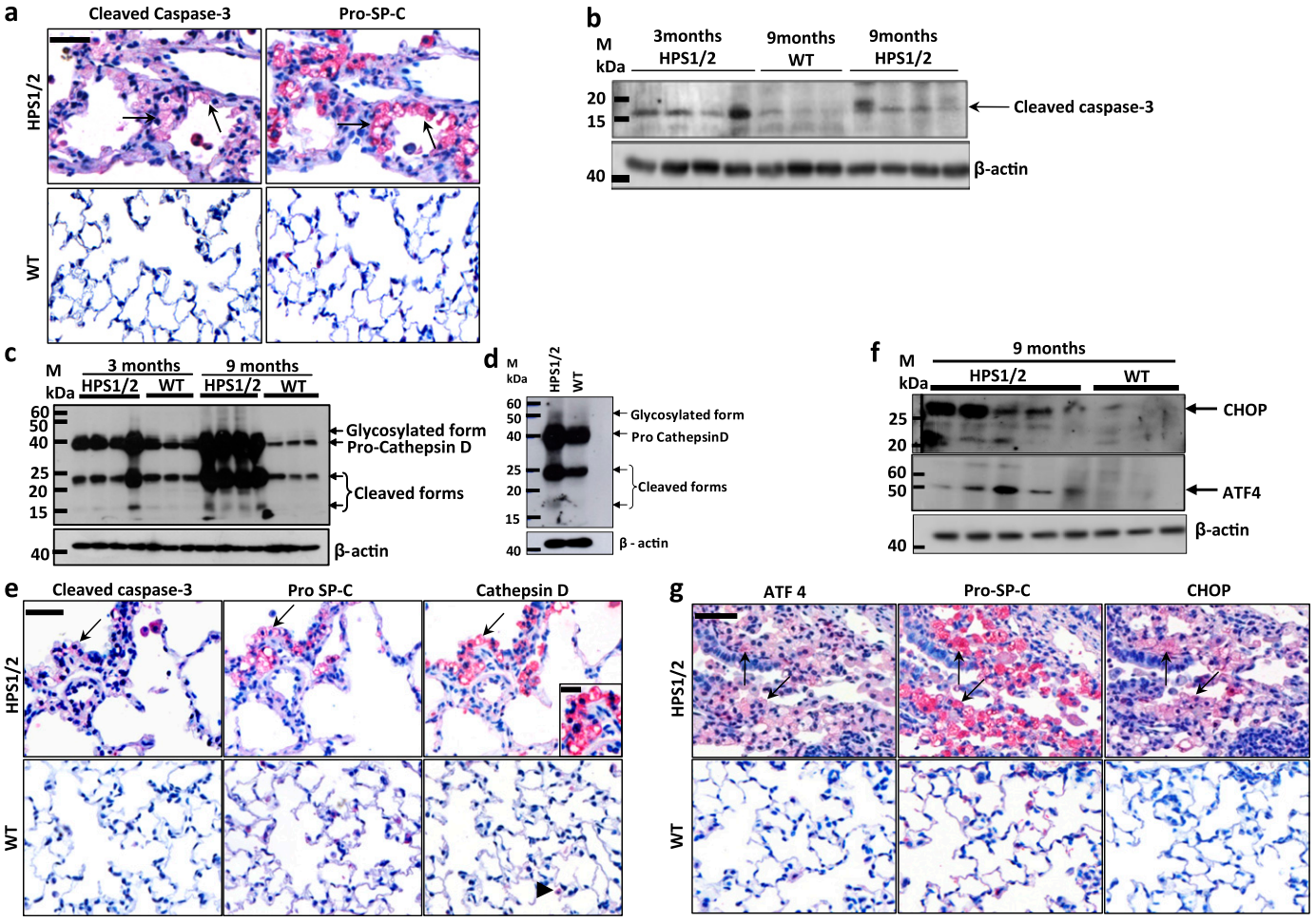

Figure 6. Alveolar epithelial type II cell (AECII) stress and apoptosis in HPS1/2 mice: (*a*) Serial paraffin-embedded lung tissue sections from (*top*) 9-month-old HPS1/2 mice and (*bottom*) wild-type (WT) controls were immunostained either for (*left*) cleaved caspase-3 or (*right*) pro–surfactant protein (SP)-C. *Arrows* indicate the same AECII stained for both proteins. (*b*) Western blot analysis of cleaved caspase-3 in lung homogenates of 3- and 9-month-old HPS1/2 mice in comparison with that of 9-month-old WT controls. (*c* and *d*) Western blot analysis of cathepsin D in (*c*) lung homogenates of HPS1/2 mice (3 and 9 mo of age) and in (*d*) isolated AECII of HPS1/2 and WT controls (3 mo of age). (*e*) Immunohistochemistry on serial sections of (*top*) HPS1/2 and (*bottom*) WT mouse lungs for (*left*) cleaved caspase-3, (*middle*) pro–SP-C, and (*right*) cathepsin D. *Arrows* indicate positive staining of AECII for all three proteins. *Inset*: High-magnification image, illustrating diffuse cytoplasmic staining of cathepsin D within the AECII of HPS1/2 mice. *Arrowhead* indicates cathepsin D staining in macrophages in a WT mouse lung tissue section. (*f*) Western blot analysis for activating transcription factor-4 (ATF4) and C/EBP homologous protein (CHOP) in lung homogenates of HPS1/2 mice and age-matched WT controls. (*g*) Serial sections were stained for either (*left*) ATF4, (*middle*) pro–SP-C, or (*right*) CHOP in 9-month-old HPS1/2 and WT controls. *Arrows* indicate the same AECII stained positive for all three proteins. Original magnification, ×400 (*scale bar*, 50 μm). Original magnification of *inset*, ×800 (*scale bar*, 20 μm). Representative blots and stainings from each group are shown, from n = 5 mice per group.

in lungs of HPS1/2 mice. To identify apoptotic AECII, we performed immunohistochemistry for cleaved, activated caspase-3, along with pro–SP-C on serial sections of HPS1/2 and control mouse lungs. It was found that the pro–SP-C–positive cells (AECII) also stained positive for cleaved caspase-3 in HPS1/2 tissue sections, whereas no signal for cleaved caspase-3 was detected in any WT control (Figure 6a). Western blot analysis for caspase-3 produced a similar result (Figure 6b). Alternatively, we performed TUNEL staining, along with immunohistochemistry, for the AECII-specific marker pro–SP-C on serial sections from all HPS and control mice. As depicted in Figure E4a in the online supplement, numerous TUNEL-positive AECII were already evident only in the lung tissue of HPS1/2 mice at an age of 3 months (but not in other mutants), indicating that AECII apoptosis is an early event in these mice. Thus, TUNEL data fully confirmed the cleaved caspase-3 immunohistochemistry and again suggest that AECII undergo extensive apoptosis in HPS1/2 mice, but not in other HPS or control mice.

Lysosomal and Endoplasmic Reticulum Stress Underlie AECII Apoptosis in HPS1/2 Mice

Observations to this point indicated that intracellular accumulation of surfactant was especially prominent in HPS1/2 mice and possibly related to the increased apoptosis of AECII, thus favoring fibrosis development in HPS1/2 double-mutants. To further study the pathways that may interconnect surfactant accumulation and AECII apoptosis in HPS1/2 mice, it was hypothesized that such surfactant accumulation may cause primarily lysosomal stress in these mice. Therefore, a well-known lysosomal aspartyl protease, cathepsin D, which has been shown to induce apoptosis by several mechanisms (21, 22), was analyzed by Western blotting. Increased levels of procathepsin D (~44 kD), its glycosylated form (~54 kD), and

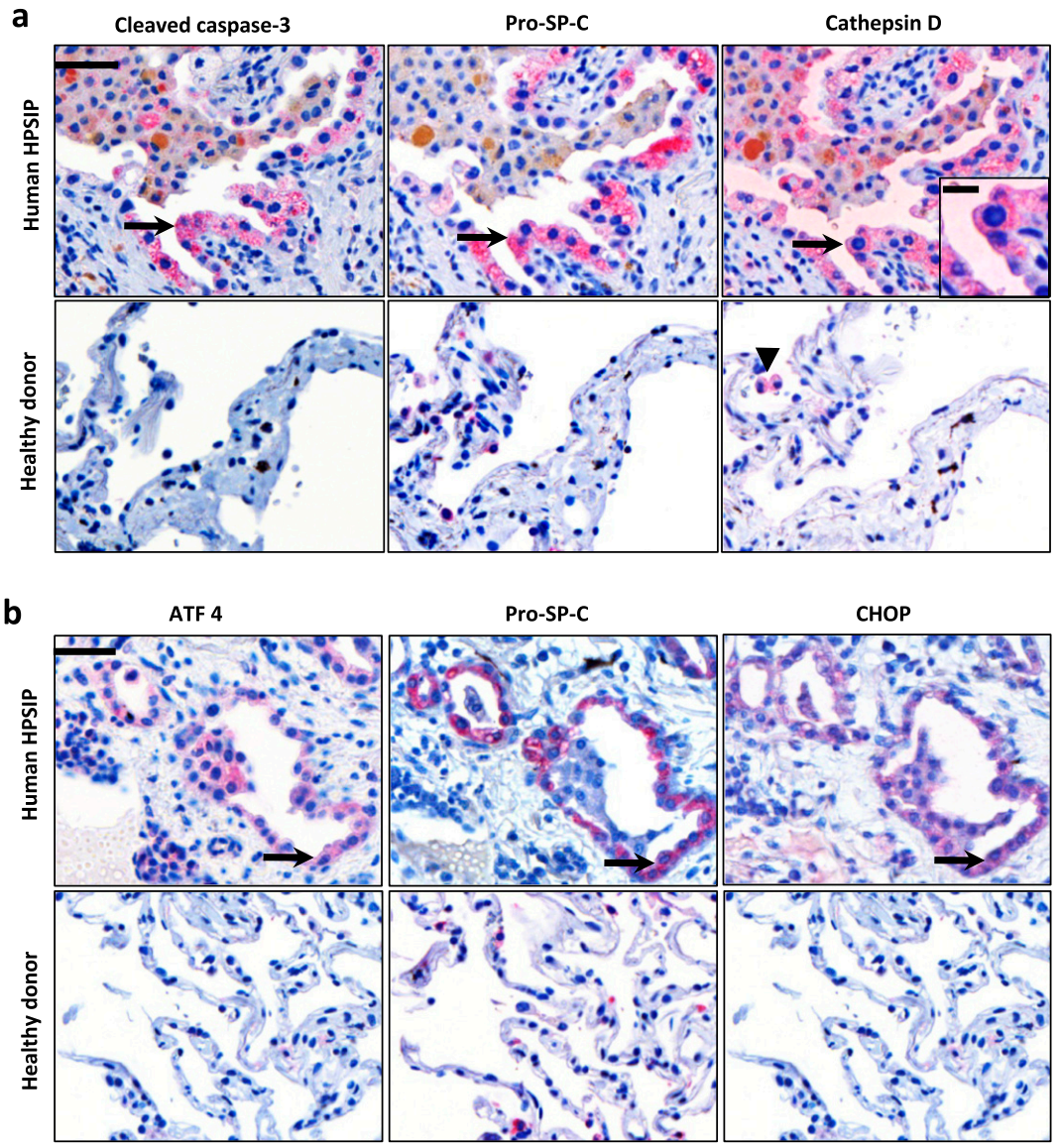

Figure 7. Apoptosis of alveolar epithelial type II cells (AECII) due to lysosomal and endoplasmic reticulum stress in human Hermansky-Pudlak syndrome–associated interstitial pneumonia (HPSIP): (*a*) Representative immunohistochemistry performed on serial paraffin-embedded lung tissue sections from (*top*) human patients with HPS and (*bottom*) healthy donors for (*left*) cleaved caspase-3, (*middle*) pro–surfactant protein (SP)-C, and (*right*) cathepsin D. *Arrows* indicate the same AECII stained for all three proteins. *Inset*: High-magnification image, illustrating diffuse cytoplasmic staining of cathepsin D within the AECII of HPSIP. *Arrowhead* indicates cathepsin D staining in macrophages in a lung tissue section of a healthy donor. (*b*) Serial lung tissue sections from (*top*) human patients with HPS and (*bottom*) healthy donors were stained for (*left*) activating transcription factor-4 (ATF4), (*middle*) pro–SP-C, or (*right*) C/EBP homologous protein (CHOP). *Arrows* indicate positive staining of an AECII for all three proteins. Representative sections from patients with HPS1 and four healthy donors are shown. Original magnification, ×400 (*scale bar*, 50 μm). Original magnification of *inset*, ×800 (scale bar, 20 μm).

subsequent cleavage products were observed in lung homogenates of 3- and 9-month-old HPS1/2 mice and in the AECII of 3-month-old HPS1/2 mice when compared with respective controls (Figures 6c and 6d). Interestingly, cathepsin D levels in lung homogenates of all other HPS mice were found to be virtually identical (*see* Figures E5a–E5c in the online supplement). Cathepsin D gene expression in HPS1/2 mice, however, did not differ from controls (Figure E5d). In colocalization studies employing immunohistochemistry for cathepsin D, cleaved caspase-3, and pro–SP-C on serial sections, we identified all three proteins on identical regions in HPS1/2 lungs (Figure 6e) with a pan-cytoplasmic distribution pattern for cathepsin D (inset in Figure 6e).

Apart from the lysosomal stress response, the possible existence of an endoplasmic reticulum (ER) stress response was also assessed in HPS mice. For this purpose, the late ER stress marker C/EBP homologous protein (CHOP; GADD153), which represents an obligatory and important proapoptotic ER stress compound, as well as activating transcription factor-4 (ATF4), which serves as a direct transcription factor for CHOP, were studied. Western blot analysis using lung homogenates revealed an up-regulation of both proteins in HPS1/2 mice, at the age of 9 months (Figure 6f) but not at an age of 3 months (data not shown). To check whether the ATF4 and CHOP signals of lung homogenates originate from AECII, immunohistochemistry of ATF4, CHOP, and pro–SP-C was performed on serial sections. Interestingly, these stainings illustrated that pro–SP-C–positive cells stained positive for ATF4 and CHOP in lung sections from 9-month-old HPS1/2 mice, whereas control mouse sections showed no positivity (Figure 6g), thus indicating that AECII from HPS1/2 mice undergo ER stress during a later stage of the disease.

AECII Apoptosis Due to Lysosomal and ER Stress Is Also a Prominent Finding in Human HPSIP

Lysosomal and ER stress pathways were characterized in human HPSIP. Lack of frozen lung material from transplanted human patients with HPS restricted the current work to available serial lung sections from paraffin-embedded lung tissues from only two patients with HPS, on which immunohistochemistry was performed. Interestingly, AECII from patients with HPSIP not only showed much more pronounced reactivity for pro–SP-C as compared with donor lungs, but also showed positive staining for both cleaved caspase-3 and cathepsin D

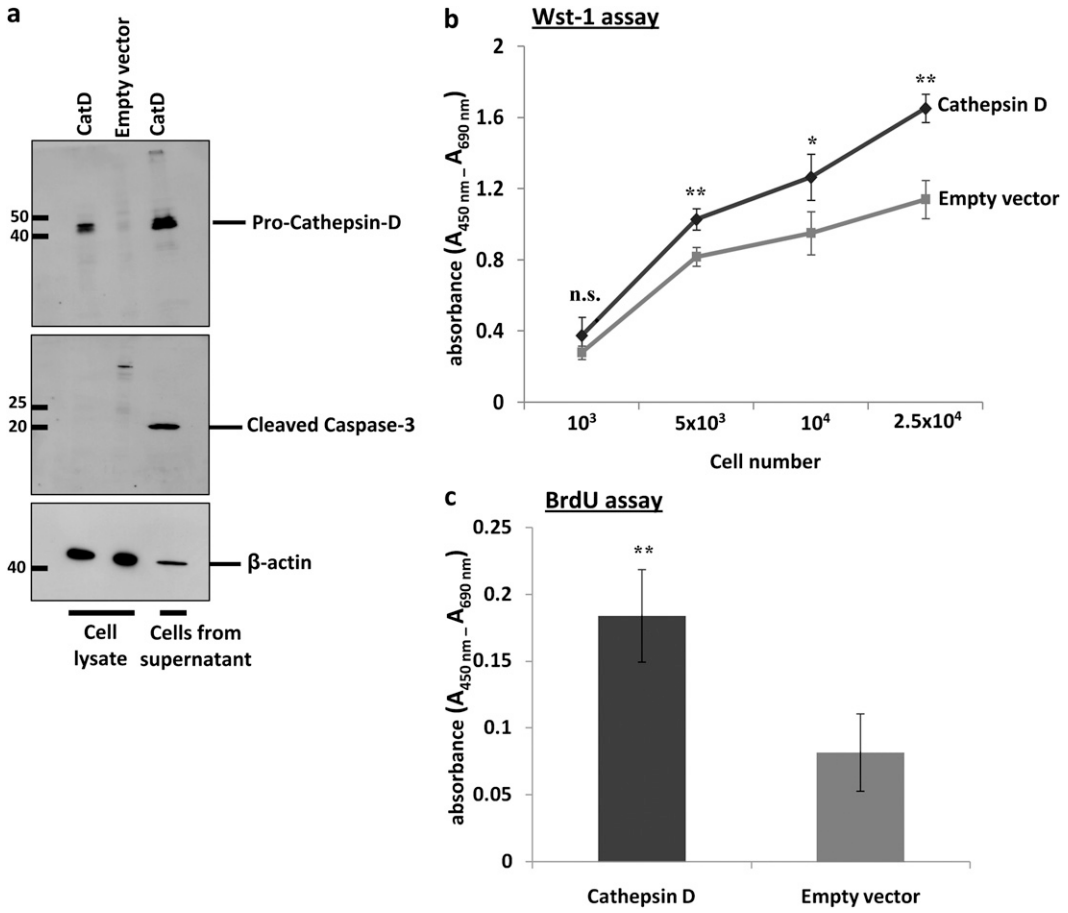

Figure 8. Overexpression of cathepsin D (CatD) drives apoptosis of an alveolar epithelial cell line and proliferation of fibroblasts: (*a*) Total protein extracts prepared from cathepsin D– and empty vector–transfected mouse lung epithelial (MLE)-12 cells as well as cells collected from supernatant after cathepsin D transfection (after 24 h) were subjected to Western blotting for (*top*) cathepsin D and for (*middle*) cleaved caspase-3, with equal protein loading (β-actin, *bottom*). Supernatant from cells transfected with empty vector did not contain enough cells (protein) to be included. (*b* and *c*) Conditioned medium from either cathepsin D– or empty vector–transfected MLE-12 cells was applied to an equal number of NIH 3T3 fibroblasts and their viability was assessed by (*b*) water-soluble tetrazolium salt (WST)-1 assay at various cell numbers or their proliferation was measured by (*c*) bromodeoxyuridine (BrdU) incorporation. $*P < 0.05$, $**P < 0.01$; n.s. = not significant.

(Figure 7a), thus fully confirming the data observed in the elder and fibrotic HPS1/2 mice. Diffuse cytoplasmic staining for cathepsin D within AECII was also observed in lung sections of HPSIP (inset in Figure 7a). Of interest, in healthy lung tissues from mice (Figure 6e) and humans (Figure 7a) cathepsin D staining was observed primarily in alveolar macrophages but not in AECII, again underscoring the significance of the observed increase in cathepsin D in AECII under conditions of HPSIP. In addition, we investigated the expression of the proapoptotic ER stress factor CHOP and its transcription factor ATF4 in human HPSIP. As depicted in Figure 7b, immunoreactivity for CHOP and ATF4 was found in AECII of HPSIP lungs, but not of donor lungs, again providing evidence for a proapoptotic ER stress response in the AECII of these patients.

Cathepsin D Promotes Apoptosis of Alveolar Epithelial Cell Line and Fibroblast Proliferation

In addition, to assess the causative role of cathepsin D overexpression in alveolar epithelial cell apoptosis and its role in fibroblast proliferation, we overexpressed full-length mouse cathepsin D in AECII-like MLE-12 cells. By analysis of cleaved caspase-3, we observed significant cell death in cathepsin D–transfected cells, as compared with empty vector–transfected cells (Figure 8a). These cells were largely detached from the culture plate, 24 hours posttransfection. Conditioned medium from cathepsin D–transfected cells was then applied on NIH 3T3 fibroblasts and this resulted in increased viability and proliferation, as measured by WST-1 assay (Figure 8b) and BrdU incorporation (Figure 8c), respectively. Incubation of NIH 3T3 fibroblasts with conditioned medium from empty vector–transfected cells resulted in a significantly depressed proliferative signal.

DISCUSSION

In patients with HPS, impaired lysosomal trafficking axis causes a complex spectrum of cell- and organ-specific disturbances, including severe pulmonary fibrosis in a larger subpopulation of patients with HPS1 and HPS4 mutations. Another entity caused by disturbed lysosomal transport is the Chédiak-Higashi syndrome (CHS), a bleeding disorder with severe and recurrent infections. In murine models of CHS (beige mice with a mutation in lysosomal trafficking regulator lyst1 [23], and chocolate mice with a rab38 mutation [24]), increased cellularity and modest interstitial inflammation have been described (23, 24), and emphysema was a prominent finding in HPS1/2 (12). In chocolate mice and in HPS1/2 mice, accumulation of mature surfactant components and giant lamellar body degeneration have been described to various extents. However, this is the first study to show spontaneous development of lung fibrosis in a murine model of HPS, which fully mimicks clinical HPSIP.

An obvious explanation for phenotypic differences in different mouse models may be that, as compared with HPS1/2, in other models, the accumulation of intracellular surfactant levels may not have reached a critical threshold level to induce chronic cellular stress and AECII apoptosis. In line with this, beige mice exhibit modest PC (~1.5-fold) and SP-B accumulation in lung homogenates, a slight reduction of SP-B in BALF at 24 weeks, and only a twofold increase in disaturated PC in adulthood (25). Regarding the surfactant pool size in tissue and

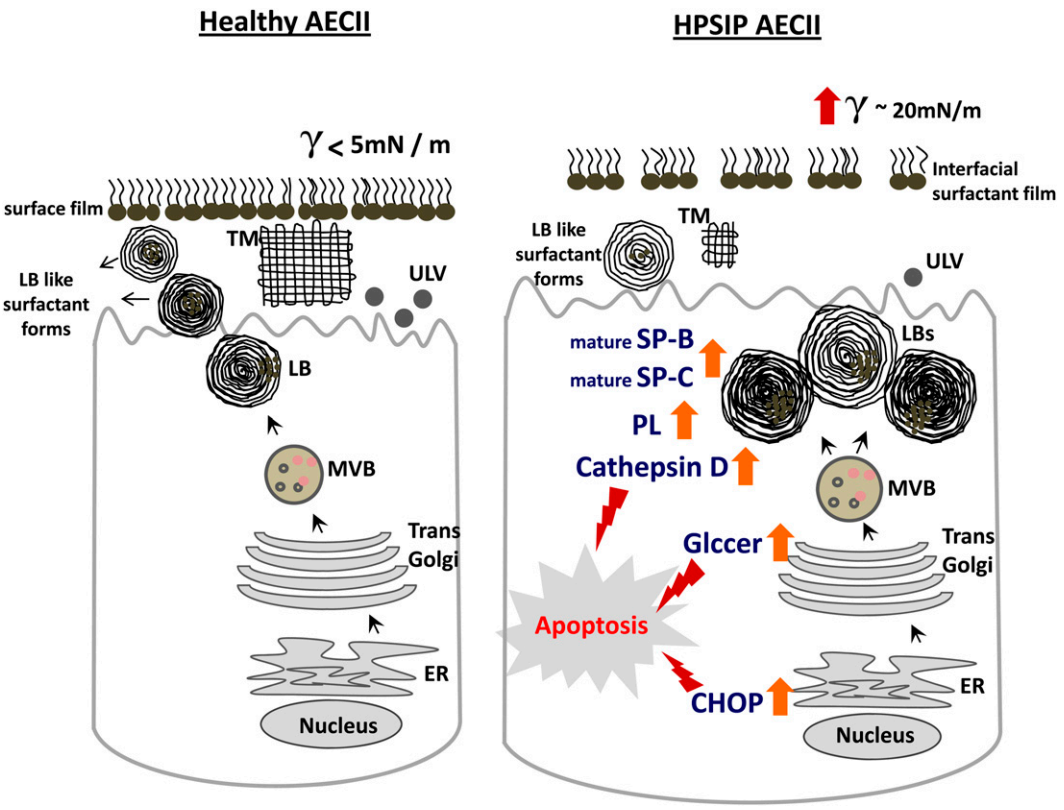

Figure 9. Proposed model for induction of apoptosis of alveolar epithelial cells type II (AECII) in Hermansky-Pudlak syndrome–associated interstitial pneumonia (HPSIP) lungs: On the *left*, a healthy AECII is shown, with regular surfactant processing, transport, and secretion. On the *right*, our data on HPSIP are summarized, in which giant lamellar bodies, defective surfactant transport, and impaired secretion of surfactant are shown. Alveolar surface tension in HPSIP lungs is increased, indicating the reduced surface activity of the alveolar surfactant pool in these lungs. Within the AECII, an increase in cathepsin D, glucosylceramides, and CHOP-induced apoptosis of the cell may result in the development of lung fibrosis. CHOP = C/EBP homologous protein; ER = endoplasmic reticulum; Glccer = glucosylceramides; LBs = lamellar bodies; MVB = multivesicular bodies; PL = phospholipids; SP = surfactant protein; TM = tubular myelin; ULV = unilamellar vesicles.

airspace enlargement, these mice are thus comparable to HPS1, HPS2, HPS6, and HPS1/6 mice (26), but they do not seem to develop fibrosis. Several factors may contribute to the development of lung fibrosis exclusively in HPS1/2.

First, activation of macrophages and elevation of basal inflammatory cytokine levels, as reported for HPS1 and HPS2 mice (23, 27), may also support fibrotic reactions. Indeed, macrophage activation has also been described in patients with HPS1 mutations (28). On the other hand, with the exception of altered morphology of macrophages (data not shown), our HPS1/2 mice did not show a significantly different differential cell count as compared with the other genotypes. Although such assessment is certainly incomplete, it does not suggest a substantially different level of inflammatory changes between mice that develop fibrosis and those that do not.

Second, changes in the extracellular surfactant pool may contribute to the development of lung fibrosis. In HPS1/2 mice, we now observed greatly increased alveolar surface tension paralleled by a far-reaching absence of both hydrophobic surfactant proteins, most likely reflecting the severity of the intracellular transport deficiency. In contrast, although also almost deficient in SP-B at the alveolar level, HPS1/6 mice still had reasonably high amounts of SP-C in the alveolar space and, accordingly, normal surface tension–reducing characteristics of the alveolar surfactant film. At a quick glance, such an observation may place SP-C at the center of a pathomechanistic concept, especially bearing in mind that SP-C may well play a role in maintaining lung mechanics (as suggested with SP-C$^{-/-}$ mice [29]). However, we believe that the loss of surface activity in HPS1/2 mice is more simply related to the simultaneous loss of SP-B and SP-C at the alveolar level, a feature well known from term babies with respiratory distress, in whom a complete (no gene expression) loss of SP-B and a functional (no processing of pro–SP-C) loss of SP-C are encountered (30). At present, we certainly cannot exclude a pathomechanistic role of the increased alveolar surface tension in the process of lung fibrosis, especially when keeping in mind the role of biomechanical forces in fibroblast activation (31). Further experiments are needed to precisely define the role of elevated alveolar surface tension, a common feature in, for example, subjects with IPF (32), in the development of lung fibrosis.

Third and, from our understanding, most importantly, an intriguing interpretation of our data and those of others is that the observed accumulation of mature and intermediate surfactant compounds in AECII may be of potential harm for this cell type and that—depending on the cellular stress level—airspace enlargement or lung fibrosis may represent the phenotypic consequences. Such an idea is supported by our observation that conditioned medium from cathepsin D–transfected epithelial cells, which are prone to apoptosis, promotes fibroblast proliferation.

In contrast to mice, in which HPSIP is provoked only by a double hit affecting both HPS1 and HPS2 (33), single mutation of HPS1 or HPS4 in humans resulted in HPSIP (4, 34, 35). In higher eukaryotes, HPS1 and HPS4 encode BLOC (biogenesis of lysosomal-related organelle complex)-3 (36), which was suggested to regulate endosomal and lysosomal movements by microtubule- and actin-dependent mechanisms (37–39). Adaptor protein (AP)-3 is affected in HPS2 and has been suggested to play a role in transporting selected proteins from *trans*-Golgi to lysosomes, endosomes, or lysosome-related organelles and was shown to form a tripartite complex with BLOC-1 and phosphatidylinositol-4-kinase type II α (PI4KIIa) (40). Interestingly, one study showed anatomically different AP-3–regulatory mechanisms in brain (41). It is also known to directly interact with some other HPS gene products (but never with BLOC-3) and cellular factors involved in lysosomal trans-

port and secretion (42, 43). Similarly, in samples from patients with HPS1 mutations, the intracellular localization of the AP-3 complex remained unaltered in fibroblasts (44, 45). Drawn against this background and observations by Feng and colleagues (46), it appears highly unlikely that AP-3 directly interacts with HPS1/BLOC-3, although these studies have never been performed in active secretory cells in general and in AECII in particular. Of note, in HPS1/2 mice, cumulative accumulation of lysosomal enzymes (β-glucuronidase, β-galactosidase) in lungs and kidneys again supports the concept of a functional redundancy of HPS1 and HPS2 in surfactant trafficking (46). Hence, only if both complexes are affected in parallel will extensive accumulation of surfactant, cell stress, and apoptosis occur, leading to fibrosis in mice (Figure 9). Although unclear at present, a lack of functional redundancy between BLOC-3 and AP-3 in humans could be a potential explanation for the development of HPSIP with single BLOC-3 or AP-3 mutations.

Another explanation for all these differences between mice and humans could involve environmental (e.g., smoking) or medical factors. Regarding the latter, steroids and β-mimetics, agents that may be frequently used in subjects with HPSIP, may in fact increase surfactant expression and production and aggravate the level of intracellular stress (47).

In general, HPS proteins were suggested to be responsible for (*1*) cargo sorting and transport vesicle formation, (*2*) movement of transport carriers across the cytoskeletal axis, and (*3*) tethering, docking, and fusion of vesicles at the target membrane (48). In view of the herein described accumulation of mature surfactant compounds in HPS1/2, it appears likely that the biosynthetic surfactant pathway is affected more in the distal part, starting at the level of the multivesicular body (MVB; Figure 9), as it is well known that the MVB is the earliest lysosomal organelle in which maturation of SP-B/C occurs. The inability of isolated AECII from HPS1/2 mice to adequately secrete surfactant even in response to ATP (13) lends credence to the assumption that a more distal transport process is altered in HPS1/2 mice.

Consistent with such reasoning, we observed an early lysosomal stress reaction in HPS1/2 mice, characterized by a significant increase in cathepsin D levels in AECII. Although representing a normal lysosomal constituent, cathepsin D potentially induces apoptosis in many cell types (21, 22) via different mechanisms (49–51). Supporting this view, in the present study, we observed apoptosis of MLE-12 cells in response to overexpression of cathepsin D, and increased proliferation of fibroblasts when incubated with conditioned medium from cathepsin D–transfected cells. These observations fully corroborate our findings in HPS mice and human samples, in which highly increased levels of cathepsin D were observed in AECII, signifying its prominent role in the development of HPSIP. The development of AECII apoptosis and lung fibrosis in HPS1/2 mice was further strengthened by lipidomic profiling of lung tissue, particularly with a significant increase in glucosylceramides. In fibroblasts isolated from patients with Gaucher's disease, such an accumulation of GlcCer was found to cause oxidative stress and apoptosis (52). Moreover, accumulation of gangliosides (gangliosidosis) or sphingomyelin (Niemann-Pick disease) were shown to provoke the unfolded protein response, causing neuronal death (53, 54). In line with such reasoning, a severe ER stress response had been previously shown to be the primary cellular consequence of mutations of the *SFTPC* gene (55), a rare reason for development of familial forms of idiopathic interstitial pneumonias. Mutations in the BRICHOS domain of the carboxy-terminal part of pro–SP-C resulted in misfolding and accumulation of the proprotein, finally also leading to induction of ER stress and AECII apoptosis (55, 56). Furthermore, severe ER stress, with the induction of ATF4 and activation of the apoptosis mediator CHOP, was observed in HPSIP (both in mice and humans) in our study, similar to previous studies by our group in patients with sporadic IPF (57). This ER stress response in HPSIP could be due to increasing amounts of accumulating SP-B/C or retrograde stacking of lysosomal surfactant compounds into the ER. In any case, such additional ER stress adds further to the lysosomal stress–induced AECII apoptosis. Drawn against observations in IPF, these data suggest that apoptosis of alveolar epithelium due to chronic lysosomal/ER stress indeed represents a common observation in HPSIP (Figure 9) and a pivotal event in the evolution of lung fibrosis in general. ER stress has been implicated in many diseases such as Alzheimer's disease, diabetes, Parkinson disease, and, more recently, also in chronic obstructive pulmonary disease (58, 59). Increasing evidence suggests that certain chemical chaperons such as sodium 4-phenyl butyrate or butylated hydroxyanisole (which is also an antioxidant) may help to dampen the unfolded protein response, thereby preventing cells from undergoing ER stress–induced apoptosis (60, 61). As an attempt to rescue AECII from ER stress–induced cell death in HPSIP, use of similar agents may be discussed, but their ability to also circumvent lysosomal stress, the primary injurious event in HPSIP to AECII, has yet to be investigated.

Regarding the clinical similarities of IPF and HPSIP, it is an intriguing thought that the herein identified HPS1/2 mice would represent a much better model as compared with the widely used bleomycin model, in which excessive inflammation before the onset of lung fibrosis and its cessation after several weeks of bleomycin challenge are ascertained drawbacks. Lack of effective treatment for IPF or HPSIP makes HPS1/2 mice a more admissible murine fibrosis model.

Conflict of Interest Statement: P.M. does not have a financial relationship with a commercial entity that has an interest in the subject of this manuscript; M.K. does not have a financial relationship with a commercial entity that has an interest in the subject of this manuscript; I.H. does not have a financial relationship with a commercial entity that has an interest in the subject of this manuscript; G.L. does not have a financial relationship with a commercial entity that has an interest in the subject of this manuscript; G.S. does not have a financial relationship with a commercial entity that has an interest in the subject of this manuscript; B.R.C. holds $10,001–$50,000 in stock ownership or options in a health care sector mutual fund; P.M. does not have a financial relationship with a commercial entity that has an interest in the subject of this manuscript; S.B. does not have a financial relationship with a commercial entity that has an interest in the subject of this manuscript; W.S. does not have a financial relationship with a commercial entity that has an interest in the subject of this manuscript; C.R. received up to $1,000 from GlaxoSmithKline in consultancy fees; A.G. received $1,001–$5,000 from GlaxoSmithKline, $1,001–$5,000 from Actelion, $1,001–$5,000 from Activaero, and $10,001–$50,000 from Nycomed in advisory board fees, and $1,001–$5,000 from Actelion in lecture fees.

Acknowledgment: The authors thank Dr. Tim Weaver for helpful comments and criticism. The authors also thank Benjamin Loeh for technical assistance.

References

1. Hermansky F, Pudlak P. Albinism associated with hemorrhagic diathesis and unusual pigmented reticular cells in the bone marrow: report of two cases with histochemical studies. *Blood* 1959;14:162–169.
2. Li W, Rusiniak ME, Chintala S, Gautam R, Novak EK, Swank RT. Murine Hermansky-Pudlak syndrome genes: regulators of lysosome-related organelles. *Bioessays* 2004;26:616–628.
3. Huizing M, Gahl WA. Disorders of vesicles of lysosomal lineage: the Hermansky-Pudlak syndromes. *Curr Mol Med* 2002;2:451–467.
4. Anderson PD, Huizing M, Claassen DA, White J, Gahl WA. Hermansky-Pudlak syndrome type 4 (HPS-4): clinical and molecular characteristics. *Hum Genet* 2003;113:10–17.
5. Wei ML. Hermansky-Pudlak syndrome: a disease of protein trafficking and organelle function. *Pigment Cell Res* 2006;19:19–42.
6. Gahl WA, Brantly M, Troendle J, Avila NA, Padua A, Montalvo C, Cardona H, Calis KA, Gochuico B. Effect of pirfenidone on the

pulmonary fibrosis of Hermansky-Pudlak syndrome. *Mol Genet Metab* 2002;76:234–242.
7. Garay SM, Gardella JE, Fazzini EP, Goldring RM. Hermansky-Pudlak syndrome: pulmonary manifestations of a ceroid storage disorder. *Am J Med* 1979;66:737–747.
8. Harmon KR, Witkop CJ, White JG, King RA, Peterson M, Moore D, Tashijian J, Marinelli A, Bitterman PB. Pathogenesis of pulmonary fibrosis: platelet-derived growth factor precedes structural alterations in the Hermansky-Pudlak syndrome. *J Lab Clin Med* 1994;123:617–627.
9. Reynolds SP, Davies BH, Gibbs AR. Diffuse pulmonary fibrosis and HPS. *Thorax* 1994;49:617–618.
10. Nakatani Y, Nakamura N, Sano J, Inayama Y, Kawano N, Yamanaka S, Miyagi Y, Nagashima Y, Ohbayashi C, Mizushima M, *et al.* Interstitial pneumonia in Hermansky-Pudlak syndrome: significance of florid foamy swelling/degeneration (giant lamellar body degeneration) of type II pneumocytes. *Virchows Arch* 2002;437:304–313.
11. Pierson DM, Ionescu D, Qing G, Yonan AM, Parkinson K, Colby TC, Leslie K. Pulmonary fibrosis in Hermansky Pudlak syndrome: a case report. *Respiration* 2000;73:382–395.
12. Lyerla TA, Rusiniak ME, Borchers M, Jahreis G, Tan J, Ohtake P, Novak EK, Swank RT. Aberrant lung structure, composition, and function in a murine model of Hermansky-Pudlak syndrome. *Am J Physiol Lung Cell Mol Physiol* 2003;285:L643–L653.
13. Guttentag SH, Akhtar A, Tao JQ, Atochina E, Rusiniak ME, Swank RT, Bates SR. Defective surfactant secretion in a mouse model of Hermansky-Pudlak syndrome. *Am J Respir Cell Mol Biol* 2005;33:14–21.
14. Mahavadi P, Korfei M, Ruppert C, Seeger W, Guenther A. Evidence of surfactant accumulation and type II pneumocyte apoptosis in Hermansky-Pudlak syndrome [abstract]. *Am J Respir Crit Care Med* 2008;177:A823.
15. Mahavadi P, Korfei M, Markart P, Schmidt R, Seeger W, Guenther A, Ruppert C. Altered post-translational processing of pulmonary surfactant components in a murine model of Hermansky-Pudlak syndrome [abstract]. *Am J Respir Crit Care Med* 2006;3:A192.
16. Woessner JF. Determination of hydroxyproline in tissue and protein samples containing small proportions of this imino acid. *Arch Biochem Biophys* 1961;93:440.
17. Brasch F, Johnen G, Brasch AW, Guttentag SH, Schmiedl A, Kapp N, Suzuki Y, Müller KM, Richter J, Hawgood S, *et al.* Surfactant protein B in type II pneumocytes and intra-alveolar surfactant forms of human lungs. *Am J Respir Cell Mol Biol* 2004;30:449–458.
18. Brasch M, Brinke AT, Johnen G, Ochs M, Kapp N, Müller KM, Beers MF, Fehrenbach H, Richter J, Batenburg JJ, *et al.* Involvement of cathepsin H in the processing of the hydrophobic surfactant-associated protein C in type II pneumocytes. *Am J Respir Cell Mol Biol* 2002;26:659–670.
19. Ihrke G, Kyttala A, Russel MRG, Rous BA, Luzio JP. Differential use of two AP-3 mediated pathways by lysosomal membrane proteins. *Traffic* 2004;5:946–962.
20. Richmond B, Huizung M, Knapp J, Koshoffer A, Zhao Y, Gahl WA, Boissy RE. Melanocytes derived from patients with Hermansky-Pudlak syndrome types 1, 2 and 3 have distinct defects in cargo trafficking. *J Invest Dermatol* 2005;124:420–427.
21. Minarowska A, Miarowski L, Karwowska A, Gacko M. Regulatory role of cathepsin D in apoptosis. *Folia Histochem Cytobiol* 2007;45:159–163.
22. Kaedgal K, Johansson U, Oellinger K. The lysosomal protease cathepsin D mediates apoptosis induced by oxidative stress. *FASEB J* 2001;15:1592–1594.
23. Tang X, Yamanaka S, Miyagi Y, Nagashima Y, Nakatani Y. Lung pathology of pale ear mouse (model of Hermansky-Pudlak syndrome 1) and beige mouse (model of Chediak-Higashi syndrome): severity of giant lamellar body degeneration of type II pneumocytes correlates with interstitial inflammation. *Pathol Int* 2005;55:137–143.
24. Osanai K, Oikawa R, Higuchi J, Kobayashi M, Tsuchihara K, Iguchi M, Jongsu H, Toga H, Voelker DR. A mutation in Rab38 small GTPase causes abnormal lung surfactant homeostasis and aberrant alveolar structure in mice. *Am J Pathol* 2008;173:1265–1274.
25. Prueitt JL, Chi EY, Lagunoff D. Pulmonary surface-active materials in the Chediak-Higashi syndrome. *J Lipid Res* 1978;19:410–415.
26. McGarry MP, Reddington M, Novak EK, Swank RT. Survival and lung pathology of mouse models of Hermansky-Pudlak syndrome and Chediak-Higashi syndrome. *Proc Soc Exp Biol Med* 2003;220:162–168.
27. Young LR, Borchers MT, Allen HL, Gibbons RS, McCormack FX. Lung-restricted macrophage activation in the pearl mouse model of Hermansky-Pudlak syndrome. *J Immunol* 2006;176:4361–4368.
28. Raouhani FN, Brantly ML, Markello TC, Helip-Wooley A, O'Brien K, Hess R, Huizung M, Gahl WA, Gochuico BR. Alveolar macrophage dysregulation in Hermansky-Pudlak syndrome type 1. *Am J Respir Crit Care Med* 2009;180:1114–1121.
29. Glasser SW, Burhans MS, Korfhagen TR, Na CL, Sly PD, Ross GF, Ikegami M, Whitsett JA. Altered stability of pulmonary surfactant in SP-C–deficient mice. *Proc Natl Acad Sci USA* 2001;98:6366–6371.
30. Nogee LM. Alterations in SP-B and SP-C expression in neonatal lung disease. *Annu Rev Physiol* 2004;66:601–623.
31. Follonier L, Schaub S, Meister JJ, Hinz B. Myofibroblast communication is controlled by intercellular mechanical coupling. *J Cell Sci* 2008;121:3305–3316.
32. Guenther A, Schmidt R, Nix F, Yabut-Perez M, Guth C, Rosseau S, Siebert C, Grimminger F, Morr H, Velcovsky HG, *et al.* Surfactant abnormalities in idiopathic pulmonary fibrosis, hypersensitivity pneumonitis and sarcoidosis. *Eur Respir J* 1999;14:565–573.
33. Young LR, Pasula R, Gulleman PM, Deutsch GH, McCormack FX. Susceptibility of Hermansky-Pudlak mice to bleomycin-induced type II cell apoptosis and fibrosis. *Am J Respir Cell Mol Biol* 2007;37:67–74.
34. Suzuki T, Li W, Zhang Q, Karim A, Novak EK, Sviderskaya EV, Hill SP, Bennett DC, Levin AV, Nieuwenhuis HK, *et al.* Hermansky-Pudlak syndrome is caused by mutations in *HPS4*, the human homolog of the mouse light-ear gene. *Nat Genet* 2002;30:321–324.
35. Chiang PW, Oiso N, Gautam R, Suzuki T, Swank RT, Spritz RA. The Hermansky Pudlak syndrome 1 (HPS1) and HPS4 proteins are components of two complexes, BLOC 3 and BLOC 4. *J Biol Chem* 2003;278:20332–20337.
36. Nazarian R, Falcón-Pérez JM, Dell'Angelica EC. Biogenesis of lysosome-related organelles complex-3 (BLOC3): a complex containing the Hermansky-Pudlak syndrome (HPS) proteins, HPS1 and HPS4. *Proc Natl Acad Sci USA* 2003;100:8770–8775.
37. Falcón-Pérez JM, Nazarian R, Sabatti C, Dell'Angelica EC. Distribution and dynamics of Lamp1-containing endocytic organelles in fibroblasts deficient in BLOC-3. *J Cell Sci* 2005;118:5243–5255.
38. Dell'Angelica EC. The building BLOC(k)s of lysosomes and related organelles. *Curr Opin Cell Biol* 2004;16:458–464.
39. Kloer DP, Rojas R, Ivan V, Moriyama K. vanVlijmen T, Murthy N, Ghirlando R, van der Sluijs P, Hurley JH, Bonifacino JS. Assembly of the biogenesis of lysosome-related organelles complex-3 (BLOC-3) and its interaction with Rab9. *J Biol Chem* 2010;285:7794–7804.
40. Salazar G, Zlatic S, Craige B, Peden AA, Pohl J, Faundez V. Hermansky-Pudlak syndrome protein complexes associate with PI4 kinase type IIα in neuronal and nonneuronal cells. *J Biol Chem* 2009;284:1790–1802.
41. Newell-Litwa K, Chintala S, Jenkins S, Pare JF, McGha L, Smith Y, Faundez V. Hermansky-Pudlak protein complexes, AP-3 and BLOC-1, differentially regulate presynaptic composition in the striatum and hippocampus. *J Neurosci* 2010;30:820–831.
42. Litwa KN, Seong E, Burmeister M, Faundez V. Neuronal and non-neuronal functions of the AP-3 sorting machinery. *J Cell Sci* 2007;120:531–541.
43. Harrison-Lavoie KJ, Michaux G, Hewlett L, Kaur J, Hannah MJ, Lui-Roberts WW, Norman KE, Cutler DF. P-selectin and CD63 use different mechanisms for delivery to Weibel-Palade bodies. *Traffic* 2006;7:647–662.
44. Dell'Angelica EC, Shotelersuk V, Aguilar RC, Gahl WA, Bonifacino JS. Altered trafficking of lysosomal proteins in Hermansky-Pudlak syndrome due to mutations in β3A subunit of AP-3 adaptor. *Mol Cell* 1999;3:11–21.
45. Dell'Angelica EC, Augilar RC, Wolins N, Hazelwood S, Gahl WA, Bonifacino JS. Molecular characterization of the protein encoded by the Hermansky-Pudlak syndrome type 1 gene. *J Biol Chem* 2000;275:1300–1306.
46. Feng L, Novak EK, Hartnell LM, Bonifacino JS, Collinson LM, Swank RT. The Hermansky-Pudlak syndrome 1 (HPS1) and HPS2 genes independently contribute to the production and function of platelet dense granules. *Blood* 2002;99:1651–1658.
47. Kristova V, Canova R. Pulmonary surfactant: properties, relation to the respiratory distress syndrome in neonates and possibilities of its prevention and therapy. *Bratisl Lek Listy (Tlacene Vyd)* 1992;93:41–49.
48. Olkkonen VM, Ikonen E. When intracellular logistics fails: genetic defects in membrane trafficking. *J Cell Sci* 2006;119:5031–5045.
49. Baumgartner HK, Gerasimenko JV, Thorne C, Ashurst LH, Barrow SL, Chvanov MA, Gillies S, Criddle DN, Tepikin AV, Petersen OH, *et al.* Caspase-8–mediated apoptosis induced by oxidative stress is inde-

pendent of the intrinsic pathway and dependent on cathepsins. *Am J Physiol* 2007;293:G296.
50. Blomgran R, Zheng L, Stendahl O. Cathepsin-cleaved Bid promotes apoptosis in human neutrophils via oxidative stress–induced lysosomal membrane permeabilization. *J Leukoc Biol* 2007;81:1213–1223.
51. Li X, Rayford H, Shu R, Zhuang J, Uhal BD. Essential role for cathepsin D in bleomycin-induced apoptosis of alveolar epithelial cells. *Am J Physiol Lung Cell Mol Physiol* 2004;287:L46–L51.
52. Deganuto M, Pittis MG, Pines A, Dominissini S, Kelley MR, Garcia R, Quadrifoglio F, Bembi B, Tell G. Altered intracellular redox status in Gaucher disease fibroblasts and impairment of adaptive response against oxidative stress. *J Cell Physiol* 2007;212:223–235.
53. Kolter T, Sandhoff K. Sphingolipid metabolism diseases. *Biochim Biophys Acta* 2006;1758:2057–2079.
54. Tessitore A, Martin MD, Sano R, Ma Y, Mann L, Ingrassia A, Laywell ED, Steindler DA, Hendershot LM, d'Azzo A.G_{M1}-ganglioside–mediated activation of the unfolded protein response causes neuronal death in a neurodegenerative gangliosidosis. *Mol Cell* 2004;15:753–766.
55. Mulugeta S, Nguyen V, Russo SJ, Muniswamy M, Beers MF. A surfactant protein C precursor protein BRICHOS domain mutation causes endoplasmic reticulum stress, proteasome dysfunction, and caspase 3 activation. *Am J Respir Cell Mol Biol* 2005;32:521–530.
56. Wang WJ, Mulugeta S, Russo SJ, Beers MF. Deletion of exon 4 from human surfactant protein C results in aggresome formation and generation of a dominant negative. *J Cell Sci* 2003;116:683–692.
57. Korfei M, Ruppert C, Mahavadi P, Henneke I, Markart P, Koch M, Lang G, Fink L, Bohle RM, Seeger W, *et al.* Epithelial endoplasmic reticulum stress and apoptosis in sporadic idiopathic pulmonary fibrosis. *Am J Respir Crit Care Med* 2008;178:838–846.
58. Yoshida H. ER stress and diseases. *FEBS J* 2007;274:630–658.
59. Malhotra D, Thimmulappa R, Vij N, Navas-Acien A, Sussan T, Merali S, Zhang L, Kelsen SG, Myers A, Wise R, *et al.* Heightened endoplasmic reticulum stress in the lungs of patients with chronic obstructive pulmonary disease: the role of Nrf2-regulated proteasomal activity. *Am J Respir Crit Care Med* 2009;180:1196–1209.
60. Yam GH, Gaplovska-Kysela K, Zuber C, Roth J. Sodium 4-phenylbutyrate acts as a chemical chaperone on misfolded myocillin to rescue cells from endoplasmic reticulum stress and apoptosis. *Invest Ophthalmol Vis Sci* 2007;48:1683–1690.
61. Malhotra JD, Miao H, Zhang K, Wolfson A, Pennathur S, Pipe SW, Kaufman RJ. Antioxidants reduce endoplasmic reticulum stress and improve protein secretion. *Proc Natl Acad Sci USA* 2008;105:18525–18530.

Reprinted with permission of the American Thoracic Society.

Copyright © 2023 American Thoracic Society. All rights reserved.

Cite: Poornima Mahavadi, Martina Korfei, Ingrid Henneke, Gerhard Liebisch, Gerd Schmitz, Bernadette R. Gochuico, Philipp Markart, Saverio Bellusci, Werner Seeger, Clemens Ruppert, and Andreas Guenther/ 2010 / Epithelial Stress and Apoptosis Underlie Hermansky-Pudlak Syndrome–associated Interstitial Pneumonia / Am J Respir Crit Care Med. / Vol 182. / pp 207–219.

The American Journal of Respiratory and Critical Care Medicine is an official journal of the American Thoracic Society.

OXFORD
SOT | Society of Toxicology
www.toxsci.oxfordjournals.org

TOXICOLOGICAL SCIENCES, 142(1), 2014, 285–297

doi: 10.1093/toxsci/kfu177
Advance Access Publication Date: August 27, 2014

Altered Surfactant Homeostasis and Alveolar Epithelial Cell Stress in Amiodarone-Induced Lung Fibrosis

Poornima Mahavadi[*,†], Ingrid Henneke[*,†], Clemens Ruppert[*,†], Lars Knudsen[‡,§,¶], Shalini Venkatesan[*,†], Gerhard Liebisch[‖], Rachel C. Chambers[‖,‖‖], Matthias Ochs[‡,§,¶], Gerd Schmitz[‖,‖‖], Carlo Vancheri[‖‖‖,#], Werner Seeger[*,†,‖‖], Martina Korfei[*,†], and Andreas Guenther[*,†,‖‖,**]

[*]Department of Internal Medicine, Justus-Liebig-University Giessen, Germany, [†]Universities of Giessen and Marburg Lung Center (UGMLC), Member of the German Center for Lung Research (DZL), Giessen, Germany, [‡]Institute of Functional and Applied Anatomy, Hannover Medical School, Hannover, Germany, [§]Biomedical Research in Endstage and Obstructive Lung Disease Hannover (BREATH), Member of the German Center for Lung Research (DZL), Hannover, Germany, [¶]REBIRTH Cluster of Excellence, Hannover, Germany, [‖]Institute of Clinical Chemistry and Laboratory Medicine, University of Regensburg, Regensburg, Germany, [‖‖]Centre for Inflammation and Tissue Repair, UCL Respiratory, University College London, London, UK, [‖‖‖]Member of the European IPF Network, [#]Department of Clinical and Molecular Biomedicine, University of Catania, Catania 95123, Italy and [**]Lung Clinic Waldhof-Elgershausen, Greifenstein, Germany

[1]To whom correspondence should be addressed at Klinikstrasse 36, 35392, Giessen, Germany. Fax: +49-641-98542509. E-mail: Andreas.Guenther@innere.med.uni-giessen.de.

ABSTRACT

Amiodarone (AD) is a highly efficient antiarrhythmic drug with potentially serious side effects. Severe pulmonary toxicity is reported in patients receiving AD even at low doses and may cause interstitial pneumonia as well as lung fibrosis. Apoptosis of alveolar epithelial type II cells (AECII) has been suggested to play an important role in this disease. In the current study, we aimed to establish a murine model of AD-induced lung fibrosis and analyze surfactant homeostasis, lysosomal, and endoplasmic reticulum (ER) stress in this model. AD/vehicle was instilled intratracheally into C57BL/6 mice, which were sacrificed on days 7, 14, 21, and 28. Extent of lung fibrosis development was assessed by trichrome staining and hydroxyproline measurement. Cytotoxicity was assessed by lactate dehydrogenase assay. Phospholipids (PLs) were analyzed by mass spectrometry. Surfactant proteins (SP) and markers for apoptosis, lysosomal, and ER stress were studied by Western blotting and immunohistochemistry. AECII morphology was evaluated by electron microscopy. Extensive lung fibrosis and AECII hyperplasia were observed in AD-treated mice already at day 7. Surfactant PL and SP accumulated in AECII over time. In parallel, induction of apoptosis, lysosomal, and ER stress was encountered in AECII of mice lungs and in MLE12 cells treated with AD. *In vitro*, siRNA-mediated knockdown of cathepsin D did not alter the AD-induced apoptotic response. Our data suggest that mice exposed to intratracheal AD develop severe pulmonary fibrosis, exhibit extensive surfactant alterations and cellular stress, but AD-induced AECII apoptosis is not mediated primarily via cathepsin D.

Key words: amiodarone; surfactant; lung fibrosis; alveolar epithelial cell apoptosis; lysosomal stress; ER stress

© The Author 2014. Published by Oxford University Press on behalf of the Society of Toxicology.
All rights reserved. For permissions, please email: journals.permissions@oup.com

Downloaded from https://academic.oup.com/toxsci/article-abstract/142/1/285/1710567 by Universitaet Giessen user on 24 October 2019

Amiodarone (AD) is an iodinated benzofuran derivative and falls under the class III antiarrhythmic drugs. Although proven highly efficient in controlling cardiac arrhythmias, its clinical use is mainly limited by its adverse effects (Chang *et al.*, 2007; Okayasu *et al.*, 2006). Black box warnings of AD include hypo and hyper thyroidism, corneal micro deposits, dermatitis, symptomatic bradycardia, and most importantly, severe pulmonary toxicity (Chang *et al.*, 2007). The frequency of pulmonary toxicity in patient cohorts receiving high dose of AD (≥400 mg/day) has been estimated at 10–17%, with fatalities occurring in about 10% of cases with pulmonary toxicity (Ott *et al.*, 2003). Low dose of AD (200 mg/day) was believed to be relatively safe, but increasing evidence suggests the risk of pulmonary complications, especially lung fibrosis, even in low dosage treatment group of patients. Apart from pulmonary fibrosis, pneumonitis and acute respiratory distress syndrome (ARDS) are also well documented as potential side effects of AD (Chang *et al.*, 2007; Charles *et al.*, 2006). According to a statistical analysis published in 1999 (Connolly, 1999), AD accounted for 24.1% of the total antiarrhythmic prescriptions in 1998. But its usage has drastically increased in the last decade. After considering its risk factors, clinicians use AD to treat atrial fibrillation (in the absence of pre-excitation) when other agents are either contra-indicated or have failed (January *et al.*, 2014). More recently, follow-up drugs have been developed such as dronedarone, which has been suggested to cause less lung, liver, and thyroid toxicity (Zimetbaum, 2009). Unfortunately, dronedarone not only caused over-mortality in a group of patients with depressed left ventricular function (Kober *et al.*, 2008) but it also appeared to be less efficient in controlling atrial fibrillation in a head-to-head comparison study with AD (Le Heuzey *et al.*, 2010). For this reason AD still represents the preferred drug.

Pathogenic and molecular events underlying AD-induced pulmonary toxicity are not clearly settled but may include direct cytotoxicity (Ashrafian and Davey, 2001), excessive intracellular phospholipid (PL) accumulation (Martin *et al.*, 1989), alterations in the angiotensin signaling pathway (Uhal *et al.*, 2007), generation of oxidants (Sarma *et al.*, 1997), and inflammatory reactions (Wilson *et al.*, 1991). In fact, AD is toxic to several types of lung cells *in vitro* (Bargout *et al.*, 2000; Chiovato *et al.*, 1994). Apart from these, it is known that AD gets enriched in lysosomes (~500-fold as compared with serum) and causes accumulation of multilamellar bodies in the cytoplasm of various cell types (Somani *et al.*, 1987).

A murine model for AD-induced lung fibrosis has not been described, with the exception of one recent study where an alkaloid, neferine, was reported to exert protective effects in AD-treated mice (Niu *et al.*, 2013). However, a systematic analysis of the ongoing cellular stress mechanisms in mice in response to amiodarone treatment is missing. The purpose of this study is to establish a mouse model of AD-induced pulmonary fibrosis and systematically analyze the surfactant alterations, lysosomal, and endoplasmic reticulum (ER) stress in this model.

MATERIALS AND METHODS

Mice. Intratracheal administration of vehicle or amiodarone (0.8 mg/kg body weight, Sigma-Aldrich, Germany) was performed in C57BL/6 mice every fifth day as detailed in the online supplement. Altogether, 10 mice per each group were included. Mice were sacrificed according to standard lab procedures as described before (Mahavadi *et al.*, 2010). Both the University Animal Care Committee and the Federal Authorities for Animal Research of the Regierungspraesidium Giessen (Hessen, Germany) approved the study protocol.

Lung compliance, histology, and electron microscopy. Mice were subjected to lung compliance measurement as described in the online supplement. Mice were sacrificed 7 and 14 days after first AD or vehicle challenge for perfusion fixation. In order to represent the whole organ a systematic uniform sampling was performed. Tissue blocks designated to transmission electron microscopy were embedded in epoxy resin. Detailed protocols are described in the online supplement.

Biochemical analysis. PLs analysis and characterization of large surfactant aggregates (LAs) was undertaken as described before (Mahavadi *et al.*, 2010). Bronchoalveolar lavage (BAL)-derived LAs were isolated by highspeed centrifugation (48,000 × g, 1 h, 4°C, Sorvall centrifuge). LA preparations were re-assessed for PL content (as described in the online supplement) and related to the originally centrifuged amount of PLs (indicating the% of LA in the original BALF). Lipids were quantified by electrospray ionization–tandem mass spectrometry in positive ion mode (Mahavadi *et al.*, 2010). Lipid species were annotated according to the recently published proposal for shorthand notation of lipid structures that are derived from mass spectrometry (Liebisch *et al.*, 2013). Details about lactate dehydrogenase (LDH) assay, Western blot, immunohistochemistry, and source of antibodies are given in the online supplement.

Cell culture. Mouse lung epithelial cell lines (MLE12) were cultured as described before (Mahavadi *et al.*, 2010). Preparation of AD solution and protocols for immunofluorescence and siRNA transfection are given in the online supplement.

Statistics. All data are expressed as means ± SEM of at least five mice for *in vivo* studies. For *in vitro* experiments, three or more independent experiments were conducted for AD treatment and triplicate transfections were performed for siRNA studies. Statistical significance was assessed employing Mann-Whitney *U* test. Significance is indicated as $^{*}p < 0.5$, $^{**}p < 0.01$, $^{***}p < 0.001$.

RESULTS

Development of Lung Fibrosis in Mice after AD Treatment

C57/Bl6 mice treated intratracheally with AD employing a microsprayer displayed significantly lowered lung compliance as compared with the vehicle-treated mice (Fig. 1A). AD treatment resulted in a significant increase in lung hydroxyproline levels compared with the vehicle-treated mice (Fig. 1B), reaching significance at day 14. Septal thickening, patchy interstitial lung fibrosis, lymphoplasmacellular infiltration, extracellular matrix deposition, areas of dense fibrosis, and areas with roughly preserved lung structure with increased AECII size were observed in AD-treated mice, right from day 7 onward (Figs. 1C and 1D). Trichrome staining of lung sections confirmed increased collagen deposition by day 7 post AD treatment (Fig. 1E). Electron microscopy demonstrated fragmentation of the alveolar lining with denudation of the basal lamina as well as interstitial edema at day 7 (Fig. 1F), which was supported by the observation of increased lung wet weight following AD treatment (Supplementary fig. 1). At day 14, an increase in collagen fibrils within thickened septal wall tissue was the most prominent finding (Fig. 1F, Supplementary fig. 2). Differential cell counts revealed a modest neutrophilic alveolitis starting at day 7, which persisted over the entire observation period (Supplementary fig. 3).

Downloaded from https://academic.oup.com/toxsci/article-abstract/142/1/285/1710567 by Universitaet Giessen user on 24 October 2019

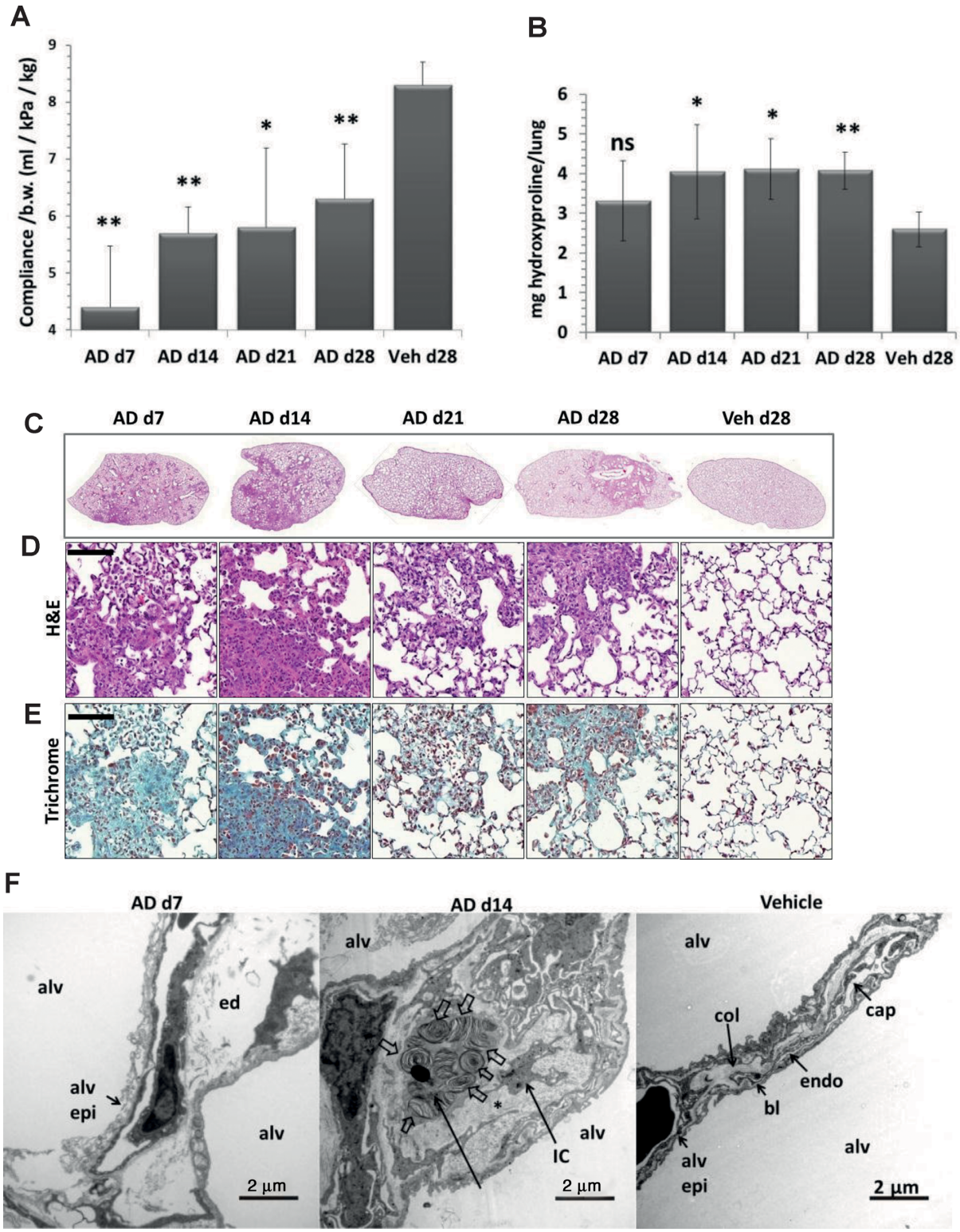

FIG. 1. Development of pulmonary fibrosis in AD-treated mice. (A) Graphical representation of dynamic lung compliance showing a significant decrease in AD-treated mice as compared with vehicle-treated controls. (B) Hydroxyproline measurement of total right lungs showing a significant increase in AD-treated mice as compared with vehicle-treated mice. (C–E) Representative H&E (C and D) and trichrome stainings (E) of complete left lungs (C) and higher magnification images (D, E) of days 7, 14, 21, and 28 AD and day 28 vehicle-treated mice showing patchy fibrosis in AD-treated mice. Scale = 100 µm, original magnification: ×200. (F) Representative transmission electron microscopic images: Fragmentation of the alveolar lining (alv epi) and denudation of basal lamina was a typical finding in d7 AD-treated mice. Interstitial edema (ed) is also visible. At d14, septal wall thickening was a consequence of deposition of collagen fibrils (asterisk) and interstitial cells (IC). Profiles of AECII containing lamellar bodies (block arrows) were observed within thickened septal walls. Vehicle-treated mice lungs showed no signs of injury or fibrosis; septal walls were slim and collagen (col) could be located on the "thick" side of the blood-gas barrier. The thin side consisted of alveolar epithelium (alv epi), basal lamina (bl), and endothelium (endo). Alv: alveolar airspace. Scale = 2 µm. $^{*}p < 0.5$, $^{**}p < 0.05$, $n = 5$ mice per group and three independent experiments were performed.

Downloaded from https://academic.oup.com/toxsci/article-abstract/142/1/285/1710567 by Universitaet Giessen user on 24 October 2019

Lung Tissue Damage and Altered Surfactant Homeostasis in AD-Treated Mice

We observed a significant increase in total protein concentration and a significant increase in LDH activity in bronchoalveolar lavage fluids (BALF) (Figs. 2A and 2B) of AD-treated mice as compared with vehicle-treated control mice, indicating an increase in lung cell permeability and lung tissue damage respectively. Parallely, we observed a significant increase in total PLs in BALF of AD- versus vehicle-treated mice (Fig. 2C), with a significant reduction in the relative content of LAs seen at day 7, but not at later time points (Fig. 2D). In agreement, lipidomic analysis of the alveolar surfactant pool forwarded modest changes in the PL profile (Table 1), but distinct changes in the fatty acid profiles, with a significant reduction in the relative amount of dipalmitoylphosphatidylcholine (DPPC) as well as saturated PC and a corresponding increase in unsaturated PC (Table 2). Likewise, saturated phosphatidylglycerol (PG) was significantly reduced at the favor of unsaturated PG species (Table 2). PE-based plasmalogens were increased in AD-treated mice as compared with vehicle-treated mice (Table 3). Analysis of mature forms of surfactant proteins (SP) B and C in BALF of AD- and vehicle-treated mice did not forward any significant differences (Fig. 2E). Taken together, we observed significant cell damage and analysis of the alveolar surfactant pool after AD treatment forwarded significant changes only with regard to PL components.

On the other hand, marked alterations of the intracellular surfactant pool were easily observed and consisted of a significant elevation of the tissue PLs (Fig. 3A) and a significant increase in the 42 kDa form of pro SP-B and a remarkable (5–10-fold) increase in mature SP-B, pro SP-C, and mature SP-C in AD-treated mice (Figs. 3B–D). Lipidomics analysis of lung tissue PLs revealed a significant increase in bis(monacylglycero)phosphate (BMP; also known as lysobisphosphatidic acid, LBPA), a PL that is present in the internal vesicles of multivesicular bodies (MVBs) and that has been suggested to be a biomarker of AD-induced phospholipidosis (Table 4) (Mortuza *et al.*, 2003). In line with this observation, we also observed the increased number of profiles of MVBs within the AECII of AD-treated mice (Supplementary fig. 4A), as compared with vehicle-treated mice (Supplementary fig. 4B). Lipidomics analysis further revealed significant increase in cholesterol esters in AD-treated mice (Table 4). In addition, small, but significant changes in other PL classes in AD-treated mice lungs were observed (Table 4), overall supporting the concept that there was a substantial intracellular accumulation of mature surfactant compounds. In full agreement, electron microscopy showed larger and more prominent AECII in close neighborhood to areas of interstitial fibrosis suggesting hypertrophy and/or hyperplasia of this cell type. Additionally, lamellar bodies were increased in number and size whereas components of intra-alveolar surfactant appeared more abundant after AD treatment (Figs. 3E and F).

AD Induces Apoptosis of AECII in Mice

Compared with the vehicle-treated mice, we observed a significant, fivefold increase in the cleaved form of caspase 3 in day 7 AD-treated mice that decreased over time (Figs. 4A and B, Supplementary fig. 5A). Immunohistochemistry for cleaved caspase 3 and the AECII marker pro SP-C on serial lung sections revealed localization of cleaved caspase 3 signal to AECII in AD-treated mice, whereas no detectable signal was seen in the lung sections of vehicle-treated mice lungs (Fig. 4C). Supporting these data, electron microscopy of lung tissues of AD-treated mice lungs showed fragmentation of the alveolar epithelium and denudation of the basal lamina in mice at d7 after AD treatment (Fig. 1F).

AD Induces Lysosomal and ER Stress in the AECII

Drawn against our previous report of cathepsin D mediated apoptosis of AECII in a mouse model of Hermansky-Pudlak syndrome associated lung fibrosis (Mahavadi *et al.*, 2010), yet another form of lung fibrosis being associated with extensive surfactant accumulation and AECII apoptosis, we investigated the regulation of cathepsin D in AD-induced lung fibrosis. We observed a significant 11-fold increase in cathepsin D levels in lung homogenates of AD-treated mice at day 7 (vs. vehicle), which gradually decreased over time (Figs. 5A and B). In addition, immunohistochemistry for cathepsin D and pro SP-C on serial lung sections showed that the increased cathepsin D was localized to the AECII in AD-treated mice whereas it was mostly restricted to macrophages in vehicle-treated control mice (Fig. 5E, Supplementary fig. 5B). Based on our previous study about induction of ER stress within the AECII of IPF patients (Korfei *et al.*, 2008), we analyzed two markers of ER stress, the activating transcription factor (ATF)-6 and C/EBP homologous protein (CHOP). We observed a significant ~10-fold increase in the p50 form of the ATF6 and ~3-fold increase in the CHOP protein in AD-treated mice lungs from day 7 through day 28 as compared with vehicle-treated mice lungs (Figs. 5A, C, and D). Immunohistochemistry revealed the induction of ATF6 within AECII and also in some, pro SP-C negative, interstitial cells (Fig. 5F, Supplementary fig. 5C). To investigate if AD may exert similar effects *in vitro*, we treated mouse lung epithelial (MLE) 12 cells with vehicle or with 10 μg/ml AD (according to Bargout *et al.*, 2000) for 8, 16, and 24 h. Western blot analysis revealed an increase in cleaved caspase 3, cathepsin D, p50ATF6, and CHOP as well as pro SP-C in AD-treated cells as compared with vehicle-treated or untreated cells (Fig. 6A). These data completely corroborated with the data obtained from AD-treated mice. Interestingly, high levels of AD-induced toxicity as evident by LDH assay were observed in MLE12 cells only after 24 h of AD treatment and not at earlier time points (Supplementary fig. 6). We then performed knockdown studies in order to investigate if AD may drive apoptosis of MLE12 cells via cathepsin D activation. We transfected cells with a cathepsin D specific versus a scrambled siRNA for 48 h and then treated with AD or vehicle for 8 h. Significant knockdown of cathepsin D was observed (Fig. 6B). In AD- versus vehicle-treated MLE12 cells, cathepsin D knockdown resulted in slightly, albeit insignificantly, reduced levels of cleaved caspase 3 (Figs. 6B and C). Interestingly, MLE12 cells treated with vehicle did show an increased level of cleaved caspase, which—most likely—originated from the stress of transfection. In these cells not treated with AD, knockdown of cathepsin D clearly attenuated the extent of apoptosis, as evident from the reduced amount of cleaved caspase 3. Hence, transfection-induced apoptosis of MLE12 cells seems to be mediated to a larger part through cathepsin D, but AD-induced alveolar epithelial cell apoptosis or pro SP-C increase is not primarily mediated via cathepsin D.

DISCUSSION

In the present study, we could show that intratracheal aerosol administration of AD, a frequently used antiarrhythmic drug causing lung fibrosis in a substantial proportion of treated patients, similarly causes a patchy interstitial fibrosis in C57Bl/6 mice alongside with increased alveolar epithelial cell apoptosis, lysosomal stress, and ER stress. To our knowledge, this is the

Downloaded from https://academic.oup.com/toxsci/article-abstract/142/1/285/1710567 by Universitaet Giessen user on 24 October 2019

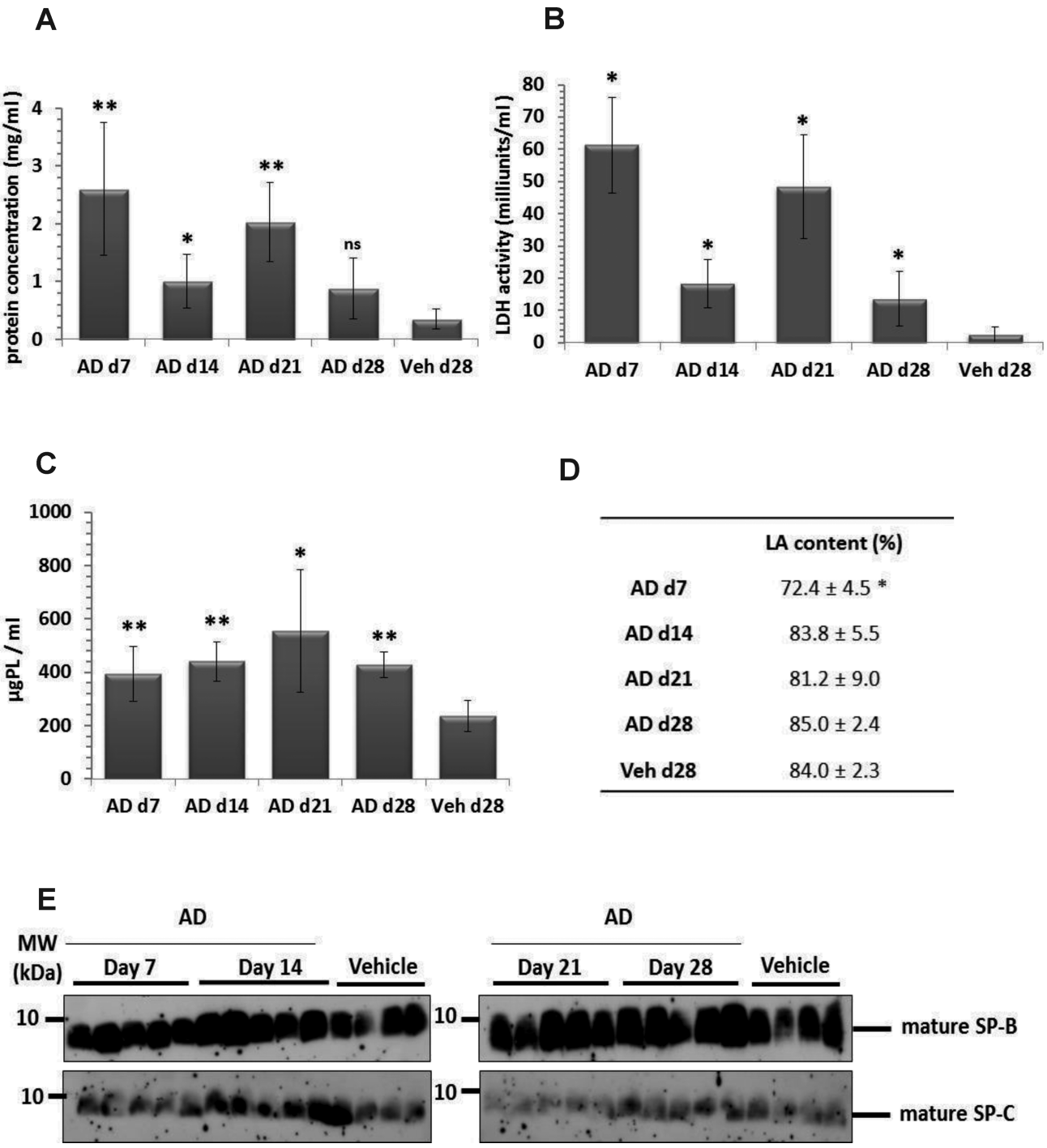

FIG. 2. Lung injury and increased surfactant in BAL fluid of AD-treated mice. Graphical representation of (A) total protein concentration and (B) LDH activity in BAL fluid from days 7, 14, 21, and 28 AD and day 28 vehicle-treated mice. (C) Total PLs were extracted from BAL fluid of AD (days 7, 14, 21, and 28) and vehicle-treated mice (day 28). The final concentrations were calculated as 'per ml' BAL fluid. (D) Data set indicating relative amount of large surfactant aggregates (LA content, given as a percentage of total PL) in BAL fluid of AD- and vehicle-treated mice. (E) Western blot analysis of mature surfactant protein (SP)-B and mature SP-C in BAL fluid of AD- and vehicle-treated mice. $^{*}p < 0.05$, $^{**}p < 0.01$; $n = 5$ mice per group and three independent experiments were performed.

first study to undertake a systematic analysis of surfactant alterations and cellular stress events with special reference to AECII in response to AD treatment in mice.

AD and its metabolites are well known to exert both direct and indirect toxicity on different cell types (Chiovato *et al.*, 1994; Martin *et al.*, 1989). Direct toxicity of AD causing disruption of cellular integrity thereby leading to tissue damage has been reported previously (Bolt *et al.*, 2001) and by us in the current study. Other important features of AD-induced cytotoxicity include intracellular phospholipidosis (Martin *et al.*, 1989), free radical formation (Sarma *et al.*, 1997), membrane destabilization due to inhibition of Na+/K+-ATPase (Chatelain *et al.*, 1985), disruption of intracellular calcium homeostasis (Lubic *et al.*, 1994), and disruption of cellular energy homeostasis (Fromenty *et al.*, 1990).

Downloaded from https://academic.oup.com/toxsci/article-abstract/142/1/285/1710567 by Universitaet Giessen user on 24 October 2019

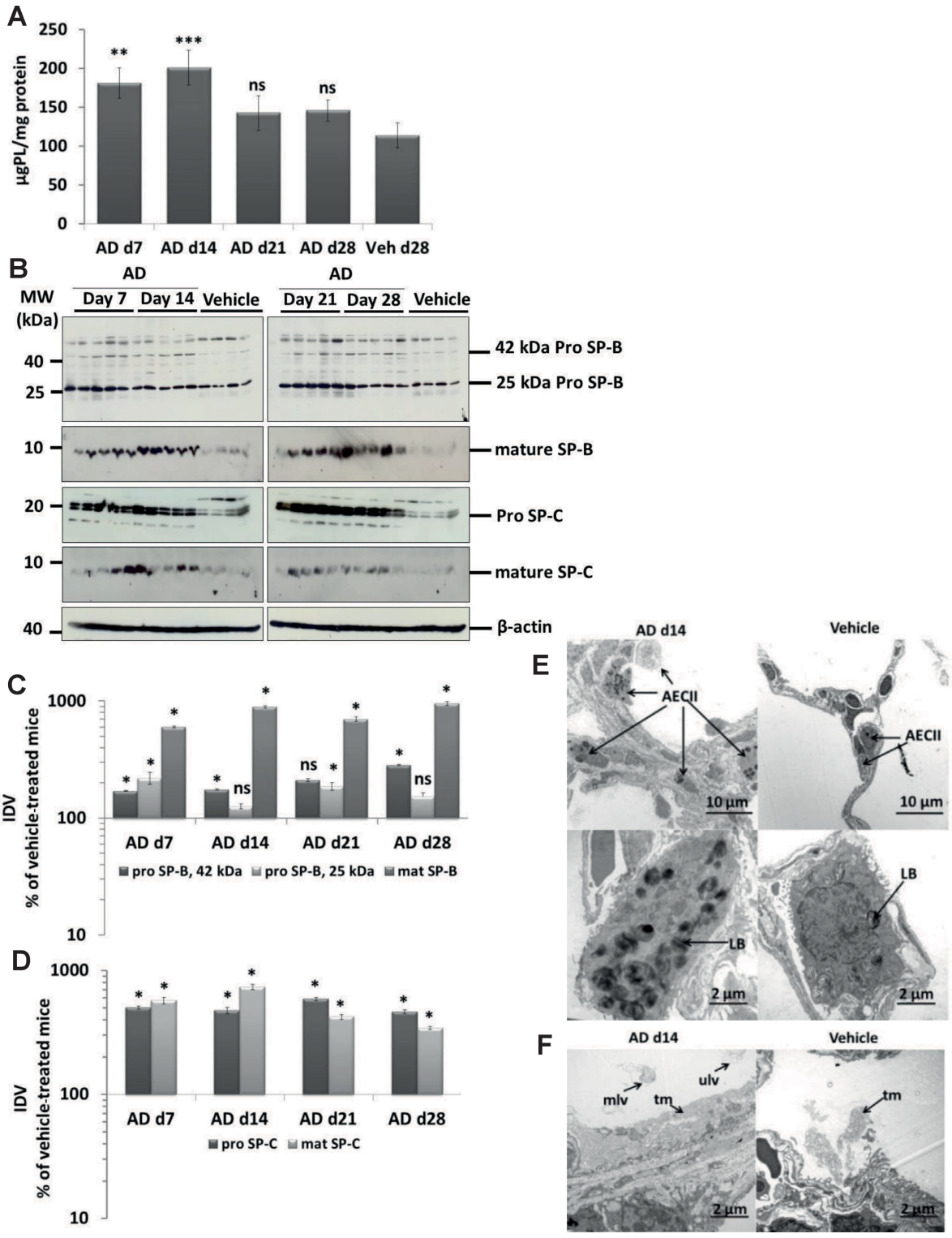

FIG. 3. Accumulation of surfactant in AD-treated lung tissues. (A) Total PLs were extracted from lung tissue of all AD- and vehicle-treated mice. The resulting PL concentrations were normalized against their respective protein concentrations and values are expressed as micrograms of PLs per milligram of protein. (B) Western blot analysis of lung homogenates of (left) AD-treated mice at days 7,14 and vehicle at day 28 and (right) AD-treated mice at days 21, 28, and vehicle at day 28 for prosurfactant protein (SP)-B, mature SP-B, pro–SP-C, and mature SP-C. Representative blots are from $n = 5$ mice per group and results of three independent experiments are shown. (C and D) Densitometry was performed on all Western blot analyses. The target protein/β-actin ratio was calculated and is given as a percentage of the respective vehicle-treated controls. $^{***}p < 0.001$,$^{**}p < 0.01$, $^{*}p < 0.05$; $n = 5$ mice per group. Representative blots and analysis from $n = 5$ mice per group and three independent experiments are shown. (E) Representative transmission electron micrographs showing increased number and size of profiles of AECII (hyperplasia; arrows) d14 post AD challenge compared with vehicle-treated mice. AECII filled with abundant and enlarged profiles of lamellar bodies (LB) are shown. Scale bar = 10 µm (upper panel); 2 µm (lower panel). (F) Alveolar areas filled with surfactant in some areas appeared more prominent in AD-treated mice lungs (left panel) as compared with vehicle-treated mice lungs (right panel). tm, tubular myelin; mlv, multilamellated vesicles; ulv, unilamellated vesicles. Scale bar = 2 µm.

Downloaded from https://academic.oup.com/toxsci/article-abstract/142/1/285/1710567 by Universitaet Giessen user on 24 October 2019

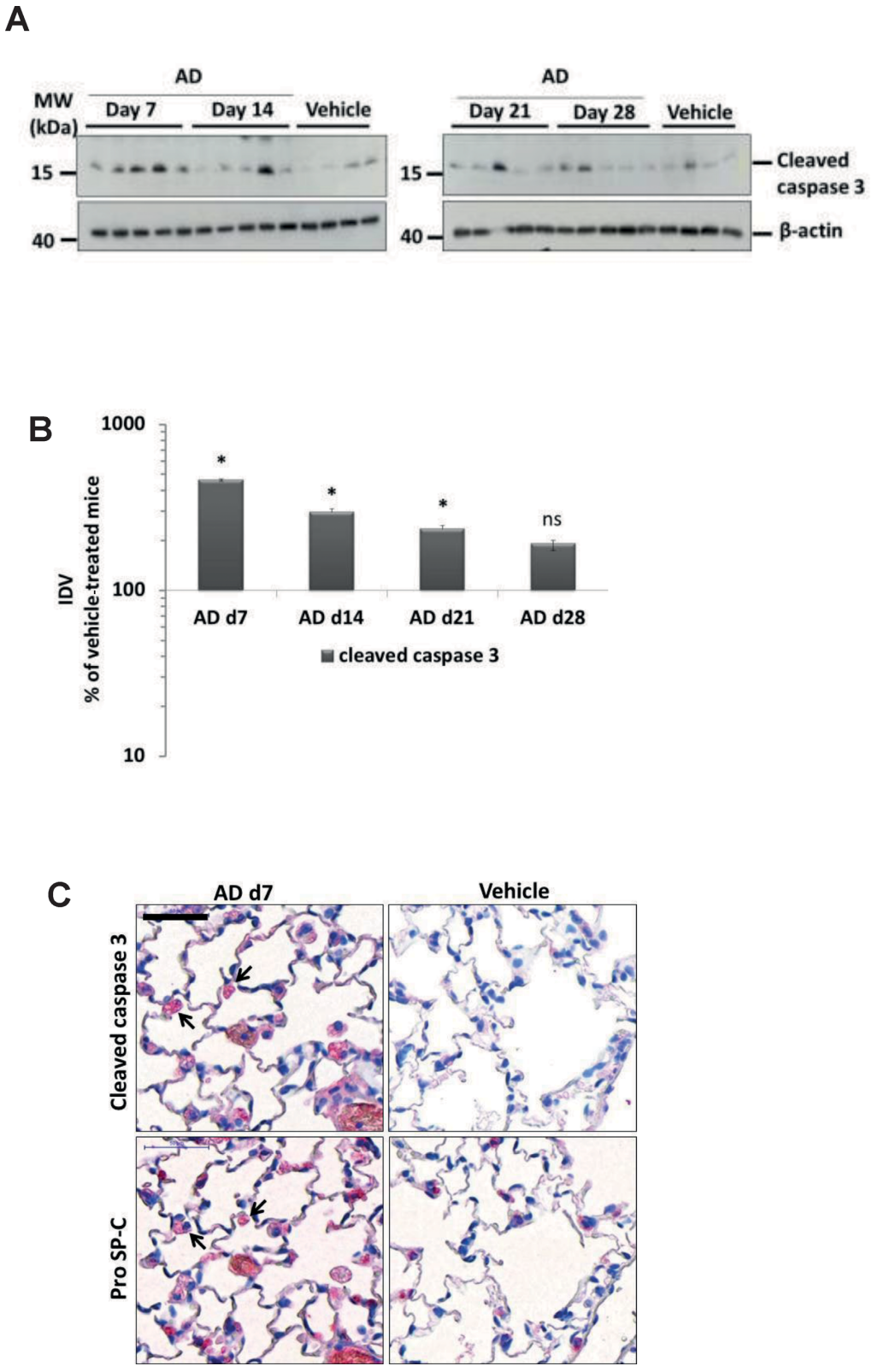

FIG. 4. Induction of AECII apoptosis in mice after AD treatment. (A) Western blot analysis of lung homogenates of (left) AD-treated mice at days 7, 14 and vehicle at day 28 and (right) AD-treated mice at days 21, 28 and vehicle at day 28 for cleaved caspase 3 and β-actin. Representative blots and analysis from $n = 5$ mice per group and three independent experiments are shown. (B) Densitometry analysis of cleaved caspase 3/β-actin ratio was calculated for all available blots and is given as a percentage of the respective vehicle-treated controls. $^*p < 0.05$. (C) Immunohistochemistry performed on serial lung sections from day 7 AD- and vehicle-treated mice for cleaved caspase 3 and pro SP-C. Arrows indicate apoptotic AECII in AD-treated mice. Scale bar = 50 μm; Original magnification of pictomicrographs: ×400. $n = 5$ mice per group and three independent experiments were performed.

Downloaded from https://academic.oup.com/toxsci/article-abstract/142/1/285/1710567 by Universitaet Giessen user on 24 October 2019

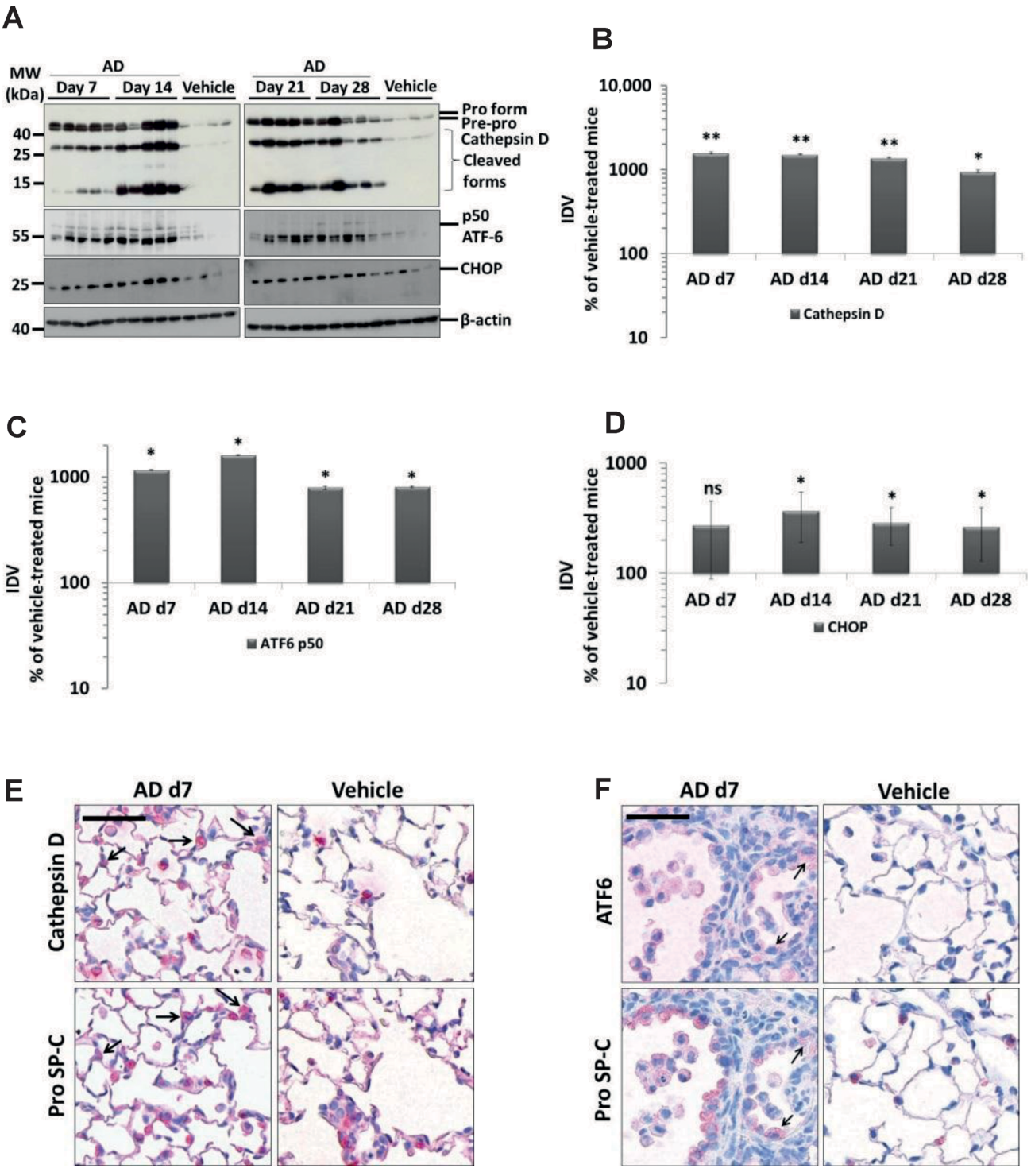

FIG. 5. Induction of lysosomal and ER stress in the AECII of AD-treated mice. (A) Western blot analysis of lung homogenates of (left) AD-treated mice at days 7, 14 and vehicle at day 28 and (right) AD-treated mice at days 21, 28 and vehicle at day 28 for cathepsin D, ATF6, CHOP, and β-actin. Representative blots and analysis from $n = 5$ mice per group and three independent experiments are shown. (B,D,E) Densitometry analysis of the cathepsin D (B) p50ATF6 (D) or CHOP (E) to β-actin ratio was calculated for all blots and is given as a percentage of the respective vehicle-treated controls. $^{**}p < 0.01$, $^{*}p < 0.05$; $n = 5$ mice per group and three independent experiments were performed. (C and F). Immunohistochemistry performed on serial lung sections from day 7 AD- and vehicle-treated mice for cathepsin D and pro SP-C (D) or for ATF6 and pro SP-C (E). Arrows indicate cathepsin D-positive and ATF6-positive AECII in C and F, respectively, in AD-treated mice. Scale bar = 50 μm. Original magnification of pictomicrographs: ×400.

Downloaded from https://academic.oup.com/toxsci/article-abstract/142/1/285/1710567 by Universitaet Giessen user on 24 October 2019

TABLE 1 PL Profile in BAL Fluid from AD- and Vehicle-Treated Mice

BAL	%PC	%SM	%PE	%PE P	%PS	%PG	%PI	%LPC	%Cer	%CE	%FC
AD d7	67.99 ± 0.01**	0.80 ± 0.12	1.00 ± 0.06	1.23 ± 0.10*	1.45 ± 0.17	9.12 ± 0.50	2.06 ± 0.26	0.93 ± 0.24	0.12 ± 0	0.77 ± 0.22	14.6 ± 1.1**
AD d14	70.85 ± 0.35	0.31 ± 0	0.9 4 ± 0.01	0.90 ± 0.02	0.93 ± 0.02	11.81 ± 0.10	1.59 ± 0.04	0.37 ± 0.01	0.07 ± 0	0.18 ± 0	12.0 ± 0.3
AD d21	70 ± 0.58	0.51 ± 0.04	0.90 ± 0	0.94 ± 0.02*	0.90 ± 0.03	10.99 ± 0.23	1.54 ± 0.05	0.77 ± 0.11	0.14 ± 0	0.57 ± 0.17	12.7 ± 0.5
AD d28	71.91 ± 0.38**	0.32 ± 0.01	0.90 ± 0.01	0.85 ± 0.01	0.8 1± 0.01	12.02 ± 0.22	1.72 ± 0.12	0.48 ± 0.06	0.07 ± 0	0.19 ± 0.03	10.7 ± 0.4**
Veh d28	68.91 ± 0.17	0.36 ± 0.02	0.889 ± 0.05	0.74 ± 0.06	0.73 ± 0.03	11.83 ± 0.3	1.52 ± 0.09	0.71 ± 0.1	0.10 ± 0	0.23 ± 0.02	13.9 ± 0.1

Note. Depicted here are the relative percentages of different PL classes in the BAL fluid of AD- and vehicle-treated mice at the indicated time points. Values are represented as means ± SEM, *p*-value summary: $^{*}p < 0.05$, $^{**}p < 0.01$. Where significance is not mentioned, values are considered as being not significant. Per group, $n = 5$ mice were analyzed. SM, Sphingomyelin; PC, Phosphatidylcholine ; LPC, Lysophosphatidylcholine ; PE, Phosphatidylethanolamine; PE P, PE-based plasmalogens; PG, Phosphatidylglycerol; PS, Phosphatidylserine; Cer, Ceramides; CE, Cholesteryl esters; FC, Free cholesterol.

TABLE 2 PC and PG Lipid Species in BAL Fluid from AD- and Vehicle-Treated Mice

BAL	% sat PC	% PC 32:0 (DPPC)	% unsat PC	% alkyl PC	% sat PG	% unsat PG
AD d7	46.7 ± 1.2**	38.2 ± 1.2**	49.2 ± 1.2**	4.21 ± 0.17	15.6 ± 1.2**	84.3 ± 1.2**
AD d14	47.1 ± 0.4*	37.1 ± 0.7**	49.1 ± 0.4*	3.77 ± 0.10	17.1 ± 0.2**	82.8 ± 0.2**
AD d21	49.7 ± 0.2**	41.8 ± 0.3**	46.7 ± 0.2*	3.51 ± 0.14	17.0 ± 0.3**	82.9 ± 0.3**
AD d28	49.5 ± 0.3**	39.6 ± 0.5**	46.9 ± 0.4**	3.53 ± 0.05	17.4 ± 0.3**	82.5 ± 0.3**
Veh d28	54.21 ± 0.5	45.7 ± 0.7	42.2 ± 0.7	3.58 ± 0.15	21.3 ± 0.5	78.6 ± 0.5

Note. Depicted here are the relative percentages of different lipid species from PC & PG phospholipds in the BAL fluid of AD and vehicle treated mice at the indicated time points. PL species annotation is based on the assumption of even numbered carbon chains only. Values are represented as means ± SEM, *p*-value summary: $^{*}p < 0.05$, $^{**}p < 0.01$. Where significance is not mentioned, values are considered as being not significant. Per group, $n = 5$ mice were analyzed. PC, Phosphatidylcholine; DPPC, Dipalmitoylated PC; PG, Phosphatidylglycerol.

TABLE 3 Lipid Species of PE-Based Plasmalogens in BAL Fluid from AD- and Vehicle-Treated Mice

BAL	PE P-16:0	PE P-18:1	PE P-18:0	Total
AD d7	5.3 ± 0.8**	0.50 ± 0.07**	0.78 ± 0.10*	6.6 ± 1.0**
AD d14	4.0 ± 0.1**	0.27 ± 0.01*	0.50 ± 0.01*	4.7 ± 0.1**
AD d21	5.1 ± 0.5**	0.42 ± 0.04*	0.61 ± 0.04*	6.1 ± 0.5**
AD d28	3.8 ± 0.5**	0.22 ± 0.02	0.40 ± 0.04	4.4 ± 0.8**
Veh d28	1.7 ± 0.2	0.18 ± 0.01	0.32 ± 0.03	2.2 ± 0.3

Note. Depicted here are the nmol/ml PE-based plamsalogens in BAL fluid of AD- and vehicle-treated mice at the indicated time points. Values are represented as means ± SEM, *p*-value summary: $^{*}p < 0.05$, $^{**}p < 0.01$. Where significance is not mentioned, values are considered as being not significant. Per group, $n = 5$ mice were analyzed. PE P, PE-based plasmalogens.

The extent of cytotoxicity is, however, dosage and time dependent. The *in vivo* and *in vitro* AD dosages used in this study are within the range of AD concentrations reported within the lungs of patients treated with this drug (Brien *et al.*, 1987; Plomp *et al.*, 1984). Because of repeated AD doses, it is logical to assume that a portion of the applied AD might get accumulated in the alveolar hypophase which associates with the layers of pulmonary surfactant due to its amphiphilic nature. But surfactant film in the hypophase is continuously renewed and lipids are removed from the alveoli with a turnover time of few hours (Wright, 1990). It has been indicated that AD does not affect the degradation of exogenous DPPC and that it does not interfere with early stages of endocytosis, a process through which surfactant is recycled by the alveolar type II cell (Baritussio *et al.*, 2001). Hence directly after AD administration there might be a high and possibly toxic local concentration in the alveolar hypophase, but due to the short turnover time of surfactant, this is also taken up by AECII, making the accumulation of toxic AD concentrations in the hypophase unlikely. Although significant tissue damage was observed in AD-treated mice in this study, *in vitro* data revealed that apoptosis is predominant, followed by direct toxic effects in AD-treated MLE 12 cells.

Full-blown AD-induced lung fibrosis was visible on day 7, in the absence of extensive inflammatory changes. As extensive AECII cell death is known to be a prominent feature in some idiopathic (IPF, cellular and fibrotic NSIP, EAA) (Jinta *et al.*, 2010; Korfei *et al.*, 2008) and drug-induced forms of interstitial pneumonia including AD (Bargout *et al.*, 2000), our data reinforce the concept that lung fibrosis may actually develop very fast, probably pending on the magnitude of epithelial cell death. In line with such reasoning, the extent of fibrosis as well as the extent of epithelial cell death seemed to slightly vanish over time despite continuous application of identical AD dosages. This to us suggests the evolution of a compensatory mechanism of the injured AECII, making these cells less susceptible towards the toxic effects of AD.

Although impairment in lung compliance and significant increase in total PL content in BALF from AD-treated mice were observed, we did not observe a remarkable difference in total surfactant pool in these mice. The decrease in lung compliance in AD-treated mice might however be a result of the increased thickness of the fibrotic lung tissue. This observation makes the AD model different to the already known Hermansky-Pudlak syndrome associated lung fibrosis, the bleomycin induced mouse model of lung fibrosis and to the clinical IPF, where pronounced disturbances in the biochemical and physical properties of lung surfactant pool were reported (Gunther *et al.*, 1999; Horiuchi *et al.*, 1996; Mahavadi *et al.*, 2010).

As mentioned earlier, AD gets enriched within the lysosomes of various cell types and gets only gradually degraded because of its uncommon long half-life (Okayasu *et al.*, 2006; Somani *et al.*, 1987). In line with such reasoning, the prominent histopatho-

Downloaded from https://academic.oup.com/toxsci/article-abstract/142/1/285/1710567 by Universitaet Giessen user on 24 October 2019

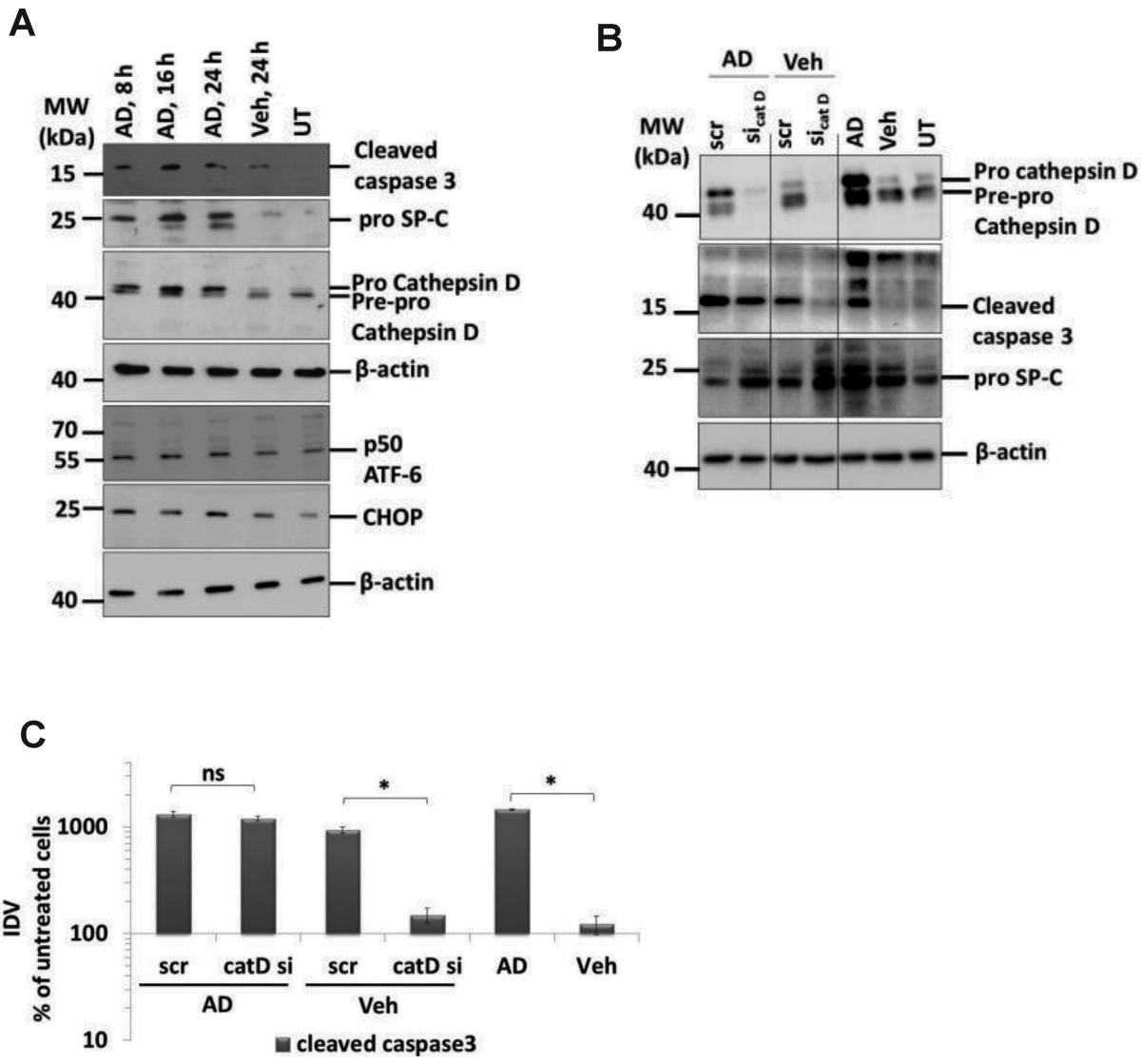

FIG. 6. AD-induced AECII apoptosis is not mediated by cathepsin D. (A) Representative Western blot images from cell lysates from AD (8, 16, and 24 h) or vehicle-treated (24 h) or untreated MLE12 cells for cleaved caspase 3, cathepsin D, pro SP-C, ATF6, CHOP, and β-actin. (B) Representative Western blot images for cathepsin D, cleaved caspase 3, pro SP-C, and β-actin from MLE12 cells treated with AD or vehicle and transfected with scrambled or siRNA for cathepsin D. Untransfected cells treated with AD, vehicle, or untreated cells were included as controls. Different parts from same Western blots are separated by vertical lines. (C) Densitometry analysis of cleaved caspase 3 to β-actin ratio was calculated and is given as a percentage of untreated cells. $^{*}p < 0.05$. Representative images and densitometry analysis from three independent experiments with triplicate transfections each are shown.

logical and biochemical read-out of AD toxicity in the alveolar epithelium was that of a substantial disturbance of lysosomal homeostasis, clearly indicated by the profound increase in the size and number of lamellar bodies within the AECII, and the significant increase in the hydrophobic SP and PL content. These findings are in agreement with previous studies reporting lamellar inclusions in several tissues including lung in AD-treated patients (Dake *et al.*, 1985). The increase in lamellar body sizes might account to the increased surfactant PLs as described before (Padmavathy *et al.*, 1993) and in our current study, and because of increased amounts of pro and mature forms of SP –B and –C within the lungs of AD-treated mice as described here.

Other important observations from our study are the increase in cholesterol and BMP in AD-treated mice lungs. This increase in cholesterol esters along with other accumulated lipids might contribute towards the characteristic foamy nature of cells due to AD treatment. This is further supported by a recent study which reported that upon AD treatment, distribution of BMP, cholesterol and other lipids were altered but the removal of cholesterol did not restore the AD-induced BMP distribution (Piccoli *et al.*, 2011). Although AD is very well-known to induce phospholipidosis in various tissues, the effects of AD on intra-alveolar surfactant pool are not reported extensively. We observed that AD increases the intra-alveolar surfactant in mice. Of note, along with an increase in the unsaturated species of PC and PG, we observed an increase in PE plasmalogens. Plasmalogens are integral components of lung surfactant and are secreted by AECII together with the other surfactant components. They are implicated to play both functional and structural roles (Rustow *et al.*, 1994). Plasmalogens are antioxidant PLs and AD has been implicated to increase oxidative stress (Sarma *et al.*, 1997). Hence, it is reasonable to speculate that the increase in

Downloaded from https://academic.oup.com/toxsci/article-abstract/142/1/285/1710567 by Universitaet Giessen user on 24 October 2019

TABLE 4 PL Profile in Lung Tissue from AD- and Vehicle-Treated Mice

Tissue	%PC	%SM	%PE	%PE P	%PS	%PG	%PI	%BMP	%PA	%LPG	%CL	%LPC	%Cer	%CE	%FC
AD d7	42.17 ± 1.13**	6.12 ± 0.09	7.95 ± 0.17*	11.36 ± 0.35*	17.35 ± 0.67*	4.23 ± 0.20	7.95 ± 0.37	0.18 ± 0.03*	0.05 ± 0.01	0.56 ± 0.11	0.07 ± 0.03	0.87 ± 0.03*	1.15 ± 0.09**	0.98 ± 0.14*	23.07±0.42
AD d14	44.02 ± 0.86**	5.77 ± 0.16*	7.04 ± 0.15	11.47 ± 0.26**	16.47 ± 0.50**	5.05 ± 0.32	6.79 ± 0.09**	0.26 ± 0.01**	0.01 ± 0	0.70 ± 0.08	0.23 ± 0.03*	1.15 ± 0.04*	1.02 ± 0.02*	0.87 ± 0.11*	21.73±0.28*
AD d21	44.35 ± 1.11**	5.58 ± 0.15*	6.85 ± 0.20	10.43 ± 0.34*	15.32 ± 0.48**	7.54 ± 1.0**	6.96 ± 0.21*	0.16 ± 0.01*	0.03 ± 0.01	0.62 ± 0.09	0.10 ± 0.03	1.10 ± 0.04	0.97 ± 0.05	0.78 ± 0.08*	20.42±0.30**
AD d28	42.52 ± 1.0**	6.01 ± 0.18	7.10 ± 0.16	11.97 ± 0.27**	17.84 ± 0.50**	4.42 ± 0.35	7.16 ± 0.12*	0.17 ± 0.01*	0.02 ± 0.01	0.64 ± 0.05	0.16 ± 0.01	0.96 ± 0.05	1.02 ± 0.02	0.59 ± 0.08*	22.13±0.29*
Veh d28	36.56 ± 0.50	6.22 ± 0.09	7.18 ± 0.07	13.14 ± 0.15	21.92 ± 0.24	4.36 ± 0.40	7.84 ± 0.20	0.11 ± 0	0.03 ± 0.01	0.56 ± 0.05	0.09 ± 0.03	1.01 ± 0.02	0.97 ± 0.01	0.57 ± 0.03	24.17±0.29

Note. Depicted here are the relative percentages of different PL classes in the lung tissue of AD- and vehicle-treated mice at the indicated time points. Glycerophospholipid species annotation is based on the assumption of even numbered carbon chains only. SM species were assigned, based on the assumption of a sphingoid base d18:1. Values are represented as means ± SEM. *p*-value summary: $^{*}p < 0.05$, $^{**}p < 0.01$. Where significance is not mentioned, values are considered as being not significant. Per group, $n = 5$ mice were analyzed. SM, Sphingomyelin; PC, Phosphatidylcholine ; LPC, Lysophosphatidylcholine ; PE, Phosphatidylethanolamine; PE P, PE-based plasmalogens; PS, Phosphatidylserine; PG, Phosphatidylglycerol; PI, Phosphatidylinositol; BMP, Bis(monacylglycero)phosphate; PA, Phosphatidic Acid; LPG, Lysophosphatidylglycerol; CL, Cardiolipin; LPC, Lysophosphatidylcholine ; Cer, Ceramides; CE, Cholesteryl esters; FC, Free cholesterol.

plasmalogens after AD treatment, as observed in the current study might be one of the rescue mechanisms of the type II cell to cope up with the increased oxidative stress. Moreover, it has been shown that increasing amount of ethanolamine plasmalogens result in reduced surface tension in synthetic PL mixtures (Rudiger *et al.*, 1998). Clinically, treatment of premature infants (with ARDS) with synthetic surfactant without plasmalogens demonstrated less efficient recovery when compared with treatment with natural surfactant extracts from bovine lungs (Ramanathan, 2009). Hence, although not experimentally proven here, the increase in plasmalogens may in part explain the ongoing compensatory mechanism of the injured AECII that makes the mice less susceptible towards the toxic effects of AD over time.

Because surfactant processing, secretion, and re-uptake in AECII take place in the lysosomal compartment, an altered intracellular surfactant homeostasis as seen in our model reflects an altered lysosomal homeostasis. In addition, because of an increase in alveolar epithelial cell apoptosis, lysosomal, and ER stress markers, at a quick glance, the AD model offers a lot of similarities with the recently described model of Hermansky-Pudlak syndrome (HPS) associated interstitial pneumonia (Mahavadi *et al.*, 2010). In agreement with this concept, we observed an increase in the levels of cathepsin D, a lysosomal aspartyl protease within the lungs of AD-treated mice and in mouse lung epithelial cells after AD treatment. Although cathepsin D is involved in activating pro-apoptotic mechanisms and terminal caspases (Kagedal *et al.*, 2001), unlike in the HPS model, we observed that AD-induced apoptosis of alveolar epithelial cells is not mediated via cathepsin D, rather the increase in cathepsin D levels after AD treatment might in fact reflect an increase in an overall lysosomal turnover in the alveolar epithelial cells, indicating that other lysosomal cell death pathways might be activated. In fact, it has been shown that AD induces cytoplasmic inclusions (Dake *et al.*, 1985; Somani *et al.*, 1987) and stimulates autophagy (Morissette *et al.*, 2009), a lysosome dependent pathway in several cell types. Whether alveolar epithelial cells undergo apoptosis in an autophagy-dependent manner has yet to be studied in our model.

Altogether, our study describes some important cellular stress mechanisms induced by AD within the AECII and paves the way for further studies on the role of these cellular stress events in the development of AD-induced lung fibrosis.

SUPPLEMENTARY DATA

Supplementary data are available online at http://toxsci.oxfordjournals.org/.

FUNDING

Part of this work has been undertaken with the enormous support of the European Commission (European IPF Network, funded from 2008 to 2012 through the frame program 7). The authors thank Stefanie Hezel and Susanne Fassbender for their superb technical assistance.

Conflict of interest: Personal fees and board membership from Intermune, Boehringer, Roche. Consultancy fees from Activaero.

REFERENCES

Ashrafian, H. and Davey, P. (2001). Is amiodarone an underrecognized cause of acute respiratory failure in the ICU? *Chest*

Downloaded from https://academic.oup.com/toxsci/article-abstract/142/1/285/1710567 by Universitaet Giessen user on 24 October 2019

120, 275–282.

Bargout, R., Jankov, A., Dincer, E., Wang, R., Komodromos, T., Ibarra-Sunga, O., Filippatos, G. and Uhal, B. D. (2000). Amiodarone induces apoptosis of human and rat alveolar epithelial cells in vitro. *Am. J. Physiol. Lung Cell. Mol. Physiol.* **278**, L1039–L1044.

Baritussio, A., Marzini, S., Agostini, M., Alberti, A., Cimenti, C., Bruttomesso, D., Manzato, E., Quaglino, D. and Pettenazzo, A. (2001). Amiodarone inhibits lung degradation of SP-A and perturbs the distribution of lysosomal enzymes. *Am. J. Physiol. Lung Cell. Mol. Physiol.* **281**, L1189–L1199.

Bolt, M W, Card, J W, Racz, W J, Brien, J F and Massey, T E (2001) Disruption of mitochondrial function and cellular ATP levels by amiodarone and N-desethylamiodarone in initiation of amiodarone-induced pulmonary cytotoxicity. J. Pharmacol. Exp. Ther., 298, 1280–1289.

Brien, J. F., Jimmo, S., Brennan, F. J., Ford, S. E. and Armstrong, P. W. (1987). Distribution of amiodarone and its metabolite, desethylamiodarone, in human tissues. *Can. J. Physiol. Pharmacol.* **65**, 360–364.

Chang, S. N., Hwang, J. J., Hsu, K. L., Tsai, C. T., Lai, L. P., Lin, J. L., Tseng, C. D. and Chiang, F. T. (2007). Amiodarone-related pneumonitis. *J. Formos. Med. Assoc.* **106**, 411–417.

Charles, P. E., Doise, J. M., Quenot, J. P., Muller, G., Aube, H., Baudouin, N., Piard, F., Besancenot, J. F. and Blettery, B. (2006). Amiodarone-related acute respiratory distress syndrome following sudden withdrawal of steroids. *Respiration* **73**, 248–249.

Chatelain, P., Laruel, R. and Gillard, M. (1985). Effect of amiodarone on membrane fluidity and Na+/K +ATPase activity in rat-brain synaptic membranes. *Biochem. Biophys. Res. Commun.* **129**, 148–154.

Chiovato, L., Martino, E., Tonacchera, M., Santini, F., Lapi, P., Mammoli, C., Braverman, L. E. and Pinchera, A. (1994). Studies on the in vitro cytotoxic effect of amiodarone. *Endocrinology* **134**, 2277–2282.

Connolly, S. J. (1999). Evidence-based analysis of amiodarone efficacy and safety. *Circulation* **100**, 2025–2034.

Dake, M. D., Madison, J. M., Montgomery, C. K., Shellito, J. E., Hinchcliffe, W. A., Winkler, M. L. and Bainton, D. F. (1985). Electron microscopic demonstration of lysosomal inclusion bodies in lung, liver, lymph nodes, and blood leukocytes of patients with amiodarone pulmonary toxicity. *Am. J. Med.* **78**, 506–512.

Fromenty, B., Fisch, C., Labbe, G., Degott, C., Deschamps, D., Berson, A., Letteron, P. and Pessayre, D. (1990). Amiodarone inhibits the mitochondrial beta-oxidation of fatty acids and produces microvesicular steatosis of the liver in mice. *J. Pharmacol. Exp. Ther.* **255**, 1371–1376.

Gunther, A., Schmidt, R., Nix, F., Yabut-Perez, M., Guth, C., Rosseau, S., Siebert, C., Grimminger, F., Morr, H., Velcovsky, H. G., *et al.* (1999). Surfactant abnormalities in idiopathic pulmonary fibrosis, hypersensitivity pneumonitis and sarcoidosis. *Eur. Respir. J.* **14**, 565–573.

Horiuchi, T., Ikegami, M., Cherniack, R. M. and Mason, R. J. (1996). Increased surface tension of the lung and surfactant in bleomycin-induced pulmonary fibrosis in rats. *Am. J. Respir. Crit. Care Med.* **154**, 1002–1005.

January, C. T., Wann, L. S., Alpert, J. S., Calkins, H., Cleveland, J. C., Jr, Cigarroa, J. E., Conti, J. B., Ellinor, P. T., Ezekowitz, M. D., Field, M. E., *et al.* (2014). 2014 AHA/ACC/HRS Guideline for the Management of Patients With Atrial Fibrillation: Executive Summary: A Report of the American College of Cardiology/American Heart Association Task Force on Practice Guidelines and the Heart Rhythm Society. *Circulation*, **129**, doi:10.1161/CIR.0000000000000040.

Jinta, T., Miyazaki, Y., Kishi, M., Akashi, T., Takemura, T., Inase, N. and Yoshizawa, Y. (2010). The pathogenesis of chronic hypersensitivity pneumonitis in common with idiopathic pulmonary fibrosis: Expression of apoptotic markers. *Am. J. Clin. Pathol.* **134**, 613–620.

Kagedal, K., Johansson, U. and Ollinger, K. (2001). The lysosomal protease cathepsin D mediates apoptosis induced by oxidative stress. *FASEB J.* **15**, 1592–1594.

Kober, L., Torp-Pedersen, C., McMurray, J. J., Gotzsche, O., Levy, S., Crijns, H., Amlie, J. and Carlsen, J. (2008). Increased mortality after dronedarone therapy for severe heart failure. *N. Engl. J. Med.* **358**, 2678–2687.

Korfei, M., Ruppert, C., Mahavadi, P., Henneke, I., Markart, P., Koch, M., Lang, G., Fink, L., Bohle, R. M., Seeger, W., *et al.* (2008). Epithelial endoplasmic reticulum stress and apoptosis in sporadic idiopathic pulmonary fibrosis. *Am. J. Respir. Crit. Care Med.* **178**, 838–846.

Le Heuzey, J. Y., De Ferrari, G. M., Radzik, D., Santini, M., Zhu, J. and Davy, J. M. (2010). A short-term, randomized, double-blind, parallel-group study to evaluate the efficacy and safety of dronedarone versus amiodarone in patients with persistent atrial fibrillation: The DIONYSOS study. *J. Cardiovasc. Electrophysiol.* **21**, 597–605.

Liebisch, G., Vizcaino, J. A., Kofeler, H., Trotzmuller, M., Griffiths, W. J., Schmitz, G., Spener, F. and Wakelam, M. J. (2013). Shorthand notation for lipid structures derived from mass spectrometry. *J. Lipid Res.* **54**, 1523–1530.

Lubic, S. P., Nguyen, K. P., Dave, B. and Giacomini, J. C. (1994). Antiarrhythmic agent amiodarone possesses calcium channel blocker properties. *J. Cardiovasc. Pharmacol.* **24**, 707–714.

Mahavadi, P., Korfei, M., Henneke, I., Liebisch, G., Schmitz, G., Gochuico, B. R., Markart, P., Bellusci, S., Seeger, W., Ruppert, C., *et al.* (2010). Epithelial stress and apoptosis underlie Hermansky-Pudlak syndrome-associated interstitial pneumonia. *Am. J. Respir. Crit. Care Med.* **182**, 207–219.

Martin, W. J. 2nd, Kachel, D. L., Vilen, T. and Natarajan, V. (1989). Mechanism of phospholipidosis in amiodarone pulmonary toxicity. *J. Pharmacol. Exp. Ther.* **251**, 272–278.

Morissette, G., Ammoury, A., Rusu, D., Marguery, M. C., Lodge, R., Poubelle, P. E. and Marceau, F. (2009). Intracellular sequestration of amiodarone: Role of vacuolar ATPase and macroautophagic transition of the resulting vacuolar cytopathology. *Br. J. Pharmacol.* **157**, 1531–1540.

Mortuza, G. B., Neville, W. A., Delaney, J., Waterfield, C. J. and Camilleri, P. (2003). Characterisation of a potential biomarker of phospholipidosis from amiodarone-treated rats. *Biochim. Biophys. Acta* **1631**, 136–146.

Niu, C. H., Wang, Y., Liu, J. D., Wang, J. L. and Xiao, J. H. (2013). Protective effects of neferine on amiodarone-induced pulmonary fibrosis in mice. *Eur. J. Pharmacol.* **714**, 112–119.

Okayasu, K., Takeda, Y., Kojima, J., Yoshizawa, A., Kobayashi, N., Sugiyama, H. and Kudo, K. (2006). Amiodarone pulmonary toxicity: A patient with three recurrences of pulmonary toxicity and consideration of the probable risk for relapse. *Intern. Med.* **45**, 1303–1307.

Ott, M. C., Khoor, A., Leventhal, J. P., Paterick, T. E. and Burger, C. D. (2003). Pulmonary toxicity in patients receiving low-dose amiodarone. *Chest* **123**, 646–651.

Padmavathy, B., Devaraj, H. and Devaraj, N. (1993). Amiodarone–induced changes in surfactant phospholipids of rat lung. *Naunyn Schmiedebergs Arch. Pharmacol.* **347**, 421–424.

Piccoli, E., Nadai, M., Caretta, C. M., Bergonzini, V., Del Vecchio,

Downloaded from https://academic.oup.com/toxsci/article-abstract/142/1/285/1710567 by Universitaet Giessen user on 24 October 2019

C., Ha, H. R., Bigler, L., Dal Zoppo, D., Faggin, E., Pettenazzo, A., *et al.* (2011). Amiodarone impairs trafficking through late endosomes inducing a Niemann-Pick C-like phenotype. *Biochem. Pharmacol.* **82**, 1234–1249.

Plomp, T. A., van Rossum, J. M., Robles de Medina, E. O., van Lier, T. and Maes, R. A. (1984). Pharmacokinetics and body distribution of amiodarone in man. *Arzneimittelforschung* **34**, 513–520.

Ramanathan, R. (2009). Choosing a right surfactant for respiratory distress syndrome treatment. *Neonatology* **95**, 1–5.

Rudiger, M., Kolleck, I., Putz, G., Wauer, R. R., Stevens, P. and Rustow, B. (1998). Plasmalogens effectively reduce the surface tension of surfactant-like phospholipid mixtures. *Am. J. Physiol.* **274**, L143–L148.

Rustow, B., Kolleck, I., Guthmann, F., Haupt, R., Kunze, D. and Stevens, P. (1994). Synthesis and secretion of plasmalogens by type-II pneumocytes. *Biochem. J.* **302**, 665–668.

Sarma, J. S., Pei, H. and Venkataraman, K. (1997). Role of oxidative stress in amiodarone-induced toxicity. *J. Cardiovasc. Pharmacol. Ther.* **2**, 53–60.

Somani, P., Bandyopadhyay, S., Gross, S. A., Morady, F. and Dicarlo, L. A. (1987). Amiodarone and multilamellar inclusion bodies. *Br. J. Clin. Pharmacol.* **24**, 237–239.

Uhal, B. D., Zhang, H., Abdul-Hafez, A., Shu, R. and Li, X. (2007). Amiodarone induces angiotensinogen gene expression in lung alveolar epithelial cells through activation protein-1. *Basic Clin. Pharmacol. Toxicol.* **100**, 59–66.

Wilson, B. D., Clarkson, C. E. and Lippmann, M. L. (1991). Amiodarone-induced pulmonary inflammation. Correlation with drug dose and lung levels of drug, metabolite, and phospholipid. *Am. Rev. Respir. Dis.* **143**, 1110–1114.

Wright, J. R. (1990). Clearance and recycling of pulmonary surfactant. *Am. J. Physiol.* **259**, L1–12.

Zimetbaum, P. J. (2009). Dronedarone for atrial fibrillation–an odyssey. *N. Engl. J. Med.* **360**, 1811–1813.

Downloaded from https://academic.oup.com/toxsci/article-abstract/142/1/285/1710567 by Universitaet Giessen user on 24 October 2019

OXFORD UNIVERSITY PRESS LICENSE
TERMS AND CONDITIONS

Feb 24, 2023

This Agreement between Justus-Liebig University Giessen -- Poornima Mahavadi ("You") and Oxford University Press ("Oxford University Press") consists of your license details and the terms and conditions provided by Oxford University Press and Copyright Clearance Center.

License Number	5495250658053
License date	Feb 24, 2023
Licensed content publisher	Oxford University Press
Licensed content publication	Toxicological Sciences
Licensed content title	Altered Surfactant Homeostasis and Alveolar Epithelial Cell Stress in Amiodarone-Induced Lung Fibrosis
Licensed content author	Mahavadi, Poornima; Henneke, Ingrid
Licensed content date	Aug 27, 2014
Type of Use	Thesis/Dissertation
Institution name	
Title of your work	Altered Surfactant Homeostasis and Alveolar Epithelial Cell Stress in Amiodarone-Induced Lung Fibrosis
Publisher of your work	Justus-Liebig University Giessen
Expected publication date	Feb 2023

Permissions cost	0.00 EUR
Value added tax	0.00 EUR
Total	0.00 EUR
Title	Altered Surfactant Homeostasis and Alveolar Epithelial Cell Stress in Amiodarone-Induced Lung Fibrosis
Institution name	Justus-Liebig University Giessen
Expected presentation date	Feb 2023
Portions	Full article with citation
Requestor Location	Justus-Liebig University Giessen Gaffkystraße 11 EG, Seltersberg haus-C Giessen, 35392 Germany Attn: Justus-Liebig University Giessen
Publisher Tax ID	GB125506730
Total	0.00 EUR
Terms and Conditions	

STANDARD TERMS AND CONDITIONS FOR REPRODUCTION OF MATERIAL FROM AN OXFORD UNIVERSITY PRESS JOURNAL

1. Use of the material is restricted to the type of use specified in your order details.

2. This permission covers the use of the material in the English language in the following territory: world. If you have requested additional permission to translate this material, the terms and conditions of this reuse will be set out in clause 12.

3. This permission is limited to the particular use authorized in (1) above and does not allow you to sanction its use elsewhere in any other format other than specified above, nor does it apply to quotations, images, artistic works etc that have been reproduced from other sources which may be part of the material to be used.

4. No alteration, omission or addition is made to the material without our written consent. Permission must be re-cleared with Oxford University Press if/when you decide to reprint.

5. The following credit line appears wherever the material is used: author, title, journal, year, volume, issue number, pagination, by permission of Oxford University Press or the sponsoring society if the journal is a society journal. Where a journal is being published on behalf of a learned society, the details of that society must be included in the credit line.

6. For the reproduction of a full article from an Oxford University Press journal for whatever purpose, the corresponding author of the material concerned should be informed of the proposed use. Contact details for the corresponding authors of all Oxford University Press journal contact can be found alongside either the abstract or full text of the article concerned, accessible from www.oxfordjournals.org Should there be a problem clearing these rights, please contact journals.permissions@oup.com

7. If the credit line or acknowledgement in our publication indicates that any of the figures, images or photos was reproduced, drawn or modified from an earlier source it will be necessary for you to clear this permission with the original publisher as well. If this permission has not been obtained, please note that this material cannot be included in your publication/photocopies.

8. While you may exercise the rights licensed immediately upon issuance of the license at the end of the licensing process for the transaction, provided that you have disclosed complete and accurate details of your proposed use, no license is finally effective unless and until full payment is received from you (either by Oxford University Press or by Copyright Clearance Center (CCC)) as provided in CCC's Billing and Payment terms and conditions. If full payment is not received on a timely basis, then any license preliminarily granted shall be deemed automatically revoked and shall be void as if never granted. Further, in the event that you breach any of these terms and conditions or any of CCC's Billing and Payment terms and conditions, the license is automatically revoked and shall be void as if never granted. Use of materials as described in a revoked license, as well as any use of the materials beyond the scope of an unrevoked license, may constitute copyright infringement and Oxford University Press reserves the right to take any and all action to protect its copyright in the materials.

9. This license is personal to you and may not be sublicensed, assigned or transferred by you to any other person without Oxford University Press's written permission.

10. Oxford University Press reserves all rights not specifically granted in the combination of (i) the license details provided by you and accepted in the course of this licensing transaction, (ii) these terms and conditions and (iii) CCC's Billing and Payment terms and conditions.

11. You hereby indemnify and agree to hold harmless Oxford University Press and CCC, and their respective officers, directors, employs and agents, from and against any and all claims arising out of your use of the licensed material other than as specifically authorized pursuant to this license.

12. Other Terms and Conditions:

v1.4

Questions? customercare@copyright.com.

Citation of this article: Poornima Mahavadi, Ingrid Henneke, Clemens Ruppert, Lars Knudsen, Shalini Venkatesan, Gerhard Liebisch, Rachel C. Chambers, Matthias Ochs, Gerd Schmitz, Carlo Vancheri, Werner Seeger, Martina Korfei, Andreas Guenther. Altered surfactant homeostasis and alveolar epithelial cell stress in amiodarone-induced lung fibrosis. **Toxicol Sci. 2014** Nov;142(1):285-97. doi: 10.1093/toxsci/kfu177. Epub 2014 Aug 27.

Am J Physiol Lung Cell Mol Physiol 309: L63–L75, 2015.
First published May 8, 2015; doi:10.1152/ajplung.00279.2014.

CALL FOR PAPERS | *Translational Research in Acute Lung Injury and Pulmonary Fibrosis*

Linking progression of fibrotic lung remodeling and ultrastructural alterations of alveolar epithelial type II cells in the amiodarone mouse model

Bastian Birkelbach,[1,2,4] Dennis Lutz,[1,2,4] Clemens Ruppert,[3,4] Ingrid Henneke,[3,4] Elena Lopez-Rodriguez,[1,2,4] Andreas Günther,[3,4,5,6,7] Matthias Ochs,[1,2,4,8] Poornima Mahavadi,[3,4]* and Lars Knudsen[1,2,4]*

[1]*Institute of Functional and Applied Anatomy, Hannover Medical School, Hannover, Germany;* [2]*Biomedical Research in Endstage and Obstructive Lung Disease Hannover (BREATH), Hannover, Germany;* [3]*Department of Internal Medicine, Justus-Liebig-University Giessen, Universities of Giessen and Marburg Lung Center (UGMLC), Giessen, Germany;* [4]*Member of the German Center for Lung Research (DZL), Germany;* [5]*European IPF Network, Giessen, Germany;* [6]*Excellence Cluster "Cardiopulmonary System ECCPS," Giessen, Germany;* [7]*Lung Clinic Waldhof-Elgershausen, Greifenstein, Germany; and* [8]*REBIRTH Cluster of Excellence, Hannover, Germany*

Submitted 2 October 2014; accepted in final form 7 May 2015

Birkelbach B, Lutz D, Ruppert C, Henneke I, Lopez-Rodriguez E, Günther A, Ochs M, Mahavadi P, Knudsen L. Linking progression of fibrotic lung remodeling and ultrastructural alterations of alveolar epithelial type II cells in the amiodarone mouse model. *Am J Physiol Lung Cell Mol Physiol* 309: L63–L75, 2015. First published May 8, 2015; doi:10.1152/ajplung.00279.2014.—Chronic injury of alveolar epithelial type II cells (AE2 cells) represents a key event in the development of lung fibrosis in animal models and in humans, such as idiopathic pulmonary fibrosis (IPF). Intratracheal delivery of amiodarone to mice results in a profound injury and macroautophagy-dependent apoptosis of AE2 cells. Increased autophagy manifested in AE2 cells by disturbances of the intracellular surfactant. Hence, we hypothesized that ultrastructural alterations of the intracellular surfactant pool are signs of epithelial stress correlating with the severity of fibrotic remodeling. With the use of design-based stereology, the amiodarone model of pulmonary fibrosis in mice was characterized at the light and ultrastructural level during progression. Mean volume of AE2 cells, volume of lamellar bodies per AE2 cell, and mean size of lamellar bodies were correlated to structural parameters reflecting severity of fibrosis like collagen content. Within 2 wk amiodarone leads to an increase in septal wall thickness and a decrease in alveolar numbers due to irreversible alveolar collapse associated with alveolar surfactant dysfunction. Progressive hypertrophy of AE2 cells and increase in mean individual size and total volume of lamellar bodies per AE2 cell were observed. A high positive correlation of these AE2 cell-related ultrastructural changes and the deposition of collagen fibrils within septal walls were established. Qualitatively, similar alterations could be found in IPF samples with mild to moderate fibrosis. We conclude that ultrastructural alterations of AE2 cells including the surfactant system are tightly correlated with the progression of fibrotic remodeling.

stereology; pulmonary fibrosis; alveolar epithelial type II cells; surfactant; collapse induration

THE FUNCTION OF THE LUNG CRITICALLY depends on its structural integrity. Within the limited space of the chest the mammalian lung provides a large surface area with a very thin diffusion barrier for efficient gas exchange (61). An economical network of connective tissue elements including collagen and elastic fibers stabilizes the lung, allowing continuous volume changes during breathing without noticeable effort at the same time. Besides the connective tissue elements, the surfactant system of the lung is of utmost importance, since it stabilizes the interior surface area of the lung by reducing surface tension within the alveoli, particularly at low lung volumes (3). The alveolar epithelium consists of alveolar epithelial type I and type II (AE2) cells. AE2 cells, also termed the "defender of the alveolus" (10), are critically involved in epithelial regeneration and surfactant metabolism. Increasing evidence suggests that dysfunction of the AE2 cells is causally linked to interstitial lung diseases in humans and in animal models. Targeted injury of AE2 cells by diphtheria toxin has been shown to be sufficient to induce fibrotic remodeling in mice lungs (51). Furthermore, disturbances in the secretion pathway of lamellar bodies, the surfactant storage organelles of AE2 cells, are linked to the development of pulmonary fibrosis in mice mimicking features of the Hermansky-Pudlak syndrome-associated interstitial pneumonia (HPSIP) (17, 34). In these mice, obvious features of AEC2 cell stress include giant lamellar bodies, early lysosomal and late endoplasmic reticulum (ER) stress, and, finally, apoptosis of this cell type (34). Supporting this, increased susceptibility for the development of pulmonary fibrosis and abnormalities in the AE2 cells were reported in animal models of Hermansky-Pudlak syndrome (64). Hence, intracellular trafficking defects of surfactant components as such might contribute to a profibrotic milieu in the lung (64). On the same line, increased surface tension within alveolar air spaces, as observed in different models of lung fibrosis (19, 34), suggests impaired alveolar dynamics, a feature that is likely to be present in sporadic IPF as well (16, 46).

In familial IPF, mutations of the surfactant protein C (SP-C) gene lead to the accumulation of misfolded and misdirected SP-C, which in turn induced an unfolded protein response, ER stress, and, ultimately, apoptosis (5, 37, 39). Ultrastructural analyses of lung explants from patients with juvenile interstitial

* P. Mahavadi and L. Knudsen contributed equally to this work.
Address for reprint requests and other correspondence: L. Knudsen, Institute for Functional and Applied Anatomy, Hannover Medical School, Carl-Neuberg Str. 1, 30625 Hannover, Germany (e-mail: Knudsen.lars@mh-hannover.de).

 1040-0605/15 Copyright © 2015 the American Physiological Society

Downloaded from www.physiology.org/journal/ajplung (141.050.134.220) on October 24, 2019.

lung disease due to SP-C mutations revealed the existence of hypertrophic AE2 cells, often containing increased number of profiles of disorganized lamellar bodies (18). Similarly, spontaneous development of lung fibrosis in domestic cats, linked to the quantitative and qualitative alterations of lamellar bodies within hypertrophic AE2 cells, was reported, suggesting similarities between feline IPF and human IPF (62). IPF is one of the most common forms of diffuse parenchymal lung diseases. It is, however, associated with a very limited prognosis (43). Effective drug therapies completely stopping disease progression are currently not available, and lung transplantation remains the only therapeutic option (49). The current pathogenetic concept suggests that fibrotic pulmonary remodeling is a consequence of repetitive minor injuries of unknown origin of the alveolar epithelial lining with denudation of the basal lamina and a disturbed alveolar reepithelialization (13). The exact mechanisms leading to the ongoing injury of the alveolar epithelium have not yet been defined in IPF, but it has been hypothesized that premature senescence of AE2 cells, disturbances of the surfactant system, and mechanical stress are involved (6, 8). Recent studies focusing on AE2 cells in IPF and animal models of pulmonary fibrosis point towards a central role of this cell type in the disease pathogenesis, since impaired regeneration capacity in concert with increased rate of apoptosis (58) and ER and lysosomal stress is consistently observed (15, 26, 34). Such "cellular stress" signature of the AE2 cells found in familial cases with SP-C mutations is at least in part shared with sporadic IPF (26, 27). According to earlier ultrastructural observations, AE2 cells located at fibrotic septal walls accompanied by signs of acute injury showed marked abnormalities of lamellar bodies' morphology in IPF (23). However, in areas with massive destruction and more progressed fibrotic remodeling like honey combing, AE2 cells were less often found and largely replaced by cuboidal cells, whose ultrastructure differed significantly from that of the AE2 cells (23). AE2 cells and myofibroblasts appear to be the most important constituents in IPF, at least in the initial phase of the disease, meaning that structural and molecular alterations of AE2 cells and the degree of fibrotic remodeling within septal walls are linked together. Hence, dysfunctional AE2 cells as morphologically characterized by hypertrophy (increase in cellular size), hyperplasia (increase in number), and abnormalities of the intracellular surfactant system might be involved in generating a profibrotic microenvironment in the lung (48).

Amiodarone, a very potent antiarrhythmic drug, accumulates within lysosomes and related organelles such as lamellar bodies. Administration of this drug is associated with interstitial fibrosis without relevant inflammation in mice paralleled with surfactant accumulation, increased ER stress and lysosomal stress, and increased autophagy and apoptosis of AE2 cells (32, 33). We have recently demonstrated that LC3B, the autophagy marker protein, was preferably localized at the limiting membrane and the interior of lamellar bodies both in healthy controls and after amiodarone challenge. Moreover, we observed classical autophagosomes, which are extremely rare in AE2 cells, in direct connection with the limiting membrane of the lamellar body after amiodarone challenge providing clear evidence that lamellar bodies and autophagosomes share the same source of membranes. In full support, knockdown of LC3B reduced amiodarone-induced accumulation of SP-C and apoptosis of alveolar epithelial cells (32). Hence, autophagy to a certain degree seems to be involved in cellular surfactant homeostasis and lamellar body formation in healthy AE2 cells while the excess of autophagy as indicated by an increase in LC3B and related increase in intracellular surfactant pool might induce dysfunction of AE2 cells and even cell death. Whether these autophagy-related disturbances of intracellular surfactant pool or whether an overall increase in autophagy would directly correlate with the severity of septal wall fibrosis is unclear. To answer this question, design-based stereology up to the electron microscopic level represents the method of choice. Design-based stereology allows sophisticated quantification of fibrotic remodeling in different compartments of the lung, e.g., within septal walls or within alveolar space, a feature that is not possible using other analytical methods. In the present study we analyzed the degree of septal wall fibrosis as a function of disturbances of the intracellular surfactant system. We tested the hypothesis whether ultrastructural alterations of AE2 cells including hypertrophy and hyperplasia as well as the alterations in the intracellular surfactant pool correlate with the severity of fibrosis in the amiodarone model of pulmonary fibrosis in mice by means of design-based stereology at the light and ultrastructural level. A high positive correlation between disturbances of the intracellular surfactant pool such as the volume of lamellar bodies on the one hand and the total amount of collagen fibrils within the septal wall tissue on the other hand could be found. These findings could be reproduced in sporadic human IPF diagnosed according to current criteria (43) at a qualitative level in areas with comparatively slight to moderate fibrosis.

MATERIALS AND METHODS

Animal models

The animal model of amiodarone-induced interstitial fibrosis has been described in detail elsewhere (33). Briefly, 20 male C57Bl/6 mice at the age of 8 wk received 0.8 mg/kg body wt amiodarone intratracheally every 5th day. Animals were randomly divided into two groups. AD d7 and AD d14 were killed 7 and 14 days after first amiodarone treatment, respectively. Seven days after first amiodarone administration, collagen content as estimated by hydroxyproline level in our previous study was significantly increased and progressive till *day 14* but remained stable thereafter up to *day 28* (33). Age-, gender-, and body weight-matched C57Bl/6 mice served as controls. Both the University Animal Care Committee and the Federal Authorities for Animal Research of the Regierungspraesidium Giessen (Hessen, Germany) approved the study protocol.

Fixation, Sampling, and Processing

The quantitative morphometric methods used in this study are based on the official research policy statement of the American Thoracic Society/European Respiratory Society on quantitative assessment of lung structure (21). Five animals each in groups wild type and AD d7 as well as six animals in group AD d14 were included in this study. The perfusion fixation process was based on a previous protocol described by Vasilescu et al. (56). A multipurpose fixative was used containing 4% paraformaldehyde, 0.1% glutaraldehyde in 0.2 M HEPES buffer. The perfusion pressure was 30 cmH_20 and the airway opening pressure during fixation was 13 cmH_2O, respectively. Fixation was started after the pulmonary vascular bed was rinsed with 0.9% NaCl solution. The airway opening pressure was adjusted during expiratory limb after recruitment maneuver (30 cmH_2O). After storage of the lungs for at least 24 h in fixative at a temperature of 4°C, the fluid displacement method was used to determine the total lung

Downloaded from www.physiology.org/journal/ajplung (141.050.134.220) on October 24, 2019.

volume (45). Afterwards, a systematic uniform randomization was carried out (54). The whole lungs were embedded in 4% agar and cut in cranio-caudal direction in eight lung slices with a thickness of 2 mm each using a tissue slicer. The aim of the systematic uniform randomization is to give every part of the lung the same chance of being considered for the stereological assessment. Hence, the stereological parameters represent the entire lung. Tissue slices designated for light microscopy were osmicated, immersed in 4% aqueous uranyl acetate, dehydrated in an acetone solution with rising concentration (e.g., 70, 90, and 100%), and embedded in glycol methacrylate according to the manufacturer's instructions (Technovit 8100; Heraeus Kulzer, Wehrheim, Germany). This protocol has been validated to minimize tissue deformation and therefore was appropriate for design-based stereology (47). The tissue slices assigned to electron microscopy had to undergo an additional unbiased sampling step. Areas from which a cube with an edge length about 1–2 mm should be taken from were randomly chosen by a point grid cast randomly on the slices. By means of this procedure, six to eight tissue blocks were obtained per lung. These small tissue blocks were postfixed in osmium tetroxide, stained en bloc in half-saturated aqueous uranyl acetate, dehydrated in a rising acetone series, and embedded in Epon. Six out of six to eight tissue blocks were taken by chance and further processed for stereological assessment.

Stereological Analysis

Design-based stereology at the light microscopic level was conducted applying a computer-assisted stereology system (newCAST; Visiopharm, Horsholm, Denmark) equipped with a computer-controlled Ludl-stage to carry out a systematic uniform random area sampling. In our study, stereological parameters to appropriately characterize lung fibrosis in animal models were based on recently published recommendations (36, 40). Following a cascade sampling design, volume fractions (V_V) of structures of interest were determined within the given reference volume at different levels of magnification using a coherent point grid for point counting. As the volume of the reference space was known, volume fractions were converted to total volumes by multiplication with the reference space. Volume fractions of parenchyma [V_V(Par,Lung)] and nonparenchyma [V_V(Nonpar,Lung)] within the lung were determined in the first step. The parenchyma includes any tissue that participates in gas exchange, which is an area with recognizable ductal and alveolar architecture (alveolar and ductal air space, septal wall tissue). Consistently, nonparenchyma was defined as structures that do not contribute to gas exchange under normal conditions, like bronchioli, all kind of blood vessels (except capillaries within septal wall tissue and corner vessels), and perivascular/peribronchiolar connective tissue. In addition, the volume fraction of destructed lung parenchyma [V_V(des,lung)] was determined. Destructed parenchyma included atelectasis, areas of alveolar edema filling the alveoli, and scars completely destroying the lung architecture. All parameters described above were determined using a primary magnification of ×5 and sections stained with toluidine blue. In a further step, with the use of a primary magnification of ×20 compartments within parenchyma were further assessed. With the use of a combination of point and intersection counting, volume fractions of alveolar air space [V_V(alv,par)], ductal air space [V_V(duc,par)], and septal wall tissue [V_V(sep,par)] as well as the surface density of the alveolar epithelium [S_V(alvepi,par)] were determined. The arithmetic mean thickness of septal wall tissue was calculated as volume-to-surface ratio [$\bar{\tau}$(sep)].

The first and fourth section of a series of sections were taken and stained with orcein and the physical disector was used to calculate the total number of alveoli per lung [*N*(alv,lung)] (22, 41). In a previous study in bleomycin-induced lung injury and fibrosis, the number of open alveoli per lung has been shown to highly correlate with lung compliance (31). The section thickness was 1.5 μm so that the disector height was 4.5 μm.

With the use of pairs of semithin sections for a physical disector counting (disector height 3 μm), the number of AE2 cells per lung [*N*(AE2,lung)] was determined at ×100 oil immersion (24, 52). In addition, the number-weighted mean volume of AE2 cells [$\bar{v}_N$(AE2)] was measured using the rotator method (53).

The electron microscopic analysis was performed using ultrathin sections (thickness ~100 nm) of the Epon-embedded tissue blocks. The ultrastructural analyses were performed by means of a transmission electron microscope (Morgagni 268; FEI, Eindhoven, The Netherlands) equipped with a Veleta camera (Olympus Soft Imaging Solutions, Münster, Germany). In wild type and AD groups, AE2 cells were recorded by meandering over the section using a magnification of ×7,100 and taking every second AE2 cell. Approximately 25 AE2 cells per section were analyzed. Images of the alveolar septal wall were recorded at a primary magnification of ×14,000 following a systematic uniform random area sampling. Every 100 μm in *x* and *y* direction an image was taken if septal wall tissue was present. A coherent test system including test points and line segments was projected on these images using the STEPanizer stereology tool (55). For the AE2 cells, volume fractions of lamellar bodies [V_V(lb/AE2)] within AE2 cells were determined by means of point counting and the volume-weighted mean volume of the lamellar bodies by point sampling of linear intercept lengths (14). The images of septal wall tissue were used to determine the volume fractions of alveolar epithelium [V_V(alvepi/sep)], basal lamina [V_V(bl/sep)], collagen [V_V(col/sep)], interstitial cells [V_V(ic/sep)], endothelial cells [V_V(endo/sep)], and capillary lumen [V_V(cap/sep)]. The arithmetic mean thickness of the blood-gas-barrier [$\bar{\tau}$(bgb)] was calculated as a volume-to-surface-ratio by point and intersection counting (60).

Function of Alveolar Surfactant

Function of alveolar surfactant was determined by means of established methods (33, 34). Mice were killed and subjected to bronchoalveolar lavage. Large surfactant aggregates were prepared by high speed centrifugation (48,000 *g*, 1 h, 4°C) and adjusted to 2 mg/ml phospholipidcontent. After a 30-min incubation period at 37°C, samples were transferred to the disposable sample chamber, and adsorption was measured over an initial period of 12 s (γ_{ads} = equilibrium surface tension). Next, pulsation was started by sinusoidally oscillating the bubble radius between 0.4 and 0.55 mm at a rate of 20 cycles/min. The pressure differences across the air/liquid interface were recorded continuously over 5 min and minimum surface tension (γ_{min} = dynamic surface tension behavior under pulsation) was calculated using the Young-Laplace equation.

Ultrastructure of Human IPF Lung Explants

Detailed ultrastructural descriptions of AE2 cells in fibrosing lung diseases including IPF have been published in 1982 (23). As diagnostic criteria of the clinical entity IPF have changed within the last decades, we processed lung tissue of two IPF lung explants diagnosed according to current criteria (43) for transmission electron microscopic evaluation. These two patients with sporadic IPF were participating in the European IPF Registry/Biobank and gave informed consent for participation. As most parts of the lungs of IPF lung explants are completely destructed and characterized by honey combing and cysts with very severe fibrosis, we focused on areas of the lung that were adjacent to such severe fibrotic areas as identified at macroscopic level but still contained air so that tissue did not descent in fixation solution. Tissue blocks with a diameter of 1–2 mm were sampled and immersion fixed in 1.5% glutaraldehyde, 1.5% paraformaldehyde in 0.15 M HEPES buffer for at least 24 h at 4°C. Afterwards, tissue was embedded in Epon as described above. The European IPF Registry and Biobank have been approved by the local ethic committee and data protection officers. Embedded tissue for electron microscopic evaluation from five healthy donor lungs was available from a previous study (41).

Downloaded from www.physiology.org/journal/ajplung (141.050.134.220) on October 24, 2019.

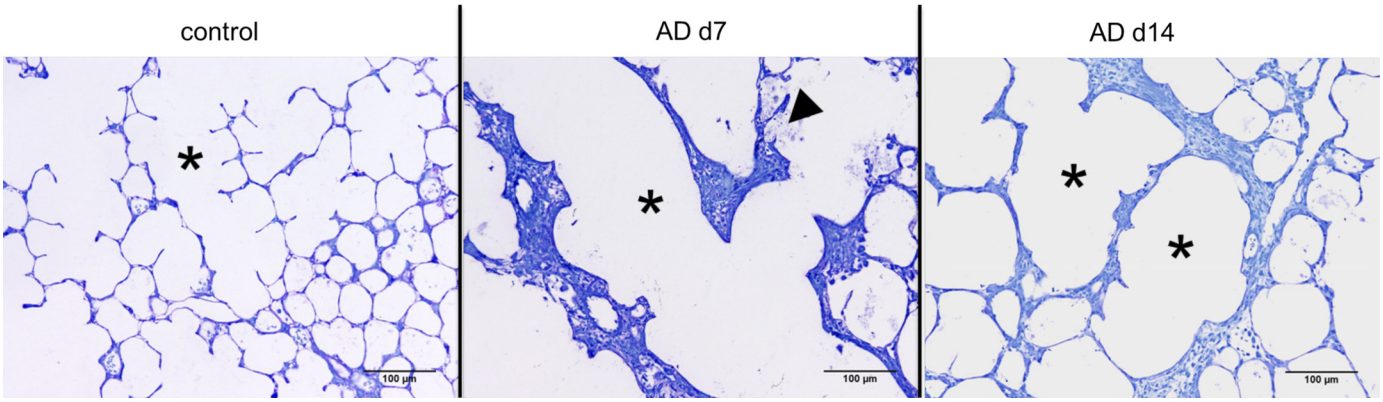

Fig. 1. Amiodarone and septal wall thickening. Representative light microscopic images of toluidine blue stained sections: enlarged alveolar ducts (asterisk) with thickened septal walls deprived of their alveoli were seen in AD d7 and AD d14 (killed 7 and 14 days after 1st amiodarone treatment, respectively). Adjacent alveoli appeared to be enlarged compared with the control group. In some alveoli surfactant material could be observed after amiodarone challenge but not in untreated controls (arrowhead).

Statistics

Data were analyzed using one-way ANOVA with a Bonferroni correction for multiple comparisons. A value of $P < 0.05$ was considered significant. Correlation analyzes were carried out using Spearman-test and pooled data. Tests were performed using Prism GraphPad 5.0 software.

RESULTS

Qualitative Findings: Animal Models

Air spaces were homogenously inflated and septal walls were slim with open corner vessels in control animals, suggesting a successful perfusion fixation (Fig. 1). After amiodarone challenge, focal thickening of septal walls was observed (Fig. 1). In some regions with thickened septal walls alveolar ducts were enlarged, lacking alveoli (Fig. 1, asterisk), hinting at high surface tension and alveolar collapse (63) and collapse induration as a mechanism for a loss of ventilated alveoli (9, 31). Some areas demonstrated accumulation of intra-alveolar surfactant in alveolar space 7 days after first amiodarone challenge (Fig. 1, arrowhead), which was absent in the control group.

At the electron microscopic level traces of interstitial and alveolar edema were occasionally seen 7 days after challenge (Fig. 2). In addition, denudation of the basal lamina due to cell death (usually oncosis) of AE1 and AE2 cells was a typical finding (Fig. 2). Interstitial edema was present 7 days after amiodarone within the thick side of the septal wall, where, as opposed to the thin side, stabilizing connective tissue elements like collagen fibrils (Fig. 2, asterisk) are found. At *day 14*, edema was not present anymore. Instead large bundles of collagen fibrils could be observed within the alveolar septal wall tissue often in close neighborhood to enlarged profiles of AE2 cells, which were completely filled with enlarged and numerous lamellar bodies (Figs. 2 and 3). In addition, the thickness of the basal lamina appeared to have increased. Some AE2 cells could be located within thickened septal wall tissue, indicating that they had lost their usual spatial orientation

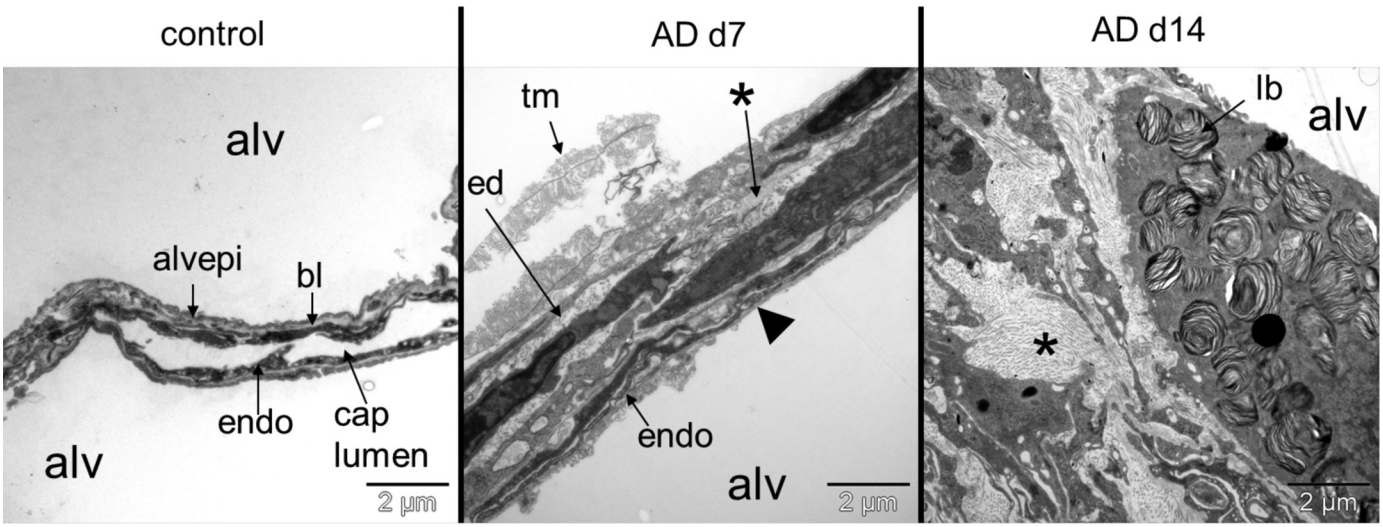

Fig. 2. Amiodarone and injury of the blood-gas barrier. Representative electron microscopic images of septal wall morphology: basal lamina was denuded in AD d7 as a consequence of epithelial cell injury (arrowhead). The endothelium was unaffected. In AD d14 bundles of collagen fibrils (asterisk) were increased and observed in thickened septal walls underneath enlarged alveolar epithelial type II (AE2) cells completely filled with lamellar bodies (lb). Alv, alveolar air space; bl, basal lamina; endo, endothelium; caplumen, capillary lumen; IC, interstitial cell; ed, interstitial edema.

Downloaded from www.physiology.org/journal/ajplung (141.050.134.220) on October 24, 2019.

regarding the contact to alveolar air space, e.g., as a consequence of alveolar collapse (Fig. 3). As published previously by our group (33), more and larger profiles of AE2 cells containing high amounts of lamellar bodies suggested hyperplasia and hypertrophy of AE2 cells in this animal model (Fig. 3).

Human IPF Lung Explants and Healthy Donor Lungs

Alveolar epithelium was injured as shown by fragmentation (Fig. 4, arrow) and denudation of the basal lamina in areas with slight septal wall thickening (Fig. 4, arrowhead). In direct neighborhood to areas of denuded basal lamina, AE2 cells were enlarged and filled with abundant lamellar bodies (Figs. 4 and 5). Some of the AE2 cells were lifted off the basal lamina and showed signs of cell death like swelling and vacuolization (Fig. 4, DC) (35). Septal walls were thickened as a consequence of an increase in components of the extracellular matrix (ECM) including collagen fibrils (Figs. 4 and 5, asterisk). A prominent finding was the marked thickening of the basal lamina in these regions. Enlarged and numerous AE2 cells were present that contained larger and above all more lamellar bodies compared with the healthy controls. Within interstitial tissue, profiles of AE2 cells occurred. Microvilli-like structures separated these AE2 cells from a surrounding basal lamina. As microvilli are usually observed at the luminal and not at the basolateral surface, this observation might be a consequence of alveolar collapse within the space between the AE2 cell and the denuded basal lamina representing the residual alveolar lumen. Alternatively, the polarization of the cell got lost and this might be considered a morphological correspondent of epithelial-mesenchymal transition.

Quantitative Findings: Amiodarone Model of Pulmonary Fibrosis

Stereological data related to general lung architecture and AE2 cells including intracellular surfactant pool and composition of the septal wall tissue are summarized in Tables 1–3 and Figs. 6–9.

General lung architecture and surfactant function. Amiodarone induced a significant increase in total volume of septal wall tissue per lung [V(sep,lung); Table 1]. While the total volume of alveolar air spaces [V(alvair,lung)] remained virtually unchanged, a marked increase in the total volume of ductal air space [V(ductair,lung)] could be found in AD d7 being in line with the qualitative finding of enlargement of alveolar ducts. In turn, the surface area of alveolar epithelium per unit

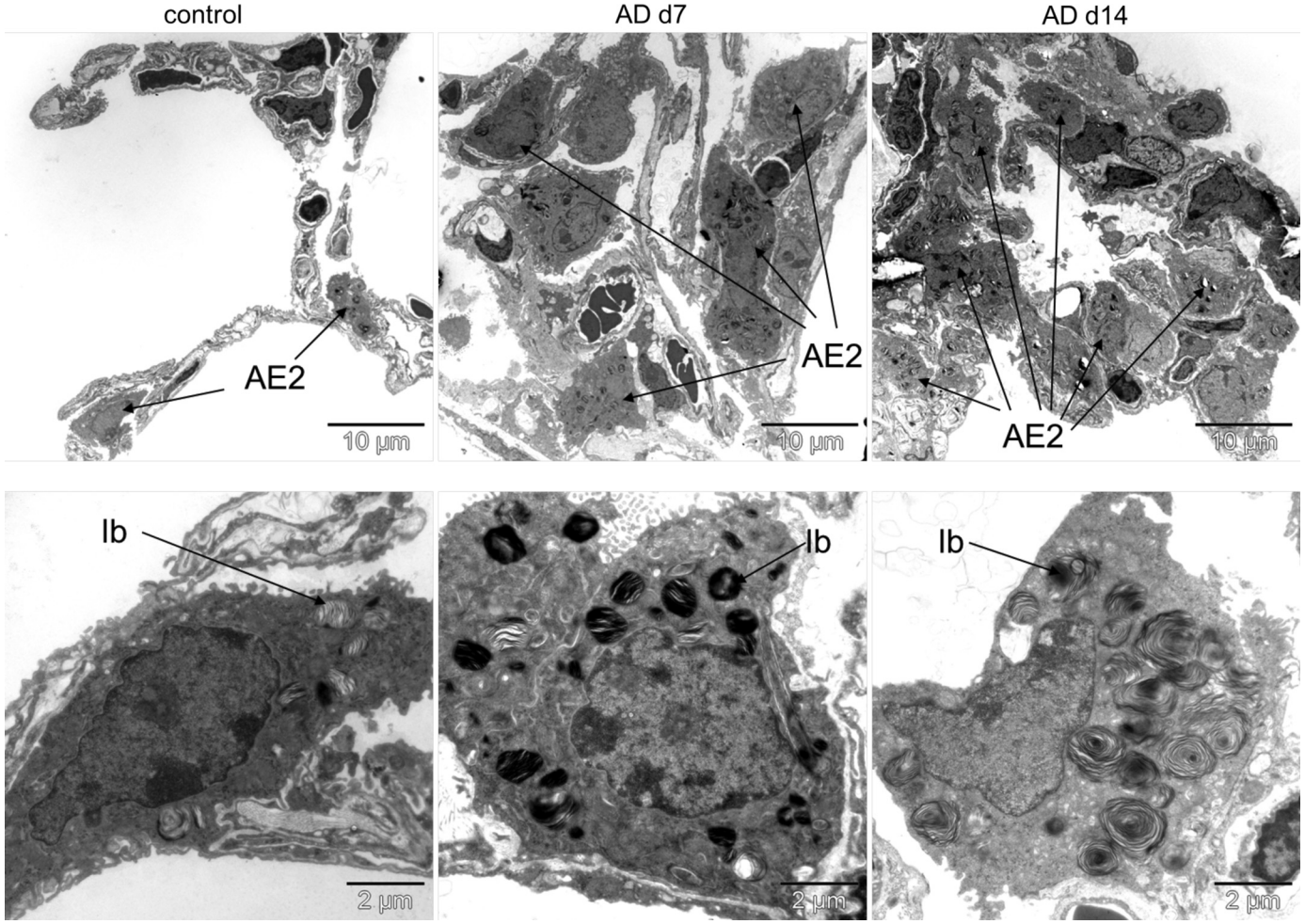

Fig. 3. Amiodarone and ultrastructure of AE2 cells. Representative electron microscopic images showing ultrastructure of AE2 cells and the surfactant system: more and larger profiles of AE2 cells were observed in AD d7 and AD d14 (arrows) in particular in areas with thickened septal walls. These enlarged AE2 cells contained more and larger profiles of lamellar bodies.

Downloaded from www.physiology.org/journal/ajplung (141.050.134.220) on October 24, 2019.

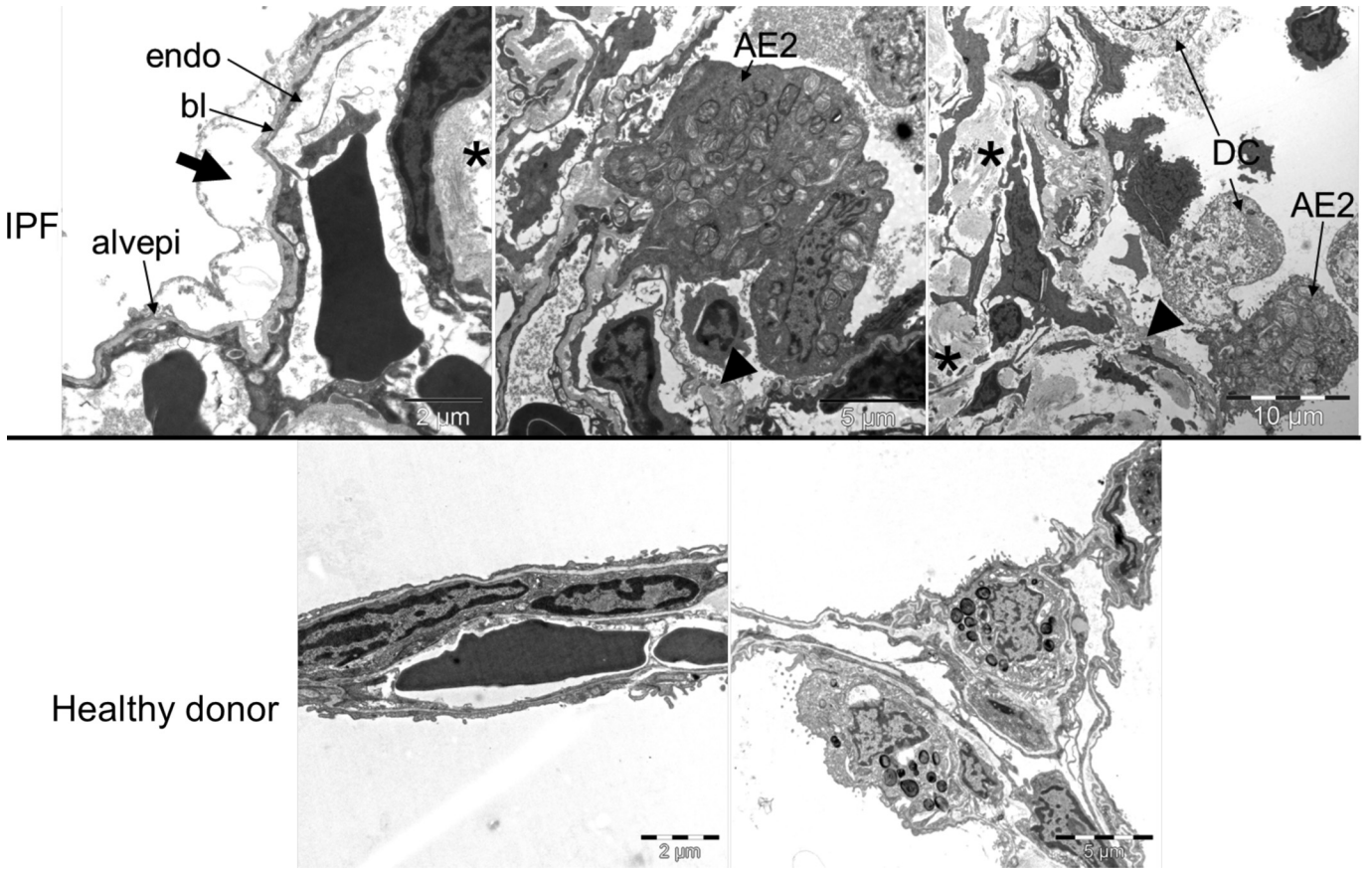

Fig. 4. Lung injury in idiopathic pulmonary fibrosis (IPF). Representative images of human IPF explants with thickened septal walls and healthy donor lungs: injury of the alveolar lining indicated by swelling of epithelial cells (arrow) and denudation of basal lamina (arrowhead). AE2 cells in these regions were enlarged in size, contained more profiles of lamellar bodies, and were sometimes lifted off the basal lamina. Some of them fulfilled ultrastructural criteria of cell death (DC). Asterisk marks bundles of collagen fibrils.

parenchyma [S_V(alvepi/par)] was significantly decreased in this group but was nearly normalized in AD d14. Alveolar number per lung [N(alv,lung)] showed a trend towards lower values in both amiodarone groups (Fig. 6*A*) while septal walls were significantly thickened (Fig. 6*B*). A significant negative correlation of pooled data between septal wall thickness and alveolar number supports the concept of collapse induration where alveolar collapse leads to septal wall thickening (Fig. 6*C*). In addition, the remaining alveoli were characterized by a larger number-weighted mean volume [$\bar{v}_N$(alv)]. This finding supports the notion that alveolar collapse and collapse induration, e.g., due to high surface tension and at later time points fibroproliferation, led to thickening of septal walls around enlarged alveolar ducts. In line with this speculation, we observed remnants of the basal lamina within thickened septal walls 7 and 14 days after first amiodarone challenge (Fig. 6, *D–F*). Remnants of the basal lamina have been suggested by Katzenstein and Myers (38) to result from collapse induration, which is likely to contribute to the loss of lung capacity in fibrosing lung diseases (31). In this context, we performed measurements to characterize the function of bronchoalveolar lavage-derived intra-alveolar surfactant by means of a pulsating bubble surfactometer. Seven days after first amiodarone challenge we observed a significant increase in minimum surface tension compared with control animals (Fig. 7). The surfactant dysfunction was associated with a decline in alveolar number and the occurance of collapse induration at the ultrastructural level. Fourteen days after first amiodarone challenge, the function of the intra-alveolar surfactant had partly recovered although the alveolar number remained stable. This suggests that collapse induration is an irreversible process.

AE2 cells and intracellular surfactant. Compared with the control group, amiodarone induces a progressive increase in the number-weighted mean volume of AE2 cells [$\bar{v}_N$(AE2)] from *day 7* to *14* (Fig. 8*A*; Table 2). The total number of AE2 cells per lung [*N*(AE2,lung)] also increased at *day 7* but remained stable thereafter (Fig. 8*B*). The hypertrophy of AE2 cells (increase in cellular volume) could partly be explained by an progressive increase in the total volume of lamellar bodies per cell [V(lb,AE2); Fig. 8*C*]. As demonstrated by the volume-weighted mean volume, the lamellar bodies as such increased in size after amiodarone challenge (Fig. 8*D*).

Composition of septal wall tissue. Although alveolar collapse as such could at least partly explain the increase in septal wall thickness after amiodarone challenge, this is not the case regarding the marked increase in the total volume of alveolar septal walls per lung (Table 3). Hence, we analyzed the composition of septal walls at the ultrastructural level by dividing alveolar septal walls into different components: alveolar epithelium, basal lamina, collagen fibrils, amorphous ECM, interstitial cells, endothelium, and capillary lumen. A slight increase in the total volume of the alveolar epithelium

Downloaded from www.physiology.org/journal/ajplung (141.050.134.220) on October 24, 2019.

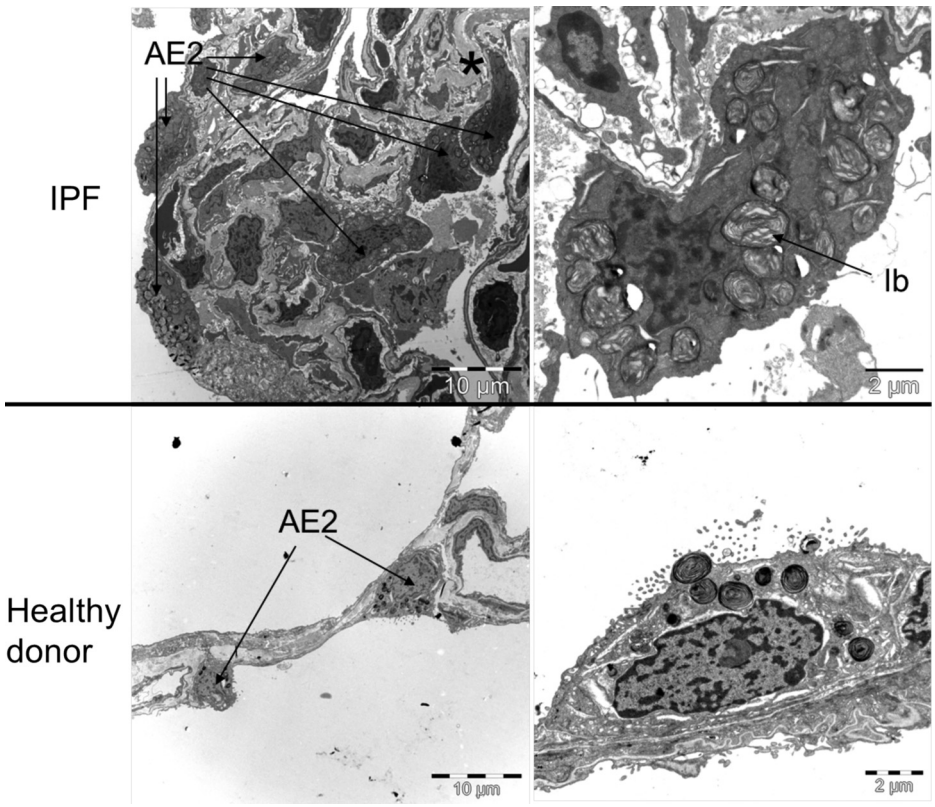

Fig. 5. IPF and the ultrastructure of AE2 cells. Characteristic ultrastructure of AE2 cells in regions with thickened septal walls of IPF lung explants and healthy human donor lungs. AE2 cells were increased in number and size containing enlarged lamellar bodies. Some AE2 cells appeared to be embedded within thickened septal walls. Asterisk indicates bundles of collagen fibrils.

[V(alvepi,sep)] was observed, which could most likely be attributed to hyperplasia and hypertrophy of AE2 cells and also to the swelling of alveolar epithelial type I cells. The total volume of endothelial cells [V(endo,sep)] and capillary lumen [V(caplumen,sep)], however, remained more or less stable after amiodarone challenge. Unlike the volume of capillaries within septal walls, the surface area of endothelium [S(endo,sep)] demonstrated a significant increase in AD d7, hinting towards angiogenesis, as a consequence of septal wall remodeling induced by amiodarone.

Table 1. *General lung architecture*

Parameter	Control	AD d7	AD d14	*P* Value
V(lung), cm^3	0.52 (0.07)	0.93 (0.07)*	0.72 (0.20)	<0.01
V(des,lung), mm^3	/	34.3 (23.6)	27.9 (7.3)	
N(alv,lung), 10^6	3.09 (0.06)	2.22 (0.83)	2.23 (0.56)	0.08
N_V(alv/par), $1/cm^3$	6.33 (0.02)	2.72 (0.83)*	3.69 (1.03)†	<0.01
$\bar{v}_N$(alv), 10^3 μm^3	93.5 (2.7)	177.6 (55.9)	144.1 (52.3)	<0.01
S(alvepi,lung), cm^2	209 (37.1)	210 (35.5)	245 (28.1)	NS
S_V(alvepi/par), cm^2/cm^3	431 (50.9)	273 (21.7)*	424 (82.6)‡	<0.01
V(alvair,lung), cm^3	0.29 (0.06)	0.37 (0.09)	0.31 (0.08)	NS
V(ductair,lung), cm^3	0.12 (0.03)	0.33 (0.06)*	0.17 (0.07)‡	<0.01
V(sep,lung), mm^3	75.0 (8.7)	146.7 (16.8)*	128.5 (21.6)†	<0.01
$\bar{\tau}$(sep), μm	7.32 (1.35)	14.5 (4.0)*	10.4 (0.9)†	<0.01
Lm, μm	78.2 (13.1)	118.6 (6.0)*	76.7 (18.3)†	<0.01

Values are means (SD). AD d7 and AD d14, killed 7 and 14 days after 1st amiodarone treatment, respectively; V, volume; *N*: number; N_V, numerical density; $\bar{v}_N$, number-weighted mean volume; S, surfacearea; S_v, surface area density; $\bar{\tau}$, arithmetic mean thickness; des, destructed lung parenchyma; alv, alveoli; par, lung parenchyma; alvepi, alveolar epithelium; alvair, alveolar air spaces; ductair, ductal airspaces; sep, septal wall tissue; Lm, mean linear intercept length. One-way ANOVA and Bonferroni test for statistical significance: *control vs. AD d7; †control vs. AD d14; ‡AD d7 vs. AD d14.

The most important factor leading to an increase in the volume of the septal walls could be assigned to the components of the interstitial tissue. The amorphous ECM [V(aECM,sep)] and collagen fibrils [V(coll,sep)] demonstrated a progressive increase after first amiodarone challenge and their volume increased by the factor 3 to 4 (Fig. 9*A*). The total volume of interstitial cells [V(IC,sep)] demonstrated an initial increase till *day 7* by the factor 3 compared with the control group but then decreased again till *day 14* after first amiodarone challenge. In essence, the described remodeling process led to an increase in the arithmetic mean thickness of the blood-gas barrier [τ(bgb)] due to deposition of connective tissue elements within the alveolar septal walls (Fig. 9*B*).

Correlation analysis. A progressive remodeling, characterized by an increase in the volume of collagen fibrils until *day 14* after amiodarone, could be observed. These findings were in line with the increase in the hydroxyproline level after the first amiodarone challenge as a typical marker used to assess the severity of pulmonary fibrosis (33). A correlation between the total volume of collagen fibrils within the alveolar septal wall (ultrastructural level) and the hydroxyproline level (biochemical level) could also be observed in the bleomycin model of pulmonary fibrosis (12). Hence, in the present study, we used the volume of collagen fibrils within the septal wall as an important severity marker of pulmonary fibrosis. High positive correlations between the volume of collagen fibrils within septal walls on the one hand and hypertrophy of AE2 cells, total volume of lamellar bodies per AE2 cell, and the volume-weighted mean size of lamellar bodies on the other hand could be established (Fig. 10, *A–C*). The same was the case taking the volume of amorphous ECM into consideration (data not

Downloaded from www.physiology.org/journal/ajplung (141.050.134.220) on October 24, 2019.

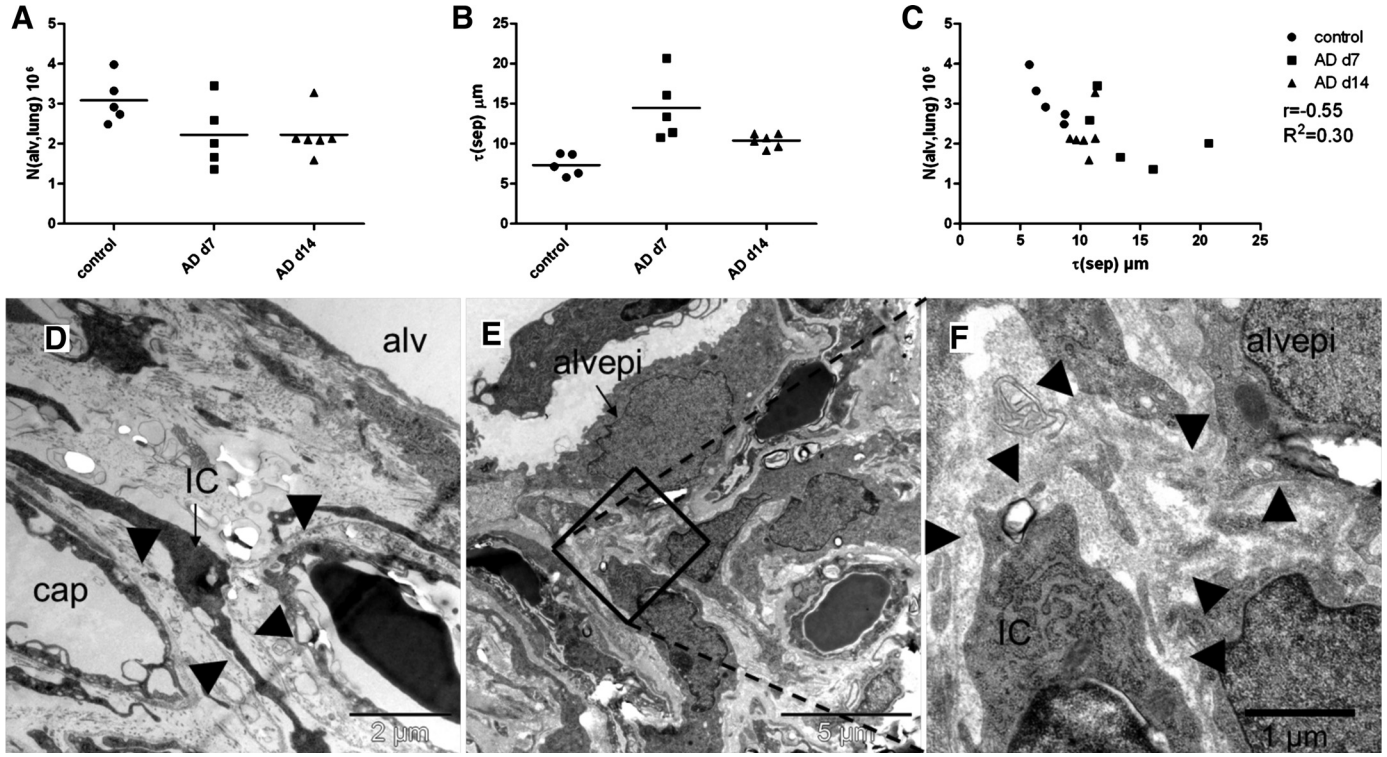

Fig. 6. Collapse induration. Total number of alveoli per lung (*A*) and arithmetic mean thickness of septal walls (*B*). Septal wall thickness and total number of alveoli demonstrated a negative correlation (*C*), meaning that alveolar collapse and collapse induration could explain at least partly the loss of alveoli in this model. *D–F*: at the ultrastructural level, basal laminae could be observed within thickened septal walls (arrowhead). Alvepi, alveolar epithelial cell. Individual data and mean are given.

shown). Altogether, alterations in intracellular surfactant pool and the severity of the pulmonary fibrosis are tightly correlated in this model.

DISCUSSION

The present study is the first stereological characterization of the amiodarone model of pulmonary fibrosis in mice. Moreover, for the first time, a quantitative link between alterations of AE2 cells and the degree of the deposition of collagen fibrils within the septal wall as a marker of severity of fibrosis could be established in an animal model. At a qualitative level these findings were reproducible in human IPF samples, where, in areas with thickened septal walls due to excessive ECM deposition but more or less maintained alveolar architecture and signs of lung injury (denuded basal lamina), AE2 cells appeared to be hypertrophic containing more and enlarged lamellar bodies. In humans amiodarone has been reported to induce a broad spectrum of pulmonary diseases ranging from acute respiratory distress syndrome to pulmonary fibrosis (7). In the current study, repetitive intratracheal instillation of amiodarone was used to mimic repetitive alveolar epithelial injury, a key characteristic of IPF. As demonstrated earlier by our group, amiodarone induces lysosomal stress (including autophagy) and endoplasmatic reticulum stress and results in autophagy-dependent apoptosis of AE2 cells (32–34). Moreover, electron microscopic tomography convincingly demonstrated that autophagosomes and lamellar bodies share the same source of membranes and that LC3B preferably localizes to the limiting membrane or the interior of lamellar bodies. It is hence reasonable to state that autophagy manifests the formation of increased and enlarged lamellar bodies in this animal model of pulmonary fibrosis (32). Therefore, the mouse model of repetitive intratracheal instillation of amiodarone was exploited to establish a correlation between disturbances of the intracellular surfactant system as a severity marker of epithelial stress defined by ultrastructural criteria and the degree of septal wall fibrosis. Therefore, we tried to translate our ultrastructural findings from the animal model to human IPF samples. AE2 cells are critical for maintaining healthy alveolar homeostasis, which is also reflected by the term "defender of the alveolus"

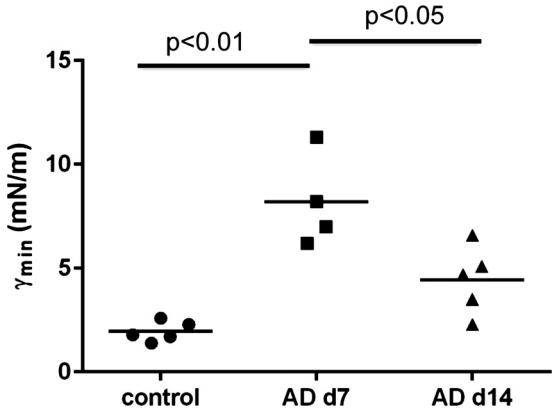

Fig. 7. Amiodarone and the function of alveolar surfactant. Seven days after first amiodarone challenge, minimum surface tension (γ_{min}) of bronchoalveolar lavage-derived alveolar surfactant is significantly increased and recovers somewhat on *day 14*. Data were obtained at a concentration of 2 mg phospholipids/ml.

Downloaded from www.physiology.org/journal/ajplung (141.050.134.220) on October 24, 2019.

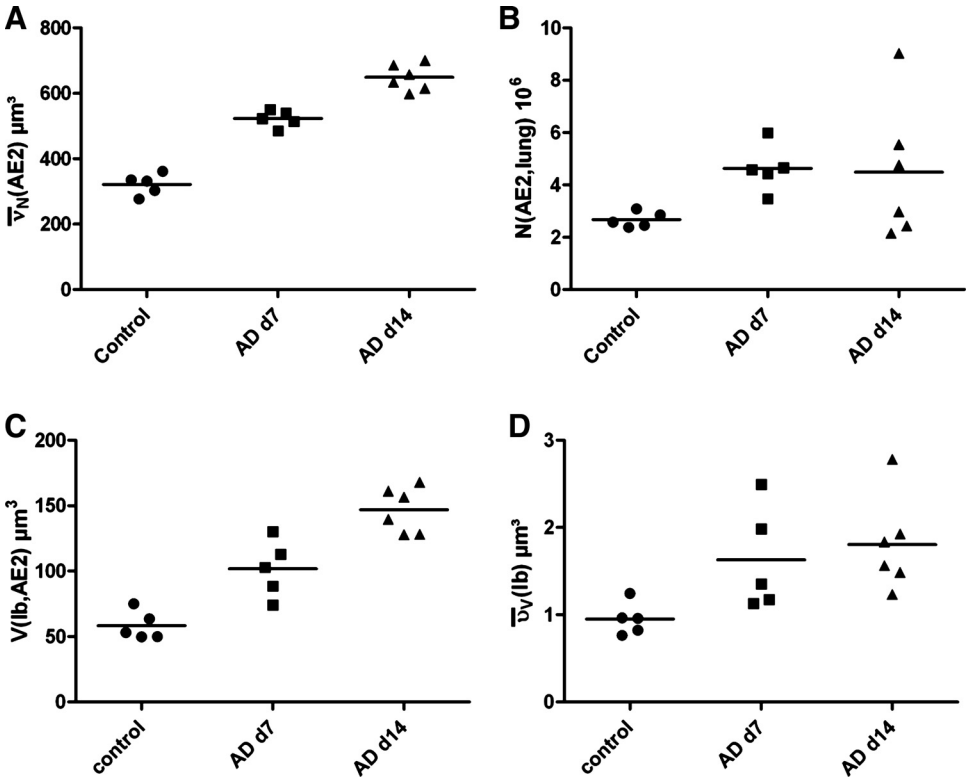

Fig. 8. Stereological data of AE2 cells. Number weighted mean volume of AE2 cells [$\bar{v}_N$(AE2); *A*], total number of AE2 cells per lung [*N*(AE2); *B*], total volume of lamellar bodies per AE2 cell [V(lb,AE2); *C*], and volume-weighted mean volume of lamellar bodies [$\bar{v}_v$(lb); *D*]. Individual data and mean are given.

(10). Besides their critical role in surfactant homeostasis which is inevitable to stabilize alveolar micro architecture during respiratory cycle, the role of AE2 cells as self-renewing stem cells of the alveolar epithelial lining is well accepted (57). Moreover, direct cell contacts with surrounding cells including fibroblasts located underneath the basal lamina (50) suggest a direct epithelial-mesenchymal communication, which is expanded by autocrine and paracrine mediators including, for instance, growth factors or inflammatory factors secreted by AE2 cells. These factors are known to regulate epithelial-mesenchymal cross talk and in turn influence alveolar micro architecture including turnover of components of the ECM under physiological and pathological conditions (20, 25, 30). In addition, in vitro studies suggested that AE2 cells, in concert with interstitial cells, are involved in the production of components of the ECM including collagen type I (11, 25) and these extracurricular functions have to be regulated very tightly in order not to interfere with the regular pulmonary functions as gas exchanger. Hence, dysfunctional AE2 cells have been suggested as key factors in generating a profibrotic microenvironment in the lung in pulmonary fibrosis (48). Recent studies linked ER stress of AE2 cells due to excessive accumulation of misfolded surfactant proteins to AE2 cell dysfunction and, as a final consequence, apoptosis in familial (37, 39) as well as sporadic IPF (26, 27). In HPSIP, AE2 cells demonstrate a massive defect in secretion of intracellular surfactant components leading to an accumulation within the cell (17). This has been proven to be a potent trigger for lysosomal and ER stress, resulting in apoptosis (34), inflammation (2), and fibrotic remodeling (64). Hence, altered surfactant homeostasis by AE2 cells might be involved in generating a profibrotic environment in the lung. In the amiodarone model, increased autophagy has been shown to be a critical mechanism for accumulation of SP-C and cell death (32). In addition, quali-

Table 2. *Alveolar type II cells and intracellular surfactant*

Parameter	Control	AD d7	AD d14	*P* Value
N(AE2,lung), 10^6	2.76 (0.30)	4.63 (0.90)	4.48 (2.59)	NS
N_V(AE2/par), 1/cm³	5.54 (0.49)	5.74 (0.81)	6.93 (3.39)	NS
$\bar{v}_N$(AE2), µm³	321 (33)	522 (25)*	648 (40)†‡	<0.01
V_V(lb/AE2)	0.18 (0.02)	0.19 (0.04)	0.23 (0.02)†	0.04
V(lb,AE2), µm³	58.3 (11.0)	101.7 (21.6)*	146.9 (17.3)†‡	<0.01
V(lb,lung), mm³	0.16 (0.04)	0.46 (0.04)	0.69 (0.47)†	0.03
ν_V(lb), µm³	0.95 (0.19)	1.63 (0.59)	1.80 (0.54)†	0.03

Values are means (SD). AE2, alveolar type II cells; lb, intracellular surfactant; V_V, volume fraction; ν_V, volume-weighted mean volume. One-way ANOVA and Bonferroni test for statistical significance: *control vs. AD d7; †control vs. AD d14; ‡AD d7 vs. AD d14.

Table 3. *Composition of septal wall tissue*

Parameter	Control	AD d7	AD d14	*P* Value
V(alvepi,sep), mm³	18.3 (2.9)	35.6 (7.20)*	31.6 (6.6)†	<0.01
V(BL,sep), mm³	3.55 (0.94)	9.02 (2.18)*	6.85 (1.83)†	<0.01
V(aECM,sep), mm³	7.48 (2.14)	27.3 (7.6)*	28.0 (11.6)†	<0.01
V(col,sep), mm³	0.73 (0.29)	2.15 (0.52)*	3.06 (1.01)†	<0.01
V(IC,sep), mm³	10.8 (3.4)	32.9 (13.9)*	23.3 (3.6)	<0.01
V(endo,sep), mm³	15.1 (3.2)	21.1 (2.6)*	17.2 (2.7)	0.02
V(caplumen,sep), mm³	19.1 (6.4)	18.5 (5.6)	17.6 (5.1)	NS
S(endo,sep), cm²	620 (138)	978 (141)*	716 (123)‡	<0.01
V(inter,sep), mm³	22.5 (3.1)	71.5 (21.8)*	61.2 (16.0)†	<0.01
$\bar{\tau}$(bgb), µm	0.43 (0.12)	0.57 (0.12)	0.60 (0.08)†	0.05

Values are means (SD). Alvepi, alveolar epithelium; BL, basal lamina; aECM, amorphous extracellular matrix; col, collagen fibrils; IC, interstitial cells; endo, endothelium; caplumen, capillary lumen; inter, interstitial tissue; bgb, blood-gas barrier. One-way ANOVA and Boferroni test for statistical significance *control vs. AD d7; †control vs. AD d14; ‡AD d7 vs. AD d14.

Downloaded from www.physiology.org/journal/ajplung (141.050.134.220) on October 24, 2019.

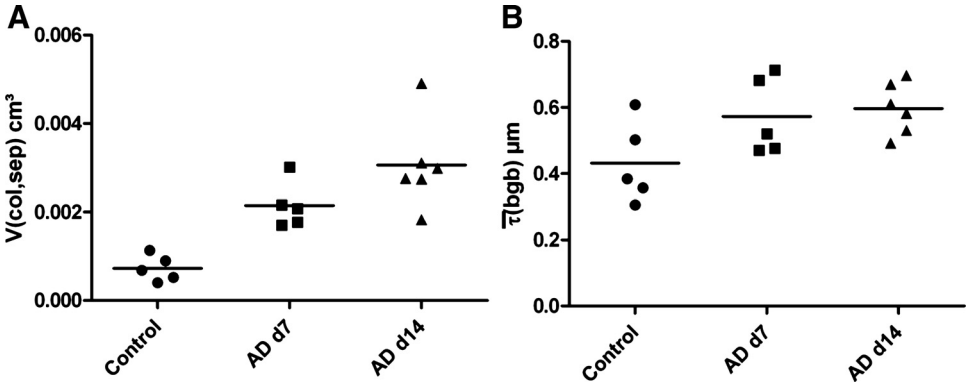

Fig. 9. Collagen content and blood-gas barrier. Total volume of collagen fibrils within septal walls per lung [V(col,sep); *A*] and the arithmetic mean thickness of the blood-gas barrier [$\bar{\tau}$(bgb); *B*]. Individual data and mean are given.

tative ultrastructural findings suggested an increase of intracellular surfactant pool size as a consequence of amiodarone treatment. Lamellar bodies are part of the lysosomal pathway and diverse mechanisms have been identified or suggested regarding the biogenesis of this organelle (42, 59). From a structural point of view autophagy has been convincingly linked to the intracellular surfactant pool, partly revealing its link to the degree of interstitial fibrosis. The volume of intracellular surfactant, defined by morphological criteria as the volume of lamellar bodies, could be an appropriate parameter of cellular stress and AE2 cell dysfunction inducing autophagy in the amiodarone model of pulmonary fibrosis.

In the present study, we quantified alterations of the intracellular surfactant pool as well as the structural remodeling process within the septal wall tissue using design-based stereology at the light and electron microscopic level. We found a progressive hypertrophy of AE2 cells within the first 14 days after amiodarone challenge, accompanied by a dramatic increase in the total volume of lamellar bodies per AE2 cell. The later could be attributed to an increase in the mean size of lamellar bodies. These changes regarding the intracellular surfactant pool were escorted by a thickening of the septal walls as indicated by an increase in the arithmetic mean thickness of septal walls, a loss of ventilated alveoli, and an increase in interstitial tissue elements within septal walls. In particular, the total volume of ECM and above all collagen fibrils as defined by ultrastructural criteria demonstrated a progressive increase till *day 14*. In IPF, alveolar collapse has been discussed to explain the observed decrease in alveolar surface area and volume of air space per lung (9). These pathological findings, however, could partly be reproduced by the amiodarone model of lung fibrosis in the present study and are most likely a consequence of an impaired intra-alveolar surfactant function, a feature this mouse model shares with human IPF as well as with the bleomycin model (16, 31).

A former study from 1982 analyzed changes of epithelial cells at the ultrastructural level in human pulmonary fibrosis including IPF (23). As opposed to healthy lung tissue, AE2 cells found in areas of thickened septal walls with slight fibrotic changes were characterized by the occurrence of giant lamellar bodies. In the present study, we also analyzed areas of thickened septal walls from two IPF patients diagnosed according to the current criteria (43). We could confirm the qualitative findings by Kawanami et al. (23) and found larger and more profiles of AE2 cells filled with abundant and larger lamellar bodies in close neighborhood to bundles of collagen fibrils and denudation of the basal lamina. These observations indicated that AE2 cell changes and interstitial remodeling are colocalized with areas of ongoing epithelial injury. Interestingly, immunohistochemical staining in areas of human IPF lungs that appeared at light microscopic level more or less normal demonstrated an increased, dot-like staining for LC3B while in areas with severe fibrosis (e.g., fibroblastic foci) LC3B was reduced, meaning that in areas with severe fibrosis and fibroblast foci autophagy seems to be insufficient while in other areas autophagy could be increased (1). In human IPF these biochemical markers of autophagy seem to be paralleled by the ultrastructural presentation of alterations of intracellular surfactant where in severely affected areas lamellar bodies are rare, disrupted, and small while in other regions, e.g., giant

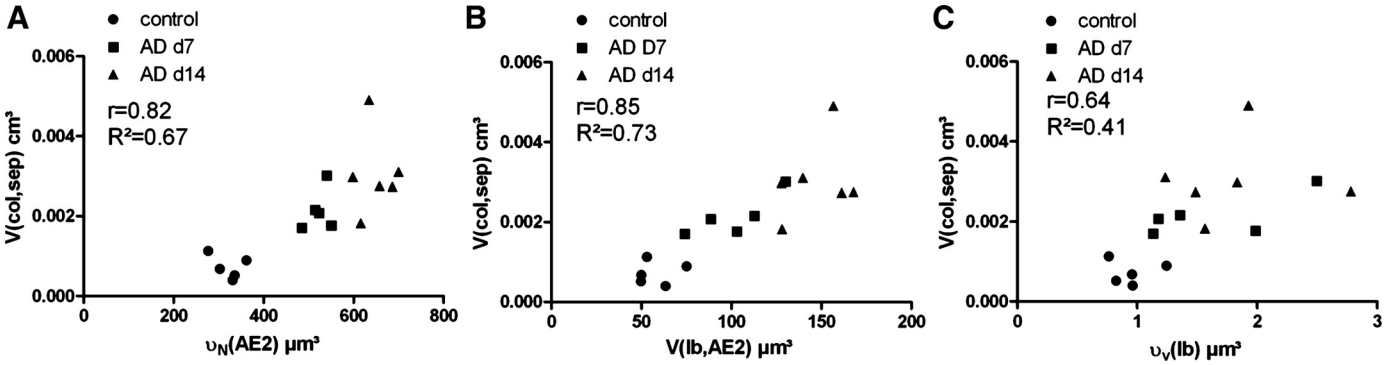

Fig. 10. AE2 cells and severity of fibrosis. Correlation analyses between the total volume of collagen within the septal walls and the number-weighted mean volume of AE2 cells (*A*) and total volume of lamellar bodies per AE2 cell (*B*) and volume-weighted mean volume of lamellar bodies (*C*).

Downloaded from www.physiology.org/journal/ajplung (141.050.134.220) on October 24, 2019.

lamellar bodies can be observed. However, severe fibrosis such as honeycombing and fibroblast foci is not present in the amiodarone model.

Intratracheal delivery of amiodarone might not truly mimic the drug delivery to the lung as it occurs clinically with systemic amiodarone therapy. Our animal model, however, exhibits histopathological alterations including patchy interstitial fibrosis, foamy AE2 cells, lung phospholipidosis, and AE2 apoptosis that resemble clinical amiodarone induced pulmonary toxicity. Of note, we recently reported severe surfactant accumulation and association of lamellar bodies with autophagosomal structures in amiodarone-treated mice. Hence, under the assumption that the increased intracellular surfactant pool is an indicator of cellular stress including autophagy with excessive accumulation of surfactant proteins and phospholipids, which might in turn be involved in driving fibrotic remodeling, we were able to establish a high positive correlation between the increase in the intracellular surfactant pool and the amount of collagen fibrils within septal wall tissue in the amiodarone model. Since both interstitial and epithelial cells are responsible for the turnover of components of the ECM, we also quantified the volume of interstitial cells within the septal walls. A correlation between the volume of interstitial cells and the degree of fibrosis was not found. These data clearly demonstrate that the alterations of AE2 cells and the septal wall fibrosis are linked together, meaning that they are either induced by the same factors or even causally linked, e.g., the excessive burden/stress due to increased surfactant pool provokes the generation of a more profibrotic environment by the AE2 cells, as seen in HPSIP.

In the amiodarone model, the total volume of destructed lung parenchyma was limited and amounted to $<4\%$ of total lung volume, which is less as has been found in the bleomycin model ($>10\%$) (31). The bleomycin model is much more complex including interstitial fibrosis within septal walls, extensive intra-alveolar fibrosis, and alveolar collapse (28, 29, 31). In the amiodarone model, the most prominent findings were thickened septal walls due to interstitial fibrosis and less intra-alveolar fibrosis or collapse induration.

Conclusion

Amiodarone challenge induces a progressive interstitial remodeling with considerable increase in components of ECM especially collagen fibrils within the septal walls. Similar alterations regarding the different ultrastructural components have also been demonstrated to occur in IPF lungs. The progressive increase in collagen fibrils could be tightly correlated to disturbances of the intracellular surfactant system suggesting that both pathological alterations are mediated by the same factors or that there is a causal relationship. In other words accumulation of intracellular surfactant potentially linked to autophagy-related dysfunction of AE2 cells and cell death after amiodarone challenge is clearly correlated with the degree of septal wall fibrosis. Qualitative findings observed in thickened septal walls with slight to moderate fibrotic remodeling from patients with IPF suggest that hypertrophy of AE2 cells and an increase in the intracellular surfactant pool could also be linked to a fibrotic remodeling process in humans at least in the early stages of the disease process.

ACKNOWLEDGMENTS

We thank Stefanie Hezel, Susanne Fassbender, and Sabine Fiedler for superb technical assistance.

GRANTS

Part of this work has been undertaken with the enormous support of the European Commission (European IPF Network, funded from 2006 to 2009 through the Frame Program 7). This work was supported by a grant of the German Research Foundation (KN 916/1-1 to L. Knudsen) and the Alexander-von-Humboldt Foundation (to E. Lopez-Rodriguez).

DISCLOSURES

No conflicts of interest, financial or otherwise are declared by the author(s).

AUTHOR CONTRIBUTIONS

Author contributions: B.B., I.H., A.G., M.O., P.M., and L.K. conception and design of research; B.B., D.L., C.R., I.H., P.M., and L.K. performed experiments; B.B., D.L., C.R., E.L.-R., A.G., M.O., P.M., and L.K. analyzed data; B.B., C.R., I.H., E.L.-R., A.G., M.O., P.M., and L.K. interpreted results of experiments; B.B., C.R., P.M., and L.K. prepared figures; B.B., P.M., and L.K. drafted manuscript; B.B., C.R., A.G., P.M., and L.K. edited and revised manuscript; B.B., D.L., C.R., I.H., E.L.-R., A.G., M.O., P.M., and L.K. approved final version of manuscript.

REFERENCES

1. **Araya J, Kojima J, Takasaka N, Ito S, Fujii S, Hara H, Yanagisawa H, Kobayashi K, Tsurushige C, Kawaishi M, Kamiya N, Hirano J, Odaka M, Morikawa T, Nishimura SL, Kawabata Y, Hano H, Nakayama K, Kuwano K.** Insufficient autophagy in idiopathic pulmonary fibrosis. *Am J Physiol Lung Cell Mol Physiol* 304: L56–L69, 2013.
2. **Atochina-Vasserman EN, Bates SR, Zhang P, Abramova H, Zhang Z, Gonzales L, Tao JQ, Gochuico BR, Gahl W, Guo CJ, Gow AJ, Beers MF, Guttentag S.** Early alveolar epithelial dysfunction promotes lung inflammation in a mouse model of Hermansky-Pudlak syndrome. *Am J Respir Crit Care Med* 184: 449–458, 2011.
3. **Bachofen H, Schürch S.** Alveolar surface forces and lung architecture. *Comp Biochem Physiol A Mol Integr Physiol* 129: 183–193, 2001.
4. **Bargout R, Jankov A, Dincer E, Wang R, Komodromos T, Ibarra-Sunga O, Filippatos G, Uhal BD.** Amiodarone induces apoptosis of human and rat alveolar epithelial cells in vitro. *Am J Physiol Lung Cell Mol Physiol* 278: L1039–L1044, 2000.
5. **Beers MF, Hawkins A, Maguire JA, Kotorashvili A, Zhao M, Newitt JL, Ding W, Russo S, Guttentag S, Gonzales L, Mulugeta S.** A nonaggregating surfactant protein C mutant is misdirected to early endosomes and disrupts phospholipid recycling. *Traffic* 12: 1196–1210, 2011.
6. **Carloni A, Poletti V, Fermo L, Bellomo N, Chilosi M.** Heterogeneous distribution of mechanical stress in human lung: a mathematical approach to evaluate abnormal remodeling in IPF. *J Theor Biol* 332: 136–140, 2013.
7. **Charles PE, Doise JM, Quenot JP, Muller G, Aube H, Baudouin N, Piard F, Besancenot JF, Blettery B.** Amiodarone-related acute respiratory distress syndrome following sudden withdrawal of steroids. *Respiration* 73: 248–249, 2006.
8. **Chilosi M, Carloni A, Rossi A, Poletti V.** Premature lung aging and cellular senescence in the pathogenesis of idiopathic pulmonary fibrosis and COPD/emphysema. *Transl Res* 162: 156–173, 2013.
9. **Coxson HO, Hogg JC, Mayo JR, Behzad H, Whittall KP, Schwartz DA, Hartley PG, Galvin JR, Wilson JS, Hunninghake GW.** Quantification of idiopathic pulmonary fibrosis using computed tomography and histology. *Am J Respir Crit Care Med* 155: 1649–1656, 1997.
10. **Fehrenbach H.** Alveolar epithelial type II cell: defender of the alveolus revisited. *Respir Res* 2: 33–46, 2001.
11. **Furuyama A, Kimata K, Mochitate K.** Assembly of basement membrane in vitro by cooperation between alveolar epithelial cells and pulmonary fibroblasts. *Cell Struct Funct* 22: 603–614, 1997.
12. **Gazdhar A, Temuri A, Knudsen L, Gugger M, Schmid RA, Ochs M, Geiser T.** Targeted gene transfer of hepatocyte growth factor to alveolar type II epithelial cells reduces lung fibrosis in rats. *Hum Gene Ther* 24: 105–116, 2013.
13. **Geiser T.** Idiopathic pulmonary fibrosis–a disorder of alveolar wound repair? *Swiss Med Wkly* 133: 405–411, 2003.

Downloaded from www.physiology.org/journal/ajplung (141.050.134.220) on October 24, 2019.

14. **Gundersen H, Jensen E.** Stereological estimation of the volume-weighted mean volume of arbitrary particles observed on random sections. *J Microsc* 138: 127–142, 1985.
15. **Günther A, Korfei M, Mahavadi P, von der Beck D, Ruppert C, Markart P.** Unravelling the progressive pathophysiology of idiopathic pulmonary fibrosis. *Eur Respir Rev* 21: 152–160, 2012.
16. **Günther A, Schmidt R, Nix F, Yabut-Perez M, Guth C, Rosseau S, Siebert C, Grimminger F, Morr H, Velcovsky H, Seeger W.** Surfactant abnormalities in idiopathic pulmonary fibrosis, hypersensitivity pneumonitis and sarcoidosis. *Eur Respir J* 14: 565–573, 1999.
17. **Guttentag SH, Akhtar A, Tao JQ, Atochina E, Rusiniak ME, Swank RT, Bates SR.** Defective surfactant secretion in a mouse model of Hermansky-Pudlak syndrome. *Am J Respir Cell Mol Biol* 33: 14–21, 2005.
18. **Hamvas A, Nogee LM, White FV, Schuler P, Hackett BP, Huddleston CB, Mendeloff EN, Hsu FF, Wert SE, Gonzales LW, Beers MF, Ballard PL.** Progressive lung disease and surfactant dysfunction with a deletion in surfactant protein C gene. *Am J Respir Cell Mol Biol* 30: 771–776, 2004.
19. **Horiuchi T, Ikegami M, Cherniack RM, Mason RJ.** Increased surface tension of the lung and surfactant in bleomycin-induced pulmonary fibrosis in rats. *Am J Respir Crit Care Med* 154: 1002–1005, 1996.
20. **Horowitz JC, Thannickal VJ.** Epithelial-mesenchymal interactions in pulmonary fibrosis. *Semin Respir Crit Care Med* 27: 600–612, 2006.
21. **Hsia C, Hyde D, Ochs M, Weibel E.** An official research policy statement of the American Thoracic Society/European Respiratory Society: standards for quantitative assessment of lung structure. *Am J Respir Crit Care Med* 181: 394–418, 2010.
22. **Hyde DM, Tyler NK, Putney LF, Singh P, Gundersen HJ.** Total number and mean size of alveoli in mammalian lung estimated using fractionator sampling and unbiased estimates of the Euler characteristic of alveolar openings. *Anat Rec A Discov Mol Cell Evol Biol* 277: 216–226, 2004.
23. **Kawanami O, Ferrans VJ, Crystal RG.** Structure of alveolar epithelial cells in patients with fibrotic lung disorders. *Lab Invest* 46: 39–53, 1982.
24. **Knudsen L, Waizy H, Fehrenbach H, Richter J, Wahlers T, Wittwer T, Ochs M.** Ultrastructural changes of the intracellular surfactant pool in a rat model of lung transplantation-related events. *Respir Res* 12: 79, 2011.
25. **Königshoff M, Kramer M, Balsara N, Wilhelm J, Amarie O, Jahn A, Rose F, Fink L, Seeger W, Schaefer L, Günther A, Eickelberg O.** WNT1-inducible signaling protein-1 mediates pulmonary fibrosis in mice and is upregulated in humans with idiopathic pulmonary fibrosis. *J Clin Invest* 119: 772–787, 2009.
26. **Korfei M, Ruppert C, Mahavadi P, Henneke I, Markart P, Koch M, Lang G, Fink L, Bohle R, Seeger W, Weaver T, Guenther A.** Epithelial endoplasmic reticulum stress and apoptosis in sporadic idiopathic pulmonary fibrosis. *Am J Respir Crit Care Med* 178: 838–846, 2008.
27. **Korfei M, von der Beck D, Henneke I, Markart P, Ruppert C, Mahavadi P, Ghanim B, Klepetko W, Fink L, Meiners S, Krämer OH, Seeger W, Vancheri C, Guenther A.** Comparative proteome analysis of lung tissue from patients with idiopathic pulmonary fibrosis (IPF), non-specific interstitial pneumonia (NSIP) and organ donors. *J Proteomics* 85: 109–128, 2013.
28. **Kuhn C, Boldt J, King TE, Crouch E, Vartio T, McDonald JA.** An immunohistochemical study of architectural remodeling and connective tissue synthesis in pulmonary fibrosis. *Am Rev Respir Dis* 140: 1693–1703, 1989.
29. **Lazenby A, Crouch E, McDonald J, Kuhn C 3rd.** Remodeling of the lung in bleomycin-induced pulmonary fibrosis in the rat. An immunohistochemical study of laminin, type IV collagen, and fibronectin. *Am Rev Respir Dis* 142: 206–214, 1990.
30. **Leuenberger A, Gazdhar A, Herrmann G, Ochs M, Geiser T, Knudsen L.** Cell-specific expression of human HGF by alveolar type II cells induces remodeling of septal wall tissue in the lung: a morphometric study. *J Appl Physiol* 113: 799–807, 2012.
31. **Lutz D, Gazdhar A, Lopez-Rodriguez E, Ruppert C, Mahavadi P, Günther A, Klepetko W, Bates JH, Smith B, Geiser T, Ochs M, Knudsen L.** Alveolar derecruitment and collapse induration as crucial mechanisms in lung injury and fibrosis. *Am J Respir Cell Mol Biol* 52: 232–243, 2015.
32. **Mahavadi P, Knudsen L, Venkatesan S, Henneke I, Hegermann J, Wrede C, Ochs M, Ahuja A, Chillappagari S, Ruppert C, Seeger W, Korfei M, Guenther A.** Regulation of macroautophagy in amiodarone induced pulmonary fibrosis. *J Pathol*. In press.
33. **Mahavadi P, Henneke I, Ruppert C, Knudsen L, Venkatesan S, Liebisch G, Chambers RC, Ochs M, Schmitz G, Vancheri C, Seeger W, Korfei M, Guenther A.** Altered surfactant homeostasis and alveolar epithelial cell stress in amiodarone-induced lung fibrosis. *Toxicol Sci* 142: 285–297, 2014.
34. **Mahavadi P, Korfei M, Henneke I, Liebisch G, Schmitz G, Gochuico BR, Markart P, Bellusci S, Seeger W, Ruppert C, Guenther A.** Epithelial stress and apoptosis underlie Hermansky-Pudlak syndrome-associated interstitial pneumonia. *Am J Respir Crit Care Med* 182: 207–219, 2010.
35. **Majno G, Joris I.** Apoptosis, oncosis, necrosis. An overview of cell death. *Am J Pathol* 146: 3–15, 1995.
36. **Mühlfeld C, Ochs M.** Quantitative microscopy of the lung: a problem-based approach. Part 2: stereological parameters and study designs in various diseases of the respiratory tract. *Am J Physiol Lung Cell Mol Physiol* 305: L205–L221, 2013.
37. **Mulugeta S, Nguyen V, Russo S, Muniswamy M, Beers M.** A surfactant protein C precursor protein BRICHOS domain mutation causes endoplasmic reticulum stress, proteasome dysfunction, and caspase 3 activation. *Am J Respir Cell Mol Biol* 32: 521–530, 2005.
38. **Myers J, Katzenstein A.** Epithelial necrosis and alveolar collapse in the pathogenesis of usual interstitial pneumonia. *Chest* 94: 1309–1311, 1988.
39. **Nogee L, Dunbar Ar Wert S, Askin F, Hamvas A, Whitsett J.** A mutation in the surfactant protein C gene associated with familial interstitial lung disease. *N Engl J Med* 344: 573–579, 2001.
40. **Ochs M, Mühlfeld C.** Quantitative microscopy of the lung: a problem-based approach. Part 1: basic principles of lung stereology. *Am J Physiol Lung Cell Mol Physiol* 305: L15–L22, 2013.
41. **Ochs M, Nyengaard JR, Jung A, Knudsen L, Voigt M, Wahlers T, Richter J, Gundersen HJ.** The number of alveoli in the human lung. *Am J Respir Crit Care Med* 169: 120–124, 2004.
42. **Perez-Gil J, Weaver TE.** Pulmonary surfactant pathophysiology: current models and open questions. *Physiology (Bethesda)* 25: 132–141, 2010.
43. **Raghu G, Collard HR, Egan JJ, Martinez FJ, Behr J, Brown KK, Colby TV, Cordier JF, Flaherty KR, Lasky JA, Lynch DA, Ryu JH, Swigris JJ, Wells AU, Ancochea J, Bouros D, Carvalho C, Costabel U, Ebina M, Hansell DM, Johkoh T, Kim DS, King TE, Kondoh Y, Myers J, Müller NL, Nicholson AG, Richeldi L, Selman M, Dudden RF, Griss BS, Protzko SL, Schünemann HJ; ATS/ERS/JRS/ALAT Committee on Idiopathic Pulmonary Fibrosis.** An official ATS/ERS/JRS/ALAT statement: idiopathic pulmonary fibrosis: evidence-based guidelines for diagnosis and management. *Am J Respir Crit Care Med* 183: 788–824, 2011.
44. **Ruppert C, Kuchenbuch T, Boensch M, Schmidt S, Mathes U, Hillebrand V, Henneke I, Markart P, Reiss I, Schermuly RT, Seeger W, Günther A.** Dry powder aerosolization of a recombinant surfactant protein-C-based surfactant for inhalative treatment of the acutely inflamed lung. *Crit Care Med* 38: 1584–1591, 2010.
45. **Scherle W.** A simple method for volumetry of organs in quantitative stereology. *Mikroskopie* 26: 57–60, 1970.
46. **Schmidt R, Meier U, Markart P, Grimminger F, Velcovsky H, Morr H, Seeger W, Günther A.** Altered fatty acid composition of lung surfactant phospholipids in interstitial lung disease. *Am J Physiol Lung Cell Mol Physiol* 283: L1079–L1085, 2002.
47. **Schneider JP, Ochs M.** Alterations of mouse lung tissue dimensions during processing for morphometry: a comparison of methods. *Am J Physiol Lung Cell Mol Physiol* 306: L341–L350, 2014.
48. **Selman M, Pardo A.** Role of epithelial cells in idiopathic pulmonary fibrosis: from innocent targets to serial killers. *Proc Am Thorac Soc* 3: 364–372, 2006.
49. **Selman M, Pardo A, Richeldi L, Cerri S.** Emerging drugs for idiopathic pulmonary fibrosis. *Expert Opin Emerg Drugs* 16: 341–362, 2011.
50. **Sirianni FE, Chu FS, Walker DC.** Human alveolar wall fibroblasts directly link epithelial type 2 cells to capillary endothelium. *Am J Respir Crit Care Med* 168: 1532–1537, 2003.
51. **Sisson T, Mendez M, Choi K, Subbotina N, Courey A, Cunningham A, Dave A, Engelhardt J, Liu X, White E, Thannickal V, Moore B, Christensen P, Simon R.** Targeted injury of type II alveolar epithelial cells induces pulmonary fibrosis. *Am J Respir Crit Care Med* 181: 254–263, 2010.
52. **Sterio DC.** The unbiased estimation of number and sizes of arbitrary particles using the disector. *J Microsc* 134: 127–136, 1984.
53. **Tandrup T, Gundersen HJ, Jensen EB.** The optical rotator. *J Microsc* 186: 108–120, 1997.

Downloaded from www.physiology.org/journal/ajplung (141.050.134.220) on October 24, 2019.

54. **Tschanz S, Schneider JP, Knudsen L.** Design-based stereology: planning, volumetry and sampling are crucial steps for a successful study. *Ann Anat* 196: 3–11, 2014.
55. **Tschanz SA, Burri PH, Weibel ER.** A simple tool for stereological assessment of digital images: the STEPanizer. *J Microsc* 243: 47–59, 2011.
56. **Vasilescu DM, Knudsen L, Ochs M, Weibel ER, Hoffman EA.** Optimized murine lung preparation for detailed structural evaluation via micro computed tomography. *J Appl Physiol* 112: 159–166, 2012.
57. **Volckaert T, De Langhe S.** Lung epithelial stem cells and their niches: Fgf10 takes center stage. *Fibrogenesis Tissue Repair* 7: 8, 2014.
58. **Waisberg D, Barbas-Filho J, Parra E, Fernezlian S, Ribeiro de Carvalho C, Kairalla R, Capelozzi V.** Abnormal expression of telomerase/apoptosis limits type II alveolar epithelial cell replication in the early remodeling of usual interstitial pneumonia/idiopathic pulmonary fibrosis. *Hum Pathol* 41: 385–391, 2010.
59. **Weaver TE, Na CL, Stahlman M.** Biogenesis of lamellar bodies, lysosome-related organelles involved in storage and secretion of pulmonary surfactant. *Semin Cell Dev Biol* 13: 263–270, 2002.
60. **Weibel E, Knight B.** A morphometric study on the thickness of the pulmonary air-blood barrier. *J Cell Biol* 21: 367–396, 1964.
61. **Weibel ER.** It takes more than cells to make a good lung. *Am J Respir Crit Care Med* 187: 342–346, 2013.
62. **Williams K, Malarkey D, Cohn L, Patrick D, Dye J, Toews G.** Identification of spontaneous feline idiopathic pulmonary fibrosis: morphology and ultrastructural evidence for a type II pneumocyte defect. *Chest* 125: 2278–2288, 2004.
63. **Wilson TA, Bachofen H.** A model for mechanical structure of the alveolar duct. *J Appl Physiol* 52: 1064–1070, 1982.
64. **Young LR, Gulleman PM, Bridges JP, Weaver TE, Deutsch GH, Blackwell TS, McCormack FX.** The alveolar epithelium determines susceptibility to lung fibrosis in Hermansky-Pudlak syndrome. *Am J Respir Crit Care Med* 186: 1014–1024, 2012.

Downloaded from www.physiology.org/journal/ajplung (141.050.134.220) on October 24, 2019.

The attached printed / pdf version of this article is part of this habilitation thesis and has been included according to the copyright permissions issued by the American Physiological Society to reuse author's own APS-published work, following the guidelines given in the website as per 24.02.2023, that says:

'Authors may reproduce whole published articles in dissertations and post to thesis repositories without charge and without requesting permission. Full citation is required'.

https://journals.physiology.org/author-info.permissions

Citation of this article: Bastian Birkelbach, Dennis Lutz, Clemens Ruppert, Ingrid Henneke, Elena Lopez-Rodriguez, Andreas Günther, Matthias Ochs, Poornima Mahavadi*, and Lars Knudsen*. Linking progression of fibrotic lung remodeling and ultrastructural alterations of alveolar epithelial type II cells in the amiodarone mouse model. **Am J Physiol Lung Cell Mol Physiol. 2015** Jul 1;309(1):L63-75. doi: 10.1152/ajplung.00279.2014. Epub 2015 May 8.

The Journal of Pathology: Clinical Research
J Path: Clin Res October 2016; **1**: 252–263
Published online 11 April 2015 in Wiley Online Library (wileyonlinelibrary.com). DOI: 10.1002/cjp2.20

Original Article

Regulation of macroautophagy in amiodarone-induced pulmonary fibrosis

Poornima Mahavadi,[1,2] Lars Knudsen,[3,4,5] Shalini Venkatesan,[1,2] Ingrid Henneke,[1,2] Jan Hegermann,[3,4,5] Christoph Wrede,[3,4,5] Matthias Ochs,[3,4,5] Saket Ahuja,[1,2] Shashi Chillappagari,[2,6] Clemens Ruppert,[1,2] Werner Seeger,[1,2,7] Martina Korfei[1,2] and Andreas Guenther[1,2,7,8]*

[1] *Department of Internal Medicine, Justus-Liebig-University, Giessen, Germany*
[2] *Universities of Giessen and Marburg Lung Center (UGMLC), German Center for Lung Research (DZL), Giessen, Germany*
[3] *Institute of Functional and Applied Anatomy, Hannover Medical School, Hannover, Germany*
[4] *Biomedical Research in Endstage and Obstructive Lung Disease Hannover (BREATH), German Center for Lung Research (DZL), Hannover, Germany*
[5] *REBIRTH Cluster of Excellence, Hannover, Germany*
[6] *Department of Medicine, Pulmonary Critical Care, Philipps-Universität Marburg, Baldingerstrasse 1, 35043 Marburg, Germany*
[7] *Member of the European IPF Network*
[8] *Lung Clinic Waldhof-Elgershausen, Greifenstein, Germany*

**Correspondence to: Andreas Guenther, Klinikstrasse 36, 35392 Giessen, Germany. e-mail: Andreas.Guenther@innere.med.uni-giessen.de*

Abstract

Amiodarone (AD) is an iodinated benzofuran derivative, especially known for its antiarrhythmic properties. It exerts serious side-effects even in patients receiving low doses. AD is well-known to induce apoptosis of type II alveolar epithelial cells (AECII), a mechanism that has been suggested to play an important role in AD-induced lung fibrosis. The precise molecular mechanisms underlying this disease are, however, still unclear. Because of its amphiphilic nature, AD becomes enriched in the lysosomal compartments, affecting the general functions of these organelles. Hence, in this study, we aimed to assess the role of autophagy, a lysosome-dependent homeostasis mechanism, in driving AECII apoptosis in response to AD. *In vitro*, AD-treated MLE12 and primary AECII cells showed increased proSP-C and LC3B positive vacuolar structures and underwent LC3B-dependent apoptosis. In addition, AD-induced autophagosome-lysosome fusion and increased autophagy flux were observed. *In vivo*, in C57BL/6 mice, LC3B was localised at the limiting membrane of lamellar bodies, which were closely connected to the autophagosomal structures in AECIIs. Our data suggest that AD causes activation of macroautophagy in AECIIs and extensive autophagy-dependent apoptosis of alveolar epithelial cells. Targeting the autophagy pathway may therefore represent an attractive treatment modality in AD-induced lung fibrosis.

Keywords: autophagy; amiodarone; alveolar epithelial cells; lamellar bodies; LC3B; apoptosis

Received 11 September 2014; accepted 31 March 2015

The authors have no conflicts of interest to declare.

Introduction

Amiodarone (AD) is pharmacologically classified as a cationic amphiphilic drug. It is an efficient antiarrhythmic drug with typical class III Vaughan-Williams properties. In spite of its beneficial effects against almost all kinds of arrhythmias, its clinical use is tempered because of its contraindications [1,2], which include corneal micro deposits, dermatitis, symptomatic bradycardia, hypo- and hyper-thyroidism and, most importantly, severe pulmonary toxicity [1]. It is estimated that 10–17% of patients receiving 400 mg AD per day develop pulmonary toxicity, with fatalities occurring in about 10% of cases [3]. Previous studies suggested that elderly patients with a pre-existing lung disease are at a high risk of developing AD-induced pulmonary toxicity. It was initially believed that a low dose of AD was relatively safe, but more recent case reports have revealed a high risk of pulmonary complications, especially confluent lung fibrosis, even with low dosage treatment of patients (200 mg per day). Acute respiratory distress syndrome and pneumonitis are also well-

© 2015 The Authors The Journal of Pathology: Clinical Research published by The Pathological Society of Great Britain and Ireland and John Wiley & Sons Ltd

This is an open access article under the terms of the Creative Commons Attribution-NonCommercial-NoDerivs License, which permits use and distribution in any medium, provided the original work is properly cited, the use is non-commercial and no modifications or adaptations are made.

20564538, 2015, 4, Downloaded from https://onlinelibrary.wiley.com/doi/10.1002/cjp2.20 by Cochrane Germany, Wiley Online Library on [29/12/2022]. See the Terms and Conditions (https://onlinelibrary.wiley.com/terms-and-conditions) on Wiley Online Library for rules of use; OA articles are governed by the applicable Creative Commons License

documented side effects of AD [1,4]. Hence, according to the recent guideline for the management of patients with atrial fibrillation, AD is prescribed to treat atrial fibrillation in the absence of pre-excitation only when other agents are unsuccessful [5].

At a cellular level, foamy macrophages and hyperplasia of type II alveolar epithelial cells (AECIIs) are the most common features of AD-induced pulmonary fibrosis. In addition, it has been demonstrated that AD induces apoptosis of alveolar epithelial cells *in vitro* and that AD induces toxicity in several types of lung cells [6,7]. In full accordance, we have recently shown that intratracheal administration of AD induces lung fibrosis in mice and that AD induces surfactant accumulation, AECII apoptosis, lysosomal stress and ER stress in this model [8]. Although the precise molecular events underlying AD-induced lung fibrosis still remain to be clearly settled, mechanisms such as excessive intracellular phospholipidosis, direct cytotoxicity, oxidative stress and the angiotensin signalling pathway [9–12], were previously suggested to contribute to the pathogenic chain of events.

It has been shown that AD becomes enriched in lysosomes (~500-fold as compared to serum) and causes accumulation of multilamellar bodies in the cytoplasm of various cell types [13,14]. Similarly, AD as well as its derivative dronedarone was shown to induce autophagy, a lysosome-mediated degradation pathway that is extremely important in maintaining cellular homeostasis [15,16]. More recently, it was claimed that activating the autophagy pathway rescues AD-induced lung fibrosis in rats [17].

Autophagy is a fundamental catabolic cellular process that degrades unnecessary proteins and damaged organelles, thereby helping in cell survival. At a molecular level, different types of autophagy pathways have been described. Macroautophagy is well characterised and is one of the important types of autophagy that involves sequestration of the cargo into a double-membrane vesicle known as an autophagosome. This process involves complex interactions between several autophagy-related (*Atg*) proteins. The autophagosome ultimately fuses with the lysosome to degrade its components. More detailed analyses of this process are given in previous reviews [18,19]. Several diseases such as cancer, neurodegenerative diseases, lysosomal storage disorders, cystic fibrosis, chronic obstructive pulmonary disease (COPD) and idiopathic pulmonary fibrosis (IPF) have been linked to altered autophagy [20].

We recently established a mouse model of AD-induced lung fibrosis and reported surfactant alterations, severe AECII apoptosis and cellular stress in this model. We reported that AD-induced AECII apoptosis is not mediated via Cathepsin D, and speculated on the involvement of other lysosomal pathways in driving AECII apoptosis in this model [8]. In the current study, we aimed to carefully analyse the role of macroautophagy (referred as autophagy hereafter) in AD-induced alveolar epithelial cell apoptosis and to identify if the autophagy marker protein microtubule-associated protein 1 light chain-3B (LC3B) is localised to the lamellar bodies of alveolar epithelial cells.

Methods

Cell culture

Mouse lung epithelial cell lines (MLE12) and isolation of primary mouse AECII and culture were performed as described before [21]. Preparations of AD solution and the protocol for siRNA transfection are described elsewhere [8]. For immunofluorescence analysis, MLE12 cells were plated in 8-well chamber slides. After overnight adherence and following treatments, cells were washed and fixed with 4% paraformaldehyde, followed by washing and permeabilisation with 0.5% Triton X-100. Permeabilised cells were then washed, blocked with 10% donkey serum and 3%BSA in PBS. Incubation with primary antibody (LC3B or LAMP2; abcam, Cambridge, UK) was performed overnight at 4 °C. Following washing, secondary antibody (Alexa Fluor 555, donkey anti rabbit or Alexa Fluor 488, donkey anti rat; Life Technologies, Darmstadt, Germany) was added for 1 h at RT in dark. Samples were then washed and mounted with mounting medium with DAPI for nuclear staining (VECTASHIELD mounting medium with DAPI, Vector Labs/Enzo Life Sciences GmbH, Lörrach, Germany) followed by microscopy (Leica Mirosystems, Germany). Protocols for RNA extraction, RT-PCR and primers used are given in Supporting Information.

Autophagy flux

10 mg/ ml stock solution of chloroquine (CQ; Chloroquine diphosphate salt, Sigma-Aldrich) was prepared by dissolving it in cell culture grade aqua dest. MLE12 cells were plated in 6-well cell culture dishes. Next day, medium was replaced with fresh culture medium and CQ or vehicle (cell culture grade aqua dest) was added. 2 or 6 µl from CQ stock solution per 2ml culture medium was added to get a final concentration of 10 or 30 µg/ml, respectively. 4 h later, AD or vehicle was added and cells were harvested after 8 h, followed by Western blotting for LC3B. Similarly, MLE12 cells were pre-incubated with DMSO or 10 µg/ml pepstatin and E64D (Enzo life sciences) dissolved in DMSO for

© 2015 The Authors The Journal of Pathology: Clinical Research published by The Pathological Society of Great Britain and Ireland and John Wiley & Sons Ltd

20564538, 2015, 4, Downloaded from https://onlinelibrary.wiley.com/doi/10.1002/cjp2.20 by Cochrane Germany, Wiley Online Library on [29/12/2022]. See the Terms and Conditions (https://onlinelibrary.wiley.com/terms-and-conditions) on Wiley Online Library for rules of use; OA articles are governed by the applicable Creative Commons License

1 h followed by incubation with AD for 8 h, after which cells were harvested and the lysates were processed for Western blotting of LC3B.

Mice

Intratracheal administration of vehicle or AD (0.8 mg/kg body weight, Sigma-Aldrich, Germany) was performed in C57BL/6 mice every fifth day as described elsewhere [8]. Ten mice were included per group. Both the University Animal Care Committee and the Federal Authorities for Animal Research of the Regierungspraesidium Giessen (Hessen, Germany) approved the study protocol.

Electron microscopy

Mice were sacrificed 7 and 14 days after first AD or vehicle challenge for perfusion fixation. In order to represent the whole organ, systematic uniform sampling was performed. Detailed protocols are described in Supporting Information.

Biochemical and statistical analysis

Details of Western blot, immunohistochemistry and sources of antibodies are given in Supporting Information. All data are expressed as means ± SEM of at least five mice for *in vivo* studies. For *in vitro* experiments, three or more independent experiments were conducted for AD treatment and triplicate transfections were performed for siRNA studies. Statistical significance was assessed using the Mann–Whitney U test. Significance is indicated as: $*p < 0.5$, $**p < 0.01$, $***p < 0.001$.

Results

AD induces macroautophagy and increases autophagy flux in murine alveolar epithelial cells

Mouse lung epithelial (MLE) 12 cells were treated with vehicle or with 10 μg/ml AD (according to [7,8]) for 8, 16 and 24 h. We observed a heavily vacuolated cytoplasm in MLE 12 cells treated with AD (Figure 1A). Immunofluorescence analysis for the macroautophagy marker, LC3B as shown in Figure 1B, revealed giant autophagosomes in AD-treated cells decorated with LC3B; vehicle-treated cells on the other hand showed occasional punctate staining, but more often a diffuse staining for LC3B. Western blot analysis showed an impressive increase in the conversion of LC3BI to LC3BII, p62 and LAMP2 in AD-treated cells as compared to vehicle treated or untreated cells (Figure 1C, Supporting Information Figure S1a). It has been indicated that p62 cannot be used as a maker for autophagy in all contexts, especially if it is transcriptionally upregulated [22]. Hence we aimed to analyse if transcriptional up-regulation of p62 might explain the marked increase at the protein level under AD treatment and, not surprisingly, semi-quantitative and q-PCR analysis showed significant time-dependent up-regulation of p62 mRNA after treating cells with AD, as compared to vehicle-treated or untreated cells (Supporting Information Figure S1b). Primary AECII treated with AD or vehicle for 24 h also showed significantly increased LC3B and proSP-C after AD treatment as compared to vehicle-treated cells (Figure 1D). As an attempt to understand if the fusion event between autophagosomes and lysosomes occurs in response to AD treatment, we performed immunofluorescence for LC3B and LAMP2. Indeed, AD-treated MLE12 cells showed giant autophagosomes, decorated with LC3B and LAMP2, which co-localised with each other (Figure 2A), demonstrating fusion between autophagosomes and lysosomes. Further, in order to evaluate the autophagy flux after AD treatment (according to current guidelines [23]), MLE12 cells were pre-treated with the vacuolar ATPase inhibitor bafilomycin A1, followed by AD versus vehicle treatment. Surprisingly, AD-induced vacuolar morphology completely disappeared upon pre-treatment of MLE12 cells with bafilomycin A1 (Supporting Information Figure S2a). This observation is in full accordance with a previous study, which reported that bafilomycin A1 significantly suppresses the uptake of AD in different cell types [15]. Hence, we excluded bafilomycin A1 and used another protease inhibitor, chloroquine, and a combination of pepstatin and E64D, which have also been suggested for assessing autophagic flux [23]. MLE12 cells were pre-incubated with saturating concentrations of chloroquine (30 μg/ml) [23], for 4 h followed by AD or vehicle treatment. We observed a significant increase in LC3BII and a marked decrease in p62 after AD treatment in the presence of chloroquine (Figure 2B,C), thus clearly indicating a slight but significant increase in autophagy flux after AD treatment. Increase in autophagic flux was also observed when cells were pre-incubated with pepstatin and E64D, followed by AD treatment (Supporting Information Figure S2b).

AD-induced AECII apoptosis is mediated by LC3B *in vitro*

In order to clarify the mechanistic role of macroautophagy in AD-induced AECII injury and apoptosis, we transfected MLE12 cells for 48 h with a LC3B-

© 2015 The Authors The Journal of Pathology: Clinical Research published by The Pathological Society of Great Britain and Ireland and John Wiley & Sons Ltd

20564538, 2015, 4, Downloaded from https://onlinelibrary.wiley.com/doi/10.1002/cjp2.20 by Cochrane Germany, Wiley Online Library on [29/12/2022]. See the Terms and Conditions (https://onlinelibrary.wiley.com/terms-and-conditions) on Wiley Online Library for rules of use; OA articles are governed by the applicable Creative Commons License

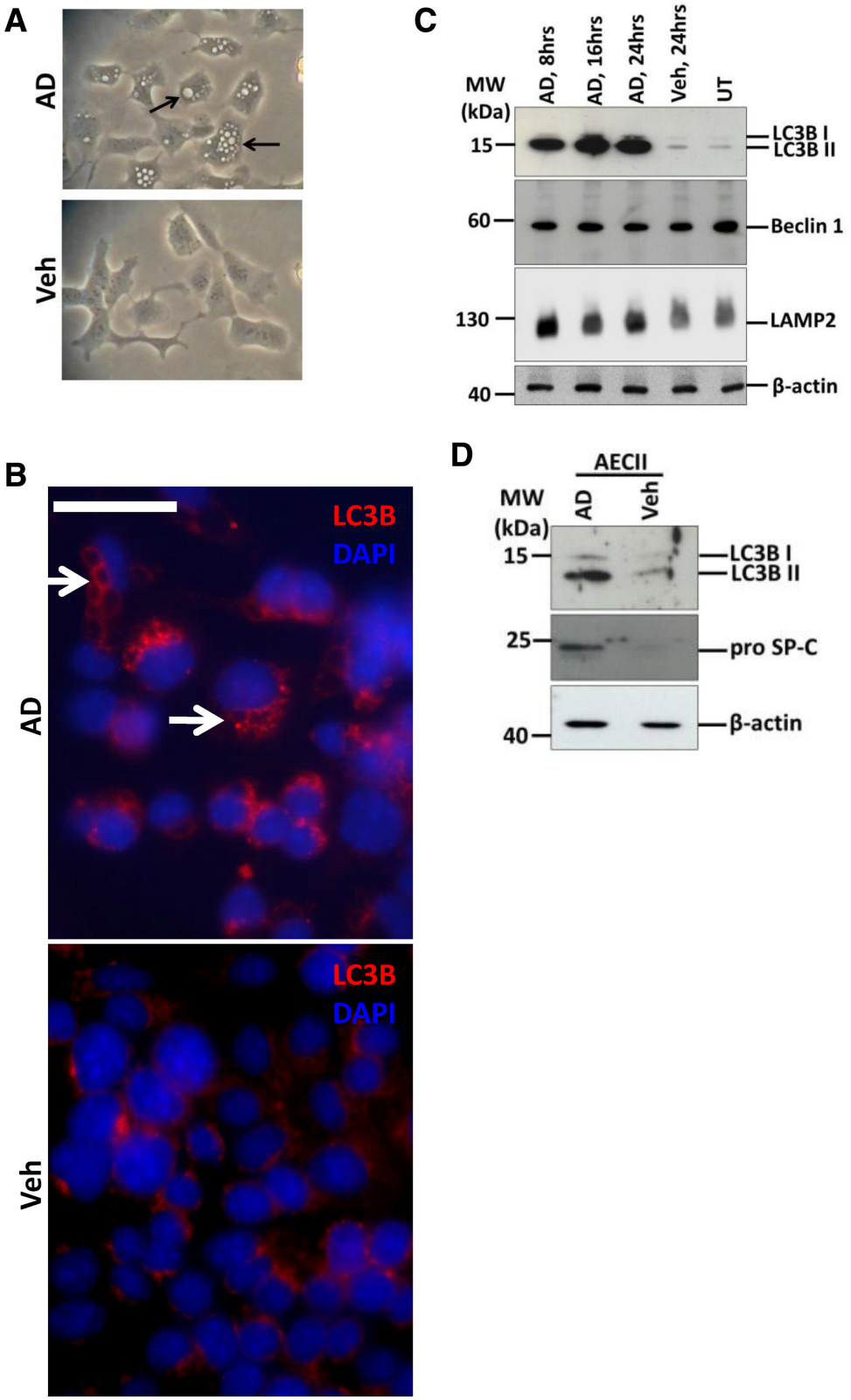

Figure 1. Increase in markers of autophagy in alveolar epithelial cells following AD treatment. (A) Phase contrast images of MLE12 cells 8 h post AD or vehicle treatment. Arrows indicate huge vacuolar structures in AD-treated MLE 12 cells. (B) Immunofluorescence images for LC3B (red) from MLE 12 cells treated with AD or vehicle for 8 h. Arrows indicate LC3B-labelled vacuolar structures in AD-treated cells. (C) Representative Western blot images from cell lysates from AD (8, 16, and 24 h) or vehicle treated (24 h) or untreated MLE12 cells for LC3B, Beclin1, LAMP2 and ß-actin. (D) Immunoblot images for LC3B and pro SP-C from AECIIs isolated from C57Bl/6 mice and treated for 24 h with AD or vehicle.

20564538, 2015, 4, Downloaded from https://onlinelibrary.wiley.com/doi/10.1002/cjp2.20 by Cochrane Germany, Wiley Online Library on [29/12/2022]. See the Terms and Conditions (https://onlinelibrary.wiley.com/terms-and-conditions) on Wiley Online Library for rules of use; OA articles are governed by the applicable Creative Commons License

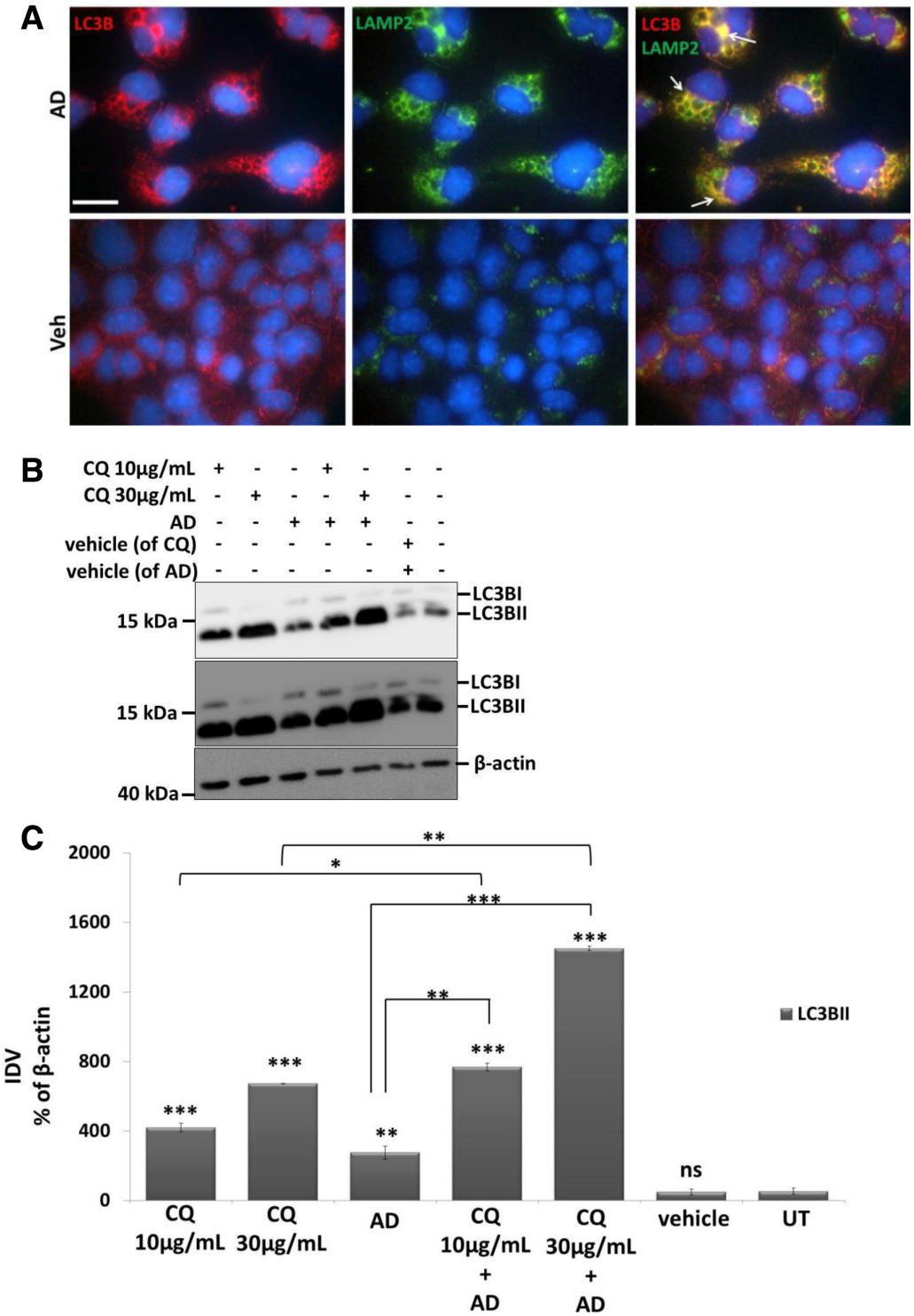

Figure 2. AD-induced increased autophagy flux in MLE 12 cells. (A) Immunofluorescence images for LC3B (red), LAMP2 (green) and overlay images of both LC3B and LAMP2 from MLE 12 cells treated with AD or vehicle for 8 h. Arrows indicate huge vacuolar structures labelled with both LC3B and LAMP2 (yellow) in AD-treated cells. Nuclei are stained with DAPI (blue). Scale bar = 50 μm. (B and C) Representative Western blot images for LC3B and β-actin after pre-incubation of MLE12 cells with chloroquine (CQ; 10 and 30 μg/ml) for 4 h followed by AD or vehicle treatment for 8 h. Upper and middle panels represent lower and higher exposures (to detect LC3BI), respectively, of the LC3B Western blot membrane and densitometry analysis performed from n = 3 independent experiments. Significance was calculated by comparing all treated groups with untreated cells and then between different treatment groups as indicated. $^{*}p < 0.05$, $^{**}p < 0.01$, $^{***}p < 0.001$.

© 2015 The Authors The Journal of Pathology: Clinical Research published by The Pathological Society of Great Britain and Ireland and John Wiley & Sons Ltd

20564538, 2015, 4, Downloaded from https://onlinelibrary.wiley.com/doi/10.1002/cjp2.20 by Cochrane Germany, Wiley Online Library on [29/12/2022]. See the Terms and Conditions (https://onlinelibrary.wiley.com/terms-and-conditions) on Wiley Online Library for rules of use; OA articles are governed by the applicable Creative Commons License

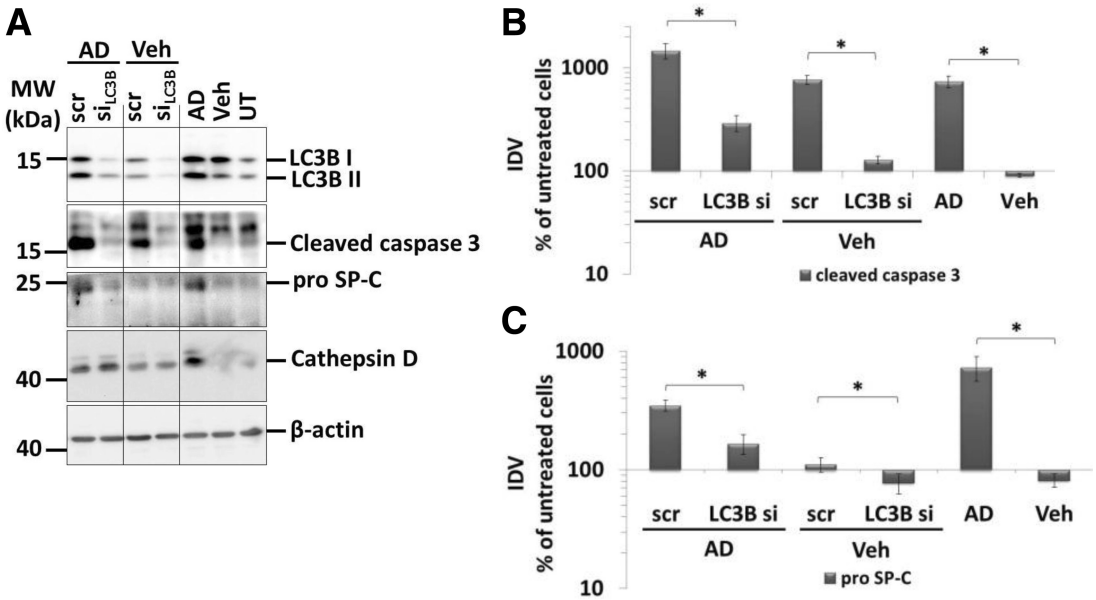

Figure 3. AD-induced AECII apoptosis is mediated by LC3B. (A) Representative Western blot images for LC3B, cleaved caspase 3, proSP-C, cathepsin D and β-actin from MLE12 cells transfected with scrambled siRNA (scr) or siRNA for LC3B (LC3B si) and treated with AD or vehicle for 8 h. Cells treated only with AD, vehicle or untreated cells were included as controls. Different parts from the same Western blots are separated by vertical lines. (B and C) Densitometry analysis of cleaved caspase 3 (B) and proSP-C (C) to β-actin ratio was calculated and is given as a percentage of untreated cells. $^*p < 0.05$.

specific and a scrambled siRNA and then treated with AD or vehicle for 8 h. Quite strikingly, cleaved caspase 3 levels, being massively increased in scrambled siRNA-transfected and AD-treated cells, returned to almost normal levels in response to LC3B knockdown (Figure 3A,B). Additionally, specific knockdown of LC3B also reversed the AD-induced proSP-C elevation almost to control levels (Figure 3A,C). Based on these observations, LC3B, either directly or indirectly, seems to regulate intracellular proSP-C content in response to AD treatment.

AD induces macroautophagy and the fusion between autophagosome and lamellar bodies in AECII

In order to identify if AD induces macroautophagy *in vivo*, we performed intratracheal administration of AD every fifth day in mice and sacrificed the animals at days 7, 14, 21 and 28. Development of lung fibrosis was observed in AD-treated mice from day 7 onwards [8]. Analysis of lung homogenates for macroautophagy markers revealed a significant (~10-fold) increase in LC3BII as well as p62 levels (~3-fold) as compared to vehicle-treated mice at all the time points analysed (Figure 4A,B, Supporting Information Figure S3a,b). The levels of Beclin1, another well-known autophagy protein, remained unaltered (Figure 4A). Moreover, the overall level of LAMP2, a lysosomal marker, increased in AD treated lungs (Figure 4A,C), indicating a marked increase in the overall lysosomal content after AD treatment. Immunohistochemistry on serial lung sections revealed numerous LC3B positive AECII in AD-treated mice as compared to vehicle-treated controls (Figure 4D, Supporting Information Figure S3c). In order to further confirm this finding, we performed immunogold labelling for LC3B on lung tissues of AD and vehicle-treated mice. This revealed preferential labelling of LC3B on the limiting membrane and the interior of lamellar bodies (LB) of AECII in AD as well as in vehicle-treated mice (Figure 5A). After AD treatment, however, gold labelling appeared to be more intense compared to vehicle-treated mice, confirming the results from our immunohistochemistry staining (Figure 5A). In addition, using EM tomography, we observed a connection between lamellar bodies and autophagosomes via membranes within the AECII of mice treated with AD (Figure 5B,C; Supporting Information video1).

Discussion

Our data indicate that AD induces enhanced fusion of autophagosomes to lysosomes as well as to lamellar bodies (which also belong to the lysosomal

© 2015 The Authors The Journal of Pathology: Clinical Research published by The Pathological Society of Great Britain and Ireland and John Wiley & Sons Ltd

20564538, 2015, 4, Downloaded from https://onlinelibrary.wiley.com/doi/10.1002/cjp2.20 by Cochrane Germany, Wiley Online Library on [29/12/2022]. See the Terms and Conditions (https://onlinelibrary.wiley.com/terms-and-conditions) on Wiley Online Library for rules of use; OA articles are governed by the applicable Creative Commons License

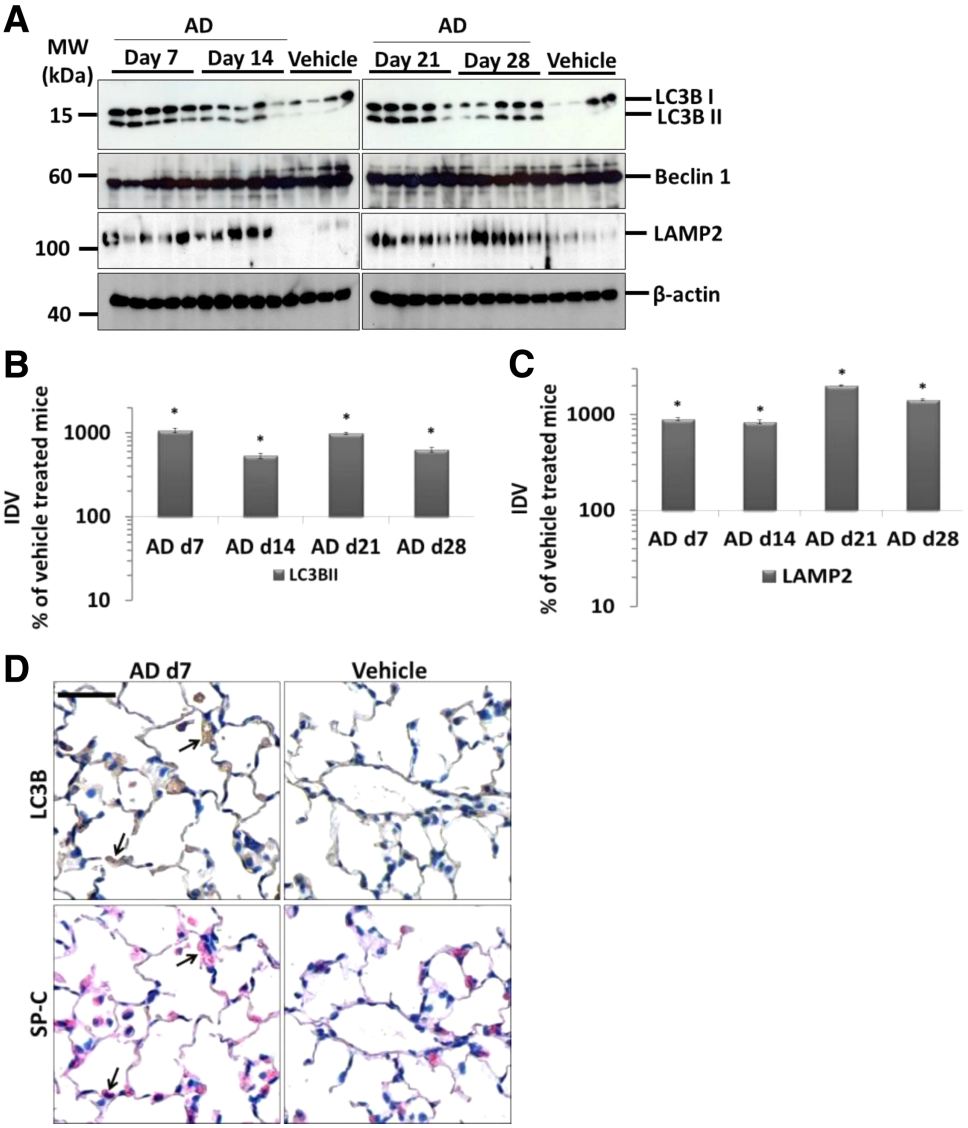

Figure 4. Increase in markers of autophagy in AECIIs from AD-treated mice. (A) Western blot analysis of lung homogenates of (left) AD-treated mice at days 7, 14 and vehicle at day 28 and (right) AD-treated mice at days 21, 28 and vehicle at day 28 for LC3BII, Beclin 1, LAMP2 and β-actin. (B and C) Graphical representation of densitometry analysis is shown for the LC3B and LAMP2 Western blots shown in (A). Representative blots and analysis from n = 5 mice. *$p < 0.05$. (D) Representative images of immunohistochemistry for LC3B and pro SP-C performed on serial lung sections from day 7 AD and vehicle-treated mice. Arrows indicate AECIIs positive for LC3B. Scale bar = 50 μm; Original magnification of pictomicrographs: x400.

compartment), increased autophagy flux and markedly increased and LC3B-dependent apoptosis of alveolar epithelial cells. We were also able to show localisation of LC3B to the lamellar bodies in AECIIs and report that the AD-driven dysregulation of proSP-C is dependent on LC3B.

AD is noted for its unusually long half-life. It accumulates within the lysosomal compartments of various types of lung cells [2,14], including AECIIs. Similarly, we also observed an increase in the size and number of lamellar bodies within AECIIs and altered intracellular surfactant homeostasis in AD-treated mice. It was previously reported that the activity of Cathepsin D, a lysosomal enzyme, is increased after AD treatment [24] and we recently showed that Cathepsin D protein levels increase in AD-treated mice lungs as well as in MLE cells [8]. All these observations reflect altered lysosomal homeostasis following AD treatment. However, we did not observe Cathepsin D-dependent apoptosis of MLE cells in response to AD treatment, indicating the involvement of other lysosome-related pathways

© 2015 The Authors The Journal of Pathology: Clinical Research published by The Pathological Society of Great Britain and Ireland and John Wiley & Sons Ltd

20564538, 2015, 4, Downloaded from https://onlinelibrary.wiley.com/doi/10.1002/cjp2.20 by Cochrane Germany, Wiley Online Library on [29/12/2022]. See the Terms and Conditions (https://onlinelibrary.wiley.com/terms-and-conditions) on Wiley Online Library for rules of use; OA articles are governed by the applicable Creative Commons License

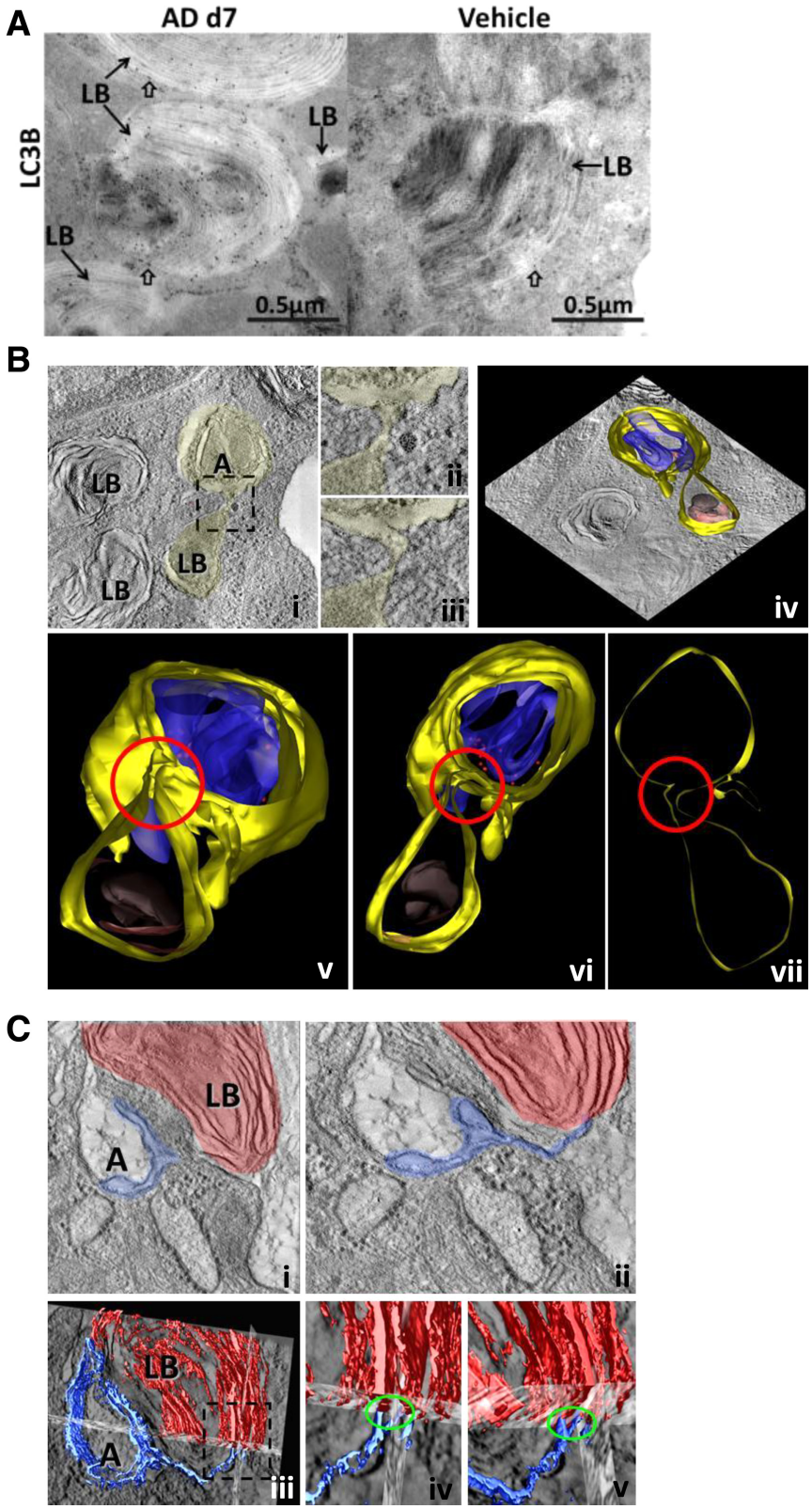

© 2015 The Authors The Journal of Pathology: Clinical Research published by The Pathological Society of Great Britain and Ireland and John Wiley & Sons Ltd

20564538, 2015, 4, Downloaded from https://onlinelibrary.wiley.com/doi/10.1002/cjp2.20 by Cochrane Germany, Wiley Online Library on [29/12/2022]. See the Terms and Conditions (https://onlinelibrary.wiley.com/terms-and-conditions) on Wiley Online Library for rules of use; OA articles are governed by the applicable Creative Commons License

in driving apoptosis [8]. Supporting this, we observed extensive vacuolisation and an increase in the autophagy markers when MLE12 cells were directly exposed to AD. This observation is in complete agreement with some previous studies, which reported AD-induced LC3B positive vacuolar structures in different human cells in culture [25,26]. It may be logical to speculate that increased autophagy could be a mechanism to degrade the deposited drug from the lysosomal compartments. Supporting this concept, in response to AD, we observed a marked increase in LAMP2 protein levels (in mice and cells) and LC3B co-localisation with LAMP2, a protein that has been shown to be pivotal for autophagosome maturation as well as for autophagosome-lysosome fusion [27,28]. At first glance, it appears that AD treatment might lead to defective autophagy due to an increase in the autophagy substrate protein p62 following AD treatment. However, we observed up-regulation of p62 transcript following AD treatment that might compensate for its protein level, questioning its use as a marker for autophagy flux. Further analysis of autophagy flux using inhibitors such as chloroquine and a combination of pepstatin and E64D (but not bafilomycin A1) revealed that AD actually increases autophagy flux in MLE12 cells. While this manuscript was in preparation, Lee *et al* [17] reported similar observations in other cell types, surprisingly using bafilomycin A1 as the inhibitor for flux studies, in spite of previous reports which impressively showed that bafilomycin A1 suppresses the uptake of AD [15].

AD is metabolised to its chief metabolite, desethylamiodarone (DES), by the P450 enzyme system [29]. DES shares some toxicological and pharmacological characters of AD and some studies have documented that DES is much more cytotoxic than AD, causing cell death even at low doses in many cell types [30]. Disruption of mitochondrial function, including production of reactive oxygen species (ROS), decrease in mitochondrial membrane potential and cytochrome c release, are well-documented effects of both AD and DES [31–34]. Since we and others have shown that AD induces autophagy in many cell types, it may not be surprising to note that DES also exerts similar effects. Accumulation of DES in tissues due to prolonged AD treatment may also contribute in part to the dysregulated autophagy pathway and thereby apoptosis of AECIIs in mice in response to AD treatment. Basal autophagy is an extremely important housekeeping process that prevents accumulation of unwanted proteins within the cytoplasm [18–20]. Under certain conditions such as cancer, it is believed to be potentially maladaptive [35] or under certain settings of uncontrolled increase in autophagy as in COPD, it might lead to cell death [19,36]. Hence, it appears important that the autophagy process is well-balanced. The interplay between autophagy and apoptosis is a matter under continuous discussion and the intricate molecular mechanisms between these two pathways are extremely complex [19,35]. Nevertheless, there exists some evidence that molecules of the autophagy pathway do play a role in executing apoptosis in certain settings. For example, knockdown of LC3 rescued p53-deficient HCT116 cells from apoptosis [37] and LC3B-/- mice were shown to be resistant to apoptosis after cigarette smoke exposure [38]. In line with these findings, we now show that AD-induced cleaved caspase 3 levels are decreased after LC3B knockdown in MLE12 cells, indicating a role for LC3B in mediating their apoptosis and, probably, also lung fibrosis.

Under physiological conditions, the autophagy pathway orchestrates with other vital cellular pathways. It is hence not surprising that autophagy influences other pivotal cellular mechanisms or *vice versa* under certain pathological conditions [39]. For example, in a previously described rat model of AD-induced pulmonary toxicity, blockade of angiotensin formation inhibited the development of lung fibrosis.

Figure 5. AD induces fusion between autophagosome and lamellar bodies in AECII. (A) Representative images from immunogold labelling for LC3B on lung sections of AD (day 7) and vehicle treated mice. Arrows indicate preferential binding of LC3B to lamellar bodies (LB) in AECII. Block arrows indicate LC3B-bound gold particles in close proximity to the limiting membrane of LB of AECII in AD and vehicle-treated mice. Scale bar=0.5 μm. (B) Single slice of EM tomogram showing a direct link between autophagosomes (A) and lamellar bodies (LB) via membranes (i); the boxed area is shown at higher magnification in (ii, iii). Different slices of the tomogram showing that the limiting membrane of the lamellar body and the autophagosome share the same membrane are shown adjacent to these images (iv). In the lower panel (v-vii), different rotation views of the model of the connection between LB and the autophagosome are shown: the junction is highlighted by a red circle. Colour code: yellow, limiting membranes; blue, membranous content of the autophagosome; red, ribosomes; grey, core of the lamellar body; brown, lipid lamellae. (C) A second example obtained by means of EM tomography showing a direct link between autophagosomes (A) and lamellar bodies (LB) via membranes (i). The membranes of the LB also protrude and form a double membrane layer of an autophagosome which separates a compartment of low density within the autophagosome from the cytosol (ii). The lower row (iii-v) represents a 3D reconstruction of the membranes of a LB (red) and the membranes of the autophagosome (blue).

© 2015 The Authors The Journal of Pathology: Clinical Research published by The Pathological Society of Great Britain and Ireland and John Wiley & Sons Ltd

20564538, 2015, 4, Downloaded from https://onlinelibrary.wiley.com/doi/10.1002/cjp2.20 by Cochrane Germany, Wiley Online Library on [29/12/2022]. See the Terms and Conditions (https://onlinelibrary.wiley.com/terms-and-conditions) on Wiley Online Library for rules of use; OA articles are governed by the applicable Creative Commons License

In fact, the angiotensin (AT) 1 receptor antagonist losartan that was used to inhibit AECII apoptosis and thereby lung fibrosis [40] is actually also an inhibitor of autophagy [41,42].

Another intriguing observation that stems from the current work is the presence of LC3B at the vicinity of the limiting membrane of lamellar bodies within the AECIIs of mouse lungs. Sometimes, especially in response to AD, membranes of these lamellar bodies were observed to be in close connection with phagophores/ autophagosomal structures. It has been shown that an autophagic process is involved in the biogenesis of multilamellar bodies [43]. However, proteomic analysis of lung lamellar bodies from rats did not reveal the presence of LC3B either on the limiting membrane or in the lumen of lamellar bodies [44]. We nevertheless could convincingly show gold-labelled LC3B particles both in the lumen as well as on the limiting membrane of lamellar bodies. Based on these observations, it may be reasonable to speculate on the role of LC3B in surfactant homeostasis in normal and, even more, in AD-injured AECIIs. In complete agreement with this, we could now show that knockdown of LC3B impressively decreased the levels of AD-induced accumulation of SP-C in MLE12 cells.

In conclusion, our current study demonstrates a critical role for macroautophagy, especially the marker LC3B, in regulating AECII cell death in response to AD. Although not addressed experimentally here, it appears reasonable to speculate that the magnitude of autophagy flux is also linked to the extent of lung fibrosis. This study enhances our understanding of the molecular mechanisms underlying AD-induced lung fibrosis. Based on our data, it appears reasonable to target autophagy pathways for improving epithelial survival and minimise AD-induced lung fibrosis. However, a careful and critical analysis is warranted when targeting the autophagy pathway as too little or too much autophagy is deleterious for the cells.

Acknowledgements

The authors thank Moritz Wattenbach, Susanne Fassbender and Sabine Fiedler for their superb technical assistance. Part of this work has been undertaken with the enormous support of the European Commission (European IPF Network, funded from 2008 to 2012 through the frame program 7).

Author contributions PM, AG conceived and designed the study. PM performed the experimental work and AG supervised the research. IH, SV, SA, SC, CR, MK participated in the experimental work. LK, JH, CW, MO performed and analysed electron microscopy and tomography.WS participated in the study design. PM, AG composed and finalised the manuscript. All authors were involved in writing the paper and had final approval of the submitted version.

References

1. Chang SN, Hwang JJ, Hsu KL, *et al*. Amiodarone-related pneumonitis. *J Formosan Med Assoc (Taiwan yi zhi)* 2007;**106**:411–417.
2. Okayasu K, Takeda Y, Kojima J, *et al*. Amiodarone pulmonary toxicity: a patient with three recurrences of pulmonary toxicity and consideration of the probable risk for relapse. *Intern Med* 2006;**45**:1303–1307.
3. Ott MC, Khoor A, Leventhal JP, *et al*. Pulmonary toxicity in patients receiving low-dose amiodarone. *Chest* 2003;**123**:646–651.
4. Charles PE, Doise JM, Quenot JP, *et al*. Amiodarone-related acute respiratory distress syndrome following sudden withdrawal of steroids. *Respiration* 2006;**73**:248–249.
5. January CT, Wann LS, Alpert JS, *et al*. 2014 AHA/ACC/HRS Guideline for the Management of Patients With Atrial Fibrillation: Executive Summary: A Report of the American College of Cardiology/American Heart Association Task Force on Practice Guidelines and the Heart Rhythm Society. *Circulation* 2014;**130**: 2071–2104.
6. Chiovato L, Martino E, Tonacchera M, *et al*. Studies on the in vitro cytotoxic effect of amiodarone. *Endocrinology* 1994;**134**: 2277–2282.
7. Bargout R, Jankov A, Dincer E, *et al*. Amiodarone induces apoptosis of human and rat alveolar epithelial cells in vitro. *Am J Physiol* 2000;**278**:L1039–L1044.
8. Mahavadi P, Henneke I, Ruppert C, *et al*. Altered surfactant homeostasis and alveolar epithelial cell stress in amiodarone-induced lung fibrosis. *Toxicol. Sci.* 2014;**142**:285–297.
9. Martin WJ, II, Kachel DL, Vilen T, *et al*. Mechanism of phospholipidosis in amiodarone pulmonary toxicity. *J Pharmacol Exp Ther* 1989;**251**:272–278.
10. Ashrafian H, Davey P. Is amiodarone an underrecognized cause of acute respiratory failure in the ICU? *Chest* 2001;**120**:275–282.
11. Sarma JS, Pei H, Venkataraman K. Role of oxidative stress in amiodarone-induced toxicity. *J Cardiov Pharmacol Ther* 1997;**2**:53–60.
12. Uhal BD, Zhang H, Abdul-Hafez A, *et al*. Amiodarone induces angiotensinogen gene expression in lung alveolar epithelial cells through activation protein-1. *Basic Clin Pharmacol. Toxicol* 2007;**100**:59–66.
13. Nagata N, Suematsu R, Yoshii C, *et al*. Characterization of amiodarone pneumonitis as related to inflammatory cells and surfactant apoprotein. *Chest* 1997;**112**:1068–1074.
14. Somani P, Bandyopadhyay S, Gross SA, *et al*. Amiodarone and multilamellar inclusion bodies. *Br J Clin Pharmacol* 1987;**24**: 237–239.
15. Morissette G, Ammoury A, Rusu D, *et al*. Intracellular sequestration of amiodarone: role of vacuolar ATPase and macroautophagic transition of the resulting vacuolar cytopathology. *Br J Pharmacol* 2009;**157**:1531–1540.
16. Piccoli E, Nadai M, Caretta CM, *et al*. Amiodarone impairs trafficking through late endosomes inducing a Niemann-Pick C-like phenotype. *Biochem Pharmacol* 2011;**82**:1234–1249.

© 2015 The Authors The Journal of Pathology: Clinical Research published by The Pathological Society of Great Britain and Ireland and John Wiley & Sons Ltd

20564538, 2015, 4, Downloaded from https://onlinelibrary.wiley.com/doi/10.1002/cjp2.20 by Cochrane Germany, Wiley Online Library on [29/12/2022]. See the Terms and Conditions (https://onlinelibrary.wiley.com/terms-and-conditions) on Wiley Online Library for rules of use; OA articles are governed by the applicable Creative Commons License

17. Lee KY, Oh S, Choi YJ, *et al*. Activation of autophagy rescues amiodarone-induced apoptosis of lung epithelial cells and pulmonary toxicity in rats. *Toxicol Sci* 2013;**136**:193–204.
18. Klionsky DJ, Emr SD. Autophagy as a regulated pathway of cellular degradation. *Science* 2000;**290**:1717–1721.
19. Mizushima N, Levine B, Cuervo AM, *et al*. Autophagy fights disease through cellular self-digestion. *Nature* 2008;**451**:1069–1075.
20. Choi AM, Ryter SW, Levine B. Autophagy in human health and disease. *New Engl J Med* 2013;**368**:1845–1846.
21. Mahavadi P, Korfei M, Henneke I, *et al*. Epithelial stress and apoptosis underlie Hermansky-Pudlak syndrome-associated interstitial pneumonia. *Am J Respir Crit Care Med* 2010;**182**:207–219.
22. Zhang XJ, Chen S, Huang KX, *et al*. Why should autophagic flux be assessed? *Acta Pharmacol Sin* 2013;**34**:595–599.
23. Klionsky DJ, Abdalla FC, Abeliovich H, *et al*. Guidelines for the use and interpretation of assays for monitoring autophagy. *Autophagy* 2012;**8**:445–544.
24. Li X, Rayford H, Shu R, *et al*. Essential role for cathepsin D in bleomycin-induced apoptosis of alveolar epithelial cells. *Am J Physiol Lung Cell Molec Physiol* 2004;**287**:L46–L51.
25. Renna M, Jimenez-Sanchez M, Sarkar S, *et al*. Chemical inducers of autophagy that enhance the clearance of mutant proteins in neurodegenerative diseases. *J Biol Chem* 2010;**285**:11061–11067.
26. Zhang L, Yu J, Pan H, *et al*. Small molecule regulators of autophagy identified by an image-based high-throughput screen. *Proc Natl Acad Sci USA* 2007;**104**:19023–19028.
27. Gonzalez-Polo RA, Boya P, Pauleau AL, *et al*. The apoptosis/autophagy paradox: autophagic vacuolization before apoptotic death. *J Cell Sci* 2005;**118**:3091–3102.
28. Saftig P, Beertsen W, Eskelinen EL. LAMP-2: a control step for phagosome and autophagosome maturation. *Autophagy* 2008;**4**:510–512.
29. Shayeganpour A, El-Kadi AO, Brocks DR. Determination of the enzyme(s) involved in the metabolism of amiodarone in liver and intestine of rat: the contribution of cytochrome P450 3A isoforms. *Drug Metab Dispos* 2006;**34**:43–50.
30. Mulder JE, Brien JF, Racz WJ, *et al*. Mechanisms of amiodarone and desethylamiodarone cytotoxicity in nontransformed human peripheral lung epithelial cells. *J Pharmacol Exp Ther* 2011;**336**:551–559.
31. Bolt MW, Card JW, Racz WJ, *et al*. Disruption of mitochondrial function and cellular ATP levels by amiodarone and N-desethylamiodarone in initiation of amiodarone-induced pulmonary cytotoxicity. *J Pharmacol Exp Ther* 2001;**298**:1280–1289.
32. Varbiro G, Toth A, Tapodi A, *et al*. Concentration dependent mitochondrial effect of amiodarone. *Biochem Pharmacol* 2003;**65**:1115–1128.
33. Varbiro G, Toth A, Tapodi A, *et al*. Protective effect of amiodarone but not N-desethylamiodarone on postischemic hearts through the inhibition of mitochondrial permeability transition. *J Pharmacol Exp Ther* 2003;**307**:615–625.
34. Zahno A, Brecht K, Morand R, *et al*. The role of CYP3A4 in amiodarone-associated toxicity on HepG2 cells. *Biochem Pharmacol* 2011;**81**:432–441.
35. Corcelle EA, Puustinen P, Jaattela M. Apoptosis and autophagy: targeting autophagy signalling in cancer cells -'trick or treats'? *FEBS J* 2009;**276**:6084–6096.
36. Ryter SW, Lee SJ, Choi AM. Autophagy in cigarette smoke-induced chronic obstructive pulmonary disease. *Expert Rev Respir Med* 2010;**4**:573–584.
37. Scherz-Shouval R, Weidberg H, Gonen C, *et al*. p53-dependent regulation of autophagy protein LC3 supports cancer cell survival under prolonged starvation. *Proc Natl Acad Sci USA* 2010;**107**:18511–18516.
38. Chen ZH, Lam HC, Jin Y, *et al*. Autophagy protein microtubule-associated protein 1 light chain-3B (LC3B) activates extrinsic apoptosis during cigarette smoke-induced emphysema. *Proc Natl Acad Sci USA* 2010;**107**:18880–18885.
39. Wang Y, Qin ZH. Coordination of autophagy with other cellular activities. *Acta Pharmacol Sin* 2013;**34**:585–594.
40. Uhal BD, Wang R, Laukka J, *et al*. Inhibition of amiodarone-induced lung fibrosis but not alveolitis by angiotensin system antagonists. *Pharmacol Toxicol* 2003;**92**:81–87.
41. Xiao R, Teng M, Zhang Q, *et al*. Myocardial autophagy after severe burn in rats. *PloS one* 2012;**7**:e39488.
42. Lin L, Tang C, Xu J, *et al*. Mechanical stress triggers cardiomyocyte autophagy through angiotensin II type 1 receptor-mediated p38MAP kinase independently of angiotensin II. *PloS one* 2014;**9**:e89629.
43. Hariri M, Millane G, Guimond MP, *et al*. Biogenesis of multilamellar bodies via autophagy. *Molec Biol Cell* 2000;**11**:255–268.
44. Ridsdale R, Na CL, Xu Y, *et al*. Comparative proteomic analysis of lung lamellar bodies and lysosome-related organelles. *PloS one* 2011;**6**:e16482.

© 2015 The Authors The Journal of Pathology: Clinical Research published by The Pathological Society of Great Britain and Ireland and John Wiley & Sons Ltd

20564538, 2015, 4, Downloaded from https://onlinelibrary.wiley.com/doi/10.1002/cjp2.20 by Cochrane Germany, Wiley Online Library on [29/12/2022]. See the Terms and Conditions (https://onlinelibrary.wiley.com/terms-and-conditions) on Wiley Online Library for rules of use; OA articles are governed by the applicable Creative Commons License

SUPPLEMENTARY MATERIAL ON THE INTERNET

Additional Supporting Information may be found in the online version of this article.

The following supplementary material may be found in the online version of this article:

Figure S1: (a) Representative Western blot images from cell lysates from AD (8, 16 & 24 hours) or vehicle treated (24 hours) or untreated (UT) MLE12 cells for p62 and ß-actin. (b). Graphical representation depicting quantification of p62 mRNA using q-PCR in MLE 12 cells upon AD treatment for the indicated time points, vehicle or untreated cells. Below, a representative agarose gel image from semi-quantitative RT-PCR for p62 is shown. β-actin was used as house-keeping gene.

Figure S2: (a) Representative phase contrast images of MLE12 cells pre-treated with bafilomycin A1, AD and both bafilomycin A1 and AD. Scale bar=100 µm. (b) Representative Western blot images for LC3B and β-actin after pre-incubation of MLE12 cells with vehicle (DMSO) or pepstatin + E64D (10 µg/mL each) for 1hour followed by AD or vehicle treatments for 8 hours.

Figure S3. (a) Western blot analysis of lung homogenates of (left) AD treated mice at days 7, 14 and vehicle at day 28 and (right) AD treated mice at days 21, 28 and vehicle at day 28 for p62 & β-actin in AD treated mice. (b) Graphical representation of densitometry analysis is shown for p62 Western blots shown in (a). Representative blots and analysis from n=5 mice. $*p < 0.05$. (c). Immunohistochemistry performed on serial lung sections from mice treated with AD at 14, 21, 28 days and vehicle at day 28 for LC3B and pro SP-C showing numerous LC3B positive AECIIs (indicated with arrows) in AD treated mice. Scale bar in all the images=50 μm; Original magnification of pictomicrographs: 400x.

Video1. Transmission electron tomography and modelling of an autophagosome connected to a lamellar body in a type II alveolar epithelial cell. Reconstructed volume is used for modelling of an autophagosome and a lamellar body (grey, core of the lamellar body; brown, lipid lamellae), sharing the same limiting membrane (yellow). The autophagosome exhibits membranous content (blue) and ribosomes (red). The 3D model reveals a junction between the lamellar body and the autophagosome and a remaining opening of the structure indicating a late phagophore/early autophagosome.

© 2015 The Authors The Journal of Pathology: Clinical Research published by The Pathological Society of Great Britain and Ireland and John Wiley & Sons Ltd

20564538, 2015, 4, Downloaded from https://onlinelibrary.wiley.com/doi/10.1002/cjp2.20 by Cochrane Germany, Wiley Online Library on [29/12/2022]. See the Terms and Conditions (https://onlinelibrary.wiley.com/terms-and-conditions) on Wiley Online Library for rules of use; OA articles are governed by the applicable Creative Commons License

The attached printed / pdf version of this article is part of this habilitation thesis and has been included according to the © 2015 The Authors The Journal of Pathology: Clinical Research published by The Pathological Society of Great Britain and Ireland and John Wiley & Sons Ltd.

This is an open access article under the terms of the Creative Commons Attribution-NonCommercial-NoDerivs License, which permits use and distribution in any medium, provided the original work is properly cited, the use is non-commercial and no modifications or adaptations are made.

Citation of this article: Poornima Mahavadi, Lars Knudsen, Shalini Venkatesan, Ingrid Henneke, Jan Hegermann, Christoph Wrede, Matthias Ochs, Saket Ahuja, Shashi Chillappagari, Clemens Ruppert, Werner Seeger, Martina Korfei, Andreas Guenther. Regulation of macroautophagy in amiodarone-induced pulmonary fibrosis. **J Pathol Clin Res. 2015** Jun 3;1(4):252-63. doi: 10.1002/cjp2.20. eCollection 2015 Oct.

Am J Physiol Lung Cell Mol Physiol 310: L519–L531, 2016.
First published December 30, 2015; doi:10.1152/ajplung.00213.2015.

CALL FOR PAPERS | *Translational Research in Acute Lung Injury and Pulmonary Fibrosis*

MAP1LC3B overexpression protects against Hermansky-Pudlak syndrome type-1-induced defective autophagy in vitro

Saket Ahuja,[1,2] Lars Knudsen,[3,4,5] Shashi Chillappagari,[1,2,6] Ingrid Henneke,[1,2] Clemens Ruppert,[1,2,7] Martina Korfei,[1,2] Bernadette R. Gochuico,[8] Saverio Bellusci,[1,2,7] Werner Seeger,[1,2,7,9] Matthias Ochs,[3,4,5] Andreas Guenther,[1,2,7,9,10]* and Poornima Mahavadi[1,2]*

[1]*Department of Internal Medicine, Justus-Liebig University, Giessen, Germany;* [2]*Universities of Giessen and Marburg Lung Center (UGMLC), Member of the German Centre for Lung Research (DZL), Giessen, Germany;* [3]*Institute of Functional and Applied Anatomy, Hannover Medical School, Hannover, Germany;* [4]*Biomedical Research in End-Stage and Obstructive Lung Disease Hannover (BREATH), Member of the German Center for Lung Research (DZL), Hannover, Germany;* [5]*REBIRTH Cluster of Excellence, Hannover, Germany;* [6]*Department of Pediatrics, Justus-Liebig-University, Giessen, Germany;* [7]*Excellence Cluster Cardiopulmonary System (ECCPS), Giessen, Germany;* [8]*Medical Genetics Branch, National Human Genome Research Institute, National Institutes of Health, Bethesda, Maryland;* [9]*Member European IPF Registry/Biobank; and* [10]*Lung Clinic Waldhof-Elgershausen, Greifenstein, Germany*

Submitted 30 June 2015; accepted in final form 24 December 2015

Ahuja S, Knudsen L, Chillappagari S, Henneke I, Ruppert C, Korfei M, Gochuico BR, Bellusci S, Seeger W, Ochs M, Guenther A, Mahavadi P. MAP1LC3B overexpression protects against Hermansky-Pudlak syndrome type-1-induced defective autophagy in vitro. *Am J Physiol Lung Cell Mol Physiol* 310: L519–L531, 2016. First published December 30, 2015; doi:10.1152/ajplung.00213.2015.—Hermansky-Pudlak syndrome (HPS) is a rare autosomal recessive disorder, and some patients with HPS develop pulmonary fibrosis, known as HPS-associated interstitial pneumonia (HPSIP). We have previously reported that HPSIP is associated with severe surfactant accumulation, lysosomal stress, and alveolar epithelial cell type II (AECII) apoptosis. Here, we hypothesized that defective autophagy might result in excessive lysosomal stress in HPSIP. Key autophagy proteins, including LC3B lipidation and p62, were increased in HPS1/2 mice lungs. Electron microscopy demonstrated a preferable binding of LC3B to the interior of lamellar bodies in the AECII of HPS1/2 mice, whereas in wild-type mice it was present on the limiting membrane in addition to the interior of the lamellar bodies. Similar observations were noted in human HPS1 lung sections. In vitro knockdown of *HPS1* revealed increased LC3B lipidation and p62 accumulation, associated with an increase in proapoptotic caspases. Overexpression of LC3B decreased the *HPS1* knockdown-induced p62 accumulation, whereas rapamycin treatment did not show the same effect. We conclude that loss of HPS1 protein results in impaired autophagy that is restored by exogenous LC3B and that defective autophagy might therefore play a critical role in the development and progression of HPSIP.

autophagy; Hermansky-Pudlak syndrome; alveolar epithelial cells; Hermansky-Pudlak syndrome-associated interstitial pneumonia; apoptosis; lung fibrosis

HERMANSKY-PUDLAK SYNDROME (HPS), a rare genetic disorder, is typically characterized by platelet dysfunction, oculocutaneous albinism, accumulation of ceroid lipofuscin in lysosomes, granulomatous colitis, and pulmonary fibrosis (16). Clinical diagnosis of HPS is established by hair and skin hypopigmentation, ocular abnormalities, and microscopic visualization of platelets revealing absence of dense bodies (16). Until now, HPS has been most frequently characterized among patients of Puerto Rican descent (2), but the disease is prevalent all over the world. Mutations in HPS genes are primarily known to affect the regulation and function of various lysosome-related organelles (LROs) such as platelet-dense granules, pigment cell melanosomes, and lung lamellar bodies (8, 12).

Several HPS mutations have been described previously, but pulmonary fibrosis known as HPS-associated interstitial pneumonia (HPSIP) seems to occur mostly in *HPS1*, *HPS2*, and *HPS4*, each encoding a different gene (1, 9, 17). HPSIP is a leading cause of death in these patients usually in the fourth or fifth decade of their life (9). Lungs of patients with HPSIP are typically characterized by swelling of alveolar epithelial type II cells (AECII) with an increase in size and number of lamellar bodies, termed "giant lamellar body degeneration" (34). Giant lamellar bodies are also observed within the AECII of HPS1/2 double-mutant mice (18), and we have previously reported that these mice spontaneously develop lung fibrosis associated with AECII-specific cellular stress and apoptosis (30). On the other hand, mice with mutations either in *HPS1* or *HPS2* genes show an increased predisposition to pulmonary fibrosis upon bleomycin challenge (56).

Whereas *HPS2* encodes the β-subunit of the adaptor protein-3 (AP-3) that sorts proteins from endosomes to LROs (40), HPS1 and HPS4 proteins are subunits of the biogenesis of LRO complex-3 (BLOC-3), which plays a role in the distribution of lysosomes and LROs (15). Such effects of HPS gene products on lysosomes was also supported by a study in the lungs of HPS1/2 mice, which demonstrated severe defects in surfactant secretion from the lamellar bodies (18), which are the LROs of the AECII. In the same vein, we previously reported accumu-

* A. Guenther and P. Mahavadi contributed equally to this work.
Address for reprint requests and other correspondence: A. Guenther, Klinikstrasse 36, 35392, Giessen, Germany (e-mail: Andreas.Guenther@innere.med.uni-giessen.de).

 1040-0605/16 Copyright © 2016 the American Physiological Society

Downloaded from www.physiology.org/journal/ajplung (141.050.134.220) on October 24, 2019.

lation of surfactant proteins associated with severe lysosomal stress and apoptosis of AECII in HPS1/2 mice as well as in a patient with HPS1 with interstitial pneumonia (30). On the basis of these observations, we hypothesized that these lysosome-associated disturbances in HPSIP might be a result of altered autophagy, a basic homeostasis mechanism of a cell that degrades long-lived proteins and organelles via lysosomes (14) to promote cellular homeostasis. Both selective (4) and nonselective forms (45) of autophagy exist. Classically, autophagy is divided into macroautophagy, microautophagy, and chaperone-mediated autophagy (33). Autophagy basically involves formation of double-membrane structures called autophagosomes, which carry long-lived proteins or dysfunctional organelles in their lumen to fuse with lysosomes and degrade their contents (25). This is a dynamic process and requires the coordinated function of several autophagy-related (Atg) gene products (33). Microtubule-associated protein 1 light chain-3β (MAP1LC3B; referred to as LC3B hereafter) is one of the important autophagy-related proteins, and its lipidated form (LC3BII) is a marker for the autophagosomes (50, 51). It interacts with sequestosome 1 (SQSTM1)/p62, a substrate for autophagy that carries the cargo to the autophagosomes for degradation (38). Autophagy is tightly regulated in the cells at a basal level, and any functional defect in this degradation pathway results in the intracellular accumulation of toxic substrates, which has deleterious effects on various biological processes (44, 55). Dysfunctional autophagy has been indicated to play an important role in the development of several pathologies, including lysosomal storage diseases (LSDs) (10, 37, 46), neurodegenerative diseases (23), and several organ-specific diseases, including lung fibrosis (3, 39).

Because lysosomal stress has been reported in HPSIP, we hypothesized that autophagy pathway plays a key role in the development and progression of HPSIP. Hence, we aimed to study this pathway in HPS1/2 mice, HPS1 human lungs, as well as to study the in vitro effects of *HPS1* knockdown on autophagy.

MATERIALS AND METHODS

Mice. Breeding pairs of HPS1 and HPS2 monomutant mice were purchased from the Jackson Laboratory, whereas the HPS1/2 double-mutant mice breeding pairs were received as a gift from Richard Swank (Roswell Park, Buffalo, NY). Background strain for these mice was C57BL/6J. All mice were kept under pathogen-free conditions and were genotyped as described before (30). Both the University Animal Care Committee and the Federal Authorities for Animal Research of the Regierungspraesidium Giessen (Hessen, Germany) approved the study protocol.

Human lung sections, immunohistochemistry, and Western blot. Written, informed consent was obtained, and subjects were enrolled in a protocol (04-HG-0211) approved by the Institutional Review Board of the National Human Genome Research Institute. For human subjects with HPS1, tissue was procured from a postmortem lung specimen and an explanted lung sample. Information about lungs from organ donors (used as controls) has been described before (24). All specimens from human and mice were fixed in 4% formaldehyde and embedded in formalin, and serial sections (3–6 μm) were performed. Immunostaining was performed using ZytoChem plus Broad Spectrum (AP-Fast red and HRP-DAB, Zytomed Systems) kit according to the manufacturer's instructions and as described before (30) for immunohistolocalization of LC3B (Abcam) and SQSTM1/p62 (Sigma-Aldrich). Stained sections were scanned with Hamamatsu scanner (Nanozoomer 2.0 RS). NDP.view2 software was used to make the images and analysis. Lung homogenates and cell lysates were denatured and subjected to Western blotting as described previously (30) to detect LC3B, green fluorescent protein (GFP), GAPDH, ATG5, myc (Abcam), p62 and ATG7 (Sigma-Aldrich), transcription factor EB (TFEB) (Proteintech), and lysosome-associated membrane protein 2 (LAMP2) (Santa Cruz Biotechnology).

Cloning, cell culture, and siRNA transfection. Full-length LC3B (gene bank accession number: NM_026160) was cloned into pEGFP-C1 expression vector and pCMV-myc-Tag3 (Agilent Technologies). Standard protocols were used for cloning, and A549 cells were transfected with GFP-LC3B or myc-LC3B plasmids. Cells were harvested after the indicated time points to isolate protein or RNA for further analysis. A549 cells were transfected with 50 nM human HPS1 siRNA (Santa Cruz Biotechnology) or scrambled siRNA (Dharmacon) in serum-free medium and cultured for the indicated time in the same medium without antibiotics followed by harvesting them for protein or RNA isolation.

Immunofluorescence. Immunofluorescence was performed according to the previously described protocols (29). Briefly, following plasmid or siRNA transfection for the indicated time points, cells were washed with ice-cold PBS and fixed in 4% paraformaldehyde. Permeabilization was performed with 0.1% Triton X-100, and nonspecific binding was blocked with 10% donkey serum followed by overnight incubation with primary antibodies against cleaved caspase-3 (Cell Signaling Technology), LC3B, LAMP1, caspase-8 (Abcam), and p62 (Sigma-Aldrich). Slides were then washed and incubated with respective Alexa Fluor probes (Alexa Fluor 488 or 555, Life Technologies) raised in donkey. Microscopy was performed using a Leica M205 FA fluorescent stereoscope (Leica Microsystems) equipped with a Leica DFC360 FX camera, and all images were captured using an ×63 objective lens. Immunofluorescence images were analyzed using Leica Application Suite Advanced Fluorescence (LAS AF) software, version 4.3. Quantification of the immunofluorescence images was performed using the JACOP plugin from ImageJ to calculate Pearson's coefficient (7). Briefly, for quantification, 15–30 random regions per well were imaged and subjected to the JACOP plugin. Image-acquisition parameters were kept constant for all images during the process of obtaining images. Pearson's coefficient of colocalization was calculated using Costes automatic threshold method for each of these pair of images having two different fluorophores.

PCR and RT-PCR. Cells were harvested, and total RNA was isolated (RNeasy Plus Mini Kit, Qiagen). RNA was reverse transcribed to cDNA (Omniscript RT Kit, Qiagen) and then subjected to PCR (HotstarTaq Polymerase PCR Kit, Qiagen) using primers for human HPS1, β-actin, GAPDH, and p62 with gene bank accession numbers NM_000195.3, NM_001101.3, NM_002046.5, and NM_003900.4 respectively, using the following primers: HPS1: forward: 5'GGACTTCTTGCTGGTGAAGAG3′, reverse: 5′CATCTGGAGTTTGTACCCCATG3′; β-actin: forward: 5′ACCCTGAAGTACCCCATCG3′, reverse: 5′CAGCCTGGATAGCAACGTAC3′; p62: forward: 5′TGGACCCATCTGTCTTCAAA3′, reverse: 5′ TCTGGGAGAGGGACTCAATC3′; GAPDH: forward: 5′ACCCAGAAGACTGTGGATGG3′, reverse: 5′GTGTCGCTGTTGAAGTCAGAG3′.

Electron microscopy and distribution pattern of immunogold labeling for LC3B in control and HPS1/2 mice. A perfusion fixation of mice lungs was performed using a multipurpose fixation solution (4% paraformaldehyde, 0.1% glutaraldehyde in 0.2 M HEPES buffer) according to recently published methods (53). Three lungs each [wild-type (WT) vs. HPS1/2] were subjected to a systematic uniform sampling (52) and embedded in lowicryl resin following a freeze substitution procedure. Immunogold labeling for LC3B (Abcam) was carried out as described before (29). Quantitative analysis of gold labeling was performed to determine cellular compartments in which a preferential labeling exists. As advocated by the current standards

Downloaded from www.physiology.org/journal/ajplung (141.050.134.220) on October 24, 2019.

for quantitative evaluation of lung structures, we determined the relative labeling index (RLI) followed by χ^2 analysis for statistical assessment of distribution pattern (19, 32). A systematic uniform area sampling was performed to sample AECII. Three lungs for each group (WT vs HPS1/2) were included, and two sections per lung were studied. The following compartments were defined, and volume fractions (Vv) and surface densities within AECII cells were determined by point and intersection counting: lumen of lamellar body, the limiting membrane (area 100 nm around the limiting membrane), mitochondria, nucleus, and cytosol. In addition, gold particles ($N_{\text{gold observed}}$) in these five compartments were counted. Supplemental Fig. S1 demonstrates examples of gold particles in different compartments of the cell (supplemental material for this article is available online at the *American Journal of Physiology Lung Cellular and Molecular Physiology* website). Gold particles were seen also in cytosol and counted accordingly. The cell size of AECII cells was much larger in HPS1/2 mice than in WT mice, and volume fractions of different compartments differed extensively (Table 1). For instance, the volume fraction of lamellar bodies in AECII was 61% in HPS1/2 and 13% in WT. Using volume fractions, the expected number of gold particles per subcellular compartment ($N_{\text{gold expected}}$) was calculated by multiplication of the sum of all counted gold particles in AECII cells and the volume fraction of the subcellular compartment. $N_{\text{gold expected}}$ is the number of particles we would have counted in the different compartments if labeling was random. $N_{\text{gold observed}}$ and $N_{\text{gold expected}}$ were used in a further step to calculate the RLI as follows: $\text{RLI} = N_{\text{gold observed}}/N_{\text{gold expected}}$.

Statistics. For statistical comparison of the difference between groups, one-way ANOVA was applied followed by Bonferroni's multiple comparison as a posttest. GraphPad Prism 5.0 was employed. P values were as follows: $^*P < 0.05$, $^{**}P < 0.01$, and $^{***}P < 0.001$. Distribution patterns of immunogold labeling in different ultrastructural compartments of AECII were assessed using χ^2 analysis and a degree of freedom of 4 (in view of 5 defined ultrastructural compartments).

Table 1. *Stereological analysis of LC3B labeling*

Compartment	$N_{\text{gold observed}}$	$V_{V(\text{comp/cell})}$	$N_{\text{gold expected}}$	RLI
		WT		
LB	246	0.13	54	4.55
LM	67	0.04	16	3.69
Mitochondria	15	0.16	66	0.22
Nucleus	4	0.19	79	0.05
Cytosol	84	0.49	203	0.41
Total	416	1	418	
		HPS1/2		
LB	1,830	0.61	1,158	1.58
LM	27	0.04	71	0.38
Mitochondria	0	0.01	18	0
Nucleus	6	0.05	100	0.06
Cytosol	34	0.30	566	0.06
Total	1,897	1	1,913	

In wild-type (WT) mice, the number of observed gold particles ($N_{\text{gold observed}}$) is larger than the expected number of gold particles ($N_{\text{gold expected}}$) in lamellar bodies (LB) and the limiting membrane (LM). Accordingly, the relative labeling index (RLI) is >1 in these compartments, suggesting a nonrandom distribution of gold particles and a preferable binding to LM and LB. To test the hypothesis that the distribution is nonrandom, a χ^2 test was added. With a total χ^2 of 997 and a degree of freedom (dF) of 4, the null hypothesis of random distribution must be rejected ($P < 0.05$). In HPS1/2 mice, $N_{\text{gold observed}} > N_{\text{gold expected}}$ was found in LB but not in LM. Hence the RLI is > 1 in LB but < 1 in LM so that a preferable binding can be attributed to the LB but not to the LM. A total χ^2 of 1013 and a dF of 4 results in a $P < 0.05$ so that the null hypothesis of random distribution of gold particles must be rejected. LC3B, light chain 3β; HPS, Hermansky-Pudlak syndrome.

RESULTS

Defective autophagy in HPSIP. To study the regulation of autophagy under HPSIP conditions, we first analyzed the lungs of 3- and 9-mo-old HPS1/2 mice. Whole-lung homogenates from these mice were subjected to Western blotting of key autophagy marker proteins. Compared with age-matched WT mice lungs as well as HPS1 and HPS2 monomutant mice, we observed an increase in LC3BII, the lipidated form of LC3B, indicating the formation of autophagosomes in HPS1/2 mice lungs (Fig. 1*A*). Supporting this, HPS1/2 mice lung homogenates (both 3 and 9 mo old) showed an increase in the levels of autophagy proteins p62, Atg7, and Atg5 and the regulator of lysosomal biogenesis, TFEB. Accumulation of p62 together with an increase in LC3BII is already indicative of a defective autophagy pathway. Interestingly, an increase in p62 was observed in the older HPS1 mice (9 mo) but not in the younger HPS1 mice (3 mo). Correspondingly, LAMP2, a lysosomal marker protein, was increased in both the double-mutant as well as in the monomutant HPS mice compared with age-matched controls (Fig. 1*A*).

Furthermore, we performed transmission electron microscopy on HPS1/2 and WT mice lungs. Immunogold labeling for LC3B was performed on a qualitative basis. Gold particles were found in lamellar bodies but occasionally also in other compartments, such as cytosol and mitochondria in both WT and HPS1/2 mice. However, whereas in WT mice gold particles were often observed in close proximity to the limiting membrane of lamellar bodies, this was not the case in HPS1/2 mice (Fig. 1*B*), in which the label was almost exclusively found inside the lamellar bodies. Hence, the distribution pattern of labeling for LC3B appeared to differ between WT and HPS1/2. To detect the preferential binding to AECII compartments in dependency of the genotype on a statistical basis, we determined the RLI, followed by the χ^2 analyses to test the distribution of labeling for randomness (Table 1), as advocated by the ATS/ERS standards for quantitative evaluation of lung structures (19). On the basis of the RLI > 1 and χ^2 analysis with a $P < 0.05$ (degree of freedom = 4), a preferential labeling for LC3B was found in the lamellar body as well as the limiting membrane in WT mice, whereas, in HPS1/2, a preferential binding of LC3B to the lamellar body, but not the limiting membrane, was encountered (RLI < 1). These data clearly demonstrate a different subcellular distribution of LC3B in WT vs. HPS1/2 mice (Fig. 1*D*, Table 1). Table 1 demonstrates a high number of observed gold particles in lamellar bodies, which is an increase of more than sevenfold compared with WT mice. The larger number of observed gold particles in lamellar bodies is above all a consequence of enlarged cells and enlarged lamellar bodies, which contribute 62% to the volume of AECII compared with WT mice, in which the lamellar bodies are smaller and contribute to only 13% of the volume of AECII (Table 1).

We next performed immunohistochemistry for p62 and surfactant protein C on serial lung sections of HPS1/2 and WT mice lung sections. Interestingly, we observed an intense staining for p62 within the AECII of HPS1/2 mice lung sections (Fig. 1, *C* and *D*), reflecting defective autophagy. Supporting these observations, AECII of one patient with HPS1 also displayed an increased staining for p62 (Fig. 2, *A* and *B*). Results until this point indicated an accumulation of

Downloaded from www.physiology.org/journal/ajplung (141.050.134.220) on October 24, 2019.

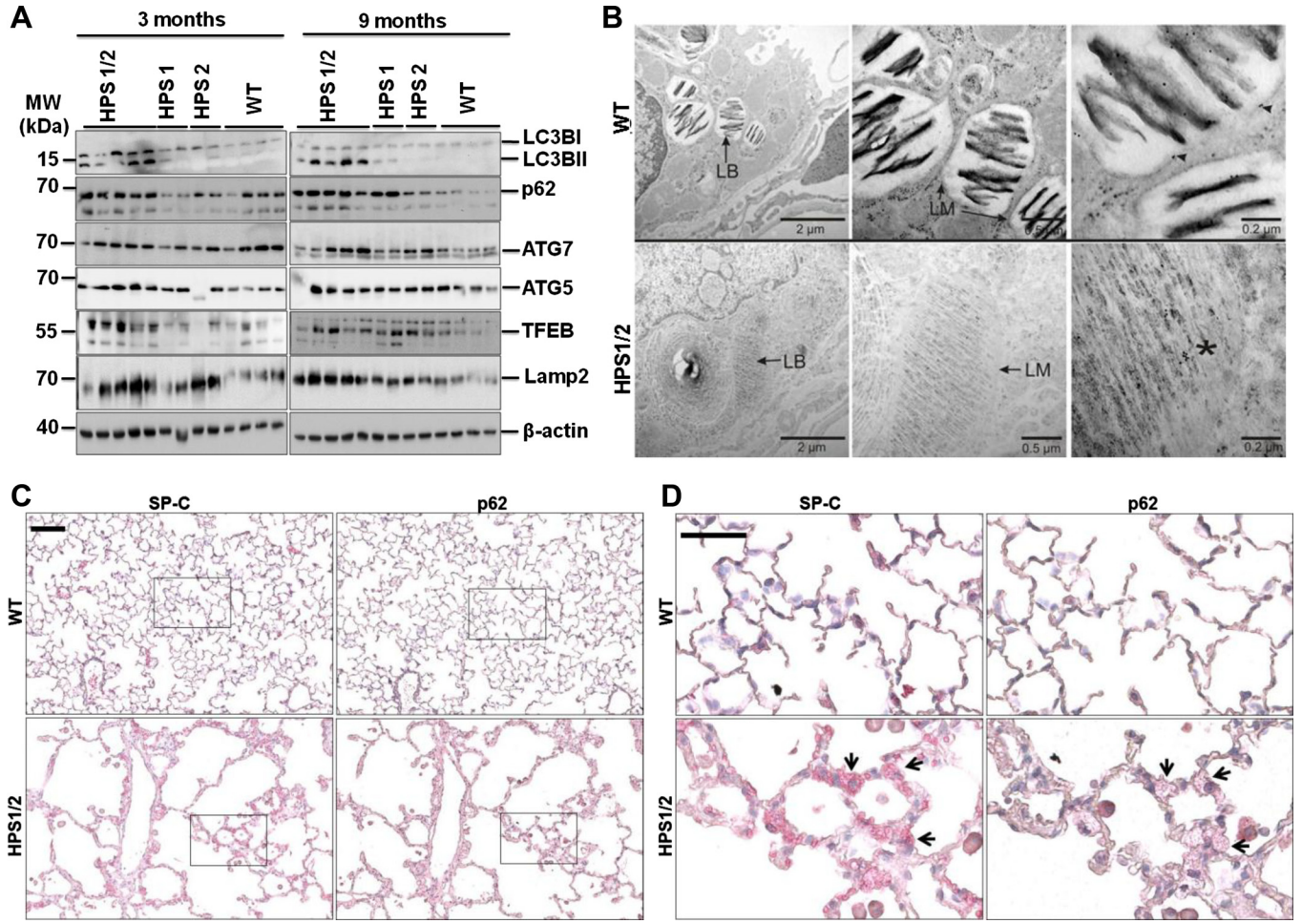

Fig. 1. Defective autophagy in the alveolar epithelial type II cells (AECII) of Hermansky-Pudlak syndrome (HPS)1/2 mice. *A*: 3- and 9-mo-old HPS1/2, HPS1, HPS2, and wild-type (WT) mice lung homogenates were subjected to Western blotting to detect the indicated markers of autophagy. *B*: immunogold labeling for light chain 3β (LC3B) on lung sections of HPS1/2 and WT mice. Lamellar bodies (LBs) within AECII of WT or HPS1/2 mice lungs are depicted here. Arrow heads indicate LC3B gold labeling on the limiting membrane of LBs in WT mice. *LC3B gold labeling within the lumen of LBs in HPS1/2 mice lungs. LM, lamellar membrane of LBs. *C* and *D*: serial sections of HPS1/2 and WT mice lungs were stained for p62 and prosurfactant protein C (SP-C). Original magnification: ×200; scale bar = 100 μm (*C*). High-magnification images for the selected regions are depicted in *D*. Arrows indicate p62-positive AECII in HPS1/2 mice lung sections. Original magnification: ×400; scale bar = 50 μm (*D*). Representative images from 3 different experiments are shown with $n = 3$–5 mice. ATG, autophagy-related gene protein; TFEB, transcription factor EB; Lamp, lysosome-associated membrane protein.

p62 within the AECII in the lungs of HPS1/2 mice and patient with HPS1, pointing toward defective autophagy under conditions of HPS-associated lung fibrosis.

Knockdown of HPS1 in A549 cells leads to defective autophagy and induces upregulation of apoptosis-related proteins. To further examine the effect of the loss of *HPS1* gene on autophagy in vitro, we performed siRNA-mediated knockdown of *HPS1* in the A549 cell line. After 24 h of transfection, knockdown of *HPS1* led to vacuolization in A549 cells, a feature that was not so prominent in scrambled or in untreated cells (Fig. 3, *A*–*C*). Supporting this observation, Western blot analysis showed a prominent and significant increase in both LC3BII and p62 in A549 cells following *HPS1* knockdown for 24 h (Fig. 3, *D*–*F*) and 48 h (not shown). It has been suggested that the transcriptional activation of p62 might counteract the degradation of p62 protein via autophagy, which might lead to either steady-state levels of p62 protein or, sometimes, an increase in p62 protein levels (41). In such cases, p62 may not be used as a marker for autophagy-mediated clearance. Hence, to identify whether the increase in p62 protein level was a mere reflection of its transcriptional regulation, we analyzed the transcript levels of p62 in untreated cells or cells transfected with scrambled siRNA or HPS1 siRNA. As indicated in Fig. 3, *G* and *H*, semiquantitative PCR showed that the transcription of *p62* is not upregulated following *HPS1* knockdown in A549 cells. Taken together, our results clearly indicate a defect in autophagy pathway, as evident by simultaneous LC3B and p62 accumulation attributable to loss of functional HPS1 protein in vitro.

In line with our previous observations (30), we observed severe cell death after 24 h of *HPS1* knockdown that was already evident under the cell culture microscope. Autophagy has been recently shown to regulate the clearance of active caspases, especially caspase-8 (57). We therefore analyzed caspase-8 and caspase-3 levels following *HPS1* knockdown. As evident from Fig. 3*I*, *HPS1* knockdown led to an increased staining of the apoptosis markers, cleaved caspase-3 and

Downloaded from www.physiology.org/journal/ajplung (141.050.134.220) on October 24, 2019.

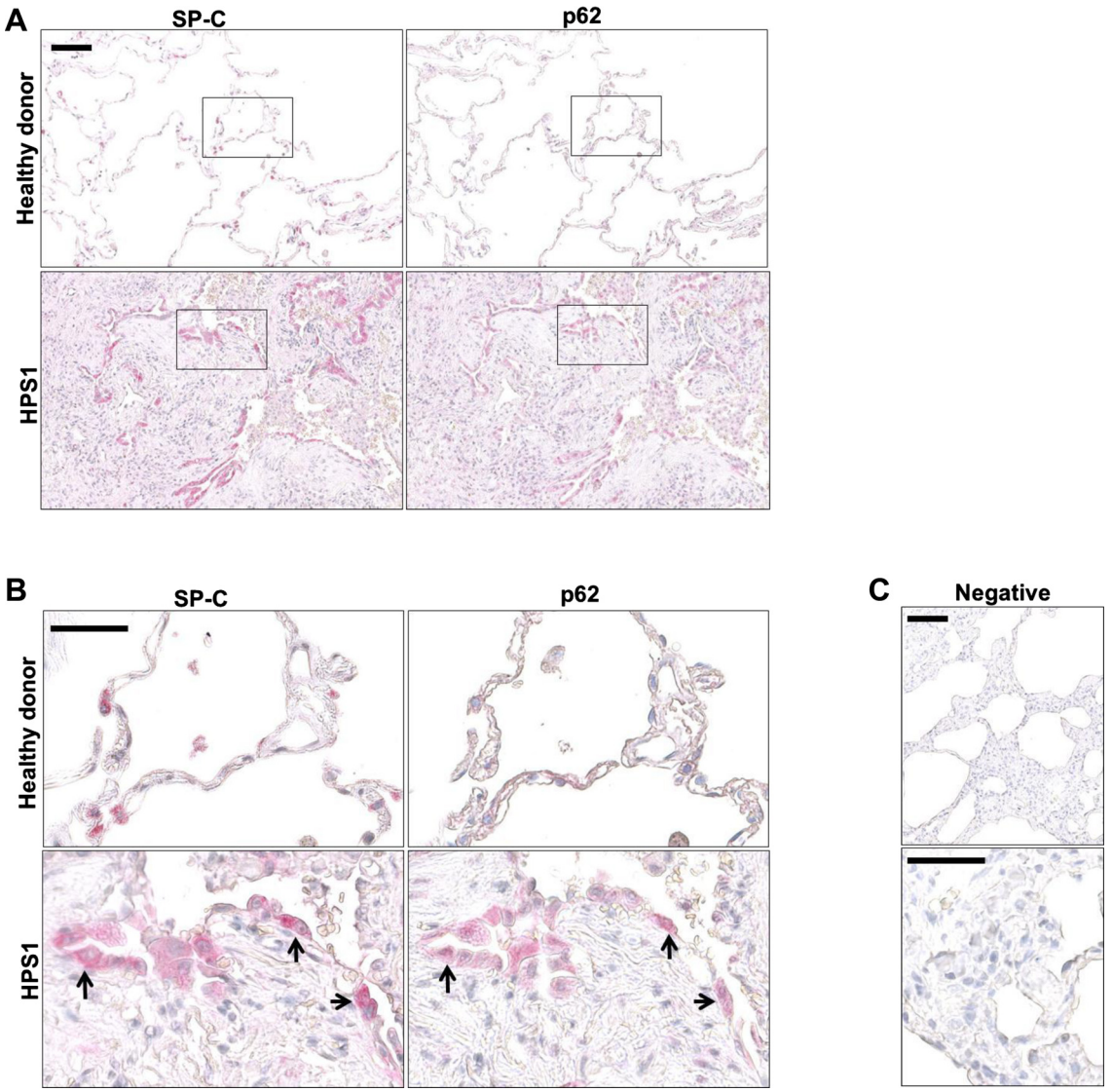

Fig. 2. Defective autophagy in AECII of lung of a patient with HPS1. Serial lung sections from 1 patient with HPS-1 and healthy donor were immunostained either for p62 or pro-SP-C. *A*: original magnification: ×200; scale bar = 100 μm. *B*: high-magnification images for the selected regions are shown, and arrows indicate p62-positive AECII in the lung sections of a patient with HPS1. Scale bar = 50 μm. *C*: low- and high-magnification images for negative control in which primary antibody was omitted are shown. Representative images from 3 independent experiments are shown.

caspase 8, compared with scrambled siRNA transfected or untransfected cells.

Overexpression of LC3B before HPS1 knockdown protects cells against p62 accumulation. On the basis of the previous results, we hypothesized that autophagy flux might be decreased following *HPS1* knockdown. To test this, we performed coimmunofluorescence for the autophagosome marker LC3B and the lysosomal marker LAMP1 following knockdown of *HPS1* gene alongside with scrambled siRNA-transfected or untreated cells to study whether the fusion event between autophagosomes and lysosomes occurs following *HPS1* knockdown. Interestingly, we observed primarily nuclear as well as cytosolic localization of LC3B, and this LC3B signal did not colocalize with LAMP1 (Fig. 4*A*). Quantification of the fluorescence signals also revealed a significant decrease in colocalization between LC3B and LAMP1 (Fig. 4*B*), again implicating defective autophagic degradation in cells with *HPS1* knockdown, whereas a diffuse staining for LC3B and normal LAMP1 distribution were observed in untreated cells or scrambled siRNA-transfected cells. Generally, use of autophagy inhibitors like bafilomycin A1 or chloroquine is recommended to study autophagy flux on a biochemical level. However, according to the guidelines of autophagy (21), prolonged exposure (>8 h) of cells to these inhibitors is not recommended because of lysosomal leakage. Hence, we aimed to assess the GFP-LC3 cleavage, which was also suggested to study the flux. In this approach, the LC3 part of the protein degrades more rapidly than the GFP, and detection of the GFP fragment alone indicates an increased autophagy flux (21). We therefore transfected A549 cells with GFP-LC3B for 24 h followed by the transfection of scrambled siRNA or HPS1 siRNA for another 24 h. Following *HPS1* knockdown, the GFP-LC3B colocalized with LAMP1 (Fig. 4, *C* and *D*), and, using anti GFP antibody, we observed free GFP fragment in cells transfected with GFP-LC3B and HPS1 siRNA, whereas bands corresponding to

Downloaded from www.physiology.org/journal/ajplung (141.050.134.220) on October 24, 2019.

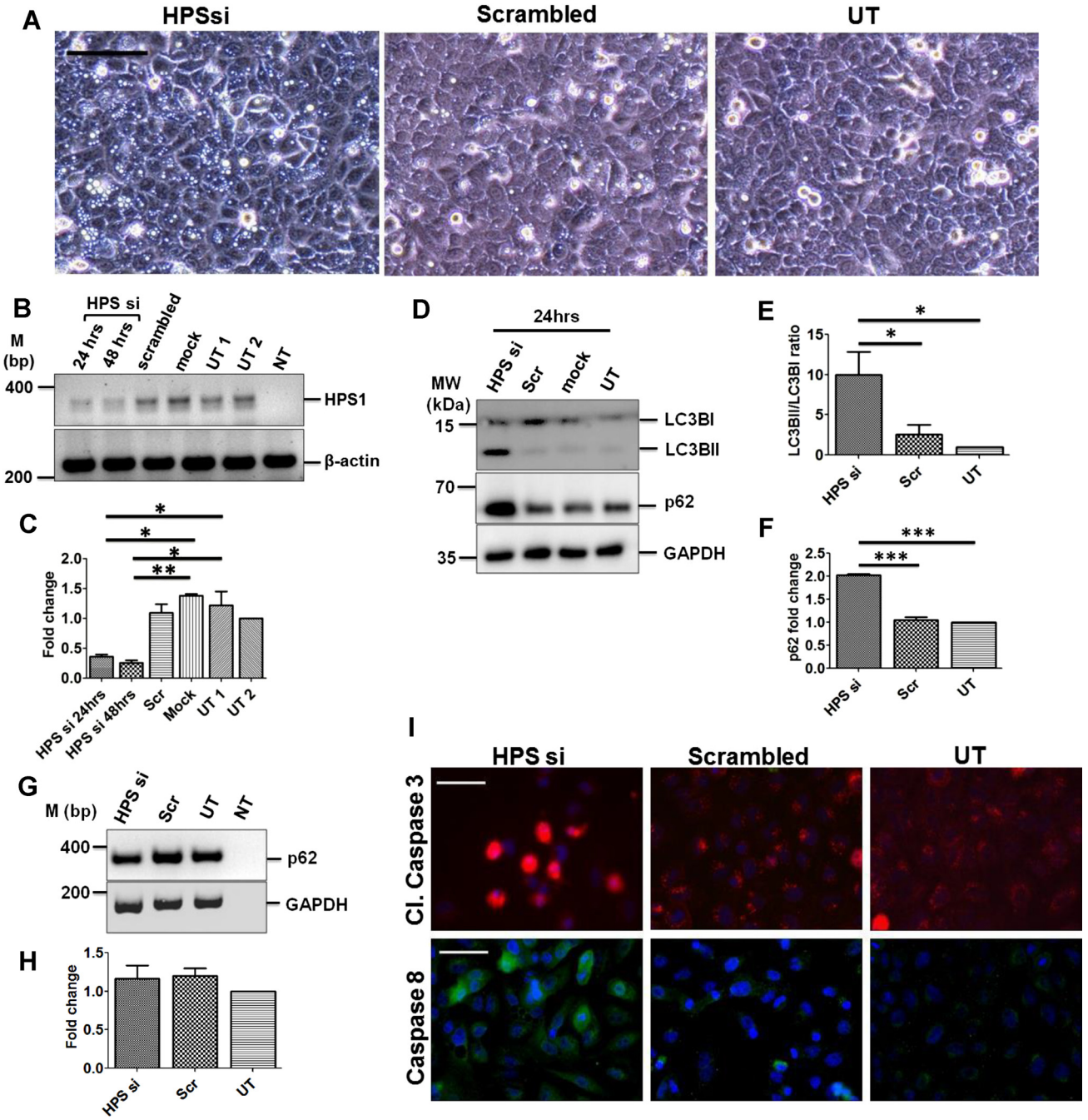

Fig. 3. siRNA-mediated knockdown of *HPS1* in A549 cells results in defective autophagy and increased apoptosis. *A*: phase-contrast images of A549 cells after 24 h of transfection with HPS1 or scrambled siRNA or untransfected cells (UT). Scale bar = 100 μm. *B*: representative agarose gel image of semiquantitative PCR performed for HPS1 and β-actin from cDNA prepared from the RNA isolated from untransfected or HPS1 or scrambled or mock-transfected A549 cells. *β-Actin* was used as a housekeeping gene. *C*: densitometric quantification of HPS1 transcript levels after HPS1 knockdown compared with scrambled, mock, and untreated cells. *D*: representative Western blot images for LC3B, p62, and GAPDH from cell lysates prepared from untransfected, mock, or scrambled (scr) siRNA or HPS1 siRNA-transfected A549 cells after 24 h. *E* and *F*: graphical representation of densitometry analysis from Western blots shown in *D* is shown as ratio of LC3BII/LC3BI (*E*) and fold change in p62 protein level (*F*) compared with untransfected controls. $^{*}P < 0.05$, $^{**}P < 0.01$, $^{***}P < 0.001$. *G*: representative agarose gel image from semiquantitative RT-PCR for *p62* is shown. *GAPDH* was used as a housekeeping gene. *H*: quantification of p62 transcript levels is represented as fold change compared with untransfected controls. *I*: representative immunofluorescence images for cleaved caspase-3 (red) and caspase-8 (green) following HPS1 or scrambled siRNA transfection or untransfected cells. DAPI (blue) was used to stain cell nuclei. Scale bar = 10 μm. Western blot images and immunofluorescence images are represented here from $n = 3$ independent experiments. UT1, untransfected sample 1; UT2, untransfected sample 2; NT, no template sample.

Downloaded from www.physiology.org/journal/ajplung (141.050.134.220) on October 24, 2019.

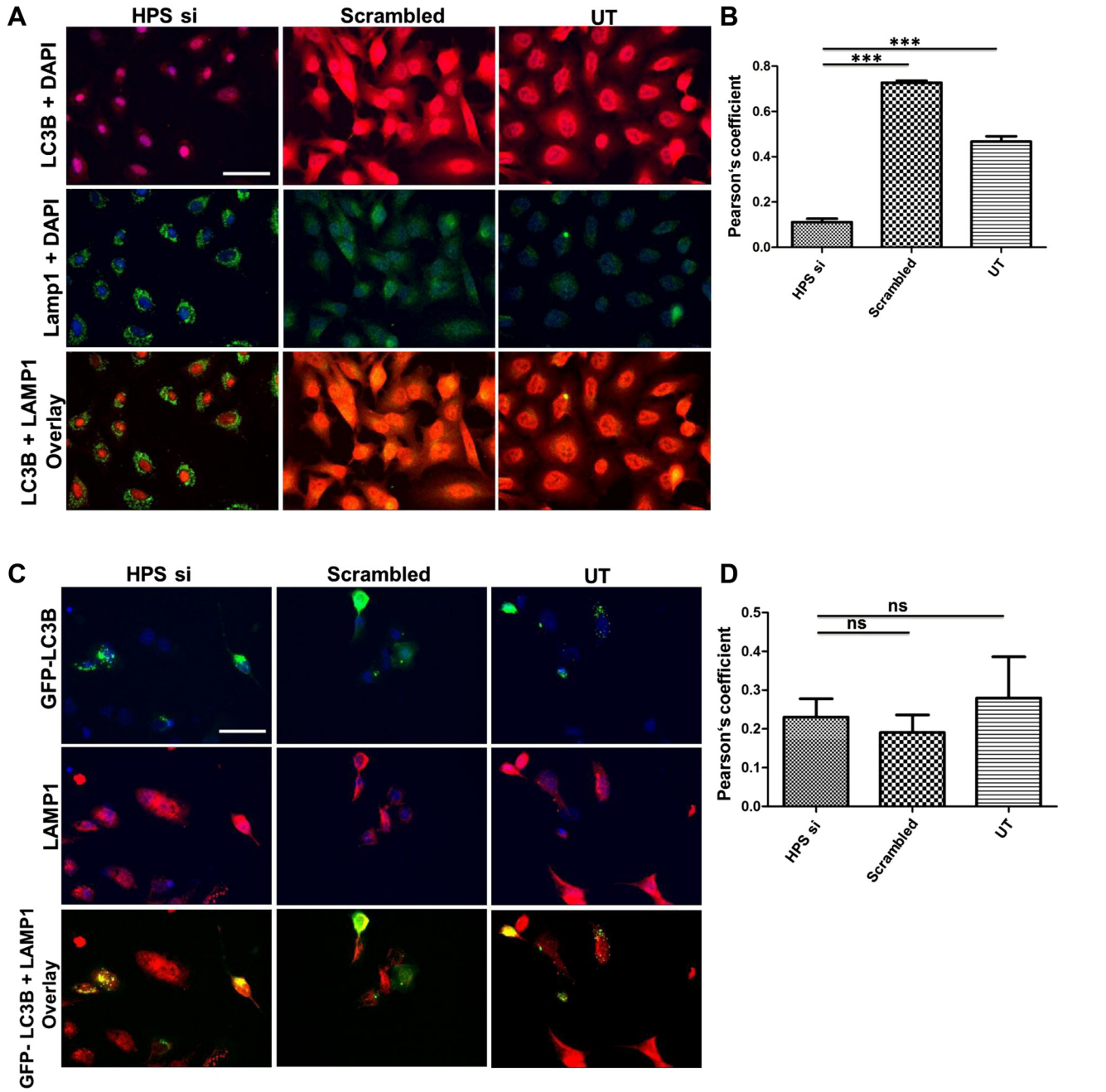

Fig. 4. Endogenous LC3B and LAMP1 do not colocalize following *HPS1* knockdown. *A*: A549 cells were either left untreated or were transfected with HPS1 siRNA or scrambled siRNA for 24 h followed by immunofluorescence for endogenous LC3B (red) and LAMP1 (green). *B*: quantification of the LC3B-LAMP1 colocalization signal is depicted as Pearson's coefficient. ***$P < 0.001$. *C*: A549 cells were transfected with GFP-LC3B plasmid for 24 h and were left untreated or transfected with HPS1 siRNA or scrambled siRNA for another 24 h followed by immunofluorescence for LAMP1. DAPI was used to stain the nuclei. Scale bar = 10 μm. *D*: quantification of the colocalization signals of LC3B with LAMP1 is depicted as Pearson's coefficient. ns, not significant. Representative images from $n = 3$ independent experiments are shown.

GFP-LC3B were observed in all samples transfected with the plasmid (Fig. 5*A*). The detection of cleaved GFP fragment in GFP-LC3B and HPS1 siRNA-transfected cells indicated an increase in autophagy flux. However, one striking observation that we noted from these experiments is that cells transfected with GFP-LC3B and HPS1 siRNA did not display the kind of severe vacuolization compared with HPS1 siRNA transfection alone (Fig. 5*B*). To understand the mechanism behind this observation, we transfected cells with GFP-LC3B, followed by HPS1 siRNA or scrambled siRNA or left them untreated. As indicated in Fig. 5*C*, cells transfected with GFP-LC3B showed a decrease in *HPS1* knockdown-induced LC3B (endogenous) as well as p62 accumulation (Fig. 5, *C* and *D*). This to us indicated that the GFP cleavage as observed in Fig. 5*A* was a result of the activation of autophagy because of GFP-LC3B transfection per se, a feature that is not observed upon *HPS1* knockdown alone. To further confirm that this induction of autophagy was due to overexpression of LC3B and not due to GFP, we transfected cells with myc-LC3B plasmid,

Downloaded from www.physiology.org/journal/ajplung (141.050.134.220) on October 24, 2019.

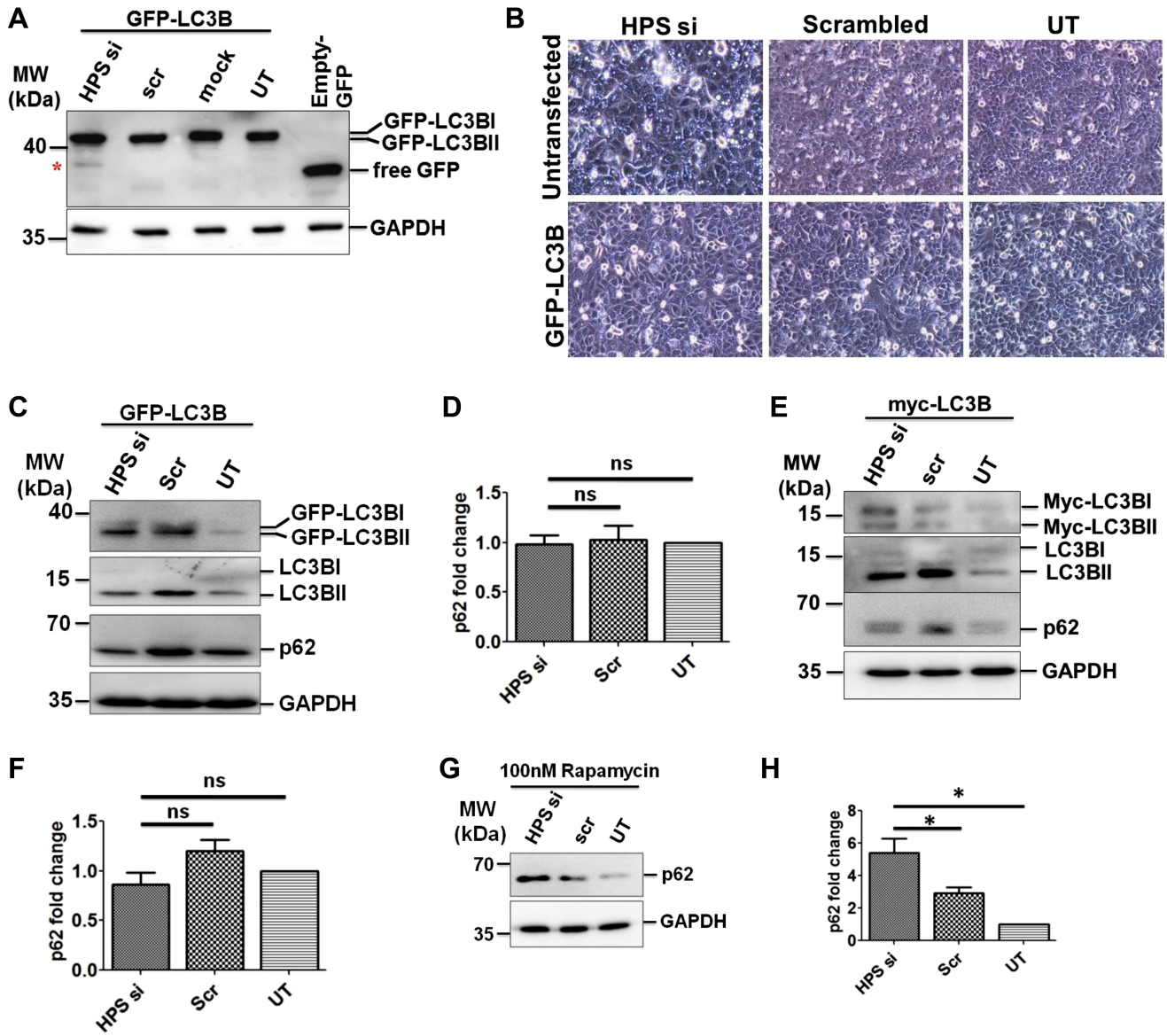

Fig. 5. Overexpression of LC3B reduces *HPS1* knockdown-induced p62 accumulation. *A*: A549 cells transfected with green fluorescent protein (GFP)-LC3B were left either untransfected or transfected with mock, HPS1, or scrambled siRNA for another 24 h. Cell lysates were subjected to Western blotting using anti-GFP antibody. Empty GFP plasmid-transfected cells were taken as controls to detect free GFP. *Bands corresponding to free GFP. *B*: phase-contrast images of cells indicating vacuolar structures in HPS1 siRNA transfection that are not detectable in GFP-LC3 and HPS1 siRNA-transfected cells. *C–F*: A549 cells were transfected with GFP-LC3B (*C* and *D*) or myc-LC3B (*E* and *F*) followed by transfection with scrambled or HPS1 siRNA for 24 h. Western blots and densitometry quantification for the indicated proteins show fold change compared with untransfected controls (*D* and *F*). *G* and *H*: representative Western blot images depicting p62 and GAPDH (*G*) and quantification of p62 Western blot (*H*) from cells transfected with HPS1 or scrambled siRNA, which were treated with 100 mM rapamycin. *$P < 0.05$. Representative images and analysis from $n = 3$ independent experiments are shown.

followed by transfection with HPS1 siRNA or scrambled siRNA or left them untreated with or without myc-LC3B transfection. We observed that cells transfected with myc-LC3B also showed a decrease in accumulation of p62 (Fig. 5, *E* and *F*), indicating that the observed effects are LC3B specific.

It is well documented that rapamycin is an inhibitor of mammalian target of rapamycin, which leads to the activation of autophagy (6). We hence asked whether activating the autophagy pathway with rapamycin in *HPS1* knockdown cells would also exert similar effects like LC3B overexpression. We treated the cells with 100 nM rapamycin followed by HPS1 siRNA or scrambled siRNA transfection or left them untransfected. Cells treated with rapamycin did show an increase in LC3BII levels (not shown), but there was no decrease in *HPS1* knockdown-induced p62 accumulation following rapamycin treatment (Fig. 5, *G* and *H*). This readout indicated that rapamycin treatment did not reverse or attenuate the p62 accumulation induced by *HPS1* knockdown.

DISCUSSION

In the present study, we document that the autophagy pathway is defective in HPS1/2 mice as well as in human patients with HPS1. In addition, we report that in vitro knockdown of

Downloaded from www.physiology.org/journal/ajplung (141.050.134.220) on October 24, 2019.

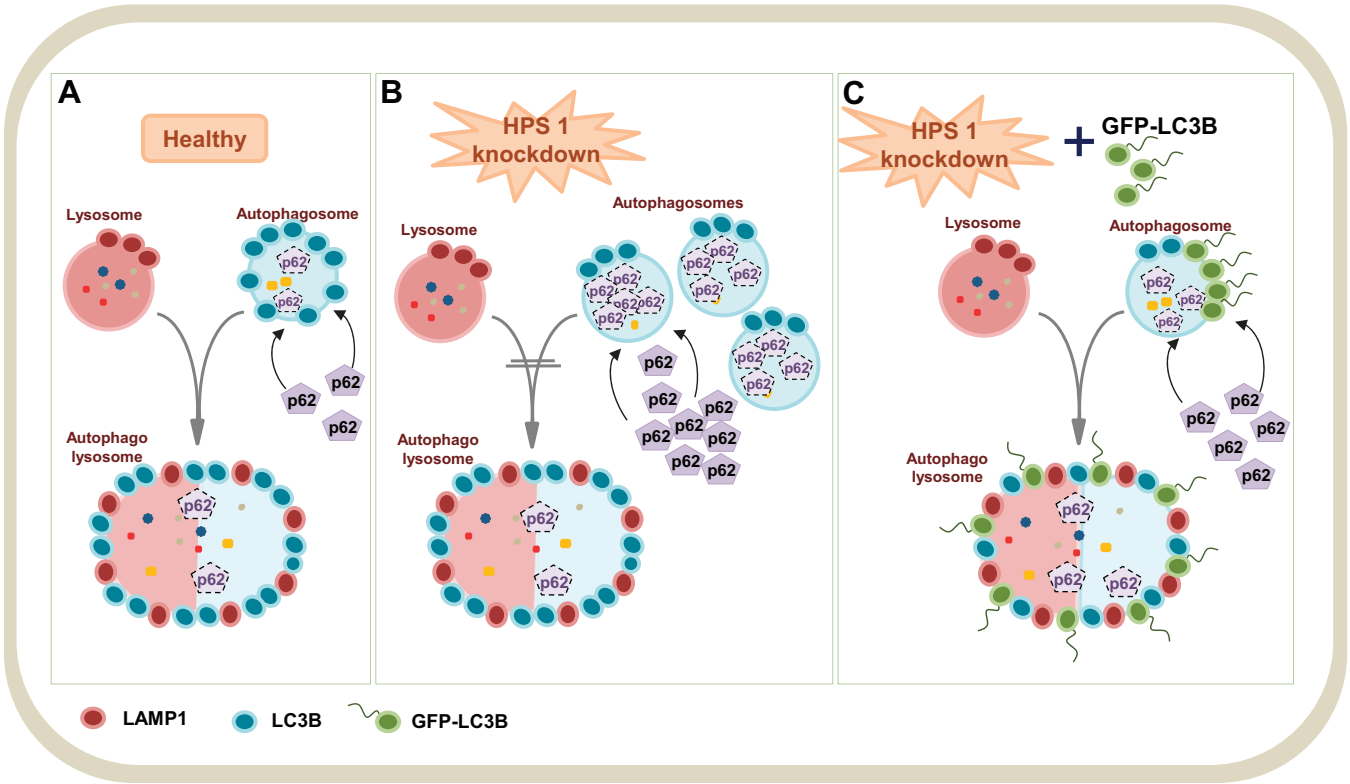

Fig. 6. Proposed model for defective autophagy following HPS1 knockdown. *A*: under healthy conditions in which autophagy is functional, p62 is recruited into the autophagosomes, which fuse with lysosomes to form autophagolysosomes, in which p62 and other contents are degraded. *B*: under conditions of HPS1 knockdown in A549 cells, fusion between autophagosomes and lysosomes is impaired, thereby resulting in defective autophagy (LC3B and p62 accumulation). *C*: overexpressing LC3B (GFP-LC3B is shown as example) before knocking down HPS1 leads to the fusion of GFP-LC3B-labeled autophagosomes and lysosomes, resulting in functional autophagolysosomes and eventually p62 degradation.

HPS1 gene in A549 cells results in apoptosis that is associated with defective autophagy. Overexpression of GFP-LC3B or myc-LC3B rescued *HPS1* knockdown-mediated defective autophagy by promoting autophagosome-lysosome fusion, thereby normalizing p62 levels (Fig. 6).

HPS gene products are known to affect LROs of the body, causing impaired lysosomal trafficking and secretion and therefore cell- and organ-specific disturbances. HPS1 and HPS4 proteins are two subunits of a large protein called BLOC-3 (35). Functions of BLOC-3 complex remain obscure, but few studies have demonstrated that this protein complex might regulate microtubule-dependent movement and distribution of LROs (15). Although direct studies reporting autophagy regulation in the absence of HPS1 are scarce, there is one study that showed that tyrosine-related proteins, LAMP1, and LAMP3 were sequestered in large membranous structures resembling macroautophagosomes in melanocytes derived from patients with HPS1 (5). In contrast, AP-3, affected in patients with HPS2, is the only HPS protein of which functions are well characterized. HPS2 encodes mutations in the β3A subunit of the AP-3 complex, and this complex has been indicated to sort membrane proteins from endosomes to lysosomes and tissue-specific LROs (40). Of note, it has been reported that AP-3-null cells selectively mistarget LAMP1 and LAMP2 proteins (47). LAMP2 is a receptor for autophagosome-lysosome fusion, and its mistargeting by AP-3-deficient fibroblasts indicates dysregulated autophagy. Likewise, our present study reveals defective autophagy in the absence of functional HPS1 protein in humans and in the absence of both HPS1 and AP-3 proteins in mice. Besides species-specific differences, loss of both HPS1 and AP-3 proteins in mice might collectively lead to accumulation of autophagosomes, thereby resulting in the early lysosomal stress events as reported for HPS1/2 mice (30).

We observed a total increase in LC3B and p62 in HPS1/2 mice as well as in vitro following HPS1 knockdown in A549 cells. According to the classical autophagy pathway, an increase in LC3B with a parallel increase in p62 indicates deficient autophagy (41). Supporting this, we also did not observe a colocalization of LC3B with the lysosomal marker LAMP1. In line with this observation, a study published by Zhen et al., (58) while this manuscript was in revision showed p62 accumulation and impaired autophagosome-lysosome fusion in brain tissue of buff mutant mice, an HPS mouse model that also exhibits hypopigmentation and platelet storage pool deficiency. Furthermore, as an attempt to study autophagy flux following knockdown of HPS1 in vitro, we performed GFP cleavage assay by transfecting cells with GFP-tagged LC3B. Interestingly, in such cells, we observed a decrease in cellular vacuolization compared with cells in which HPS1 knockdown alone was performed, indicating that exogenous LC3B was protective, in part through induction of autophagy. This observation is in agreement with previously reported studies, in which overexpression of autophagy-related genes leading to antiapoptotic effects were shown (31, 42).

Altered autophagy has been indicated in the pathophysiology of several LSDs. In Niemann-Pick type C (NPC), a

Downloaded from www.physiology.org/journal/ajplung (141.050.134.220) on October 24, 2019.

complex sphingolipidosis disorder, accumulation of autophagosomes was reported in skin fibroblasts from patients with NPC (37) and in brains of NPC mice (26). It has been suggested that induction of autophagy with impairment of autophagy flux leads to the severe aspects like generation of reactive oxygen species and accumulation of ubiquitinated proteins in the NPC neuropathology (28). Similarly, in other sphingolipidoses like Gaucher disease and Fabry disease, induction of autophagy and accumulation of autophagy substrates including p62 were reported in several tissues of patients as well as in mouse models of these diseases (11, 27, 36, 48). Such impaired autophagy flux was observed also in other LSDs like mucolipidosis (54), Pompe disease (43), Dannon disease (49), and neuronal ceroid lipofuscinoses (22). Similarly, we now report impaired autophagy resulting in accumulation of autophagy substrate p62 in vitro in the absence of HPS1 protein. Supporting this, we observed that LC3B immunogold labeling could preferentially be located in the lumen of lamellar bodies but not on the limiting membrane of lamellar bodies of the HPS1/2 mice compared with control mice. Whether this impaired autophagy contributes to the giant lamellar body degeneration that is characteristic to the HPSIP needs to be further studied. Another intriguing observation that stems from our present work is the nuclear localization of LC3B in cells in which the *HPS1* gene was knocked down. Both LC3BI and LC3BII were shown to localize to nucleus (13), and it is known that nuclear LC3B is deacetylated to drive autophagy under starvation conditions (20); however, the function of nuclear LC3B under other settings is not yet clear. Why *HPS1* gene knockdown should drive nuclear localization of endogenous LC3B remains an open question.

Altered autophagy has been reported in lung fibrosis recently. In a mouse model of amiodarone-induced lung fibrosis, we showed an increase in autophagy flux and autophagy-dependent apoptosis of alveolar epithelial cells (29). In patients with idiopathic pulmonary fibrosis, it was reported that autophagy was not induced despite the activation of the upstream pathways that induce autophagy (39). In the present study, we report that autophagy is impaired in HPS-associated lung fibrosis. On the basis of this information, it seems that autophagy is regulated differently depending on the kind of insult. Considering the complex regulation of autophagy and the integrated functions of the autophagosomes, lysosomes, and LROs, this observation may not be surprising. In any case, one of the important features shared by these different types of lung fibrosis is lysosomal stress in the alveolar epithelial cells that results from altered autophagy, either too much or too little.

We conclude that defective autophagy may be an important mechanism behind lysosomal stress events and epithelial cell apoptosis in the development of HPS-associated lung fibrosis.

GRANTS

This work was funded in part by the Excellence Cluster Cardio-Pulmonary System (ECCPS), Giessen, Germany and in part by the Intramural Research Program of the National Human Genome Research Institute, National Institutes of Health.

DISCLOSURES

No conflicts of interest, financial or otherwise, are declared by the authors.

AUTHOR CONTRIBUTIONS

Author contributions: S.A., L.K., S.C., I.H., C.R., M.K., B.R.G., S.B., M.O., and P.M. performed experiments; S.A., L.K., A.G., and P.M. analyzed data; S.A., L.K., M.O., A.G., and P.M. interpreted results of experiments; S.A. and P.M. prepared figures; S.A. and P.M. drafted manuscript; S.A., L.K., S.C., I.H., C.R., M.K., B.R.G., S.B., W.S., M.O., A.G., and P.M. approved final version of manuscript; S.C., B.R.G., A.G., and P.M. edited and revised manuscript; W.S., A.G., and P.M. conception and design of research.

REFERENCES

1. **Anderson PD, Huizing M, Claassen DA, White J, Gahl WA.** Hermansky-Pudlak syndrome type 4 (HPS-4): clinical and molecular characteristics. *Hum Genet* 113: 10–17, 2003.
2. **Anikster Y, Huizing M, White J, Shevchenko YO, Fitzpatrick DL, Touchman JW, Compton JG, Bale SJ, Swank RT, Gahl WA, Toro JR.** Mutation of a new gene causes a unique form of Hermansky-Pudlak syndrome in a genetic isolate of central Puerto Rico. *Nat Genet* 28: 376–380, 2001.
3. **Araya J, Kojima J, Takasaka N, Ito S, Fujii S, Hara H, Yanagisawa H, Kobayashi K, Tsurushige C, Kawaishi M, Kamiya N, Hirano J, Odaka M, Morikawa T, Nishimura SL, Kawabata Y, Hano H, Nakayama K, Kuwano K.** Insufficient autophagy in idiopathic pulmonary fibrosis. *Am J Physiol Lung Cell Mol Physiol* 304: L56–L69, 2013.
4. **Blommaart EF, Luiken JJ, Meijer AJ.** Autophagic proteolysis: control and specificity. *Histochem J* 29: 365–385, 1997.
5. **Boissy RE, Zhao Y, Gahl WA.** Altered protein localization in melanocytes from Hermansky-Pudlak syndrome: support for the role of the HPS gene product in intracellular trafficking. *Lab Invest* 78: 1037–1048, 1998.
6. **Boland B, Kumar A, Lee S, Platt FM, Wegiel J, Yu WH, Nixon RA.** Autophagy induction and autophagosome clearance in neurons: relationship to autophagic pathology in Alzheimer's disease. *J Neurosci* 28: 6926–6937, 2008.
7. **Bolte S, Cordelieres FP.** A guided tour into subcellular colocalization analysis in light microscopy. *J Microsc* 224: 213–232, 2006.
8. **Bonifacino JS.** Insights into the biogenesis of lysosome-related organelles from the study of the Hermansky-Pudlak syndrome. *Ann NY Acad Sci* 1038: 103–114, 2004.
9. **Brantly M, Avila NA, Shotelersuk V, Lucero C, Huizing M, Gahl WA.** Pulmonary function and high-resolution CT findings in patients with an inherited form of pulmonary fibrosis, Hermansky-Pudlak syndrome, due to mutations in HPS-1. *Chest* 117: 129–136, 2000.
10. **Cao Y, Espinola JA, Fossale E, Massey AC, Cuervo AM, MacDonald ME, Cotman SL.** Autophagy is disrupted in a knock-in mouse model of juvenile neuronal ceroid lipofuscinosis. *J Biol Chem* 281: 20483–20493, 2006.
11. **Chevrier M, Brakch N, Celine L, Genty D, Ramdani Y, Moll S, Djavaheri-Mergny M, Brasse-Lagnel C, Annie Laquerriere AL, Barbey F, Bekri S.** Autophagosome maturation is impaired in Fabry disease. *Autophagy* 6: 589–599, 2010.
12. **Dell'Angelica EC, Mullins C, Caplan S, Bonifacino JS.** Lysosome-related organelles. *FASEB J* 14: 1265–1278, 2000.
13. **Drake KR, Kang M, Kenworthy AK.** Nucleocytoplasmic distribution and dynamics of the autophagosome marker EGFP-LC3. *PLoS One* 5: e9806, 2010.
14. **Eskelinen EL.** New insights into the mechanisms of macroautophagy in mammalian cells. *Int Rev Cell Mol Biol* 266: 207–247, 2008.
15. **Falcon-Perez JM, Nazarian R, Sabatti C, Dell'Angelica EC.** Distribution and dynamics of Lamp1-containing endocytic organelles in fibroblasts deficient in BLOC-3. *J Cell Sci* 118: 5243–5255, 2005.
16. **Gahl WA, Brantly M, Kaiser-Kupfer MI, Iwata F, Hazelwood S, Shotelersuk V, Duffy LF, Kuehl EM, Troendle J, Bernardini I.** Genetic defects and clinical characteristics of patients with a form of oculocutaneous albinism (Hermansky-Pudlak syndrome). *N Engl J Med* 338: 1258–1264, 1998.
17. **Gochuico BR, Huizing M, Golas GA, Scher CD, Tsokos M, Denver SD, Frei-Jones MJ, Gahl WA.** Interstitial lung disease and pulmonary fibrosis in Hermansky-Pudlak syndrome type 2, an adaptor protein-3 complex disease. *Mol Med* 18: 56–64, 2012.
18. **Guttentag SH, Akhtar A, Tao JQ, Atochina E, Rusiniak ME, Swank RT, Bates SR.** Defective surfactant secretion in a mouse model of Hermansky-Pudlak syndrome. *Am J Respir Cell Mol Biol* 33: 14–21, 2005.

Downloaded from www.physiology.org/journal/ajplung (141.050.134.220) on October 24, 2019.

19. **Hsia CC, Hyde DM, Ochs M, Weibel ER.** An official research policy statement of the American Thoracic Society/European Respiratory Society: standards for quantitative assessment of lung structure. *Am J Respir Crit Care Med* 181: 394–418, 2010.
20. **Huang R, Xu Y, Wan W, Shou X, Qian J, You Z, Liu B, Chang C, Zhou T, Lippincott-Schwartz J, Liu W.** Deacetylation of nuclear LC3 drives autophagy initiation under starvation. *Mol Cell* 57: 456–466, 2015.
21. **Klionsky DJ, Abdalla FC, Abeliovich H, Abraham RT, Acevedo-Arozena A, Adeli K, Agholme L, Agnello M, Agostinis P, Aguirre-Ghiso JA, Ahn HJ, Ait-Mohamed O, Ait-Si-Ali S, Akematsu T, Akira S, Al-Younes HM, Al-Zeer MA, Albert ML, Albin RL, Alegre-Abarrategui J, Aleo MF, Alirezaei M, Almasan A, Almonte-Becerril M, Amano A, Amaravadi R, Amarnath S, Amer AO, Andrieu-Abadie N, Anantharam V, Ann DK, Anoopkumar-Dukie S, Aoki H, Apostolova N, Arancia G, Aris JP, Asanuma K, Asare NY, Ashida H, Askanas V, Askew DS, Auberger P, Baba M, Backues SK, Baehrecke EH, Bahr BA, Bai XY, Bailly Y, Baiocchi R, Baldini G, Balduini W, Ballabio A, Bamber BA, Bampton ET, Banhegyi G, Bartholomew CR, Bassham DC, Bast RC Jr, Batoko H, Bay BH, Beau I, Bechet DM, Begley TJ, Behl C, Behrends C, Bekri S, Bellaire B, Bendall LJ, Benetti L, Berliocchi L, Bernardi H, Bernassola F, Besteiro S, Bhatia-Kissova I, Bi X, Biard-Piechaczyk M, Blum JS, Boise LH, Bonaldo P, Boone DL, Bornhauser BC, Bortoluci KR, Bossis I, Bost F, Bourquin JP, Boya P, Boyer-Guittaut M, Bozhkov PV, Brady NR, Brancolini C, Brech A, Brenman JE, Brennand A, Bresnick EH, Brest P, Bridges D, Bristol ML, Brookes PS, Brown EJ, Brumell JH, Brunetti-Pierri N, Brunk UT, Bulman DE, Bultman SJ, Bultynck G, Burbulla LF, Bursch W, Butchar JP, Buzgariu W, Bydlowski SP, Cadwell K, Cahova M, Cai D, Cai J, Cai Q, Calabretta B, Calvo-Garrido J, Camougrand N, Campanella M, Campos-Salinas J, Candi E, Cao L, Caplan AB, Carding SR, Cardoso SM, Carew JS, Carlin CR, Carmignac V, Carneiro LA, Carra S, Caruso RA, Casari G, Casas C, Castino R, Cebollero E, Cecconi F, Celli J, Chaachouay H, Chae HJ, Chai CY, Chan DC, Chan EY, Chang RC, Che CM, Chen CC, Chen GC, Chen GQ, Chen M, Chen Q, Chen SS, Chen W, Chen X, Chen YG, Chen Y, Chen YJ, Chen Z, Cheng A, Cheng CH, Cheng Y, Cheong H, Cheong JH, Cherry S, Chess-Williams R, Cheung ZH, Chevet E, Chiang HL, Chiarelli R, Chiba T, Chin LS, Chiou SH, Chisari FV, Cho CH, Cho DH, Choi AM, Choi D, Choi KS, Choi ME, Chouaib S, Choubey D, Choubey V, Chu CT, Chuang TH, Chueh SH, Chun T, Chwae YJ, Chye ML, Ciarcia R, Ciriolo MR, Clague MJ, Clark RS, Clarke PG, Clarke R, Codogno P, Coller HA, Colombo MI, Comincini S, Condello M, Condorelli F, Cookson MR, Coombs GH, Coppens I, Corbalan R, Cossart P, Costelli P, Costes S, Coto-Montes A, Couve E, Coxon FP, Cregg JM, Crespo JL, Cronje MJ, Cuervo AM, Cullen JJ, Czaja MJ, D'Amelio M, Darfeuille-Michaud A, Davids LM, Davies FE, De Felici M, de Groot JF, de Haan CA, De Martino L, De Milito A, De Tata V, Debnath J, Degterev A, Dehay B, Delbridge LM, Demarchi F, Deng YZ, Dengjel J, Dent P, Denton D, Deretic V, Desai SD, Devenish RJ, Di Gioacchino M, Di Paolo G, Di Pietro C, Diaz-Araya G, Diaz-Laviada I, Diaz-Meco MT, Diaz-Nido J, Dikic I, Dinesh-Kumar SP, Ding WX, Distelhorst CW, Diwan A, Djavaheri-Mergny M, Dokudovskaya S, Dong Z, Dorsey FC, Dosenko V, Dowling JJ, Doxsey S, Dreux M, Drew ME, Duan Q, Duchosal MA, Duff K, Dugail I, Durbeej M, Duszenko M, Edelstein CL, Edinger AL, Egea G, Eichinger L, Eissa NT, Ekmekcioglu S, El-Deiry WS, Elazar Z, Elgendy M, Ellerby LM, Eng KE, Engelbrecht AM, Engelender S, Erenpreisa J, Escalante R, Esclatine A, Eskelinen EL, Espert L, Espina V, Fan H, Fan J, Fan QW, Fan Z, Fang S, Fang Y, Fanto M, Fanzani A, Farkas T, Farre JC, Faure M, Fechheimer M, Feng CG, Feng J, Feng Q, Feng Y, Fesus L, Feuer R, Figueiredo-Pereira ME, Fimia GM, Fingar DC, Finkbeiner S, Finkel T, Finley KD, Fiorito F, Fisher EA, Fisher PB, Flajolet M, Florez-McClure ML, Florio S, Fon EA, Fornai F, Fortunato F, Fotedar R, Fowler DH, Fox HS, Franco R, Frankel LB, Fransen M, Fuentes JM, Fueyo J, Fujii J, Fujisaki K, Fujita E, Fukuda M, Furukawa RH, Gaestel M, Gailly P, Gajewska M, Galliot B, Galy V, Ganesh S, Ganetzky B, Ganley IG, Gao FB, Gao GF, Gao J, Garcia L, Garcia-Manero G, Garcia-Marcos M, Garmyn M, Gartel AL, Gatti E, Gautel M, Gawriluk TR, Gegg ME, Geng J, Germain M, Gestwicki JE, Gewirtz DA, Ghavami S, Ghosh P, Giammarioli AM, Giatromanolaki AN, Gibson SB, Gilkerson RW, Ginger ML, Ginsberg HN, Golab J, Goligorsky MS, Golstein P, Gomez-Manzano C, Goncu E, Gongora C, Gonzalez CD, Gonzalez R, Gonzalez-Estevez C, Gonzalez-Polo RA, Gonzalez-Rey E, Gorbunov NV, Gorski S, Goruppi S, Gottlieb RA, Gozuacik D, Granato GE, Grant GD, Green KN, Gregorc A, Gros F, Grose C, Grunt TW, Gual P, Guan JL, Guan KL, Guichard SM, Gukovskaya AS, Gukovsky I, Gunst J, Gustafsson AB, Halayko AJ, Hale AN, Halonen SK, Hamasaki M, Han F, Han T, Hancock MK, Hansen M, Harada H, Harada M, Hardt SE, Harper JW, Harris AL, Harris J, Harris SD, Hashimoto M, Haspel JA, Hayashi S, Hazelhurst LA, He C, He YW, Hebert MJ, Heidenreich KA, Helfrich MH, Helgason GV, Henske EP, Herman B, Herman PK, Hetz C, Hilfiker S, Hill JA, Hocking LJ, Hofman P, Hofmann TG, Hohfeld J, Holyoake TL, Hong MH, Hood DA, Hotamisligil GS, Houwerzijl EJ, Hoyer-Hansen M, Hu B, Hu CA, Hu HM, Hua Y, Huang C, Huang J, Huang S, Huang WP, Huber TB, Huh WK, Hung TH, Hupp TR, Hur GM, Hurley JB, Hussain SN, Hussey PJ, Hwang JJ, Hwang S, Ichihara A, Ilkhanizadeh S, Inoki K, Into T, Iovane V, Iovanna JL, Ip NY, Isaka Y, Ishida H, Isidoro C, Isobe K, Iwasaki A, Izquierdo M, Izumi Y, Jaakkola PM, Jaattela M, Jackson GR, Jackson WT, Janji B, Jendrach M, Jeon JH, Jeung EB, Jiang H, Jiang JX, Jiang M, Jiang Q, Jiang X, Jimenez A, Jin M, Jin S, Joe CO, Johansen T, Johnson DE, Johnson GV, Jones NL, Joseph B, Joseph SK, Joubert AM, Juhasz G, Juillerat-Jeanneret L, Jung CH, Jung YK, Kaarniranta K, Kaasik A, Kabuta T, Kadowaki M, Kagedal K, Kamada Y, Kaminskyy VO, Kampinga HH, Kanamori H, Kang C, Kang KB, Kang KI, Kang R, Kang YA, Kanki T, Kanneganti TD, Kanno H, Kanthasamy AG, Kanthasamy A, Karantza V, Kaushal GP, Kaushik S, Kawazoe Y, Ke PY, Kehrl JH, Kelekar A, Kerkhoff C, Kessel DH, Khalil H, Kiel JA, Kiger AA, Kihara A, Kim DR, Kim DH, Kim EK, Kim HR, Kim JS, Kim JH, Kim JC, Kim JK, Kim PK, Kim SW, Kim YS, Kim Y, Kimchi A, Kimmelman AC, King JS, Kinsella TJ, Kirkin V, Kirshenbaum LA, Kitamoto K, Kitazato K, Klein L, Klimecki WT, Klucken J, Knecht E, Ko BC, Koch JC, Koga H, Koh JY, Koh YH, Koike M, Komatsu M, Kominami E, Kong HJ, Kong WJ, Korolchuk VI, Kotake Y, Koukourakis MI, Kouri Flores JB, Kovacs AL, Kraft C, Krainc D, Kramer H, Kretz-Remy C, Krichevsky AM, Kroemer G, Kruger R, Krut O, Ktistakis NT, Kuan CY, Kucharczyk R, Kumar A, Kumar R, Kumar S, Kundu M, Kung HJ, Kurz T, Kwon HJ, La Spada AR, Lafont F, Lamark T, Landry J, Lane JD, Lapaquette P, Laporte JF, Laszlo L, Lavandero S, Lavoie JN, Layfield R, Lazo PA, Le W, Le Cam L, Ledbetter DJ, Lee AJ, Lee BW, Lee GM, Lee J, Lee JH, Lee M, Lee MS, Lee SH, Leeuwenburgh C, Legembre P, Legouis R, Lehmann M, Lei HY, Lei QY, Leib DA, Leiro J, Lemasters JJ, Lemoine A, Lesniak MS, Lev D, Levenson VV, Levine B, Levy E, Li F, Li JL, Li L, Li S, Li W, Li XJ, Li YB, Li YP, Liang C, Liang Q, Liao YF, Liberski PP, Lieberman A, Lim HJ, Lim KL, Lim K, Lin CF, Lin FC, Lin J, Lin JD, Lin K, Lin WW, Lin WC, Lin YL, Linden R, Lingor P, Lippincott-Schwartz J, Lisanti MP, Liton PB, Liu B, Liu CF, Liu K, Liu L, Liu QA, Liu W, Liu YC, Liu Y, Lockshin RA, Lok CN, Lonial S, Loos B, Lopez-Berestein G, Lopez-Otin C, Lossi L, Lotze MT, Low P, Lu B, Lu Z, Luciano F, Lukacs NW, Lund AH, Lynch-Day MA, Ma Y, Macian F, MacKeigan JP, Macleod KF, Madeo F, Maiuri L, Maiuri MC, Malagoli D, Malicdan MC, Malorni W, Man N, Mandelkow EM, Manon S, Manov I, Mao K, Mao X, Mao Z, Marambaud P, Marazziti D, Marcel YL, Marchbank K, Marchetti P, Marciniak SJ, Marcondes M, Mardi M, Marfe G, Marino G, Markaki M, Marten MR, Martin SJ, Martinand-Mari C, Martinet W, Martinez-Vicente M, Masini M, Matarrese P, Matsuo S, Matteoni R, Mayer A, Mazure NM, McConkey DJ, McConnell MJ, McDermott C, McDonald C, McInerney GM, McKenna SL, McLaughlin B, McLean PJ, McMaster CR, McQuibban GA, Meijer AJ, Meisler MH, Melendez A, Melia TJ, Melino G, Mena MA, Menendez JA, Menna-Barreto RF, Menon MB, Menzies FM, Mercer CA, Merighi A, Merry DE, Meschini S, Meyer CG, Meyer TF, Miao CY, Miao JY, Michels PA, Michiels C, Mijaljica D, Milojkovic A, Minucci S, Miracco C, Miranti CK, Mitroulis I, Miyazawa K, Mizushima N, Mograbi B, Mohseni S, Molero X, Mollereau B, Mollinedo F, Momoi T, Monastyrska I, Monick MM, Monteiro MJ, Moore MN, Mora R, Moreau K, Moreira PI, Moriyasu Y, Moscat J, Mostowy S, Mottram JC, Motyl T, Moussa CE, Muller S, Munger K, Munz C, Murphy LO, Murphy ME, Musaro A, Mysorekar I, Nagata E, Nagata K, Nahimana A, Nair U, Nakagawa T, Nakahira K, Nakano H, Nakatogawa H, Nanjundan M, Naqvi NI, Narendra DP, Narita M, Navarro M, Nawrocki ST, Nazarko TY, Nemchenko A, Netea MG, Neufeld TP, Ney PA, Nezis IP, Nguyen HP, Nie D, Nishino I, Nislow C, Nixon RA, Noda T, Noegel AA, Nogalska A, Noguchi S, Notterpek L, Novak I, Nozaki T, Nukina N, Nurnberger T, Nyfeler B, Obara K,**

Downloaded from www.physiology.org/journal/ajplung (141.050.134.220) on October 24, 2019.

Oberley TD, Oddo S, Ogawa M, Ohashi T, Okamoto K, Oleinick NL, Oliver FJ, Olsen LJ, Olsson S, Opota O, Osborne TF, Ostrander GK, Otsu K, Ou JH, Ouimet M, Overholtzer M, Ozpolat B, Paganetti P, Pagnini U, Pallet N, Palmer GE, Palumbo C, Pan T, Panaretakis T, Pandey UB, Papackova Z, Papassideri I, Paris I, Park J, Park OK, Parys JB, Parzych KR, Patschan S, Patterson C, Pattingre S, Pawelek JM, Peng J, Perlmutter DH, Perrotta I, Perry G, Pervaiz S, Peter M, Peters GJ, Petersen M, Petrovski G, Phang JM, Piacentini M, Pierre P, Pierrefite-Carle V, Pierron G, Pinkas-Kramarski R, Piras A, Piri N, Platanias LC, Poggeler S, Poirot M, Poletti A, Pous C, Pozuelo-Rubio M, Praetorius-Ibba M, Prasad A, Prescott M, Priault M, Produit-Zengaffinen N, Progulske-Fox A, Proikas-Cezanne T, Przedborski S, Przyklenk K, Puertollano R, Puyal J, Qian SB, Qin L, Qin ZH, Quaggin SE, Raben N, Rabinowich H, Rabkin SW, Rahman I, Rami A, Ramm G, Randall G, Randow F, Rao VA, Rathmell JC, Ravikumar B, Ray SK, Reed BH, Reed JC, Reggiori F, Regnier-Vigouroux A, Reichert AS, Reiners JJ Jr, Reiter RJ, Ren J, Revuelta JL, Rhodes CJ, Ritis K, Rizzo E, Robbins J, Roberge M, Roca H, Roccheri MC, Rocchi S, Rodemann HP, Rodriguez de Cordoba S, Rohrer B, Roninson IB, Rosen K, Rost-Roszkowska MM, Rouis M, Rouschop KM, Rovetta F, Rubin BP, Rubinsztein DC, Ruckdeschel K, Rucker EB 3rd, Rudich A, Rudolf E, Ruiz-Opazo N, Russo R, Rusten TE, Ryan KM, Ryter SW, Sabatini DM, Sadoshima J, Saha T, Saitoh T, Sakagami H, Sakai Y, Salekdeh GH, Salomoni P, Salvaterra PM, Salvesen G, Salvioli R, Sanchez AM, Sanchez-Alcazar JA, Sanchez-Prieto R, Sandri M, Sankar U, Sansanwal P, Santambrogio L, Saran S, Sarkar S, Sarwal M, Sasakawa C, Sasnauskiene A, Sass M, Sato K, Sato M, Schapira AH, Scharl M, Schatzl HM, Scheper W, Schiaffino S, Schneider C, Schneider ME, Schneider-Stock R, Schoenlein PV, Schorderet DF, Schuller C, Schwartz GK, Scorrano L, Sealy L, Seglen PO, Segura-Aguilar J, Seiliez I, Seleverstov O, Sell C, Seo JB, Separovic D, Setaluri V, Setoguchi T, Settembre C, Shacka JJ, Shanmugam M, Shapiro IM, Shaulian E, Shaw RJ, Shelhamer JH, Shen HM, Shen WC, Sheng ZH, Shi Y, Shibuya K, Shidoji Y, Shieh JJ, Shih CM, Shimada Y, Shimizu S, Shintani T, Shirihai OS, Shore GC, Sibirny AA, Sidhu SB, Sikorska B, Silva-Zacarin EC, Simmons A, Simon AK, Simon HU, Simone C, Simonsen A, Sinclair DA, Singh R, Sinha D, Sinicrope FA, Sirko A, Siu PM, Sivridis E, Skop V, Skulachev VP, Slack RS, Smaili SS, Smith DR, Soengas MS, Soldati T, Song X, Sood AK, Soong TW, Sotgia F, Spector SA, Spies CD, Springer W, Srinivasula SM, Stefanis L, Steffan JS, Stendel R, Stenmark H, Stephanou A, Stern ST, Sternberg C, Stork B, Stralfors P, Subauste CS, Sui X, Sulzer D, Sun J, Sun SY, Sun ZJ, Sung JJ, Suzuki K, Suzuki T, Swanson MS, Swanton C, Sweeney ST, Sy LK, Szabadkai G, Tabas I, Taegtmeyer H, Tafani M, Takacs-Vellai K, Takano Y, Takegawa K, Takemura G, Takeshita F, Talbot NJ, Tan KS, Tanaka K, Tang D, Tanida I, Tannous BA, Tavernarakis N, Taylor GS, Taylor GA, Taylor JP, Terada LS, Terman A, Tettamanti G, Thevissen K, Thompson CB, Thorburn A, Thumm M, Tian F, Tian Y, Tocchini-Valentini G, Tolkovsky AM, Tomino Y, Tonges L, Tooze SA, Tournier C, Tower J, Towns R, Trajkovic V, Travassos LH, Tsai TF, Tschan MP, Tsubata T, Tsung A, Turk B, Turner LS, Tyagi SC, Uchiyama Y, Ueno T, Umekawa M, Umemiya-Shirafuji R, Unni VK, Vaccaro MI, Valente EM, Van den Berghe G, van der Klei IJ, van Doorn W, van Dyk LF, van Egmond M, van Grunsven LA, Vandenabeele P, Vandenberghe WP, Vanhorebeek I, Vaquero EC, Velasco G, Vellai T, Vicencio JM, Vierstra RD, Vila M, Vindis C, Viola G, Viscomi MT, Voitsekhovskaja OV, von Haefen C, Votruba M, Wada K, Wade-Martins R, Walker CL, Walsh CM, Walter J, Wan XB, Wang A, Wang C, Wang D, Wang F, Wang G, Wang H, Wang HG, Wang HD, Wang J, Wang K, Wang M, Wang RC, Wang X, Wang YJ, Wang Y, Wang Z, Wang ZC, Wansink DG, Ward DM, Watada H, Waters SL, Webster P, Wei L, Weihl CC, Weiss WA, Welford SM, Wen LP, Whitehouse CA, Whitton JL, Whitworth AJ, Wileman T, Wiley JW, Wilkinson S, Willbold D, Williams RL, Williamson PR, Wouters BG, Wu C, Wu DC, Wu WK, Wyttenbach A, Xavier RJ, Xi Z, Xia P, Xiao G, Xie Z, Xu DZ, Xu J, Xu L, Xu X, Yamamoto A, Yamashina S, Yamashita M, Yan X, Yanagida M, Yang DS, Yang E, Yang JM, Yang SY, Yang W, Yang WY, Yang Z, Yao MC, Yao TP, Yeganeh B, Yen WL, Yin JJ, Yin XM, Yoo OJ, Yoon G, Yoon SY, Yorimitsu T, Yoshikawa Y, Yoshimori T, Yoshimoto K, You HJ, Youle RJ, Younes A, Yu L, Yu SW, Yu WH, Yuan ZM, Yue Z, Yun CH, Yuzaki M, Zabirnyk O, Silva-Zacarin E, Zacks D, Zacksenhaus E, Zaffaroni N, Zakeri Z, Zeh HJ 3rd, Zeitlin SO, Zhang H, Zhang HL, Zhang J, Zhang JP, Zhang L, Zhang MY, Zhang XD, Zhao M, Zhao YF, Zhao Y, Zhao ZJ, Zheng X, Zhivotovsky B, Zhong Q, Zhou CZ, Zhu C, Zhu WG, Zhu XF, Zhu X, Zhu Y, Zoladek T, Zong WX, Zorzano A, Zschocke J, Zuckerbraun B. Guidelines for the use and interpretation of assays for monitoring autophagy. *Autophagy* 8: 445–544, 2012.

22. **Koike M, Shibata M, Waguri S, Yoshimura K, Tanida I, Kominami E, Gotow T, Peters C, von Figura K, Mizushima N, Saftig P, Uchiyama Y.** Participation of autophagy in storage of lysosomes in neurons from mouse models of neuronal ceroid-lipofuscinoses (Batten disease). *Am J Pathol* 167: 1713–1728, 2005.
23. **Komatsu M, Waguri S, Chiba T, Murata S, Iwata J, Tanida I, Ueno T, Koike M, Uchiyama Y, Kominami E, Tanaka K.** Loss of autophagy in the central nervous system causes neurodegeneration in mice. *Nature* 441: 880–884, 2006.
24. **Korfei M, von der Beck D, Henneke I, Markart P, Ruppert C, Mahavadi P, Ghanim B, Klepetko W, Fink L, Meiners S, Kramer OH, Seeger W, Vancheri C, Guenther A.** Comparative proteome analysis of lung tissue from patients with idiopathic pulmonary fibrosis (IPF), non-specific interstitial pneumonia (NSIP) and organ donors. *J Proteomics* 85: 109–128, 2013.
25. **Lawrence BP, Brown WJ.** Autophagic vacuoles rapidly fuse with pre-existing lysosomes in cultured hepatocytes. *J Cell Sci* 102: 515–526, 1992.
26. **Liao G, Yao Y, Liu J, Yu Z, Cheung S, Xie A, Liang X, Bi X.** Cholesterol accumulation is associated with lysosomal dysfunction and autophagic stress in Npc1 −/− mouse brain. *Am J Pathol* 171: 962–975, 2007.
27. **Liebau MC, Braun F, Hopker K, Weitbrecht C, Bartels V, Muller RU, Brodesser S, Saleem MA, Benzing T, Schermer B, Cybulla M, Kurschat CE.** Dysregulated autophagy contributes to podocyte damage in Fabry's disease. *PLoS One* 8: e63506, 2013.
28. **Lieberman AP, Puertollano R, Raben N, Slaugenhaupt S, Walkley SU, Ballabio A.** Autophagy in lysosomal storage disorders. *Autophagy* 8: 719–730, 2012.
29. **Mahavadi P, Knudsen L, Venkatesan S, Henneke I, Hegermann J, Wrede C, Ochs M, Ahuja S, Chillappagari S, Ruppert C, Seeger W, Korfei M, Guenther A.** Regulation of macroautophagy in amiodarone induced pulmonary fibrosis. *J Pathol Clin Res* 1: 252–263, 2015.
30. **Mahavadi P, Korfei M, Henneke I, Liebisch G, Schmitz G, Gochuico BR, Markart P, Bellusci S, Seeger W, Ruppert C, Guenther A.** Epithelial stress and apoptosis underlie Hermansky-Pudlak syndrome-associated interstitial pneumonia. *Am J Respir Crit Care Med* 182: 207–219, 2010.
31. **Mai S, Muster B, Bereiter-Hahn J, Jendrach M.** Autophagy proteins LC3B, ATG5 and ATG12 participate in quality control after mitochondrial damage and influence lifespan. *Autophagy* 8: 47–62, 2012.
32. **Mayhew TM, Lucocq JM.** Quantifying immunogold labelling patterns of cellular compartments when they comprise mixtures of membranes (surface-occupying) and organelles (volume-occupying). *Histochem Cell Biol* 129: 367–378, 2008.
33. **Mizushima N.** Autophagy: process and function. *Genes Dev* 21: 2861–2873, 2007.
34. **Nakatani Y, Nakamura N, Sano J, Inayama Y, Kawano N, Yamanaka S, Miyagi Y, Nagashima Y, Ohbayashi C, Mizushima M, Manabe T, Kuroda M, Yokoi T, Matsubara O.** Interstitial pneumonia in Hermansky-Pudlak syndrome: significance of florid foamy swelling/degeneration (giant lamellar body degeneration) of type-2 pneumocytes. *Virchows Arch* 437: 304–313, 2000.
35. **Nazarian R, Falcon-Perez JM, Dell'Angelica EC.** Biogenesis of lysosome-related organelles complex 3 (BLOC-3): a complex containing the Hermansky-Pudlak syndrome (HPS) proteins HPS1 and HPS4. *Proc Natl Acad Sci USA* 100: 8770–8775, 2003.
36. **Osellame LD, Duchen MR.** Defective quality control mechanisms and accumulation of damaged mitochondria link Gaucher and Parkinson diseases. *Autophagy* 9: 1633–1635, 2013.
37. **Pacheco CD, Kunkel R, Lieberman AP.** Autophagy in Niemann-Pick C disease is dependent upon Beclin-1 and responsive to lipid trafficking defects. *Hum Mol Genet* 16: 1495–1503, 2007.
38. **Pankiv S, Clausen TH, Lamark T, Brech A, Bruun JA, Outzen H, Overvatn A, Bjorkoy G, Johansen T.** p62/SQSTM1 binds directly to Atg8/LC3 to facilitate degradation of ubiquitinated protein aggregates by autophagy. *J Biol Chem* 282: 24131–24145, 2007.

Downloaded from www.physiology.org/journal/ajplung (141.050.134.220) on October 24, 2019.

39. **Patel AS, Lin L, Geyer A, Haspel JA, An CH, Cao J, Rosas IO, Morse D.** Autophagy in idiopathic pulmonary fibrosis. *PLoS One* 7: e41394, 2012.
40. **Peden AA, Oorschot V, Hesser BA, Austin CD, Scheller RH, Klumperman J.** Localization of the AP-3 adaptor complex defines a novel endosomal exit site for lysosomal membrane proteins. *J Cell Biol* 164: 1065–1076, 2004.
41. **Puissant A, Fenouille N, Auberger P.** When autophagy meets cancer through p62/SQSTM1. *Am J Cancer Res* 2: 397–413, 2012.
42. **Pyo JO, Yoo SM, Ahn HH, Nah J, Hong SH, Kam TI, Jung S, Jung YK.** Overexpression of Atg5 in mice activates autophagy and extends lifespan. *Nat Commun* 4: 2300, 2013.
43. **Raben N, Baum R, Schreiner C, Takikita S, Mizushima N, Ralston E, Plotz P.** When more is less: excess and deficiency of autophagy coexist in skeletal muscle in Pompe disease. *Autophagy* 5: 111–113, 2009.
44. **Schultz ML, Tecedor L, Chang M, Davidson BL.** Clarifying lysosomal storage diseases. *Trends Neurosci* 34: 401–410, 2011.
45. **Seglen PO, Gordon PB, Holen I.** Non-selective autophagy. *Semin Cell Biol* 1: 441–448, 1990.
46. **Settembre C, Fraldi A, Jahreiss L, Spampanato C, Venturi C, Medina D, de Pablo R, Tacchetti C, Rubinsztein DC, Ballabio A.** A block of autophagy in lysosomal storage disorders. *Hum Mol Genet* 17: 119–129, 2008.
47. **Styers ML, Salazar G, Love R, Peden AA, Kowalczyk AP, Faundez V.** The endo-lysosomal sorting machinery interacts with the intermediate filament cytoskeleton. *Mol Biol Cell* 15: 5369–5382, 2004.
48. **Sun Y, Liou B, Ran H, Skelton MR, Williams MT, Vorhees CV, Kitatani K, Hannun YA, Witte DP, Xu YH, Grabowski GA.** Neuronopathic Gaucher disease in the mouse: viable combined selective saposin C deficiency and mutant glucocerebrosidase (V394L) mice with glucosylsphingosine and glucosylceramide accumulation and progressive neurological deficits. *Hum Mol Genet* 19: 1088–1097, 2010.
49. **Tanaka Y, Guhde G, Suter A, Eskelinen EL, Hartmann D, Lullmann-Rauch R, Janssen PM, Blanz J, von Figura K, Saftig P.** Accumulation of autophagic vacuoles and cardiomyopathy in LAMP-2-deficient mice. *Nature* 406: 902–906, 2000.
50. **Tanida I, Ueno T, Kominami E.** Human light chain 3/MAP1LC3B is cleaved at its carboxyl-terminal Met121 to expose Gly120 for lipidation and targeting to autophagosomal membranes. *J Biol Chem* 279: 47704–47710, 2004.
51. **Tanida I, Ueno T, Kominami E.** LC3 conjugation system in mammalian autophagy. *Int J Biochem Cell Biol* 36: 2503–2518, 2004.
52. **Tschanz S, Schneider JP, Knudsen L.** Design-based stereology: Planning, volumetry and sampling are crucial steps for a successful study. *Ann Anat* 196: 3–11, 2014.
53. **Vasilescu DM, Gao Z, Saha PK, Yin L, Wang G, Haefeli-Bleuer B, Ochs M, Weibel ER, Hoffman EA.** Assessment of morphometry of pulmonary acini in mouse lungs by nondestructive imaging using multiscale microcomputed tomography. *Proc Natl Acad Sci USA* 109: 17105–17110, 2012.
54. **Vergarajauregui S, Connelly PS, Daniels MP, Puertollano R.** Autophagic dysfunction in mucolipidosis type IV patients. *Hum Mol Genet* 17: 2723–2737, 2008.
55. **Vitner EB, Platt FM, Futerman AH.** Common and uncommon pathogenic cascades in lysosomal storage diseases. *J Biol Chem* 285: 20423–20427, 2010.
56. **Young LR, Pasula R, Gulleman PM, Deutsch GH, McCormack FX.** Susceptibility of Hermansky-Pudlak mice to bleomycin-induced type II cell apoptosis and fibrosis. *Am J Respir Cell Mol Biol* 37: 67–74, 2007.
57. **Zhang L, Huang X, Qin C, Brinkman K, Gong Y, Wang S, Huang K.** First spectroscopic identification of pyrocarbonate for high CO2 flux membranes containing highly interconnected three dimensional ionic channels. *Phys Chem Chem Phys* 15: 13147–13152, 2013.
58. **Zhen Y, Li W.** Impairment of autophagosome-lysosome fusion in the buff mutant mice with the VPS33A(D251E) mutation. *Autophagy* 11: 1608–1622, 2015.

Downloaded from www.physiology.org/journal/ajplung (141.050.134.220) on October 24, 2019.

The attached printed / pdf version of this article is part of this habilitation thesis and has been included according to the copyright permissions issued by the American Physiological Society to reuse author's own APS-published work, following the guidelines given in the website as per 24.02.2023, that says:

'Authors may reproduce whole published articles in dissertations and post to thesis repositories without charge and without requesting permission. Full citation is required'.

https://journals.physiology.org/author-info.permissions

Citation of this article: Saket Ahuja, Lars Knudsen, Shashi Chillappagari, Ingrid Henneke, Clemens Ruppert, Martina Korfei, Bernadette R. Gochuico, Saverio Bellusci, Werner Seeger, Matthias Ochs, Andreas Guenther*, and Poornima Mahavadi*. MAP1LC3B overexpression protects against Hermansky-Pudlak syndrome type-1-induced defective autophagy in vitro. **Am J Physiol Lung Cell Mol Physiol. 2016** Mar 15; 310(6):L519-31. doi: 10.1152/ajplung.00213.2015. Epub 2015 Dec 30.

THE FASEB JOURNAL • RESEARCH • www.fasebj.org

15306860, 2019, 11, Downloaded from https://faseb.onlinelibrary.wiley.com/doi/10.1096/fj.201900854R by Justus-Liebig-Universitat, Wiley Online Library on [29/12/2022]. See the Terms and Conditions (https://onlinelibrary.wiley.com/terms-and-conditions) on Wiley Online Library for rules of use; OA articles are governed by the applicable Creative Commons License

Susceptibility of microtubule-associated protein 1 light chain 3β (MAP1LC3B/LC3B) knockout mice to lung injury and fibrosis

Vidya Sagar Kesireddy,[*,†] Shashi Chillappagari,[‡] Saket Ahuja,[*,†] Lars Knudsen,[§,¶,‖] Ingrid Henneke,[*,†] Johannes Graumann,[#,] Silke Meiners,[††] Matthias Ochs,[§,¶,‖,‡‡] Clemens Ruppert,[*,†] Martina Korfei,[*,†] Werner Seeger,[*,†,§§] and Poornima Mahavadi[*,†,1]**

[*]Department of Internal Medicine, [‡]Department of Biochemistry, Faculty of Medicine, and [§§]The Cardio-Pulmonary Institute, Justus-Liebig University (JLU) Giessen, Giessen, Germany; [†]Universities of Giessen and Marburg Lung Center (UGMLC), German Centre for Lung Research (DZL), Giessen, Germany; [§]Institute of Functional and Applied Anatomy, Hannover Medical School, Hannover, Germany, [¶]Biomedical Research in Endstage and Obstructive Lung Disease Hannover (BREATH), DZL, Hannover, Germany; [‖]Regenerative Biology and Reconstructive Therapies (REBIRTH) Cluster of Excellence, Hannover, Germany; [#]Biomolecular Mass Spectrometry, Max Planck Institute for Heart and Lung Research, Bad Nauheim, Germany; **German Centre for Cardiovascular Research (DZHK), Partner Site Rhine-Main, Frankfurt, Germany; [††]Comprehensive Pneumology Center (CPC), DZL, University Hospital of Ludwig-Maximilians-University (LMU)–Helmholtz Zentrum München, Munich, Germany; and [‡‡]Institute of Vegetative Anatomy, Charité–Universitaetsmedizin Berlin, Berlin, Germany

ABSTRACT: Insufficient autophagy has been reported in idiopathic pulmonary fibrosis (IPF) lungs. Specific roles of autophagy-related proteins in lung fibrosis development remain largely unknown. Here, we investigated the role of autophagy marker protein microtubule-associated protein 1 light chain 3β (LC3B) in the development of lung fibrosis. LC3B$^{-/-}$ mice upon aging show smaller lamellar body profiles, increased cellularity, alveolar epithelial cell type II (AECII) apoptosis, surfactant alterations, and lysosomal and endoplasmic reticulum stress. Autophagosomal soluble *N*-ethylmaleimide–sensitive factor attachment protein receptor syntaxin 17 is increased in the AECII of aged LC3B$^{-/-}$ mice and patients with IPF. Proteasomal activity, however, remained unaltered in LC3B$^{-/-}$ mice. *In vitro* knockdown of *LC3B* sensitized mouse lung epithelial cells to bleomycin-induced apoptosis, but its overexpression was protective. *In vivo*, LC3B$^{-/-}$ mice displayed increased susceptibility to bleomycin-induced lung injury and fibrosis. We identified cathepsin A as a novel LC3B binding partner and its overexpression *in vitro* drives MLE12 cells to apoptosis. Additionally, cathepsin A is increased in the AECII of aged LC3B$^{-/-}$ mice and in the lungs of patients with IPF. Our study reveals that LC3B mediated autophagy plays essential roles in AECII by modulating the functions of proteins like cathepsin A and protects alveolar epithelial cells from apoptosis and subsequent lung injury and fibrosis.—Kesireddy, V. S., Chillappagari, S., Ahuja, S., Knudsen, L., Henneke, I., Graumann, J., Meiners, S., Ochs, M., Ruppert, C., Korfei, M., Seeger, W., Mahavadi, P. Susceptibility of microtubule-associated protein 1 light chain 3β (MAP1LC3B/LC3B) knockout mice to lung injury and fibrosis. FASEB J. 33, 12392–12408 (2019). www.fasebj.org

KEY WORDS: alveolar epithelial cells · lamellar bodies · autophagy · aging · lysosome

Idiopathic pulmonary fibrosis (IPF) represents one of the most aggressive forms of organ fibrosis, killing patients within a few years of diagnosis (1). IPF has a remarkable age-related onset and is characterized by a progressive decline in lung function with the histologic appearance of usual interstitial pneumonia. The pathogenesis of IPF

ABBREVIATIONS: ABCA3, ATP binding cassette subfamily A member 3; AECII, alveolar epithelial cell type II; ATF6, activating transcription factor 6; Atg, autophagy-related; CHOP, C/EBP homologous protein; ER, endoplasmic reticulum; GABARAP1, γ-aminobutyric acid receptor-associated protein-like 1; GFP, green fluorescent protein; H&E, hematoxylin and eosin; HPS, Hermansky-Pudlak syndrome; IPF, idiopathic pulmonary fibrosis; LAMP, lysosome-associated membrane protein; LIR, LC3 interacting region; MAP1LC3B/LC3B, microtubule-associated protein 1 light chain 3β; NT, nontargeting; proSP-C, prosurfactant protein C; PSMD11, 26S proteasome non-ATPase regulatory subunit 11; siRNA, small interfering RNA; SNARE, soluble *N*-ethylmaleimide–sensitive factor attachment protein receptor; SP-B, surfactant protein B; ULK, mammalian orthologs of yeast Atg1; WT, wild type

[1] Correspondence: Department of Internal Medicine, Justus-Liebig University Giessen, University of Giessen–Marburg Lung Center, Seltersberg House-C, EG, Gaffkystrasse 11, 35392 Giessen, Germany. E-mail: poornima.mahavadi@innere.med.uni-giessen.de

doi: 10.1096/fj.201900854R

This article includes supplemental data. Please visit *http://www.fasebj.org* to obtain this information.

0892-6638/19/0033-12392 © FASEB

remains to be fully elucidated but may be based on chronic epithelial injury, disturbed epithelial-mesenchymal crosstalk, activation of fibroblasts, excessive collagen deposition, and disruption of the delicate alveolar architecture, altogether resulting in progressive dyspnea, decline of lung function and, ultimately, death (2, 3). Several studies published in the past underscore the importance of the alveolar epithelium in the evolution of IPF and lung fibrosis in general; already, the very first report by Myers and Katzenstein on IPF disclosed extensive alveolar epithelial type II cell (AECII) death and suggested a pathomechanistic role for the epithelium (4). AECII are secretory cells, and lamellar bodies of the AECII are lysosome-related organelles that are responsible for the storage and secretion of lung surfactant (5, 6). Qualitative and quantitative alterations in lamellar bodies within the hypertrophic AECII are well reported in patients with IPF as well as in several animal models. Likewise, alterations in the lysosomal compartment within the AECII in both clinical as well as experimental models of lung fibrosis are well documented. Firstly, pronounced changes in surfactant properties in patients with IPF have been reported (7–11). Furthermore, giant lamellar bodies, alterations in the surfactant secretion pathway, and lysosomal stress were linked to the development of pulmonary fibrosis in Hermansky-Pudlak syndrome (HPS)-associated and in amiodarone-induced lung fibrosis (12, 13). Along the same lines, we and others have shown that autophagy, a lysosome-dependent protein quality control mechanism of a cell, is either defective as in IPF and in HPS-associated lung fibrosis or excessively active as in the amiodarone model (10, 14–16), which, in either case, indicates the pathologic relevance of autophagy in the development of lung fibrosis.

Autophagy is a tightly regulated intracellular housekeeping mechanism that degrades long-lived proteins and unnecessary/nonfunctional organelles (17). It involves the function and interaction of several autophagy-related (Atg) gene products, which result in the conversion of the cytosolic form of the microtubule-associated protein 1 light chain 3β (MAP1LC3B/LC3B) to the membrane-bound, lipidated LC3BII form that labels the double membraned structures called autophagosomes (17, 18). These autophagosomes fuse with lysosomes to degrade their contents. Recently, it was shown that mammalian orthologs of yeast Atg1 (ULK)1 and 2 double knockout mice display lung abnormalities including glycogen-laden AECII (19). In addition, autophagy was shown to be altered in the widely used bleomycin model of lung fibrosis and that mice deficient for the deconjugation protease, Atg4, display accelerated apoptosis and lung fibrosis following bleomycin challenge (20).

We previously demonstrated that LC3B is localized to the limiting membrane of lamellar bodies of AECII in 2 models of lung fibrosis: the amiodarone model and the HPS model (10, 16). In addition, in the amiodarone model, we reported that the autophagosomes and lamellar bodies share the same membrane (16) and under conditions of HPS1 knockdown, overexpression of LC3B rescued cells from defective autophagy (10). Based on these observations, we now aimed to further understand the role of LC3B in the development of lung fibrosis.

MATERIALS AND METHODS

Mice and human lung tissue

Homozygous LC3B$^{-/-}$ mice (B6; 129P2-Map1lc3btm1Mrab/J) and wild-type (WT) control mice (B6129PF2/J) were purchased from The Jackson Laboratory (Bar Harbor, ME, USA). Both the University Animal Care Committee and the Federal Authorities for Animal Research of the Regierungspraesidium Giessen (Hessen, Germany) approved the study protocol. Mice were bred and maintained in specific pathogen-free conditions. Thirteen- and 42-wk-old mice were euthanized following the protocols previously described (12, 13). Mice that were ~13 wk old were treated with vehicle (0.9% NaCl) or 1.5 U/kg bodyweight bleomycin (Hexal AG, Holzkirchen, Germany) intratracheally. Each group consisted of about 5–10 animals: LC3B$^{-/-}$ or WT mice. Mice were euthanized according to the protocols previously described (10, 13). Shock-frozen lung tissue samples from 16 patients with IPF (mean age 54 ± SD: 9.14) and 6 nondiseased control subjects (donors; mean age 48.16 ± SD: 8) were used for homogenization and subsequent Western blot analysis. Additionally, formalin-fixed, paraffin-embedded lung tissue samples from 5 patients with sporadic IPF (mean age 54.8 ± SD: 11.07) and 5 nondiseased control subjects (mean age 50.8 ± SD: 9.41) were used for immunohistochemistry. All IPF diagnoses were made according to the American Thoracic Society (ATS)/European Respiratory Society (ERS) consensus criteria (21). The Universities of Giessen and Marburg Lung Center (UGMLC) Giessen Biobank [member of the German Centre for Lung Research (DZL) Platform Biobanking] provided all human lung tissue samples. The study protocol was approved by the Ethics Committee of the Justus-Liebig University Giessen (111/08 and 58/15).

Electron microscopy

After fixation of the lungs by instillation of 1.5% glutaraldehyde, 1.5% paraformaldehyde in 0.15 M 4-(2-hydroxyethyl)-1-piperazineethanesulfonic acid buffer, lungs were subjected to a systematic uniform random sampling, and 4–6 tissue pieces per lung were sampled (22), post fixed with osmium and uranyl acetate, and embedded in epoxy resin (Epon; Miller-Stephenson, Danbury, CT, USA). Afterwards, ultrathin sections were cut (thickness 80 nm). Electron microscopic evaluation of 4 sections per organ was performed using a Morgagni 268 Electron Microscope (Thermo Fisher Scientific, Waltham, MA, USA). A systematic uniform random area sampling was performed to sample 150–200 profiles of AECII for stereological assessment of the intracellular surfactant pool defined by ultrastructural criteria as the amount of lamellar bodies. Random test points were used to count points hitting lamellar bodies or all other structures of the sampled AECII to determine the volume fraction of lamellar bodies within AECII. In addition, the point sampled intercept method was used to determine the volume-weighted mean volume of lamellar bodies, a parameter that is dependent on the number-weighted mean volume as well as the coefficient of variation of lamellar bodies (23).

Histology and immunofluorescence

Lung tissues harvested from mice were fixed in 4% formaldehyde and embedded in formalin, and serial sections of thickness

15306860, 2019, 11, Downloaded from https://faseb.onlinelibrary.wiley.com/doi/10.1096/fj.201900854R by Justus-Liebig-Universitat, Wiley Online Library on [29/12/2022]. See the Terms and Conditions (https://onlinelibrary.wiley.com/terms-and-conditions) on Wiley Online Library for rules of use; OA articles are governed by the applicable Creative Commons License

3–6 μm were prepared. Hematoxylin and eosin (H&E) and masson goldner staining were performed according to the previously described protocols (12). A ZytomedChem Plus Broad Spectrurm Kit (AP-Fast Fed, AP008RED-MS; Zytomed Systems, Berlin, Germany) was used to perform immunostaining of cleaved caspase-3 (9664; Cell Signaling Technology, Danvers, MA, USA), pro SP-C (AB3786; MilliporeSigma, Burlington, MA, USA), syntaxin 17 (PA5-40127; Thermo Fisher Scientific), and cathepisin A (ab184553; Abcam, Cambridge, United Kingdom) as per the manufacturer's instructions and as previously described (13). Hamamatsu scanner (Nanozoomer 2.0 RS; Hamamatsu Photonics, Hamamatsu City, Japan) was used for scanning the stained sections. NDP.view 2.0 software was used for preparing and analyzing the images. For quantifying immunohistochemistry images, 5–6 regions from 5 mice per group were randomly analyzed for intensity quantification using ImageJ software (National Institutes of Health, Bethesda, MD, USA) following the instructions given in the ImageJ documentation (*https://www.unige.ch/medecine/bioimaging/files/1914/1208/6000/Quantification.pdf*). For staining on lung sections, prosurfactant protein C (proSP-C) antibody (AB3786; MilliporeSigma) was labeled with Alexa Fluor 488 using the Alexa Fluor 488 antibody labeling kit from Thermo Fisher Scientific (A20181), following the manufacturer's instructions, and was used to stain AECII on mouse lung sections for costaining studies. For human sections, ATP binding cassette subfamily A member 3 (ABCA3) antibody was used to stain AECII. Microscopy was performed using a Leica M205 FA Fluorescent Stereoscope (Leica Microsystems, Buffalo Grove, IL, USA) equipped with a Leica DFC360 FX camera. Immunofluorescence images were quantified using Leica LAS X LS software on 10–15 randomly selected regions per mouse or human sections and represented as mean fluorescence intensity, using the SEM. Four to 5 mice or human sections per group were used for each staining with subsequent quantification.

Western blot

Denatured lung homogenates and cell lysates were used for Western blotting as previously described (12). Antibodies used for Western blots are listed in **Table 1**.

Proteasome activity assay

Total lung extracts from young and old LC3B$^{-/-}$ and WT control mice were generated using native lysis conditions. Proteasome activity was monitored in total extracts for the chymotrypsin-like and caspase-like proteasome activities using the Promega Glo Assay (Madison, WI, USA) as previously described (24).

Cell culture

Small interfering RNA (siRNA) for LC3B was purchased from Santa Cruz Biotechnology (Dallas, TX, USA), and transfections in MLE12 cells were performed according to the previously described protocols (16). Cells were plated 1 d before the experiment, and when they reached confluency, they were transfected with nontargeting (NT) siRNA or with siRNA against mouse LC3B (Santa Cruz Biotechnology) for 24 h followed by treatment with bleomycin for 4 h and then harvesting. Green fluorescent protein (GFP)-LC3B was generated as previously described (16), and mouse cathepsin A tagged with myc was from OriGene

TABLE 1. *List of antibodies used*

Name	Catalog no.	Company
Immunoblotting and immunoprecipitation		
β-actin	ab8227	Abcam
ATF6	NBP1-77251	Novus Biologicals, Centennial, CO, USA
Cleaved caspase-3	9664	Cell Signaling Technology
Cathepsin D	AF1029	R&D Systems, Minneapolis, MN, USA
Cathepsin A	ab184553 and ab217857	Abcam
Cathepsin L ()	ab58991	Abcam
Gadd163	sc-7351 HRP	Santa Cruz Biotechnology
GFP	ab5450	Abcam
GABBARAPL1		Genetex, Irvine, CA, USA
Glyceraldehyde 3-phosphate dehydrogenase	2118s	Cell Signaling Technology
LC3B	ab48394 and 2775s	Abcam and Cell Signaling Technology
Lamp1	ab24170	Abcam
Lamp2	MABC40	MilliporeSigma
Myc	ab9106	Abcam
Mature SP-C	WRAB-76694	Seven Hills, Cincinnati, OH, USA
Mature SP-B	WRAB-48604	Seven Hills
PSMD11	14786-1-1AP	Proteintech, Rosemont, IL, USA
Proteasome 20s core subunit	BML-PW8155-0100	Enzo Life Sciences, Farmingdale, NY, USA
ProSP-C	AB3786	MilliporeSigma
Pro-SP-B	WRAB-55522	Seven Hills
P62	P0067	MilliporeSigma
Syntaxin 17 ()	PA5-40127	Thermo Fisher Scientific
Immunohistochemistry and immunofluorescence		
ABCA3	WAMB-ABCA3-17	Seven Hills
Cleaved caspase-3	9664	Cell Signaling Technology
Cathepsin A	ab184553 and ab217857	Abcam
Pro-SP-C	AB3786	MilliporeSigma
Syntaxin 17	PA5-40127	Thermo Fisher Scientific
P62	P0067	MilliporeSigma

15306860, 2019, 11, Downloaded from https://faseb.onlinelibrary.wiley.com/doi/10.1096/fj.201900854R by Justus-Liebig-Universitat, Wiley Online Library on [29/12/2022]. See the Terms and Conditions (https://onlinelibrary.wiley.com/terms-and-conditions) on Wiley Online Library for rules of use; OA articles are governed by the applicable Creative Commons License

Technologies (Rockville, MD, USA; NM_001038492; MR207589). Cotransfection of these plasmids in MLE12 cells was performed using Lipofectamine 2000 (Thermo Fisher Scientific), and cells were harvested after 24 h. Alveolar epithelial cells from LC3B$^{-/-}$ or WT mice were isolated as previously described (12). Briefly, 42-wk-old LC3B$^{-/-}$ (5 mice) or WT mice (5 mice) were anesthetized and dissected followed by lung lavaging. Lungs were flushed with 0.9% NaCl through the left ventricle, and 1.5 ml dispase and 0.5 ml melted agarose were injected, and then the dissected lung was incubated in dispase at room temperature for 45 min. Lung tissue was then minced. Cell populations were not pooled, and cells from each mouse were analyzed separately. Following panning on antibody-coated dishes (using CD16/CD45; BD Biosciences, San Jose, CA, USA), cells were coated on noncoated dishes for 30 min at 37°C/4% CO_2 incubator. Suspensions were centrifuged and pellets were frozen for further analysis. Control staining was performed using proSP-C (AB3786; MilliporeSigma) antibody as well as Nile red staining.

Coimmunoprecipitation

Tosylactivated dynabeads (Thermo Fisher Scientific) were used for all coimmunoprecipitation experiments, and immunoprecipitation was performed according to the manufacturer's protocol. Briefly, dynabeads were coupled to the antibody (anti-myc, anti-cathepsin A, or rabbit IgG) by incubating them overnight at room temperature on a tube rotator. The next day, supernatant was removed by placing the tubes in a magnetic stand. After washing, antibody coupled beads were added to the sample [freshly harvested MLE12 cells using immunoprecipitated lysis buffer (Thermo Fisher Scientific)] and incubated in a tube rotator overnight at 4°C. An aliquot of 10% of the lysate, before adding it to the beads, was used as input. The next day, an unbound sample was discarded by placing the tubes in a magnetic stand. Following washing, the immunoprecipitated samples or input were then denatured at 98°C for 10 min in buffer containing SDS and were subjected to Western blotting.

Statistics

All data are expressed as means ± SD of ≥5 mice for *in vivo* studies. For *in vitro* experiments, ≥ independent experiments were conducted for bleomycin treatment and triplicate transfections were performed for siRNA/GFP-LC3B/cathepsin A-myc studies. Statistical significance was assessed using the Mann-Whitney *U* test. Results were significant when $P < 0.05$.

RESULTS

LC3B$^{-/-}$ mice display age-dependent alteration in lung structure

In view of our previous studies that showed a critical role of LC3B in HPS-associated lung fibrosis as well as in the amiodarone model of lung fibrosis and based on observations from other studies that reported lung-specific alterations in certain autophagy gene knockout mouse models, we now asked if LC3B knockout mice would display lung alterations. A careful histologic analysis of the lungs of 13-wk-old LC3B$^{-/-}$ mice (young mice) and age-matched WT control mice revealed normal lung architecture. However, 42-wk-old LC3B$^{-/-}$ mice (aged mice) did show areas with increased cellularity and reduced airspaces (**Fig. 1*A*** and Supplemental Fig. S1). Because immunogold labeling demonstrated a preferential binding of LC3B antibodies to the limiting membrane of lamellar bodies in our previous studies (10, 25), we closely examined the ultrastructure of AECII in LC3B$^{-/-}$ mice. The morphology of lamellar bodies with respect to the densely packed lipid layers as well as the limiting membrane did not differ between WT and LC3B$^{-/-}$ mice. At best, in some AECII of the LC3B$^{-/-}$ mice, there were fewer and smaller profiles of lamellar bodies compared with WT mice (Fig. 1*B*). Thus, we added a stereological assessment and determined the volume fraction of lamellar bodies within AECII as well as the volume-weighted mean volume of lamellar bodies. The volume fraction was significantly reduced in LC3B$^{-/-}$ mice compared with WT mice, meaning that per volume of AECII, the cells contained less intracellular surfactant (Fig. 1*C*). Also, the volume-weighted mean volume was significantly reduced in LC3B mice, indicating that lamellar bodies were smaller or characterized by a reduced size variability (Fig. 1*D*). Analysis of surfactant proteins revealed significant difference only in pro and mature surfactant protein B (SP-B) levels in lung homogenates between LC3B$^{-/-}$ and WT mice (Supplemental Fig. S2*A–F*).

Aged LC3B$^{-/-}$ mice display apoptosis of AECII

Because apoptosis of AECII is a hallmark in the development of lung fibrosis, we further asked if the AECII of LC3B$^{-/-}$ mice undergo apoptosis. Immunoblots from total lung homogenates revealed significant cleavage of caspase-3, the terminal apoptosis marker in the older but not in the younger LC3B$^{-/-}$ mice as compared with age-matched WT mice (**Fig. 2*A*, *B***). Interestingly, histologic staining for cleaved caspase-3 as well as proSP-C, an AECII marker on serial sections revealed that AECII in the 42-wk-old LC3B$^{-/-}$ mice display extensive apoptosis, especially in the patchy fibrotic regions (Fig. 2*C–E*).

LC3B$^{-/-}$ mice display lysosomal and endoplasmic reticulum stress and increase in syntaxin 17 within their AECII

By immunoblotting, we also analyzed the lysosomal markers, lysosome-associated membrane protein (LAMP) 1 and 2, the lysosomal stress marker, cathepsin D as well as the standard autophagy substrate and receptor protein p62. Cathepsin D and LAMP1 levels did not differ between LC3B$^{-/-}$ and WT control mice, but p62 and LAMP2 levels were significantly increased in the older LC3B$^{-/-}$ mice as compared with their age-matched controls (**Fig. 3*A–E***). Interestingly, the pro form of cathepsin D is decreased in the younger LC3B$^{-/-}$ mice. In the older mice, on the other hand, we observed an increase in the pro and cleaved forms of cathepsin D, albeit a nonsignificant increase (Fig. 3*A, E*). Furthermore, in order to analyze whether these mice develop alternate cellular stress mechanisms, we queried 2 endoplasmic reticulum (ER) stress markers, activating transcription factor 6 (ATF6), and C/EBP homologous protein (CHOP).

15306860, 2019, 11, Downloaded from https://faseb.onlinelibrary.wiley.com/doi/10.1096/fj.201900854R by Justus-Liebig-Universitat, Wiley Online Library on [29/12/2022]. See the Terms and Conditions (https://onlinelibrary.wiley.com/terms-and-conditions) on Wiley Online Library for rules of use; OA articles are governed by the applicable Creative Commons License

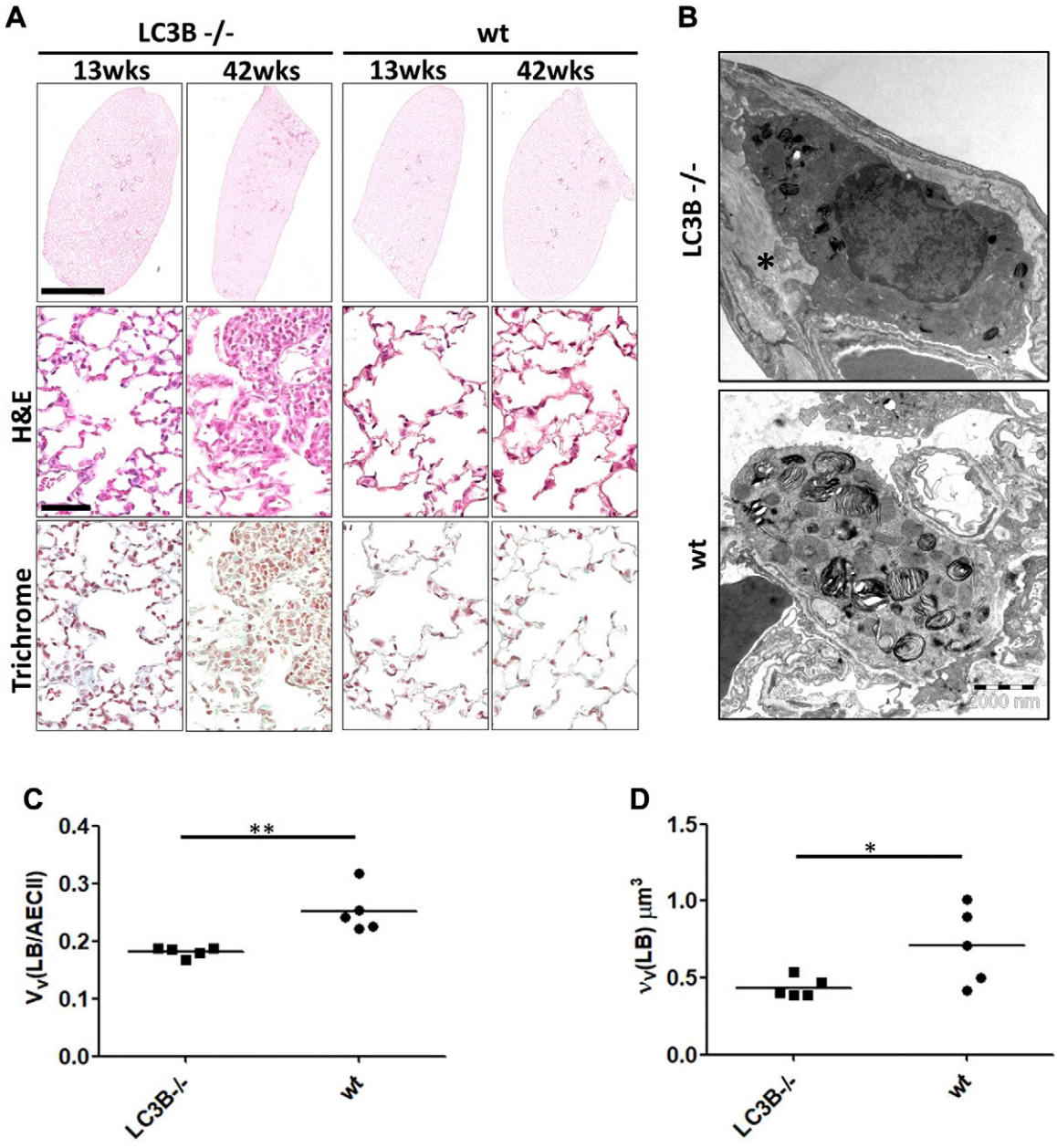

Figure 1. Decreased airspaces and diameter of distal air spaces in aged LC3B$^{-/-}$ mice. *A*) Representative H&E staining of complete left lungs (upper panel) and higher magnification images of the H&E staining (middle panel) and trichrome staining (lower panel) of 13- and 42-wk-old LC3B$^{-/-}$ and WT mice. Scale for the whole lungs, 2 mm; scale for the higher magnification pictures, 100 µm; original magnification, ×200. *B*) Representative transmission electron microscopic images from 42-wk-old LC3B$^{-/-}$ and age-matched WT mice showing an example of smaller profiles of lamellar bodies in LC3B$^{-/-}$ compared with WT (primary original magnification, ×8900). *C, D*) Stereological data revealed a reduced volume fraction of lamellar bodies in AECII [V_V(LB/AECII)] (*C*) combined with a reduced volume-weighted mean volume of lamellar bodies [v_V(LB)] (*D*).

Immunoblotting analysis revealed that the activated form (p50) of ATF6 and CHOP significantly increased in LC3B$^{-/-}$ mice in an age-correlated manner as compared with WT controls (Fig. 3*F–H*), indicating that lysosomal has a retrograde stress effect on the ER, thereby activating the ER stress proteins in aged LC3B$^{-/-}$ mice.

Of note and as indicated in Fig. 3*A*, *B* and Supplemental Fig. S3*A*, the autophagy substrate and receptor protein p62 accumulated in the aged mice as compared with the younger LC3B$^{-/-}$ mice. We interpreted this finding as an activation of compensatory mechanisms in the absence of LC3B-mediated autophagy in the younger LC3B$^{-/-}$ mice. We thus hypothesized that knockout of *LC3B* may result in a compensatory activation of the proteasome in younger LC3B$^{-/-}$ mice. To test this, we analyzed 2 proteasomal subunits: the 20S core subunit and the 26S proteasome non-ATPase regulatory subunit 11 (PSMD11). Interestingly, a significant increase in the 20S core subunit expression was observed in the younger mice, whereas its levels were significantly decreased in older LC3B$^{-/-}$ mice relative to WT controls and the levels of PSMD11 remained unaltered (**Fig. 4*A, B***). In total lung

15306860, 2019, 11, Downloaded from https://faseb.onlinelibrary.wiley.com/doi/10.1096/fj.201900854R by Justus-Liebig-Universitat, Wiley Online Library on [29/12/2022]. See the Terms and Conditions (https://onlinelibrary.wiley.com/terms-and-conditions) on Wiley Online Library for rules of use; OA articles are governed by the applicable Creative Commons License

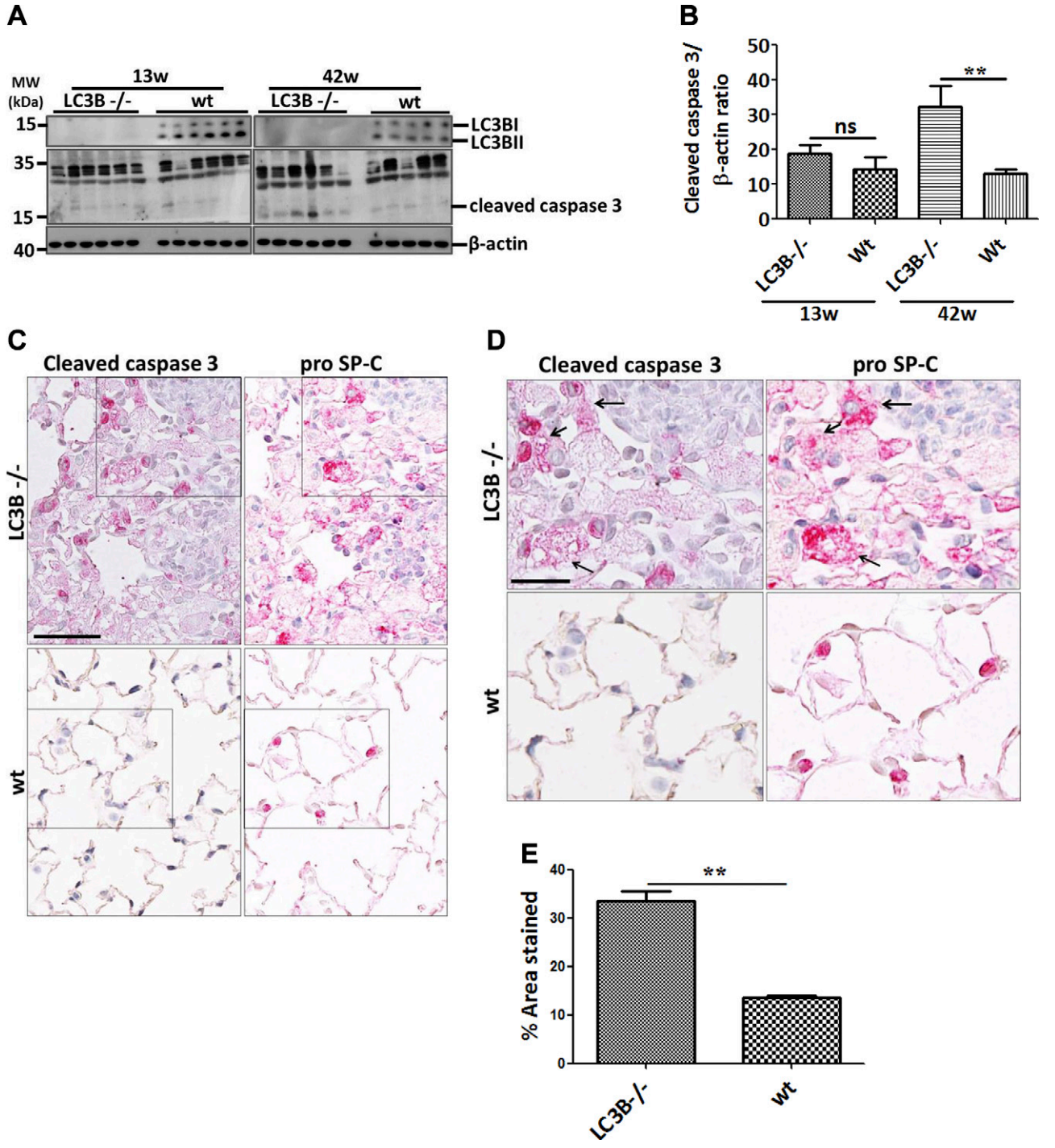

Figure 2. AECII apoptosis in aged LC3B$^{-/-}$ mice. *A*) Western blot analysis of lung homogenates of 13-wk-old (left) or 42-wk-old (right) LC3B$^{-/-}$ and WT mice for cleaved caspase-3 and β-actin. *B*) Densitometry analysis of cleaved caspase-3/β-actin ratio. *C*, *D*) Representative immunohistochemistry images of serial lung sections of 42-wk-old LC3B$^{-/-}$ and WT mice for cleaved caspase-3 and proSP-C. Original magnification of images are ×200 (*C*) and 400, (*D*). Scale bars, 50 and 25 μm, respectively. Arrows in *D* indicate apoptotic AECII in LC3B$^{-/-}$ mice. *E*) Immunohistological staining for cleaved caspase-3 in several regions of the lungs were quantified and depicted as a bar graph. Representative blots and analysis from $n = 5$ mice/group and ≥3 independent experiments are shown. $^{**}P < 0.01$.

extracts, however, we did not consistently observe differences in either chymotrypsin-like or caspase-like proteasomal activities between LC3B$^{-/-}$ and WT or between younger and older mice (Fig. 4C, *D*). This indicated that the proteasome is not activated to compensate for the loss of LC3B-mediated autophagy function in the LC3B$^{-/-}$ mice. In addition, we also analyzed γ-aminobutyric acid receptor-associated protein-like 1 (GABARAP1), another ATG8 family member that is involved in autophagosome maturation, to understand whether GABARAP1L would compensate for the loss of LC3B function in LC3B$^{-/-}$ mice. However, GABARAP1L

15306860, 2019, 11, Downloaded from https://faseb.onlinelibrary.wiley.com/doi/10.1096/fj.201900854R by Justus-Liebig-Universitat, Wiley Online Library on [29/12/2022]. See the Terms and Conditions (https://onlinelibrary.wiley.com/terms-and-conditions) on Wiley Online Library for rules of use; OA articles are governed by the applicable Creative Commons License

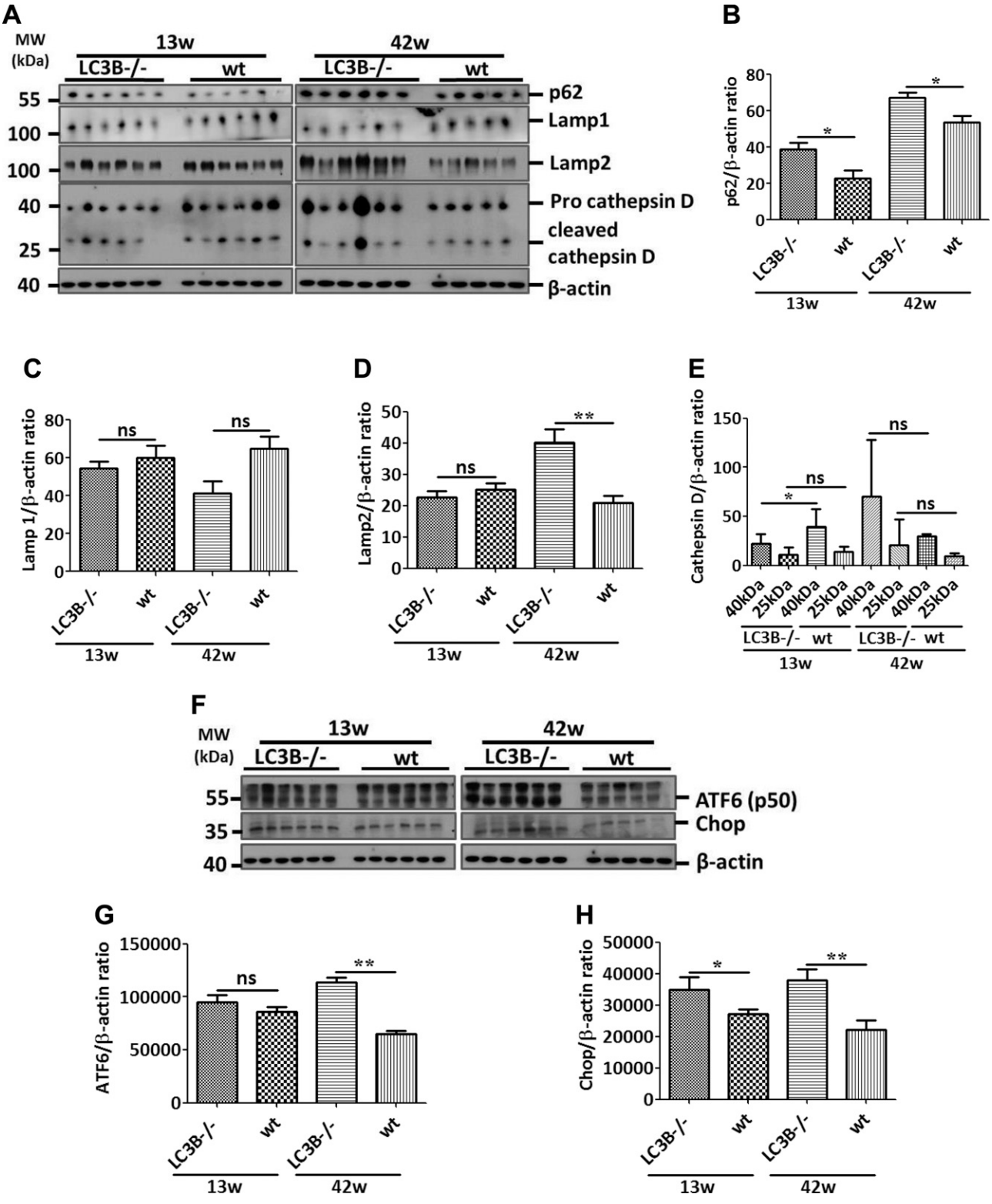

Figure 3. Lysosomal and ER stress in LC3B$^{-/-}$ mice. *A*) Western blot analysis of lung homogenates of 13-wk-old (left) or 42-wk-old (right) LC3B$^{-/-}$ and WT mice for the autophagy marker protein, p62, lysosomal markers, LAMP1 and 2, and cathepsin D and β-actin. *B–E*) Graphical representation of the densitometry analysis of the respective protein to β-actin ratio is shown. *F*) Western blot analysis of lung homogenates of 13- (left) or 42-wk-old (right) LC3B$^{-/-}$ and WT mice for the ER stress marker proteins, cleaved form of ATF6 and CHOP. *G*, *H*) Graphical representation of the densitometry analysis of the respective protein to β-actin ratio is shown. Representative blots and analysis from $n = 5$ mice/group and 3 independent experiments are shown; ns, not significant. $^{*}P < 0.05$, $^{**}P < 0.01$.

15306860, 2019, 11, Downloaded from https://faseb.onlinelibrary.wiley.com/doi/10.1096/fj.201900854R by Justus-Liebig-Universitat, Wiley Online Library on [29/12/2022]. See the Terms and Conditions (https://onlinelibrary.wiley.com/terms-and-conditions) on Wiley Online Library for rules of use; OA articles are governed by the applicable Creative Commons License

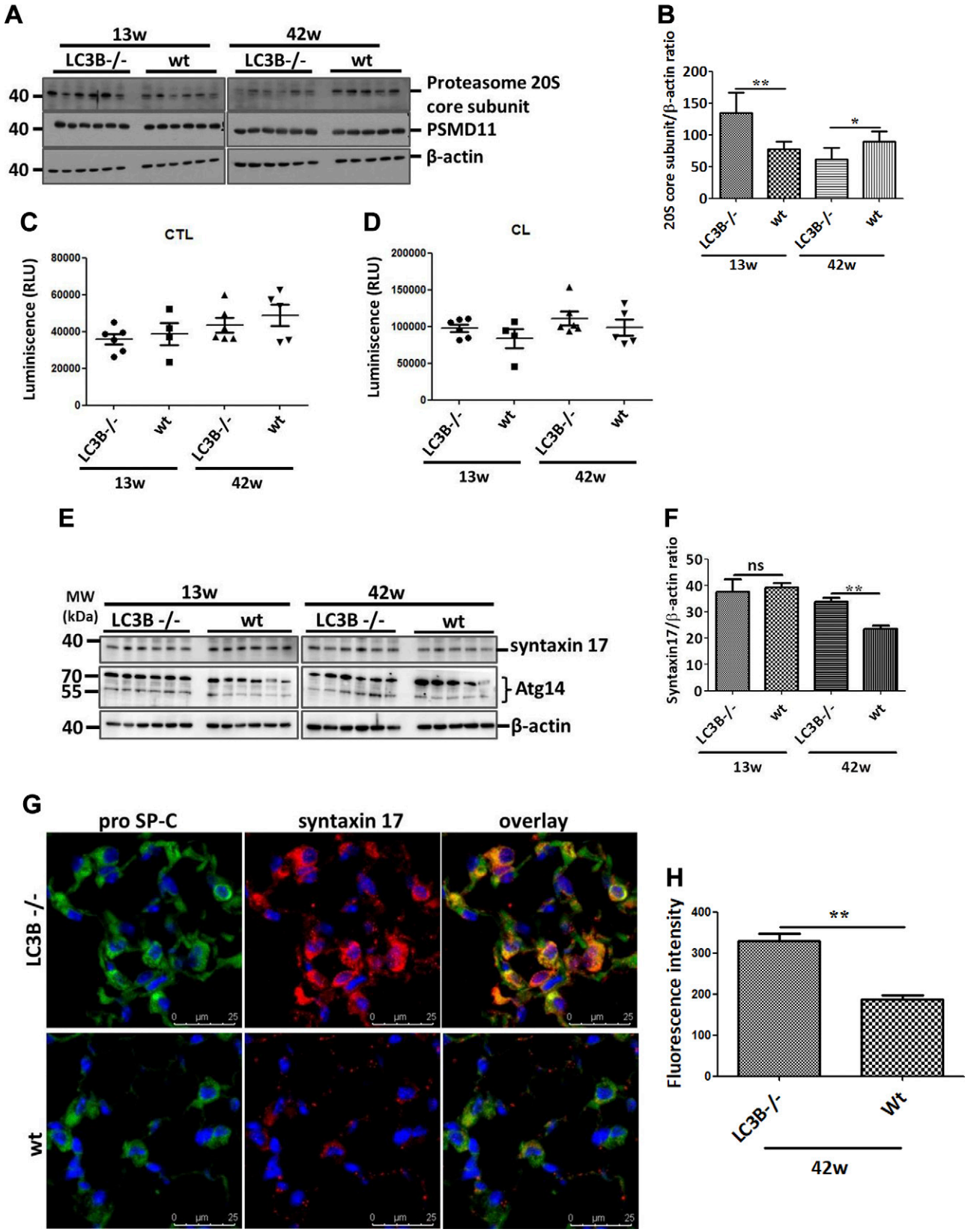

Figure 4. Up-regulation of syntaxin 17 in LC3B$^{-/-}$ mice. *A*) Western blot analysis of lung homogenates of 13-wk-old (left) or 42-wk-old (right) LC3B$^{-/-}$ and WT mice for the 20S core subunit of the 20S proteasome, the PSMD11 and β-actin. *B*) Graphical representation of densitometric quantification for 20S core subunit. *C, D*) Chymotrypsin-like (CTL) (*C*) and caspase-like (CL) (*D*) proteasome activity was measured in total lung extracts of LC3B$^{-/-}$ and WT control mice. *E*) Western blot analysis of lung homogenates of 13-wk-old (left) or 42-wk-old (right) LC3B$^{-/-}$ and WT mice for syntaxin 17, Atg14, and β-actin. *F*) Graphical representation of densitometric quantification for syntaxin 17. *G*) Immunofluorescence staining on paraffin sections from

(*continued on next page*)

15306860, 2019, 11, Downloaded from https://faseb.onlinelibrary.wiley.com/doi/10.1096/fj.201900854R by Justus-Liebig-Universitat, Wiley Online Library on [29/12/2022]. See the Terms and Conditions (https://onlinelibrary.wiley.com/terms-and-conditions) on Wiley Online Library for rules of use; OA articles are governed by the applicable Creative Commons License

protein levels in both young and old LC3B$^{-/-}$ mice did not differ from their age-matched WT mice (Supplemental Fig. S3*B*). This observation is in full accordance with a previous study from mouse embryonic fibroblasts of LC3B$^{-/-}$ mice (26).

Maturation of autophagosomes and, more importantly, their fusion with lysosomes involve the autophagosomal soluble *N*-ethylmaleimide–sensitive factor attachment protein receptor (SNARE) syntaxin 17. It was shown that in cells lacking the classic ATG conjugation system, syntaxin 17–positive autophagosome-like structures are formed at a reduced rate and fuse with lysosomes (27). Likewise, it has been suggested that Atg14 might also compensate for the role of LC3B to form syntaxin 17–positive autophagosomes (28). However, we did not find consistent difference in the protein levels of Atg14 in LC3B$^{-/-}$ mice compared with WT mice (Fig. 4*E*). Interestingly, syntaxin 17 protein levels did not alter in the younger LC3B$^{-/-}$ mice but were significantly increased in older LC3B$^{-/-}$ mice both in lung homogenates as well as in primary AECII (Fig. 4*E, F* and Supplemental Fig. S4*A, B*). In fact, punctate staining for syntaxin 17 was observed in WT and in younger LC3B$^{-/-}$ mice, but the older LC3B$^{-/-}$ mice displayed increased and diffused staining for syntaxin 17 within the AECII as compared with WT mice (Fig. 4*G, H*). Taken together, these readouts indicate that syntaxin 17–mediated autophagy may be defective in older LC3B$^{-/-}$ mice but not in younger mice. Next, we also evaluated syntaxin 17 in the explanted lungs of patients with IPF as well as healthy donors. Protein levels of syntaxin 17 were significantly increased in total lung extracts of patients with IPF as compared with donor lungs (Supplemental Fig. S4*C, D*). Likewise, immunohistochemical analysis revealed increased staining for syntaxin 17 within the AECII of patients with IPF as compared with the AECII of donor lungs (Supplemental Fig. S4*E, F*). This indicates that upon aging, defective autophagy, as seen in both aged LC3B$^{-/-}$ mice as well as in patients with IPF, results in a concomitant increase in syntaxin 17–positive structures within the AECII.

LC3B$^{-/-}$ mice display increased susceptibility to bleomycin-induced lung fibrosis

We further sought to study the role of *LC3B* in driving apoptosis of AECII and subsequent lung fibrosis both *in vivo* as well as *in vitro.* To this end, we performed siRNA-mediated knockdown of *LC3B* in MLE12 cells followed either by treatment with bleomycin or vehicle for 4 h or by leaving them untreated (**Fig. 5*A, B***). Cells transfected with NT siRNA served as controls. It is well documented that bleomycin induces apoptosis of alveolar epithelial cells and subsequent lung fibrosis (29, 30). Replicating these findings, we also observed significant increase in the apoptosis marker, cleaved caspase-3 levels in MLE12 cells transfected with NT siRNA, followed by bleomycin treatment (Fig. 5*A, C*). Next, in cells transfected with siRNA against *LC3B* followed by bleomycin treatment, a further increase of the level of cleaved caspase-3 protein was observed (Fig. 5*A, C*). We interpreted this observation as a sensitization of MLE12 cells to bleomycin-induced apoptosis through knockdown of *LC3B*. On the contrary, cells overexpressing GFP-LC3B followed by bleomycin treatment displayed reduced levels of cleaved caspase-3 and thus apoptosis as signaling compared with cells overexpressing empty GFP followed by bleomycin treatment (Fig. 5*D, E*), indicating the protective role of GFP-LC3B upon bleomycin treatment. These data reconfirm previous studies from our group as well as from others about the protective role of LC3B in lung pathologies (16, 31, 32).

Based on these readouts and to further delineate the role of LC3B in lung fibrosis, we treated the younger LC3B$^{-/-}$ as well as WT mice with a single low dose (1.5 U/kg) of bleomycin and euthanized them at d 7 or 14. As indicated in **Fig. 6*A–D***, LC3B$^{-/-}$ mice challenged with bleomycin at d 7 displayed increased cellularity and reduced airspaces as compared with bleomycin-challenged WT mice. Such differences were not clearly seen in mice challenged with bleomycin for 14 d (unpublished data). LC3B$^{-/-}$ at d 7 following bleomycin challenge displayed a nonsignificant increase in apoptosis as indicated by cleaved caspase-3 immunoblots in Supplemental Fig. S5*E, F* compared with WT mice challenged with bleomycin. These data supported our previous observations from Figs. 1 and 2, wherein the older LC3B$^{-/-}$ mice displayed increased lung alterations. In addition, we also analyzed for cellular stress (lysosomal and ER stress) markers in LC3B$^{-/-}$ and WT mice challenged with bleomycin. Significant differences were observed in cathepsin D levels at d 14 after bleomycin challenge of LC3B$^{-/-}$ *vs.* WT mice and ATF6 (p50) between d 7 bleomycin *vs.* wt mice (Supplemental Fig. S5*E, G, H*). In addition, p62 and LAMP2 protein levels were significantly different between bleomycin-challenged LC3B$^{-/-}$ mice on d 14 *vs.* WT mice (Supplemental Fig. S5*A, D*). The levels of lysosomal marker protein, LAMP1 remained unaffected (Supplemental Fig. S5*A, C*).

Cathepsin A is an LC3B binding partner and is increased in the AECII of LC3B$^{-/-}$ mice and the lungs of patients with IPF

The results described above point toward a significant contribution of LC3B to lung fibrosis. We then sought to analyze the underlying molecular mechanisms. In this context, one intriguing observation deriving from our analysis is the increased levels of cathepsin L as well as cathepsin A levels in LC3B$^{-/-}$ mice lungs *vs.* WT control lungs (**Fig. 7*A–C***and Supplemental Fig. S3*B, C*). Cathepsin L is a cysteine protease involved in functions including protein turnover and antigen presentation. Cathepsin A, on the other hand, was identified as a lysosomal protective

42-wk-old LC3B$^{-/-}$ or WT control mice for the AECII marker, proSP-C (green) and syntaxin 17 (red). DAPI was used to stain the nuclei in blue. *H*) Syntaxin 17 fluorescence signal intensity was quantified and depicted as a bar graph. Representative blots and analysis from $n = 5$ mice/group and 3 independent experiments are shown; ns, not significant. $^{*}P < 0.05$, $^{**}P < 0.01$.

15306860, 2019, 11, Downloaded from https://faseb.onlinelibrary.wiley.com/doi/10.1096/fj.201900854R by Justus-Liebig-Universitat, Wiley Online Library on [29/12/2022]. See the Terms and Conditions (https://onlinelibrary.wiley.com/terms-and-conditions) on Wiley Online Library for rules of use; OA articles are governed by the applicable Creative Commons License

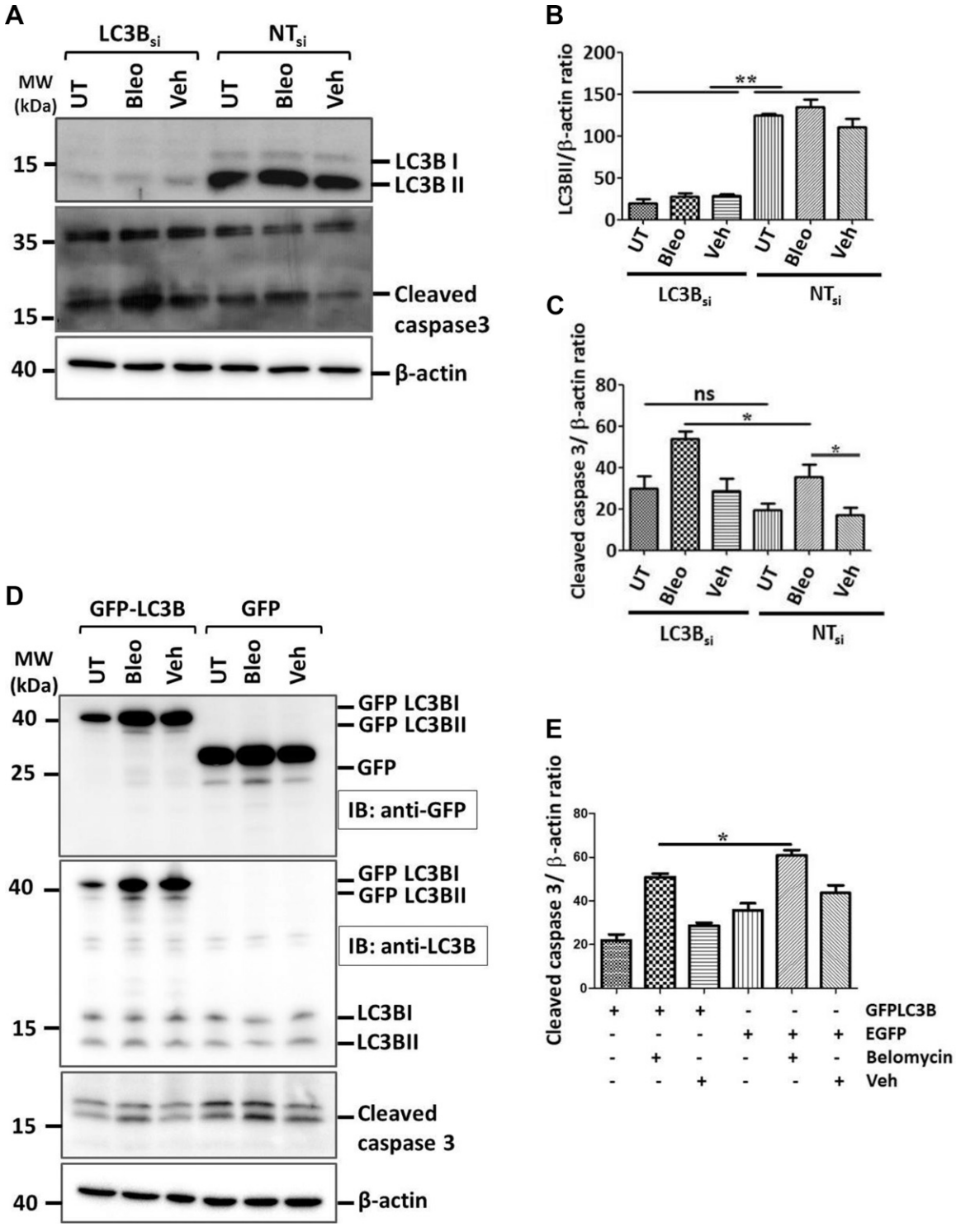

Figure 5. Knockdown of *LC3B* sensitizes MLE12 cells to bleomycin-induced apoptosis. *A*) MLE12 cells were either transfected with LC3B siRNA or NT siRNA for 24 h followed by bleomycin (Bleo) or vehicle (Veh) treatment for 4 h. Representative Western blot images are shown from these cell lysates for LC3B, cleaved caspase-3, and β-actin. *B*, *C*) Graphical representation of densitometric quantification for LC3B/β-actin (*B*) and cleaved caspase-3/β-actin (*C*) ratio are shown. *D*) MLE12 cells were either transfected with GFP-LC3B or empty GFP vector for 24 h followed by Bleo or Veh treatment for 4 h. Representative Western blot images are shown from these cell lysates for GFP-LC3B using anti-GFP antibody or for both GFP-LC3B and endogenous LC3B using anti-LC3B antibody, cleaved caspase-3, and β-actin. *E*) Graphical representation of densitometric quantification for cleaved caspase-3 is shown. Representative blots and analysis from 4 independent experiments are shown; ns, not significant. $*P < 0.05$, $**P < 0.01$.

15306860, 2019, 11, Downloaded from https://faseb.onlinelibrary.wiley.com/doi/10.1096/fj.201900854R by Justus-Liebig-Universitat, Wiley Online Library on [29/12/2022]. See the Terms and Conditions (https://onlinelibrary.wiley.com/terms-and-conditions) on Wiley Online Library for rules of use; OA articles are governed by the applicable Creative Commons License

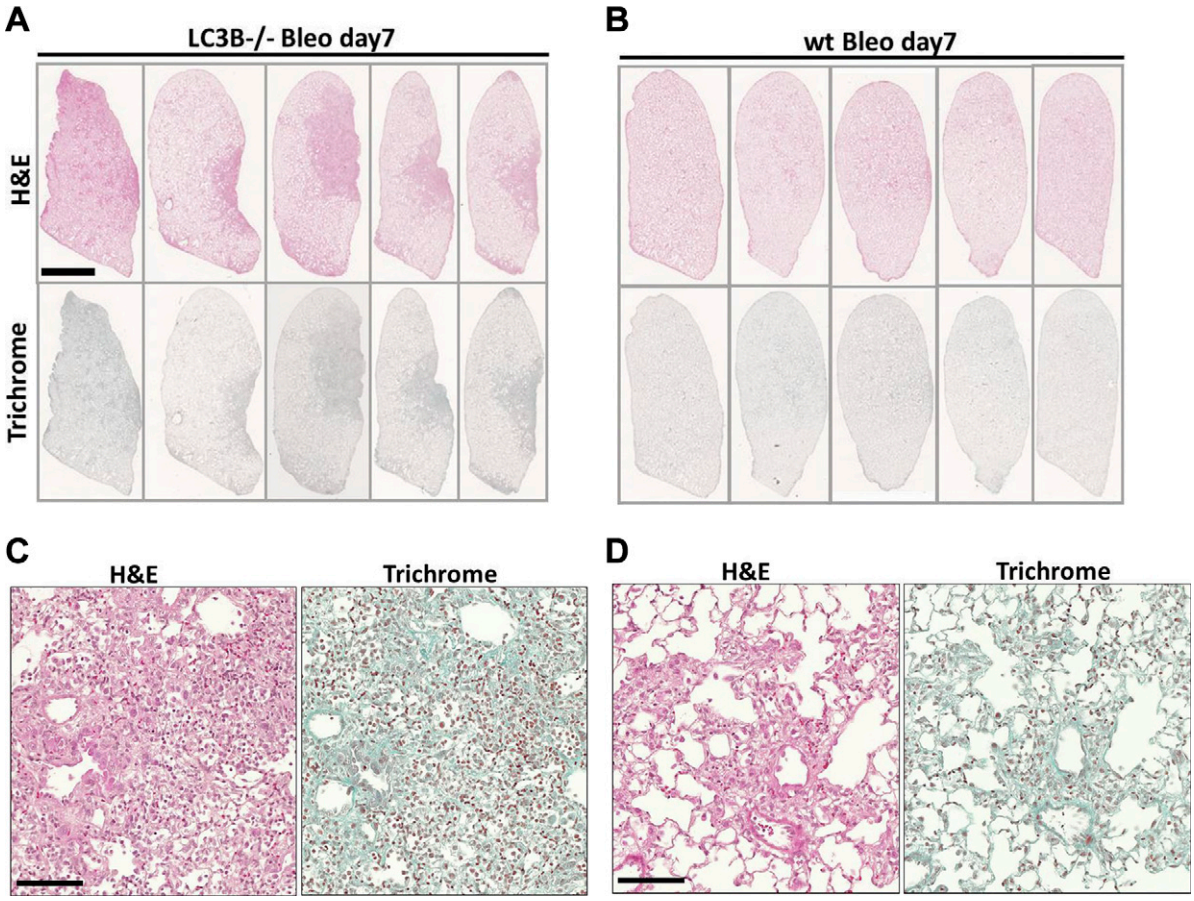

Figure 6. LC3B$^{-/-}$ mice are susceptible to bleomycin-induced lung injury and fibrosis. Representative H&E (upper panel) and trichrome staining (lower panel) of complete left lungs of LC3B$^{-/-}$ (*A*) or WT mice (*C*) treated with bleomycin (Bleo) for 7 d and their respective higher magnification images are shown (*B*, *D*). Original magnification, ×200. Scale bars: 2.5 mm (whole lung);100 μm (high magnification).

protein because it protects β-galactosidase and neuraminidase from intralysosomal proteolysis. It is a multicatalytic enzyme with carboxypeptidase, deamidase, and esterase activities (33). Cathepsin A shares its structural homology with the yeast carboxypeptidase Y and has been shown to regulate chaperone-mediated autophagy (34). We did not observe any changes in the protein levels of LAMP2a or GABARAP (Supplemental Fig. S3*B*), but proSP-C–positive AECII in LC3B$^{-/-}$ mice showed increased cathepsin A staining as compared with the AECII of WT control mice lungs (Fig. 7*D*, *E*). In full support, primary AECII isolated from 42-wk-old LC3B$^{-/-}$ mice displayed significantly increased cathepsin A protein levels as compared with those of age-matched WT mice (Fig. 7*F*, *G*). We thus hypothesized that apart from the chaperone-mediated autophagy, cathepsin A might also contribute to the macroautophagy pathway. To study this, we first analyzed the protein sequence of cathepsin A. As shown in **Fig. 8*A***, the mouse cathepsin A protein has 5 core LC3 interacting regions (LIRs), of which 3 are Y-type (YxxL), 1 is a W-type (WxxL), and 1 is F-type (FxxI) LIR. We next overexpressed myc-cathepsin A, and GFP-LC3B in MLE12 cells performed coimmunoprecipitation experiments, which revealed an interaction between the 2 overexpressed proteins (Fig. 8*B*). In addition, endogenous cathepsin A immunoprecipitation revealed an interaction with endogenous LC3B protein (Fig. 8*C*). Apart from its protective activity, cathepsin A overexpression has been shown to exert oxidative stress and cell death in cardiac tissue (35). Thus, to study the biologic significance of cathepsin A overexpression as seen in LC3B$^{-/-}$ mice, we overexpressed cathepsin A in MLE12 cells and analyzed cleaved caspase-3 as the terminal apoptosis marker. Cells overexpressing cathepsin A alone showed significant increase in cleaved caspase-3 as compared with cells overexpressing both LC3B as well as cathepsin A (Fig. 8*D*, *E*), indicating the importance of their interaction in regulating apoptosis. These data are fully supported by data from patients with IPF, where defective autophagy has been reported (15). As shown in **Fig. 9**, cathepsin A protein levels were significantly increased in the total lung extracts of patients with IPF as compared with those of donors (Fig. 9*A*, *B*). The increased cathepsin A protein levels in IPF could be ascribed to the AECII and by immunohistochemistry where serial lung sections of IPF, and donor lungs were stained for proSP-C and cathepsin A (Fig. 9*C*, *D*) as well as by immunofluorescence where the sections were costained for ABCA3, the marker of the limiting membrane of lamellar bodies in AECII and for cathepsin A (Fig. 9*E*, *F*).

15306860, 2019, 11, Downloaded from https://faseb.onlinelibrary.wiley.com/doi/10.1096/fj.201900854R by Justus-Liebig-Universitat, Wiley Online Library on [29/12/2022]. See the Terms and Conditions (https://onlinelibrary.wiley.com/terms-and-conditions) on Wiley Online Library for rules of use; OA articles are governed by the applicable Creative Commons License

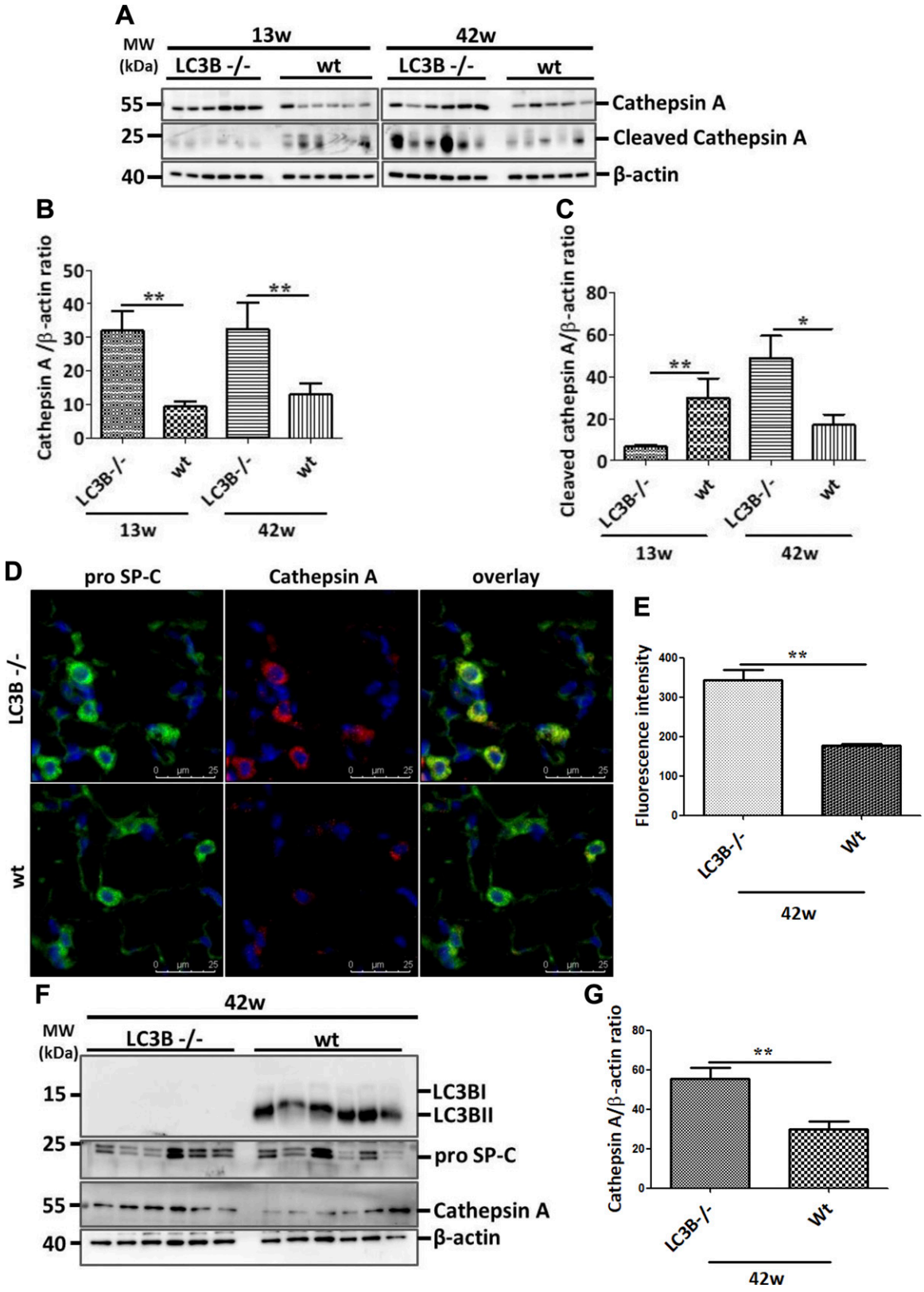

Figure 7. Increase in cathepsin A in LC3B$^{-/-}$ mice. *A–C*) Western blot analysis (*A*) of lung homogenates of 13-wk-old (left) or 42-wk-old (right) LC3B$^{-/-}$ and WT mice for cathepsin A (pro form), for cleaved form of cathepsin A and β-actin followed by their densitometric quantifications in (*B, C*) respectively. *D*) Immunofluorescence staining on paraffin sections from 42-wk-old LC3B$^{-/-}$ or WT control mice for the AECII marker, proSP-C (green), and cathepsin A (red). DAPI was used to stain the nuclei in blue. *E*) Cathepsin A fluorescence signal intensity was quantified and depicted as a bar graph. *F*) Representative Western blots for the indicated proteins from primary AECII isolated from 42-wk-old LC3B$^{-/-}$ or WT mice. *G*) Densitometric quantification for cathepsin A from AECII is shown. Representative blots and analysis from $n = 5$ mice/group and 3 independent experiments are shown. *$P < 0.05$, **$P < 0.01$.

15306860, 2019, 11, Downloaded from https://faseb.onlinelibrary.wiley.com/doi/10.1096/fj.201900854R by Justus-Liebig-Universitat, Wiley Online Library on [29/12/2022]. See the Terms and Conditions (https://onlinelibrary.wiley.com/terms-and-conditions) on Wiley Online Library for rules of use; OA articles are governed by the applicable Creative Commons License

DISCUSSION

In the current study, we report that the LC3B$^{-/-}$ mice at 42 wk display reduced airspaces and diameter of distal airspaces and increased cellularity. These older mice also display AECII apoptosis and increased lysosomal and ER stress without any concomitant increase in the proteasomal activity. However, syntaxin 17, the lysosomal SNARE that is involved in the autophagosome-lysosome fusion is accumulated in the AECII of aged LC3B$^{-/-}$ mice (**Fig. 10**) as well as in the AECII of human patients with IPF. Furthermore, *in vitro* knockdown of *LC3B* followed by bleomycin treatment in MLE12 cells resulted in increased apoptosis. Likewise, *in vivo*, LC3B$^{-/-}$ mice upon bleomycin challenge showed increased susceptibility to lung injury as reflected by reduced airspaces, increased cellularity, as well as increased apoptosis. In addition to this, we identified cathepsin A as a novel interacting partner of LC3B and its protein levels to be increased in the AECII of LC3B$^{-/-}$ mice as well as in patients with IPF. Furthermore, *in vitro* overexpression of cathepsin A resulted in increased apoptosis, which was reduced in the presence of overexpressed LC3B. To our knowledge, this is the first study to reveal lung defects in LC3B$^{-/-}$ mice and their susceptibility to lung injury upon bleomycin treatment as well as the significance of the cathepsin A overexpression in fibrotic lungs.

Our current observations are in line with our previous study where we showed that overexpression of GFP-LC3B protects lung epithelial cells from *HPS1* knockdown–induced defective autophagy (16). Although protective effects of LC3B in several settings have been reported (16, 31, 32), this is the first study to show that its loss can result in lung injury. Our data also complement a recent study by Cheong and colleagues (19) who reported that serine/threonine-protein kinases, ULK1/2 double knockout mice, and ATG5 knockout mice display lung defects at a very early age. ULK1 and 2 are mammalian orthologs of yeast ATG1, which is the first protein in the autophagy pathway (36, 37). ULK1/2 double knockout results in the deactivation of all the downstream autophagy gene products, thus resulting in a cumulative knockout situation of the autophagy pathway that may have resulted in the neonatal mortality of ULK1/2$^{-/-}$ mice. Here, we show that the loss of LC3B, the distal protein in the autophagy pathway is sufficient to result in lung injury, albeit in older mice. That said, we cannot exclude nonautophagy functions of LC3B to contribute to the phenotype observed in LC3B$^{-/-}$ mice.

It has been reported that LC3B$^{-/-}$ mice develop normally without any compensatory increase in LC3α or proteins associated with fibronectin, the synthesis of which is used to study LC3-regulated mRNA translational control. The same study emphasized the activation of novel compensatory mechanisms in the absence of LC3B (26). In line with this notion, one striking observation of our current study is that the autophagy substrate protein p62 is increased slightly in younger, but significantly in older, LC3B$^{-/-}$ mice as compared with age-matched WT control mice. A straightforward explanation of that observation is that compensatory autophagy pathways might be activated in the younger mice in the absence of LC3B. Indeed, it has been suggested that other proteins that are involved in the homeostatic processes might compensate for the loss of LC3B (31, 38). However, we did not observe significant increase in GABARAP proteins that could compensate for the loss of LC3B-mediated autophagy in LC3B$^{-/-}$ mice.

It is well established that the ubiquitin proteasome system and autophagy are the 2 fundamental protein quality control mechanisms of the cell (39). In fact, under certain settings of defective proteasomal degradation, autophagic degradation has been shown to be activated in order to alleviate proteotoxic stress (40–42). Although there is no direct evidence showing the inverse, recent reports reinforce the notion that coordinated and complementary action of these pathways is extremely important to rescue cells from cellular stress (39). Hence, we hypothesized that the increased accumulation of p62 in older as compared with younger LC3B$^{-/-}$ mice may be a result of the compensatory function of the proteasome in the younger mice. Although we observed an increase in the 20S core subunit protein levels in the younger LC3B$^{-/-}$ mice, we did not observe an increase in the proteasome activity. This led us to study the regulation of other autophagy-related proteins potentially compensating for the loss of LC3B in the younger LC3B$^{-/-}$ mice. It has been shown that the lysosomal SNARE protein syntaxin 17 is recruited to the completed autophagosomes and aids in the fusion of autophagosomes and lysosomes also in the absence of the classic ATG conjugation mechanisms. Agreeing with this notion, we also identified that syntaxin 17 was accumulated in the AECII of older LC3B$^{-/-}$ mice but not in the younger mice, indicating that syntaxin 17–mediated autophagy may compensate part of LC3B functions in the younger mice, but upon aging, its functions are discounted. Likewise, in the AECII of patients with IPF where defective autophagy has been reported, we now identified elevated syntaxin 17 protein levels thereby supporting the data from LC3B$^{-/-}$ mice.

Next, we observed that the younger LC3B$^{-/-}$ mice are susceptible to bleomycin-induced lung injury. The most pronounced effects were observed 7 d after a single low-dose bleomycin application in which LC3B$^{-/-}$ mice display increased cellularity and patchy fibrotic consolidations as compared with the WT mice treated with bleomycin. A note of caution here is that this time point coincides with inflammatory response to bleomycin. LC3B$^{-/-}$ and WT mice treated with bleomycin showed no perceivable differences at d 14 posttreatment. Our observation regarding the susceptibility of LC3B$^{-/-}$ mice supports the findings of a previous study in which deficiency of ATG4B resulted in increased sensitivity of mice to bleomycin-induced lung fibrosis (20). ATG4B is a cysteine protease that cleaves LC3B at its C terminus, a cleavage that is essential to conjugate it to phosphatidylethanolamine and insert it on the membranes (43) and absence of ATG4B might result in the inhibition of LC3B cleavage and thereby autophagy.

Another interesting observation from this study is the increase of cathepsin A protein levels in the aged LC3B$^{-/-}$ mice and in the AECII of the lungs of patients with IPF, as

15306860, 2019, 11, Downloaded from https://faseb.onlinelibrary.wiley.com/doi/10.1096/fj.201900854R by Justus-Liebig-Universitat, Wiley Online Library on [29/12/2022]. See the Terms and Conditions (https://onlinelibrary.wiley.com/terms-and-conditions) on Wiley Online Library for rules of use; OA articles are governed by the applicable Creative Commons License

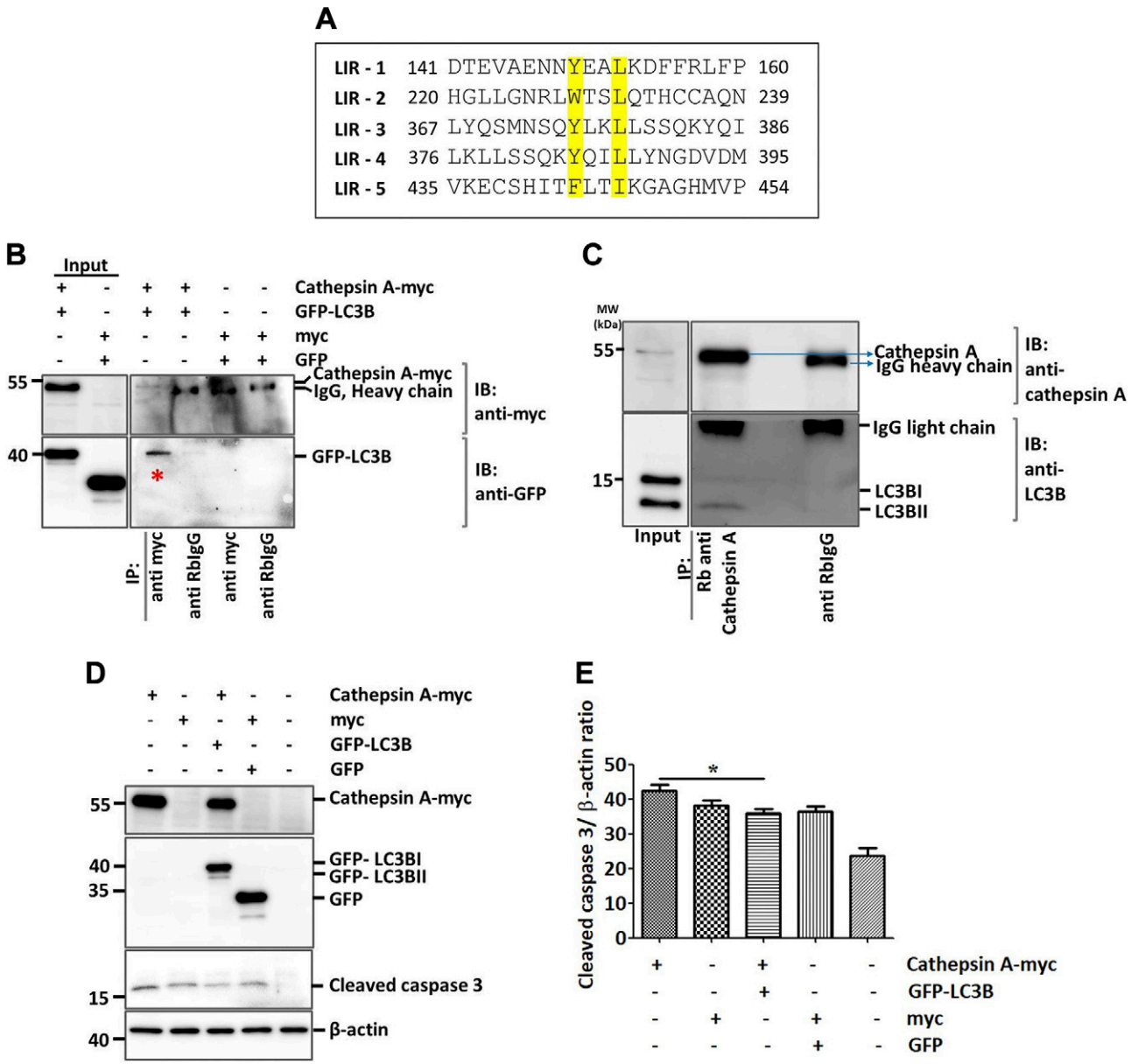

Figure 8. Cathepsin A is an LC3B interacting protein. *A*) Alignment of 5 putative LIRs of mouse cathepsin A, highlighting the N- and C-terminal amino acids of the core motif in yellow. *B*) Cathepsin A is coimmunoprecipitated with LC3B in MLE12 cells coexpressing cathepsin A (myc tagged) and LC3B (GFP tagged). *C*) Representative Western blots for cathepsin A and LC3B following immunoprecipitation of endogenous cathepsin A from MLE12 cells. *D*) Overexpression of cathepsin A, LC3B, empty myc, or GFP plasmids followed by Western blots using anti-myc, GFP, cleaved caspase-3, and β-actin. *E*) Densitometric quantification for cleaved caspase-3 is shown. Representative blots and analysis from 3 independent experiments are shown. $*P < 0.05$.

well as the interaction between these 2 proteins. To our knowledge, the interaction between these 2 proteins has not yet been reported. Our data indicate that the increase in cathepsin A in the absence of LC3B may contribute to the apoptosis of AECII. Cathepsin A has been suggested to elicit oxidative stress and cell death in cardiomyocytes. Although not shown directly in our study, it is plausible to speculate that the apoptosis of mouse lung epithelial cells upon cathepsin A overexpression *in vitro* or the overexpression of cathepsin A in the AECII of LC3B$^{-/-}$ mice may retrogradely elicit oxidative stress and subsequent apoptosis. Our data do suggest, however that modulation of cathepsin A protein levels by LC3B is important in defining the physiologic roles of cathepsin A in AECII. Our *in vitro* as well as *in vivo* observations are fully supported by the data from the lungs of patients with IPF, altogether suggesting that the increased cathepsin A protein levels may contribute to the increased cellular stress and apoptosis of AECII in lung fibrosis.

Our current study ascertains the pathomechanistic role of autophagy in general and LC3B in particular in the development of pulmonary fibrosis. This study also raises the possibility that in IPF, LC3B-mediated regulation of cellular mechanisms may play an integral role in eliciting

15306860, 2019, 11, Downloaded from https://faseb.onlinelibrary.wiley.com/doi/10.1096/fj.201900854R by Justus-Liebig-Universitat, Wiley Online Library on [29/12/2022]. See the Terms and Conditions (https://onlinelibrary.wiley.com/terms-and-conditions) on Wiley Online Library for rules of use; OA articles are governed by the applicable Creative Commons License

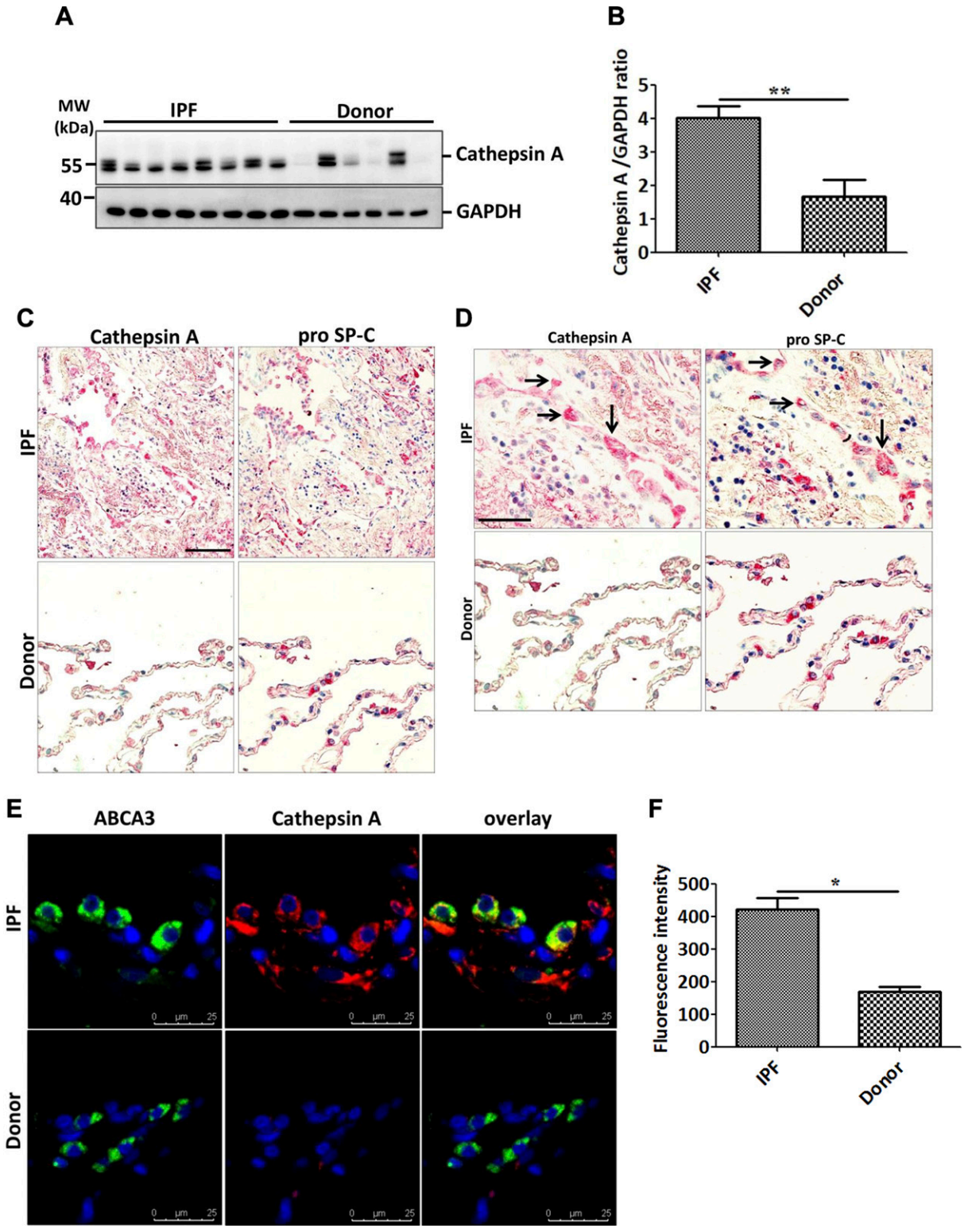

Figure 9. Increase in cathepsin A in AECII of IPF lungs. *A*, *B*) Western blot analysis of lung homogenates of patients with IPF and age-matched donors for cathepsin A and glyceraldehyde 3-phosphate dehydrogenase as loading control (*A*) followed by densitometric quantification for cathesin A (*B*). *C*, *D*) Serial paraffin sections from IPF and donor lungs were stained for cathepsin A and the AECII marker proSP-C and pictomicrographs were performed for the same areas from both types of staining. High magnification images (*D*) show several AECII cells also stained positively for cathepsin A, as indicated by the arrows. *E*) Immunofluorescence staining for the AECII lamellar body limiting membrane marker, ABCA3 (green) and cathepsin A (red). DAPI was used to stain nuclei in blue. *F*) Cathepsin A fluorescence signal intensity was quantified and depicted as a bar graph. Scale bars, 100 μm. Representative pictures are shown from ~10–15 patients with IPF and donors. $^{**}P < 0.01$.

15306860, 2019, 11, Downloaded from https://faseb.onlinelibrary.wiley.com/doi/10.1096/fj.201900854R by Justus-Liebig-Universitat, Wiley Online Library on [29/12/2022]. See the Terms and Conditions (https://onlinelibrary.wiley.com/terms-and-conditions) on Wiley Online Library for rules of use; OA articles are governed by the applicable Creative Commons License

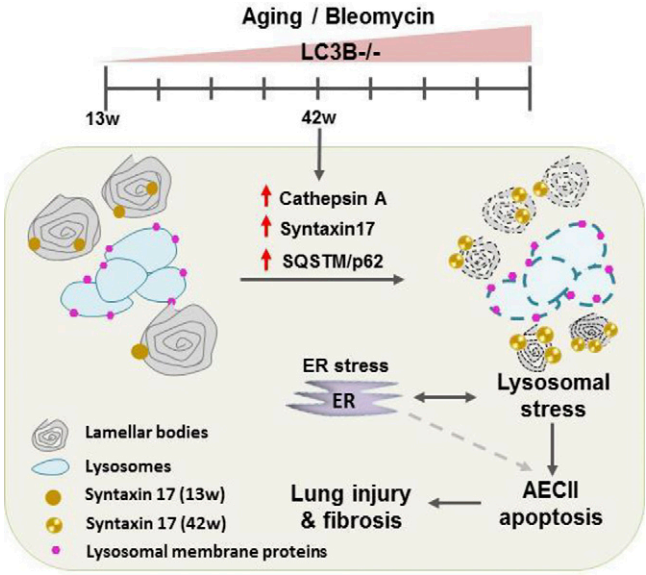

Figure 10. Schematic representation of pathomechanistic events in LC3B$^{-/-}$ mice. Aged LC3B$^{-/-}$ mice (42 w) lungs show increased cellularity and AECII apoptosis with smaller lamellar body profiles. AECII show increase in syntaxin 17, lysosomal, and ER stress with a concomitant increase in the novel LC3B interacting partner, cathepsin A that contributes to AECII apoptosis. Furthermore, LC3B$^{-/-}$ mice display increased susceptibility to bleomycin-induced lung injury and fibrosis. Similar observations from the lungs of patients with IPF emphasized the pathomechanistic role of autophagy in lung fibrosis.

cellular stress in the AECII, which, in addition to the activation of concomitant stress pathways, subsequently results in pulmonary fibrosis. Fj

ACKNOWLEDGMENTS

The authors thank the German Research Foundation for supporting this study through an independent research grant to P.M. The authors also thank Silke Haendel, Stefanie Hezel [Department of Internal Medicine, Justus-Liebig University (JLU) Giessen], and Susanne Faßbender (Institute of Functional and Applied Anatomy, Hannover Medical School) for their excellent technical support. The authors also thank Prof. Dr. Saverio Bellusci (Department of Internal Medicine, JLU Giessen) and laboratory members for help with fluorescence miscroscopy. The authors declare no conflicts of interest.

AUTHOR CONTRIBUTIONS

V. S. Kesireddy, S. Chillappagari, S. Ahuja, I. Henneke, J. Graumann, C. Ruppert, and M. Korfei performed experiments; V. S. Kesireddy and P. Mahavadi developed the project, analyzed and interpreted the data, and wrote the article; S. Chillappagari and J. Graumann critically read the manuscript; L. Knudsen and M. Ochs performed electron microscopy and interpreted the data; S. Meiners performed proteasome analysis; W. Seeger and P. Mahavadi supervised the study; P. Mahavadi designed the study; and all authors approved the final version of the manuscript.

REFERENCES

1. King, T. E., Jr., Pardo, A., and Selman, M. (2011) Idiopathic pulmonary fibrosis. *Lancet* **378**, 1949–1961
2. Selman, M., and Pardo, A. (2006) Role of epithelial cells in idiopathic pulmonary fibrosis: from innocent targets to serial killers. *Proc. Am. Thorac. Soc.* **3**, 364–372
3. American Thoracic Society; European Respiratory Society. (2002) American Thoracic Society/European Respiratory Society International Multidisciplinary Consensus Classification of the Idiopathic Interstitial Pneumonias. [This joint statement of the American Thoracic Society (ATS) and the European Respiratory Society (ERS) was adopted by the ATS board of directors, June 2001 and by the ERS Executive Committee, June 2001.] *Am. J. Respir. Crit. Care Med.* **165**, 277–304; erratum: **166**, 426
4. Myers, J. L., and Katzenstein, A. L. (1988) Epithelial necrosis and alveolar collapse in the pathogenesis of usual interstitial pneumonia. *Chest* **94**, 1309–1311
5. Fehrenbach, H. (2001) Alveolar epithelial type II cell: defender of the alveolus revisited. *Respir. Res.* **2**, 33–46
6. Weaver, T. E., Na, C. L., and Stahlman, M. (2002) Biogenesis of lamellar bodies, lysosome-related organelles involved in storage and secretion of pulmonary surfactant. *Semin. Cell Dev. Biol.* **13**, 263–270
7. Lutz, D., Gazdhar, A., Lopez-Rodriguez, E., Ruppert, C., Mahavadi, P., Günther, A., Klepetko, W., Bates, J. H., Smith, B., Geiser, T., Ochs, M., and Knudsen, L. (2015) Alveolar derecruitment and collapse induration as crucial mechanisms in lung injury and fibrosis. *Am. J. Respir. Cell Mol. Biol.* **52**, 232–243
8. Thomas, A. Q., Lane, K., Phillips J. III, Prince, M., Markin, C., Speer, M., Schwartz, D. A., Gaddipati, R., Marney, A., Johnson, J., Roberts, R., Haines, J., Stahlman, M., and Loyd, J. E. (2002) Heterozygosity for a surfactant protein C gene mutation associated with usual interstitial pneumonitis and cellular nonspecific interstitial pneumonitis in one kindred. *Am. J. Respir. Crit. Care Med.* **165**, 1322–1328
9. Schmitz, G., and Müller, G. (1991) Structure and function of lamellar bodies, lipid-protein complexes involved in storage and secretion of cellular lipids. *J. Lipid Res.* **32**, 1539–1570
10. Mahavadi, P., Knudsen, L., Venkatesan, S., Henneke, I., Hegermann, J., Wrede, C., Ochs, M., Ahuja, S., Chillappagari, S., Ruppert, C., Seeger, W., Korfei, M., and Guenther, A. (2015) Regulation of macroautophagy in amiodarone-induced pulmonary fibrosis. *J. Pathol. Clin. Res.* **1**, 252–263
11. Miller, B. E., and Hook, G. E. (1990) Hypertrophy and hyperplasia of alveolar type II cells in response to silica and other pulmonary toxicants. *Environ. Health Perspect.* **85**, 15–23
12. Mahavadi, P., Korfei, M., Henneke, I., Liebisch, G., Schmitz, G., Gochuico, B. R., Markart, P., Bellusci, S., Seeger, W., Ruppert, C., and Guenther, A. (2010) Epithelial stress and apoptosis underlie Hermansky-Pudlak syndrome-associated interstitial pneumonia. *Am. J. Respir. Crit. Care Med.* **182**, 207–219
13. Mahavadi, P., Henneke, I., Ruppert, C., Knudsen, L., Venkatesan, S., Liebisch, G., Chambers, R. C., Ochs, M., Schmitz, G., Vancheri, C., Seeger, W., Korfei, M., and Guenther, A. (2014) Altered surfactant homeostasis and alveolar epithelial cell stress in amiodarone-induced lung fibrosis. *Toxicol. Sci.* **142**, 285–297
14. Patel, A. S., Lin, L., Geyer, A., Haspel, J. A., An, C. H., Cao, J., Rosas, I. O., and Morse, D. (2012) Autophagy in idiopathic pulmonary fibrosis. *PLoS One* **7**, e41394
15. Bueno, M., Lai, Y. C., Romero, Y., Brands, J., St Croix, C. M., Kamga, C., Corey, C., Herazo-Maya, J. D., Sembrat, J., Lee, J. S., Duncan, S. R., Rojas, M., Shiva, S., Chu, C. T., and Mora, A. L. (2015) PINK1 deficiency impairs mitochondrial homeostasis and promotes lung fibrosis. *J. Clin. Invest.* **125**, 521–538
16. Ahuja, S., Knudsen, L., Chillappagari, S., Henneke, I., Ruppert, C., Korfei, M., Gochuico, B. R., Bellusci, S., Seeger, W., Ochs, M., Guenther, A., and Mahavadi, P. (2016) MAP1LC3B overexpression protects against Hermansky-Pudlak syndrome type-1-induced

15306860, 2019, 11, Downloaded from https://faseb.onlinelibrary.wiley.com/doi/10.1096/fj.201900854R by Justus-Liebig-Universitat, Wiley Online Library on [29/12/2022]. See the Terms and Conditions (https://onlinelibrary.wiley.com/terms-and-conditions) on Wiley Online Library for rules of use; OA articles are governed by the applicable Creative Commons License

defective autophagy in vitro. *Am. J. Physiol. Lung Cell. Mol. Physiol.* **310**, L519–L531
17. Mizushima, N. (2007) Autophagy: process and function. *Genes Dev.* **21**, 2861–2873
18. Codogno, P., and Meijer, A. J. (2005) Autophagy and signaling: their role in cell survival and cell death. *Cell Death Differ.* **12** (Suppl 2), 1509–1518
19. Cheong, H., Wu, J., Gonzales, L. K., Guttentag, S. H., Thompson, C. B., and Lindsten, T. (2014) Analysis of a lung defect in autophagy-deficient mouse strains. *Autophagy* **10**, 45–56
20. Cabrera, S., Maciel, M., Herrera, I., Nava, T., Vergara, F., Gaxiola, M., López-Otín, C., Selman, M., and Pardo, A. (2015) Essential role for the ATG4B protease and autophagy in bleomycin-induced pulmonary fibrosis. *Autophagy* **11**, 670–684
21. Raghu, G., Collard, H. R., Egan, J. J., Martinez, F. J., Behr, J., Brown, K. K., Colby, T. V., Cordier, J. F., Flaherty, K. R., Lasky, J. A., Lynch, D. A., Ryu, J. H., Swigris, J. J., Wells, A. U., Ancochea, J., Bouros, D., Carvalho, C., Costabel, U., Ebina, M., Hansell, D. M., Johkoh, T., Kim, D. S., King, T. E., Jr., Kondoh, Y., Myers, J., Müller, N. L., Nicholson, A. G., Richeldi, L., Selman, M., Dudden, R. F., Griss, B. S., Protzko, S. L., and Schünemann, H. J.; ATS/ERS/JRS/ALAT Committee on Idiopathic Pulmonary Fibrosis. (2011) An official ATS/ERS/JRS/ALAT statement: idiopathic pulmonary fibrosis: evidence-based guidelines for diagnosis and management. *Am. J. Respir. Crit. Care Med.* **183**, 788–824
22. Tschanz, S., Schneider, J. P., and Knudsen, L. (2014) Design-based stereology: planning, volumetry and sampling are crucial steps for a successful study. *Ann. Anat.* **196**, 3–11
23. Gundersen, H. J., Bagger, P., Bendtsen, T. F., Evans, S. M., Korbo, L., Marcussen, N., Møller, A., Nielsen, K., Nyengaard, J. R., and Pakkenberg, B., et al. (1988) The new stereological tools: disector, fractionator, nucleator and point sampled intercepts and their use in pathological research and diagnosis. *APMIS* **96**, 857–881
24. Welk, V., Coux, O., Kleene, V., Abeza, C., Trümbach, D., Eickelberg, O., and Meiners, S. (2016) Inhibition of proteasome activity induces formation of alternative proteasome complexes. *J. Biol. Chem.* **291**, 13147–13159
25. Ahuja, S., Knudsen, L., Chillappagari, S., Henneke, I., Ruppert, C., Korfei, M., Gochuico, B. R., Bellusci, S., Seeger, W., Ochs, M., Guenther, A., and Mahavadi, P. (2016) MAP1LC3B overexpression protects against Hermansky-Pudlak syndrome type-1-induced defective autophagy in vitro. *Am. J. Physiol. Lung Cell. Mol. Physiol.* **310**, L519–L531
26. Cann, G. M., Guignabert, C., Ying, L., Deshpande, N., Bekker, J. M., Wang, L., Zhou, B., and Rabinovitch, M. (2008) Developmental expression of LC3alpha and beta: absence of fibronectin or autophagy phenotype in LC3beta knockout mice. *Dev. Dyn.* **237**, 187–195
27. Tsuboyama, K., Koyama-Honda, I., Sakamaki, Y., Koike, M., Morishita, H., and Mizushima, N. (2016) The ATG conjugation systems are important for degradation of the inner autophagosomal membrane. *Science* **354**, 1036–1041
28. Hamasaki, M., Furuta, N., Matsuda, A., Nezu, A., Yamamoto, A., Fujita, N., Oomori, H., Noda, T., Haraguchi, T., Hiraoka, Y., Amano, A., and Yoshimori, T. (2013) Autophagosomes form at ER-mitochondria contact sites. *Nature* **495**, 389–393
29. Wang, R., Ibarra-Sunga, O., Verlinski, L., Pick, R., and Uhal, B. D. (2000) Abrogation of bleomycin-induced epithelial apoptosis and lung fibrosis by captopril or by a caspase inhibitor. *Am. J. Physiol. Lung Cell. Mol. Physiol.* **279**, L143–L151
30. Lee, V. Y., Schroedl, C., Brunelle, J. K., Buccellato, L. J., Akinci, O. I., Kaneto, H., Snyder, C., Eisenbart, J., Budinger, G. R., and Chandel, N. S. (2005) Bleomycin induces alveolar epithelial cell death through JNK-dependent activation of the mitochondrial death pathway. *Am. J. Physiol. Lung Cell. Mol. Physiol.* **289**, L521–L528
31. Lee, S. J., Smith, A., Guo, L., Alastalo, T. P., Li, M., Sawada, H., Liu, X., Chen, Z. H., Ifedigbo, E., Jin, Y., Feghali-Bostwick, C., Ryter, S. W., Kim, H. P., Rabinovitch, M., and Choi, A. M. (2011) Autophagic protein LC3B confers resistance against hypoxia-induced pulmonary hypertension. *Am. J. Respir. Crit. Care Med.* **183**, 649–658
32. Lahm, T., and Petrache, I. (2012) LC3 as a potential therapeutic target in hypoxia-induced pulmonary hypertension. *Autophagy* **8**, 1146–1147
33. Hiraiwa, M. (1999) Cathepsin A/protective protein: an unusual lysosomal multifunctional protein. *Cell. Mol. Life Sci.* **56**, 894–907
34. Cuervo, A. M., Mann, L., Bonten, E. J., d'Azzo, A., and Dice, J. F. (2003) Cathepsin A regulates chaperone-mediated autophagy through cleavage of the lysosomal receptor. *EMBO J.* **22**, 47–59
35. Petrera, A., Kern, U., Linz, D., Gomez-Auli, A., Hohl, M., Gassenhuber, J., Sadowski, T., and Schilling, O. (2016) Proteomic profiling of cardiomyocyte-specific cathepsin a overexpression links cathepsin a to the oxidative stress response. *J. Proteome Res.* **15**, 3188–3195
36. Alers, S., Löffler, A. S., Wesselborg, S., and Stork, B. (2012) Role of AMPK-mTOR-Ulk1/2 in the regulation of autophagy: cross talk, shortcuts, and feedbacks. *Mol. Cell. Biol.* **32**, 2–11
37. Alers, S., Löffler, A. S., Wesselborg, S., and Stork, B. (2012) The incredible ULKs. *Cell Commun. Signal.* **10**, 7
38. Martens, S. (2016) No ATG8s, no problem? How LC3/GABARAP proteins contribute to autophagy. *J. Cell Biol.* **215**, 761–763
39. Nedelsky, N. B., Todd, P. K., and Taylor, J. P. (2008) Autophagy and the ubiquitin-proteasome system: collaborators in neuroprotection. *Biochim. Biophys. Acta* **1782**, 691–699
40. Zhu, K., Dunner, K., Jr., and McConkey, D. J. (2010) Proteasome inhibitors activate autophagy as a cytoprotective response in human prostate cancer cells. *Oncogene* **29**, 451–462
41. Tang, B., Cai, J., Sun, L., Li, Y., Qu, J., Snider, B. J., and Wu, S. (2014) Proteasome inhibitors activate autophagy involving inhibition of PI3K-Akt-mTOR pathway as an anti-oxidation defense in human RPE cells. *PLoS One* **9**, e103364
42. Jänen, S. B., Chaachouay, H., and Richter-Landsberg, C. (2010) Autophagy is activated by proteasomal inhibition and involved in aggresome clearance in cultured astrocytes. *Glia* **58**, 1766–1774
43. Skytte Rasmussen, M., Mouilleron, S., Kumar Shrestha, B., Wirth, M., Lee, R., Bowitz Larsen, K., Abudu Princely, Y., O'Reilly, N., Sjøttem, E., Tooze, S. A., Lamark, T., and Johansen, T. (2017) ATG4B contains a C-terminal LIR motif important for binding and efficient cleavage of mammalian orthologs of yeast Atg8. *Autophagy* **13**, 834–853

Received for publication April 2, 2019.
Accepted for publication July 23, 2019.

15306860, 2019, 11, Downloaded from https://faseb.onlinelibrary.wiley.com/doi/10.1096/fj.201900854R by Justus-Liebig-Universitat, Wiley Online Library on [29/12/2022]. See the Terms and Conditions (https://onlinelibrary.wiley.com/terms-and-conditions) on Wiley Online Library for rules of use; OA articles are governed by the applicable Creative Commons License

JOHN WILEY AND SONS LICENSE
TERMS AND CONDITIONS

Feb 24, 2023

This Agreement between Justus-Liebig University Giessen -- Poornima Mahavadi ("You") and John Wiley and Sons ("John Wiley and Sons") consists of your license details and the terms and conditions provided by John Wiley and Sons and Copyright Clearance Center.

License Number	5495251221353
License date	Feb 24, 2023
Licensed Content Publisher	John Wiley and Sons
Licensed Content Publication	THE FASEB JOURNAL
Licensed Content Title	Susceptibility of microtubule-associated protein 1 light chain 3β (MAP1LC3B/LC3B) knockout mice to lung injury and fibrosis
Licensed Content Author	Poornima Mahavadi, Werner Seeger, Martina Korfei, et al
Licensed Content Date	Aug 20, 2019
Licensed Content Volume	33
Licensed Content Issue	11
Licensed Content Pages	17
Type of use	Dissertation/Thesis
Requestor type	Author of this Wiley article

Format	Print and electronic
Portion	Full article
Will you be translating?	No
Title	Susceptibility of microtubule-associated protein 1 light chain 3β (MAP1LC3B/LC3B) knockout mice to lung injury and fibrosis
Institution name	Justus-Liebig University Giessen
Expected presentation date	Feb 2023
Requestor Location	Justus-Liebig University Giessen Gaffkystraße 11 EG, Seltersberg haus-C Giessen, 35392 Germany Attn: Justus-Liebig University Giessen
Publisher Tax ID	EU826007151
Total	0.00 EUR
Terms and Conditions	

TERMS AND CONDITIONS

This copyrighted material is owned by or exclusively licensed to John Wiley & Sons, Inc. or one of its group companies (each a"Wiley Company") or handled on behalf of a society with which a Wiley Company has exclusive publishing rights in relation to a particular work (collectively "WILEY"). By clicking "accept" in connection with completing this licensing transaction, you agree that the following terms and conditions apply to this transaction (along with the billing and payment terms and conditions established by the Copyright Clearance Center Inc., ("CCC's Billing and Payment terms and conditions"), at the time that you opened your RightsLink account (these are available at any time at http://myaccount.copyright.com).

Terms and Conditions

- The materials you have requested permission to reproduce or reuse (the "Wiley Materials") are protected by copyright.

- You are hereby granted a personal, non-exclusive, non-sub licensable (on a stand-alone basis), non-transferable, worldwide, limited license to reproduce the Wiley Materials for the purpose specified in the licensing process. This license, **and any CONTENT (PDF or image file) purchased as part of your order,** is for a one-time use only and limited to any maximum distribution number specified in the license. The first instance of republication or reuse granted by this license must be completed within two years of the date of the grant of this license (although copies prepared before the end date may be distributed thereafter). The Wiley Materials shall not be used in any other manner or for any other purpose, beyond what is granted in the license. Permission is granted subject to an appropriate acknowledgement given to the author, title of the material/book/journal and the publisher. You shall also duplicate the copyright notice that appears in the Wiley publication in your use of the Wiley Material. Permission is also granted on the understanding that nowhere in the text is a previously published source acknowledged for all or part of this Wiley Material. Any third party content is expressly excluded from this permission.

- With respect to the Wiley Materials, all rights are reserved. Except as expressly granted by the terms of the license, no part of the Wiley Materials may be copied, modified, adapted (except for minor reformatting required by the new Publication), translated, reproduced, transferred or distributed, in any form or by any means, and no derivative works may be made based on the Wiley Materials without the prior permission of the respective copyright owner.**For STM Signatory Publishers clearing permission under the terms of the STM Permissions Guidelines only, the terms of the license are extended to include subsequent editions and for editions in other languages, provided such editions are for the work as a whole in situ and does not involve the separate exploitation of the permitted figures or extracts,** You may not alter, remove or suppress in any manner any copyright, trademark or other notices displayed by the Wiley Materials. You may not license, rent, sell, loan, lease, pledge, offer as security, transfer or assign the Wiley Materials on a stand-alone basis, or any of the rights granted to you hereunder to any other person.

- The Wiley Materials and all of the intellectual property rights therein shall at all times remain the exclusive property of John Wiley & Sons Inc, the Wiley Companies, or their respective licensors, and your interest therein is only that of having possession of and the right to reproduce the Wiley Materials pursuant to Section 2 herein during the continuance of this Agreement. You agree that you own no right, title or interest in or to the Wiley Materials or any of the intellectual property rights therein. You shall have no rights hereunder other than the license as provided for above in Section 2. No right, license or interest to any trademark, trade name, service mark or other branding ("Marks") of WILEY or its licensors is granted hereunder, and you agree that you shall not assert any such right, license or interest with respect thereto

- NEITHER WILEY NOR ITS LICENSORS MAKES ANY WARRANTY OR REPRESENTATION OF ANY KIND TO YOU OR ANY THIRD PARTY, EXPRESS, IMPLIED OR STATUTORY, WITH RESPECT TO THE MATERIALS OR THE ACCURACY OF ANY INFORMATION CONTAINED IN THE MATERIALS, INCLUDING, WITHOUT LIMITATION, ANY IMPLIED WARRANTY OF MERCHANTABILITY, ACCURACY, SATISFACTORY QUALITY, FITNESS FOR A PARTICULAR PURPOSE, USABILITY, INTEGRATION OR NON-INFRINGEMENT AND ALL SUCH WARRANTIES ARE HEREBY EXCLUDED BY WILEY AND ITS LICENSORS AND WAIVED BY YOU.

- WILEY shall have the right to terminate this Agreement immediately upon breach of this Agreement by you.

- You shall indemnify, defend and hold harmless WILEY, its Licensors and their respective directors, officers, agents and employees, from and against any actual or threatened claims, demands, causes of action or proceedings arising from any breach

of this Agreement by you.

- IN NO EVENT SHALL WILEY OR ITS LICENSORS BE LIABLE TO YOU OR ANY OTHER PARTY OR ANY OTHER PERSON OR ENTITY FOR ANY SPECIAL, CONSEQUENTIAL, INCIDENTAL, INDIRECT, EXEMPLARY OR PUNITIVE DAMAGES, HOWEVER CAUSED, ARISING OUT OF OR IN CONNECTION WITH THE DOWNLOADING, PROVISIONING, VIEWING OR USE OF THE MATERIALS REGARDLESS OF THE FORM OF ACTION, WHETHER FOR BREACH OF CONTRACT, BREACH OF WARRANTY, TORT, NEGLIGENCE, INFRINGEMENT OR OTHERWISE (INCLUDING, WITHOUT LIMITATION, DAMAGES BASED ON LOSS OF PROFITS, DATA, FILES, USE, BUSINESS OPPORTUNITY OR CLAIMS OF THIRD PARTIES), AND WHETHER OR NOT THE PARTY HAS BEEN ADVISED OF THE POSSIBILITY OF SUCH DAMAGES. THIS LIMITATION SHALL APPLY NOTWITHSTANDING ANY FAILURE OF ESSENTIAL PURPOSE OF ANY LIMITED REMEDY PROVIDED HEREIN.

- Should any provision of this Agreement be held by a court of competent jurisdiction to be illegal, invalid, or unenforceable, that provision shall be deemed amended to achieve as nearly as possible the same economic effect as the original provision, and the legality, validity and enforceability of the remaining provisions of this Agreement shall not be affected or impaired thereby.

- The failure of either party to enforce any term or condition of this Agreement shall not constitute a waiver of either party's right to enforce each and every term and condition of this Agreement. No breach under this agreement shall be deemed waived or excused by either party unless such waiver or consent is in writing signed by the party granting such waiver or consent. The waiver by or consent of a party to a breach of any provision of this Agreement shall not operate or be construed as a waiver of or consent to any other or subsequent breach by such other party.

- This Agreement may not be assigned (including by operation of law or otherwise) by you without WILEY's prior written consent.

- Any fee required for this permission shall be non-refundable after thirty (30) days from receipt by the CCC.

- These terms and conditions together with CCC's Billing and Payment terms and conditions (which are incorporated herein) form the entire agreement between you and WILEY concerning this licensing transaction and (in the absence of fraud) supersedes all prior agreements and representations of the parties, oral or written. This Agreement may not be amended except in writing signed by both parties. This Agreement shall be binding upon and inure to the benefit of the parties' successors, legal representatives, and authorized assigns.

- In the event of any conflict between your obligations established by these terms and conditions and those established by CCC's Billing and Payment terms and conditions, these terms and conditions shall prevail.

- WILEY expressly reserves all rights not specifically granted in the combination of (i) the license details provided by you and accepted in the course of this licensing transaction, (ii) these terms and conditions and (iii) CCC's Billing and Payment terms and conditions.

- This Agreement will be void if the Type of Use, Format, Circulation, or Requestor Type was misrepresented during the licensing process.

- This Agreement shall be governed by and construed in accordance with the laws of the State of New York, USA, without regards to such state's conflict of law rules. Any legal action, suit or proceeding arising out of or relating to these Terms and Conditions or the breach thereof shall be instituted in a court of competent jurisdiction in New York County in the State of New York in the United States of America and each party hereby consents and submits to the personal jurisdiction of such court, waives any objection to venue in such court and consents to service of process by registered or certified mail, return receipt requested, at the last known address of such party.

WILEY OPEN ACCESS TERMS AND CONDITIONS

Wiley Publishes Open Access Articles in fully Open Access Journals and in Subscription journals offering Online Open. Although most of the fully Open Access journals publish open access articles under the terms of the Creative Commons Attribution (CC BY) License only, the subscription journals and a few of the Open Access Journals offer a choice of Creative Commons Licenses. The license type is clearly identified on the article.

The Creative Commons Attribution License

The Creative Commons Attribution License (CC-BY) allows users to copy, distribute and transmit an article, adapt the article and make commercial use of the article. The CC-BY license permits commercial and non-

Creative Commons Attribution Non-Commercial License

The Creative Commons Attribution Non-Commercial (CC-BY-NC)License permits use, distribution and reproduction in any medium, provided the original work is properly cited and is not used for commercial purposes.(see below)

Creative Commons Attribution-Non-Commercial-NoDerivs License

The Creative Commons Attribution Non-Commercial-NoDerivs License (CC-BY-NC-ND) permits use, distribution and reproduction in any medium, provided the original work is properly cited, is not used for commercial purposes and no modifications or adaptations are made. (see below)

Use by commercial "for-profit" organizations

Use of Wiley Open Access articles for commercial, promotional, or marketing purposes requires further explicit permission from Wiley and will be subject to a fee.

Further details can be found on Wiley Online Library
http://olabout.wiley.com/WileyCDA/Section/id-410895.html

Other Terms and Conditions:

v1.10 Last updated September 2015

Questions? customercare@copyright.com.

Citation of this article: Vidya Sagar Kesireddy, Shashi Chillappagari, Saket Ahuja, Lars Knudsen, Ingrid Henneke, Johannes Graumann, Silke Meiners, Matthias Ochs, Clemens Ruppert, Martina Korfei, Werner Seeger, Poornima Mahavadi. Susceptibility of microtubule - associated protein 1 light chain 3β (MAP1LC3B/LC3B) knockout mice to lung injury and fibrosis. **FASEB J. 2019** Nov;33(11):12392-12408. doi: 10.1096/fj.201900854R. Epub 2019 Aug 20.

9. Acknowledgements

Foremost, I acknowledge and pay my special regards to my advisor Prof. Dr. Andreas Guenther. His professional guidance and support have been invaluable for which I am extremely grateful. As my teacher, guide and a well-wisher, his encouragement and constructive criticism helped endlessly to reach the goals of my work. I consider it to be a great privilege and honor to work with Andreas whose vision and sincerity always inspired me.

My sincere thanks goes to my senior colleague and my good friend, Dr. Martina Korfei from whom I learnt the intricacies of research work. Her suggestions and co-operation contributed invaluably to my work.

I thank my very good friend Dr. Ingrid Henneke with whom I love to work. I am extremely thankful to her for helping me with her expertise in establishing animal models of lung fibrosis and for making the animal work happen as smoothly as possible.

A big thank you goes to all my students for being a strong part of this work and for helping me grow as a teacher. I cannot name my students individually here, but teaching them was a rewarding and an extremely satisfying experience.

I also thank Silke Haendel, Stefanie Hezel, Ann-Christin Beitel and Moritz Wattenbach for their technical assistance all through this work. My sincere thanks goes to my colleague Dr. Clemens Ruppert for his co-operation. I thank my collaborator Prof. Dr. Lars Knudsen whose expertise in lung ultrastructural analysis greatly contributed to this work. My sincere thanks also goes to all my collaborators for making this work possible. I thank Dr. Jasmin Wagner, a former colleague, a great friend and a well-wisher who always supported me through my work. A warm thank you for my colleague and a wonderful friend, Dr. Jutta Schlegel, who always managed to simplify the unending paper and bureautic work related to my projects and with whom I had the best telephone and corridor chats. Her translational skills and prompt responses have been extremely helpful. A special thanks to Mr. Patrice Schlegel for editing the summary of my thesis.

A special vote of thanks goes to the research and funding organizations: Excellence Cluster Cardio-Pulmonary System (ECCPS), Deutsche Forscungsgemeinschaft (DFG), Von Behring-Röntgen-Stiftung and Universitätsklinikum Gießen & Marburg (UKGM). Their contribution undoubtedly helped to accomplish the goals of this work for which I am extremely thankful.

Finally, I would like to extend my gratitude to my family for always being there for me. My special thanks to my husband Dr. Shashi Chillappagari for all his love and understanding and with whom I share moments of deep anxiety and of big excitement. I am always thankful to my lovely children, Aaraadhya and Agastya for understanding mommy's many late nights

work and scientific trips. My parents, Prof. Dr. Subhash Mahavadi and Mrs. Radha Rani Suvarna have been my pillars of support all through. A big thanks to mummy-nana and my younger brother Dr. Phanindra Mahavadi for their unconditional love, affection and for their moral and spiritual support.

10. Declaration

„Hiermit erkläre ich, dass ich die vorliegende Arbeit bzw. die mir zuzuordnenden Teile im Rahmen einer kumulativen Habilitationsschrift, selbstständig und ohne unzulässige Hilfe oder Benutzung anderer als der angegebenen Hilfsmittel angefertigt habe. Alle Textstellen, die wörtlich oder sinngemäß aus veröffentlichten oder nichtveröffentlichten Schriften entnommen sind, und alle Angaben, die auf mündlichen Auskünften beruhen, sind als solche kenntlich gemacht. Ich versichere, dass ich für die nach §2 (3) der Habilitationsordnung angeführten bereits veröffentlichten Originalarbeiten als Erst-oder Seniorautor fungiere, da ich den größten Teil der Daten selbst erhoben habe, für das Design der Arbeiten verantwortlich bin und die Manuskripte maßgeblich gestaltet habe. Für alle von mir erwähnten Untersuchungen habe ich die in der „Satzung der Justus-Liebig-Universität zur Sicherung guter wissenschaftlicher Praxis“ niedergelegten Grundsätze befolgt. Ich versichere, dass alle an der Finanzierung der Arbeiten beteiligten Geldgeber in den jeweiligen Publikationen genannt worden sind. Ich versichere außerdem, dass die vorgelegte Arbeit weder im Inland noch im Ausland in gleicher oder ähnlicher Weise einer anderen Prüfungsbehörde vorgelegt wurde oder Gegenstand eines anderen Prüfungsverfahrens war. Mit der Überprüfung meiner Arbeit durch eine Plagiatserkennungssoftware bzw. ein internetbasiertes Softwareprogramm erkläre ich mich einverstanden.“

Gießen, den 09.08.2021